UAB
Universitat Autònoma de Barcelona

DECIPHERING HETEROGENEITY: IMMUNE AND EPIGENETIC BIOMARKERS AND MODULATORS OF PARTIAL REMISSION IN TYPE 1 DIABETES

Laia Gómez Muñoz

DECIPHERING HETEROGENEITY: IMMUNE AND EPIGENETIC BIOMARKERS AND MODULATORS OF PARTIAL REMISSION IN TYPE 1 DIABETES

Laia Gómez Muñoz

DOCTORAL THESIS

Badalona, 2024

Thesis director:

Marta Vives-Pi, PhD

Immunology Department

Germans Trias i Pujol Research Institute

PhD programme in Advanced Immunology

Department of Cellular Biology, Physiology and Immunology

Universitat Autònoma de Barcelona

DECIPHERING HETEROGENEITY: IMMUNE AND EPIGENETIC BIOMARKERS AND MODULATORS OF PARTIAL REMISSION IN TYPE 1 DIABETES

Thesis presented by **Laia Gómez Muñoz** to qualify for the PhD degree in Advanced Immunology by the Universitat Autònoma de Barcelona.

The presented work has been performed in the Immunology of Diabetes group at the Germans Trias i Pujol Research Institute (IGTP) and directed by Dr **Marta Vives Pi**.

Badalona, 20th November 2024

Laia Gómez Muñoz

PhD Candidate

Marta Vives Pi

Director

This work has been supported by Instituto de Salud Carlos III through the projects PI18/00436 and PI22/00045 co-financed with the European Regional Development Funds 'A way to make Europe' (FEDER), and by CERCA Programme/*Generalitat de Catalunya*. A grant to support research groups recognized by the Government of Catalonia (No. 2021 SGR 00002), and entities such as *Fundación Diabetes Cero*, *Mi Dulce Guerrero* and *Amics de Can Ruti* also supported part of this work. Laia Gómez Muñoz has been supported by both the Health Department of the *Generalitat de Catalunya* through the predoctoral contract PIF-Salut (Grant No. SLT017/20/000049) and by *Fundació Universitària Agustí Pedro i Pons* through a grant for studies or projects outside Catalonia. The director of this thesis is the co-founder and CSO of Ahead Therapeutics SL, a biotech spin-off created to advance the development of therapies for autoimmune diseases. The author of the present PhD thesis declares no conflict of interest.

Dr. Marta Vives Pi, a biomedical researcher at the Germans Trias i Pujol Research Institute and Associate Professor at the Department of Cellular Biology, Physiology, and Immunology at the Autonomous University of Barcelona,

Certifies:

That the experimental work and the writing of the Doctoral Thesis titled '***Deciphering heterogeneity: immune and epigenetic biomarkers and modulators of partial remission in type 1 diabetes***' were conducted by Laia Gómez Muñoz under her supervision and considers the dissertation suitable for presentation to opt for the degree of Doctor in Advanced Immunology.

And so for the record, she signs this document in Badalona,

Dra. Marta Vives Pi

A mis padres, por creer siempre en mí.

Ja sé que les coses no s'acaben ni comencen: s'entrecreuen.

Sí, ja sé que viure és provar-ho infinites vegades.

Extracte del poema “Per què tot comença?” de Màrius Sampere i Passarell

TABLE OF CONTENTS

ABBREVIATIONS

6-FAM	6-Carboxyfluorescein
7-AAD	7-amino-actinomycin D
APC	Allophycocyanin
APC-H7	Allophycocyanin-hilite 7
APCs	Antigen-presenting cells
AUC	Area under the curve
BCR	B-cell receptor
BFP	Blue fluorescent protein
BMI	Body mass index
BMP	Bone morphogenetic protein
Bregs	Regulatory B cells
BSA	Bovine serum albumin
BV	Brilliant violet
Cav	Voltage-gated Ca^{2+}
CBA	Cytometric Bead Array
CCL	Chemokine ligand
CCR	Chemokine receptor
cDCs	Conventional dendritic cell
cDNA	complementary DNA
CM	central memory
C_t	Cycle threshold
CTLA-4	Cytotoxic T lymphocyte-associated protein 4
CTV	CellTrace Violet
CXCL	CXC chemokine ligand
CXCR	CXC chemokine receptor
DAISY	Diabetes Autoimmunity Study in the Young
DCs	Dendritic cells
DEGs	Differentially expressed genes
DEMs	Differentially expressed miRNAs
DIPP	Type 1 Diabetes Prediction and Prevention
DMSO	Dimethyl sulfoxide
DN	Double negative
DNA	Deoxyribonucleic acid
DoRothEA	Discriminant Regulon Expression Analysis
dsRed	Red fluorescent protein
ECS	Euro-Collins Solution
ELISA	Enzyme-linked immunosorbent assay
EM	Effector memory

ER	Endoplasmic reticulum
FACS	Fluorescence-activated cell sorting
FBS	Fetal bovine serum
FC	Fold change
FcR	Fc receptor
FDA	Food and Drug Administration
FDR	False discovery rate
FITC	Fluorescein isothiocyanate
FMO	Fluorescence minus one
FoxP3	Forkhead box protein 3
FSC	Forward scatter
GADA	Glutamic acid decarboxylase autoantibodies
GO	Gene ontology
GWAS	Genome-wide association studies
HbA1c	Glycated hemoglobin
HIP	Human insulin promoter
HLA	Human leukocyte antigen
HPSs	Human pancreatic slices
HRP	Horseradish peroxidase
i.p.	intraperitoneal
IA-2A	Insulinoma Associated-2 Autoantibodies
IAA	Insulin autoantibodies
ICIs	Insulin-containing islets
IDAA1c	Insulin dose-adjusted glycated hemoglobin
IFN	Interferon
IGF-1	Insulin-like growth factor 1
IL	Interleukin
IL-1Ra	IL-1 receptor antagonist
IL-22RA1	IL-22 receptor alpha 1
IRS-1	Insulin receptor substrate 1
ISL-1	Islet-1
KEGG	Kyoto Encyclopedia of Genes and Genomes
LAG-3	Lymphocyte activation gene 3
LNA	Locked Nucleic Acid
LXR-β	Liver X receptor beta
mDCs	Myeloid dendritic cells
MFI	Mean fluorescence intensity
MHC	Major histocompatibility complex
miRNA	microRNA
NC	Negative control

NES	Normalized Enrichment Score
NETs	Neutrophil extracellular traps
NK	Natural killer
NKeffs	Effector natural killer cells
NKG2D	Natural killer group 2 member D
NKregs	Regulatory natural killer cells
NOD	Non-obese diabetic
non-PR	Non-partial remission
nPOD	Network for Pancreatic Organ Donors
OD	Optical density
PBMCs	Peripheral blood mononuclear cells
PBS	Phosphate buffered saline
PD-1	Programmed Cell Death Protein 1
pDCs	Plasmacytoid dendritic cells
PD-L1	Programmed Cell Death Ligand 1
PE	Phycoerythrin
PE-Cy5	Phycoerythrin-cyanine 5
PE-Cy7	Phycoerythrin-cyanine 7
PerCP	Peridinin-chlorophyll-protein
PerCP-Cy5.5	Peridinin-chlorophyll-cyanine 5.5
PLN	Pancreatic lymph nodes
PR	Partial Remission
RISC	RNA-induced silencing complex
RNA	Ribonucleic acid
RNA-seq	RNA sequencing
ROC	Receiver operating characteristic
ROS	reactive oxygen species
RTEs	Recent thymic emigrants
RT-qPCR	Reverse transcription–quantitative polymerase chain reaction
SASP	Senescence-associated secretory phenotype
SC-islets	Stem cell-derived islets
SD	Standard deviation
SEM	Standard error of the mean
SSC	Side scatter
T1D	Type 1 diabetes
T2D	Type 2 diabetes
TCR	T–cell receptor
TEDDY	The Environmental Determinants of Diabetes in the Young
TEMRA	Terminally differentiated effector memory T cells
TF	Transcription factor

Tfh	T follicular helper
TGF	Transforming growth factor
Th	T helper
TIGIT	T cell immunoreceptor with Ig and ITIM domains
TIM-3	T cell immunoglobulin and mucin domain containing-3
TLR	Toll-like receptor
TMB	Tetramethylbenzidine
TNF	Tumor necrosis factor
Treg	Regulatory T cell
TTR	Transthyretin
U	Units
UPR	Unfolded protein response
UTR	Untranslated regions
VNTR	Variable number of tandem repeats
ZnT8A	Zinc transporter 8 autoantibodies

Type 1 diabetes (T1D) is an autoimmune disease with complex, heterogeneous pathogenesis. Following initiation of insulin therapy, the majority of pediatric patients experience a period of partial remission (PR), commonly referred to as the "honeymoon" phase. During this stage, pancreatic β-cells experience a transient functional recovery with improved endogenous insulin secretion, which reduces the need for exogenous insulin and maintains better glycemic control. The mechanisms behind this phase are unclear but may involve reduced β-cell stress due to corrected hyperglycemia, as well as improved viability, insulin sensitivity, regeneration, and immune regulation. It is therefore of great importance to understand not only the immunological fluctuations that precede the diagnosis of the disease but also those occurring subsequent to it. This can provide valuable insights into the pathways leading to β-cell protection and immune modulation, impacting patient stratification, immune intervention timing, and therapeutic precision. We hypothesize that the identification and characterization of metabolic, immunological, and epigenetic alterations in T1D can lead to the development of predictive algorithms and monitoring biomarkers of remission and can provide insights into the mechanisms underlying the PR phase. Thus, the main aim of the present work is to identify novel immunological and epigenetic biomarkers of PR in pediatric patients with T1D and to elucidate the mechanisms underlying the intersection of immunometabolism and epigenetic regulation, with the potential to provide insights into β-cell protective pathways.

To this end, we initially characterized quantitative changes in up to fifty-five peripheral immune cell subpopulations at T1D diagnosis in order to identify which variables are predictive of remission. Subsequently, a PR prediction model was developed based on an index of immunologic variables, exhibiting a discriminatory power of 81%. This index, in combination with age, may serve as a means of early monitoring of these patients and may assist in stratifying those who will have better or worse prognoses, thereby enabling a more personalized approach to therapeutic management. Subsequently, in a longitudinal study, we characterized quantitative changes in these same leukocyte subpopulations and different cytokines and microRNAs (miRNAs) in plasma to define specific monitoring biomarkers of the PR phase. Our findings indicate that this phenomenon is associated with alterations in the percentage and/or concentration of effector and regulatory T lymphocytes, regulatory and transitional B lymphocytes, regulatory NK cells, monocytes, and IL-17A concentration. Furthermore, remitter patients exhibit a distinctive plasma miRNA profile associated with immune, apoptosis, and metabolic processes. Among the identified miRNAs, miR-30d-5p exhibited the most pronounced upregulation during the PR phase. This miRNA was enriched for many different biological processes, including responses to stress, insulin signaling, cell death,

and immune-related processes such as antigen processing and presentation or TGF-β signaling. Moreover, it was also associated with regeneration, differentiation, and proliferation pathways. Based on the premise that miR-30d-5p plays a role in regulating pivotal pathways that contribute to the pathogenesis of T1D, we sought to investigate whether it can promote immunoregulation and β-cell regeneration and functional recovery. Inhibition of this miRNA in electroporated T lymphocytes demonstrated that it is necessary for the expression of different inhibitory molecules, including PD-1, CTLA-4, CD200, TIM-3 and LAG-3, as well as for the secretion of IFN-γ. These findings indicate that the miRNA has immunoregulatory potential in halting autoimmune responses. Moreover, lineage trace studies on human pancreatic tissue showed that miR-30d-5p stimulates the formation of new insulin-expressing β-cells. Dynamic perifusion experiments also revealed that it can activate the synthesis and secretion of insulin, as determined by the analysis of C-peptide. Using RNA sequencing, we verified that miR-30d-5p can indeed regulate genes related to both the function and regeneration of human β-cells. Finally, we sought to ascertain whether miR-30d-5p could modify the ongoing autoimmune attack in the non-obese diabetic mouse, —the experimental model for T1D. Inhibition of this miRNA resulted in an aggravation of the autoimmune attack, marked by an increase in the degree of islet leukocytic infiltrate and the promotion of an effector phenotype in T lymphocytes. In addition, its silencing resulted in a reduction in PD-1 expression within the spleen and an increase in the number of Tregs within the pancreatic lymph nodes, which can be associated with the upregulation of *CD200*. As a result, we have identified novel immune and epigenetic biomarkers for the PR phase and described, for the first time, a role for miR-30d-5p in immunoregulation and human β-cell function and regeneration. In summary, the findings presented here not only shed light on the complex interplay of immune and epigenetic factors during the PR phase in T1D but also open new avenues for therapeutic strategies aimed at enhancing β-cell preservation and regeneration, potentially revolutionizing the management of pediatric diabetes. While further research is necessary, this work represents a significant initial step toward the specific characterization of this intriguing period and the processes driving it.

La diabetes tipo 1 (DT1) es una enfermedad autoinmunitaria con una patogenia compleja y heterogénea. Tras el inicio del tratamiento con insulina, la mayoría de los pacientes pediátricos experimentan un periodo de remisión parcial (RP), comúnmente conocido como "luna de miel". Durante esta fase, las células β pancreáticas experimentan una recuperación de la propia síntesis y secreción de insulina, lo que reduce la necesidad de insulina exógena y mantiene un mejor control glucémico. Los mecanismos que subyacen a esta fase están aún por determinar, pero pueden implicar una reducción del estrés sobre las células β debida a la corrección de la hiperglucemia, así como a una mejora de la viabilidad y sensibilidad a la insulina o a procesos de regeneración y regulación inmunitaria. Por lo tanto, es importante comprender no sólo las fluctuaciones inmunológicas que preceden al diagnóstico de la enfermedad, sino también las que se producen después. Esto puede aportar información sobre las vías que conducen a la protección de las células β y la modulación del sistema inmunitario, lo que puede repercutir en la estratificación de los pacientes, en determinar el momento óptimo de las inmunointervenciones y la precisión terapéutica. Nuestra hipótesis es que la identificación y caracterización de las alteraciones metabólicas, inmunológicas y epigenéticas en la DT1 puede conducir al desarrollo de algoritmos predictivos y biomarcadores de seguimiento de la remisión, proporcionando información sobre los mecanismos que subyacen a la fase de RP. Por lo tanto, el objetivo principal de esta tesis doctoral es identificar nuevos biomarcadores inmunológicos y epigenéticos de la RP en pacientes pediátricos con DT1 y esclarecer los mecanismos subyacentes a la intersección del inmunometabolismo y la regulación epigenética, con el potencial de proporcionar información sobre las vías de protección de las células β.

Para ello, inicialmente caracterizamos los cambios cuantitativos en hasta cincuenta y cinco subpoblaciones de células inmunitarias periféricas en el momento del diagnóstico de la DT1, con el fin de identificar qué variables son predictivas de la remisión. Posteriormente, se desarrolló un modelo de predicción de la RP basado en un índice de variables inmunológicas, que mostró un poder discriminatorio del 81%. Este índice, en combinación con la edad, puede servir para el seguimiento precoz de estos pacientes y puede ayudar a estratificar aquellos que tendrán mejor o peor pronóstico, permitiendo así un abordaje más personalizado del manejo terapéutico. Posteriormente, en un estudio longitudinal, caracterizamos los cambios cuantitativos en estas mismas subpoblaciones leucocitarias y en diferentes citoquinas y microARN (miARN) en plasma, con el objetivo de definir biomarcadores de seguimiento específicos de la fase de RP. Nuestros hallazgos indican que este fenómeno se asocia a alteraciones en el porcentaje y/o concentración de linfocitos T efectores y reguladores, linfocitos B reguladores y transicionales, células NK reguladoras, monocitos y en la concentración de IL-17A.

Además, los pacientes remitentes presentan un perfil plasmático de miARN distintivo asociado a procesos inmunitarios, de apoptosis y metabólicos. Entre los miARN identificados, el miR-30d-5p mostró la mayor regulación al alza durante la fase de RP. Este miARN está enriquecido para una serie de procesos biológicos que incluyen la respuesta al estrés, la señalización de la insulina, la muerte celular y diferentes vías relacionadas con el sistema inmunitario, como el procesamiento y la presentación de antígenos o la señalización del TGF-β. Además, también se asocia a vías de regeneración, diferenciación y proliferación. Partiendo de la premisa de que el miR-30d-5p desempeña un papel en la regulación de vías fundamentales que contribuyen a la patogénesis de la DT1, tratamos de investigar si también puede promover la inmunorregulación y la regeneración y recuperación funcional de las células β. La inhibición de este miARN en linfocitos T electroporados demostró que es necesario para la expresión de diferentes moléculas inhibidoras, incluyendo PD-1, CTLA-4, CD200, TIM-3 y LAG-3, así como para la secreción de IFN-γ. Estos hallazgos indican que el miARN tiene potencial inmunorregulador para frenar las respuestas autoinmunitarias. Además, estudios de trazado de linaje en tejido pancreático humano demostraron que el miR-30d-5p estimula la formación de nuevas células β que expresan insulina. Los experimentos de perifusión dinámica también revelaron que puede activar la síntesis y secreción de insulina, según se determinó mediante el análisis del péptido C. Mediante la secuenciación del ARN comprobamos que efectivamente el miR-30d-5p puede regular genes relacionados tanto con la función como con la regeneración de las células β humanas. Por último, se llevó a cabo experimentos en el ratón diabético no obeso —el modelo experimental de la DT1— para mostrar si el miR-30d-5p podía modificar el ataque autoinmunitario en curso. La inhibición de este miARN provocó un agravamiento de la autoinmunidad, marcado por un aumento del grado de infiltrado leucocitario en los islotes y la promoción de un fenotipo efector en los linfocitos T. Además, su silenciamiento resultó en una reducción de la expresión de PD-1 en los esplenocitos y un aumento en el porcentaje de Tregs en los ganglios linfáticos pancreáticos, el cual puede estar relacionado con la regulación al alza de CD200, un gen diana del miRNA. En conclusión, hemos identificado nuevos biomarcadores inmunitarios y epigenéticos para la fase de RP y hemos descrito, por primera vez, el papel del miR-30d-5p en la inmunorregulación y en la función y regeneración de las células β humanas. Los hallazgos presentados en este trabajo no sólo arrojan luz sobre la compleja interacción entre factores inmunitarios y epigenéticos durante la fase de RP en la DT1, sino que también abren nuevas vías para estrategias terapéuticas dirigidas a mejorar la preservación y regeneración de las células β, revolucionando potencialmente el tratamiento de la diabetes pediátrica. Aunque es necesario seguir investigando, este trabajo representa un paso inicial importante hacia la caracterización específica de esta intrigante fase y de los procesos que la impulsan.

La diabetis tipus 1 (DT1) és una malaltia autoimmunitària amb una patogènia complexa i heterogènia. Després de l'inici del tractament amb insulina, la majoria dels pacients pediàtrics experimenten un període de remissió parcial (RP), comunament conegut com a "lluna de mel". Durant aquesta fase, les cèl·lules β pancreàtiques experimenten una recuperació de la pròpia síntesi i secreció d'insulina, la qual cosa redueix la necessitat d'insulina exògena i manté un millor control glucèmic. Els mecanismes que subjauen a aquesta fase estan encara per determinar, però poden implicar una reducció de l'estrès sobre les cèl·lules β deguda a la correcció de la hiperglucèmia, així com a una millora de la viabilitat i sensibilitat a la insulina o a processos de regeneració i regulació immunitària. Per tant, és important comprendre no sols les fluctuacions immunològiques que precedeixen al diagnòstic de la malaltia, sinó també les que es produeixen després. Això pot aportar informació sobre les vies que condueixen a la protecció de les cèl·lules β i la modulació del sistema immunitari, la qual cosa repercutirà en l'estratificació dels pacients, en la determinació del moment òptim de les immunointervencions i la precisió terapèutica. La nostra hipòtesi és que la identificació i caracterització de les alteracions metabòliques, immunològiques i epigenètiques en la DT1 pot conduir al desenvolupament d'algoritmes predictius i biomarcadors de seguiment de la remissió, proporcionant informació sobre els mecanismes que subjauen a la fase de RP. Per tant, l'objectiu principal d'aquesta tesi doctoral és identificar nous biomarcadors immunològics i epigenètics de la RP en pacients pediàtrics amb DT1 i esclarir els mecanismes subjacents a la intersecció del immunometabolisme i la regulació epigenètica, amb el potencial de proporcionar informació sobre les vies de protecció de les cèl·lules β.

Per a això, inicialment vam caracteritzar canvis quantitatius en fins a cinquanta-cinc subpoblacions de cèl·lules immunitàries perifèriques en el moment del diagnòstic de la DT1, amb la finalitat d'identificar quines variables són predictives de la remissió. Posteriorment, es va desenvolupar un model de predicció de la RP basat en un índex de variables immunològiques, que va mostrar un poder discriminatori del 81%. Aquest índex, en combinació amb l'edat, pot servir per al seguiment precoç d'aquests pacients i ajudar a estratificar aquells que tindran millor o pitjor pronòstic, cosa que permet un abordatge més personalitzat del maneig terapèutic. Posteriorment, en un estudi longitudinal, vam caracteritzar canvis quantitatius en aquestes mateixes subpoblacions leucocitàries i en diferents citocines i microARN (miARN) en plasma, amb l'objectiu de definir biomarcadors de seguiment específics de la fase RP. Les nostres troballes indiquen que aquest fenomen s'associa a alteracions en el percentatge i/o concentració de limfòcits T efectors i reguladors, limfòcits B reguladors i transicionals, cèl·lules NK reguladores, monòcits i en la concentració de IL-17A. A més, els pacients

remitents presenten un perfil plasmàtic de miARN distintiu associat a processos immunitaris, d'apoptosis i metabòlics. Entre els miARN identificats, el miR-30d-5p va mostrar la regulació més gran a l'alça durant la fase de RP. Aquest miARN està enriquit per a una sèrie de processos biològics que inclouen la resposta a l'estrès, la senyalització de la insulina, la mort cel·lular i diferents vies relacionades amb el sistema immunitari, com el processament i la presentació d'antígens o la senyalització del TGF-β. A més, també s'associa a vies de regeneració, diferenciació i proliferació. Partint de la premissa que el miR-30d-5p exerceix un paper en la regulació de vies fonamentals que contribueixen a la patogènesi de la DT1, vam investigar si també pot promoure la regulació del sistema immunitari i la regeneració i recuperació funcional de les cèl·lules β. La inhibició d'aquest miARN en limfòcits T electroporats va demostrar que és necessari per a l'expressió de diferents molècules inhibidores, incloent-hi PD-1, CTLA-4, CD200, TIM-3 i LAG-3, així com per a la secreció de IFN-γ. Aquestes troballes indiquen que el miARN té potencial immunorregulador per a frenar les respostes autoimmunitàries. A més, estudis de traçat de llinatge en teixit pancreàtic humà van demostrar que el miR-30d-5p estimula la formació de noves cèl·lules β que expressen insulina. Els experiments de perifusió dinàmica també van revelar que pot activar la síntesi i secreció d'insulina, segons es va determinar mitjançant l'anàlisi del pèptid C. Mitjançant la seqüenciació de l'ARN vam comprovar que efectivament el miR-30d-5p pot regular gens que estan relacionats tant amb la funció com amb la regeneració de les cèl·lules β humanes. Finalment, es va dur a terme experiments en el ratolí diabètic no obès—el model experimental de la DT1—per a mostrar si aquest miARN podia modificar l'atac autoimmunitari en curs. La seva inhibició va provocar un agreujament de l'autoimmunitat, marcat per un augment del grau d'infiltrat leucocitari en els illots i la promoció d'un fenotip efector en els limfòcits T. A més, el seu silenciament va resultar en una reducció de l'expressió de PD-1 en els esplenòcits i un augment en el percentatge de Tregs en els ganglis limfàtics pancreàtics, el qual pot estar relacionat amb la regulació a l'alça de CD200, un gen diana del miARN. En conclusió, hem identificat nous biomarcadors immunitaris i epigenètics per a la fase de RP i hem descrit, per primera vegada, el paper del miR-30d-5p en la immunorregulació i en la funció i regeneració de les cèl·lules β humanes. Les troballes presentades en aquest treball no sols llancen llum sobre la complexa interacció entre factors immunitaris i epigenètics durant la fase de RP en la DT1, sinó que també obren noves vies per a estratègies terapèutiques dirigides a millorar la preservació i regeneració de les cèl·lules β, revolucionant potencialment el tractament de la diabetis pediàtrica. Encara que és necessari continuar investigant, aquest treball representa un pas inicial important cap a la caracterització específica d'aquesta intrigant fase i dels processos que la impulsen.

1

INTRODUCTION

1. TYPE 1 DIABETES

Type 1 diabetes (T1D) is an autoimmune disease that results from the destruction of insulin-producing β-cells in genetically predisposed individuals, leading to metabolic failure requiring lifelong insulin treatment [1]. β-cells are located in the islets of Langerhans, the endocrine portion of the pancreas that secret hormones into the bloodstream and that consists of clusters of different endocrine cell types: α (~20%), β (~70%), δ (<10%), γ (<5%), and ε (<1%). The islets of Langerhans make up only 5% of the adult pancreas, while the remaining 95% is exocrine tissue that produces enzymes that aid digestion. Each endocrine cell type is specialized in secreting specific hormones: α cells secrete glucagon, δ cells secrete somatostatin, γ cells secrete pancreatic polypeptide, and ε cells secrete ghrelin. Regarding β-cells, these specialized endocrine cells are chiefly responsible for the synthesis and secretion of insulin, a hormone crucial for glucose uptake and utilization by various tissues. Upon stimulation by elevated blood glucose levels, β-cells promptly release insulin into the bloodstream in a tightly regulated manner, thereby facilitating the uptake of glucose by insulin-sensitive tissues such as skeletal muscle, adipose tissue, and the liver. In T1D, the progressive T-cell mediated autoimmune loss of β-cell mass and/or function results in inadequate insulin production and manifests clinically as hyperglycemia, an increase in blood glucose levels [2].

T1D accounts for approximately 5–10% of all diagnosed cases of diabetes. A systematic review and meta-analysis reported a global prevalence of 9.5% for T1D, alongside an incidence rate of 15 per 100,000 individuals [3]. In 2021, the number of individuals living with T1D was estimated to be approximately 8.4 million worldwide, with 500,000 new cases that year [4]. Presently, this disease stands as the predominant form of diabetes observed in pediatric populations. Although it can be diagnosed at any age, the symptomatic onset usually occurs during childhood (0–14 years). Statistical approximations suggest around 100,000 diagnosed total new cases of T1D globally among children and adolescents, with an estimated 1.2 million individuals under the age of 20 worldwide grappling with its manifestations [5,6]. Moreover, T1D is increasing both in incidence and prevalence across all age groups, with overall annual increases in incidence of about 2–3% [5,7]. The greatest observed increases in the incidence of T1D are among children younger than 15 years, particularly in those younger than 5 years [8]. The cause of this rise remains unclear, but it could be attributed to shifts in diet and environmental factors. Unlike other autoimmune diseases, T1D does not have a higher prevalence in women (with a male-to-female incidence rate ratio of about 1.32), although this may vary in different populations [9,10]

Worldwide, there is also a considerable geographic variation in incidence that follows a north-south gradient. The highest incidence rates are found in populations residing in Northern European regions and North America, with a growing number of countries in the Middle East and North Africa also experiencing elevated rates. Conversely, incidence rates are lowest in countries located in South America, as well as in the southern regions of Asia and Africa [11]. By country, Finland (52.2 cases per 100,000 people/year) and Sweden (44.1 cases per 100,000 people/year) are the top countries for incidence rates of T1D in children. In Spain, the mean incidence rate is 13.7 cases per 100,000 people/year [12]. India now has the highest estimated number of prevalent T1D cases in people under 20 years of age (229,400), followed by the USA (157,900) and Brazil (92,300) [11]

1.1. The natural history of type 1 diabetes

The precise mechanisms leading to T1D remain elusive, although much progress has been made in understanding the natural history of this disease. In 1986, George Eisenbarth proposed a model to explain T1D development, which has helped us to understand and predict the onset of the disease [13]. The model comprises six phases, starting with the individual's genetic susceptibility (mainly associated with the human leukocyte antigen (HLA) region), passing through a triggering event of autoimmunity and a gradual and progressive loss of β-cells, and ending with their near-total destruction. This model has been of great service to the community by offering guidance for investigations that have significantly advanced our comprehension of the natural progression of this disease.

In the initiation of the autoimmune attack, an interplay between genetic, environmental, and immunological factors occurs in order to generate and activate autoreactive diabetogenic T cells (detailed in ***section 1.2.***). However, the definitive triggering factors causing the loss of self-tolerance to β-cells are still elusive. The current model suggests that the natural progression of T1D in genetically susceptible individuals consists of four stages (**Figure 1**) [1,14,15], where stages 1 and 2 are collectively referred to as prediabetes. During this period, the individual may not experience any symptoms of the disease, but there is already evidence of β-cell autoimmunity and loss. In this sense, the leukocytic infiltrate (insulitis) has started invading the islet and attacking β-cells. In **stage 1**, normoglycemia is accompanied by two or more islet autoantibodies, which are considered the earliest biomarkers of β-cell autoimmunity. Autoantibodies to insulin (IAA), glutamic acid decarboxylase (GADA), insulinoma associated-2 (IA-2A), and zinc transporter 8 (ZnT8A) are currently employed in the diagnosis and identification of individuals at high risk of developing T1D, especially when combined with the risk

genotype [16]. An increase in autoantibody number indicates autoantigen spreading and progression towards the clinical onset, with a >80% risk of developing T1D in those children presenting two or more autoantibodies [17]. However, it is currently understood that these autoantibodies do not directly cause β-cell damage, instead, they develop as the result of β-cell destruction [18]. In **stage 2**, the autoantibodies are accompanied by dysglycemia reflecting inadequate insulin secretion after a glucose or nutrient challenge, which arises from further loss of β-cell function. Jointly, this so-called prediabetes stage is highly variable and can last from months to years, and may never even progress to hyperglycemia requiring insulin treatment.

On the other hand, a new paradigm in the pathogenesis of T1D has recently emerged which suggests that β-cell perturbations precede the development of the autoimmune attack. So far it was thought that the intersection of various genetic and environmental factors led to the onset of autoimmunity, which resulted in elevated blood glucose levels as a result of β-cell destruction. However, Warncke et al. detected a sharp rise in postprandial blood glucose two months before the detection of islet autoantibodies [19]. Indeed, various triggers or "stressors" that could prompt β-cells to elicit an immune response have been suggested, encompassing factors such as pancreas size, β-cell mass, viral infections, and metabolic stress [20]. In fact, a type I interferon (IFN) signaling can be found before seroconversion, which is typically triggered by viral infections [21]. Then, the elevated levels of blood glucose could potentially hasten the progression of T1D by increasing antigen exposure by β-cells or by other means, such as enhancing cell death, which would precipitate total β-cell demise [22] (**Figure 2**).

In **stage 3**, insulin secretion is not enough to maintain glycemic control due to substantial β-cell destruction (there is a decline of 60–80% in the β-cell mass depending on the age at onset [23]), overt hyperglycemia ensues and the patient presents with clinical symptoms. The typical trio of symptoms —polydipsia (excessive thirst), polyphagia (excessive appetite), and polyuria (abnormally large production of urine)— will appear along with weight loss, extreme fatigue, or blurry vision. In some cases, the person may develop diabetic ketoacidosis, as the body will begin to break down muscle and fat for energy, causing an accumulation of ketone bodies in the blood and urine, which if left untreated, can result in unconsciousness and even death [16]. Indeed, approximately half of the children present diabetic ketoacidosis at the time of diagnosis [24].

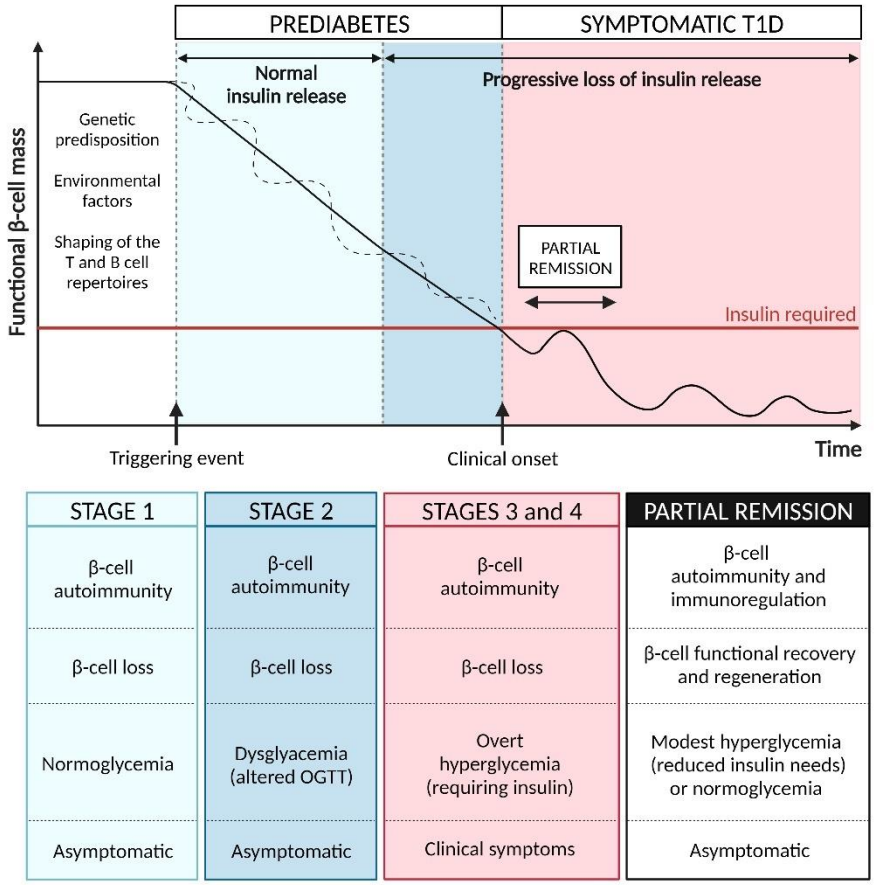

Figure 1. ***The natural history of type 1 diabetes.*** *T1D is triggered by an unknown event wherein the interplay between genetic predisposition, environmental factors, and the shaping of immune responses (impaired central tolerance to islet antigens) is important. As the disease progresses during the prediabetes period (before the clinical onset of the disease), a progressive loss of β-cell mass and function (black line) is observed, together with the appearance of autoantibodies targeting islet epitopes (autoimmunity) in the context of normoglycemia. Stage 2 is characterized by the appearance of dysglycemia. The decline in β-cell function might not be constant over time (black dashed line), generating a relapsing-remitting pattern. When β-cell function falls below the threshold required to maintain a proper glucose metabolism, hyperglycemia becomes overt, clinical symptoms appear, and insulin therapy is needed (stage 3). A few months after insulin therapy, most patients experience a partial remission phase. During this period, there is a functional recovery and possible regeneration of β-cells and immunoregulatory attempts that result in a reduced need for exogenous insulin and an improvement in glycemic control. New biomarkers are emerging to better recapitulate the immunometabolic pathways that lead to β-cell protection. However, the increase in neoantigens and epitope spreading may also stoke the autoimmune attack, ending this period and continuing the decline in β-cell function with time (stage 4), although with possible subclinical periods of remission. Figure created using BioRender and from [25].*

Upon diagnosis, patients with T1D rely on insulin therapy for life to help manage their blood glucose levels and delay the appearance of secondary complications. T1D can be diagnosed based on a fasting plasma glucose of ≥126 mg/dL or a random plasma glucose of ≥200 mg/dL. However, other parameters are usually tested, such as glycated hemoglobin (HbA1c) levels, which indicate the average blood sugar level over three months. An HbA1c ≥6.5% or 48 mmol/mol indicates the presence of diabetes [16]. Also, residual β-cell mass function can be measured through basal or stimulated C-peptide concentration. After cleavage of proinsulin, insulin and C-peptide (31 amino acid peptide) are produced in equal amounts. Measuring C-peptide levels is more reliable than measuring insulin itself, because insulin levels may be altered by the administration of exogenous insulin or hepatic clearance, whereas C-peptide is minimally affected by this process. A fasting C-peptide level of less than 0.6 ng/mL is consistent with β-cell failure and patients with T1D have low or undetectable C-peptide levels [26]. Moreover, to confirm the autoimmune nature of the absence of insulin, islet autoantibodies in the sera are measured. The primary autoantigen in the development of β-cell autoimmunity seems to strongly correlate with age, indicating heterogeneity in the initiation of the disease process [27]. Finally, HLA allele typing is useful to determine if an individual has a predisposing HLA haplotype.

In the last years, the term endotype has been proposed to explain heterogeneity at and after T1D diagnosis [28,29]. First, histological examination of the pancreas from patients with T1D revealed that fewer than 10% of islets are infiltrated, a threshold typically reached with a minimum of 15 leukocytes per islet, which only doubles the levels found in healthy controls [30]. Regarding insulitis, differences have been observed according to age at diagnosis. T1D endotype 1 includes individuals diagnosed at <13 years of age who are characterized by an abundance of $CD20^{high}$ B cells and $CD8^+$ T cells in the islets, few residual insulin-containing islets (ICIs), and abnormal insulin processing. In contrast, T1D endotype 2 includes patients who are diagnosed at ≥13 years of age and who are characterized by $CD20^+$ B cells and $CD8^+$ T cells-poor insulitis, more ICIs, and normal insulin processing [23,31,32]. These features may reflect distinct immunopathological processes and accelerated β-cell destruction in children. In addition, it should be considered that there are immunometabolic changes inherent to the patient's physiology depending on their age. A tendency to decrease B cells in the blood with increasing age has already been described [33], which could also explain part of the higher proportion of B cells in the islets of the young.

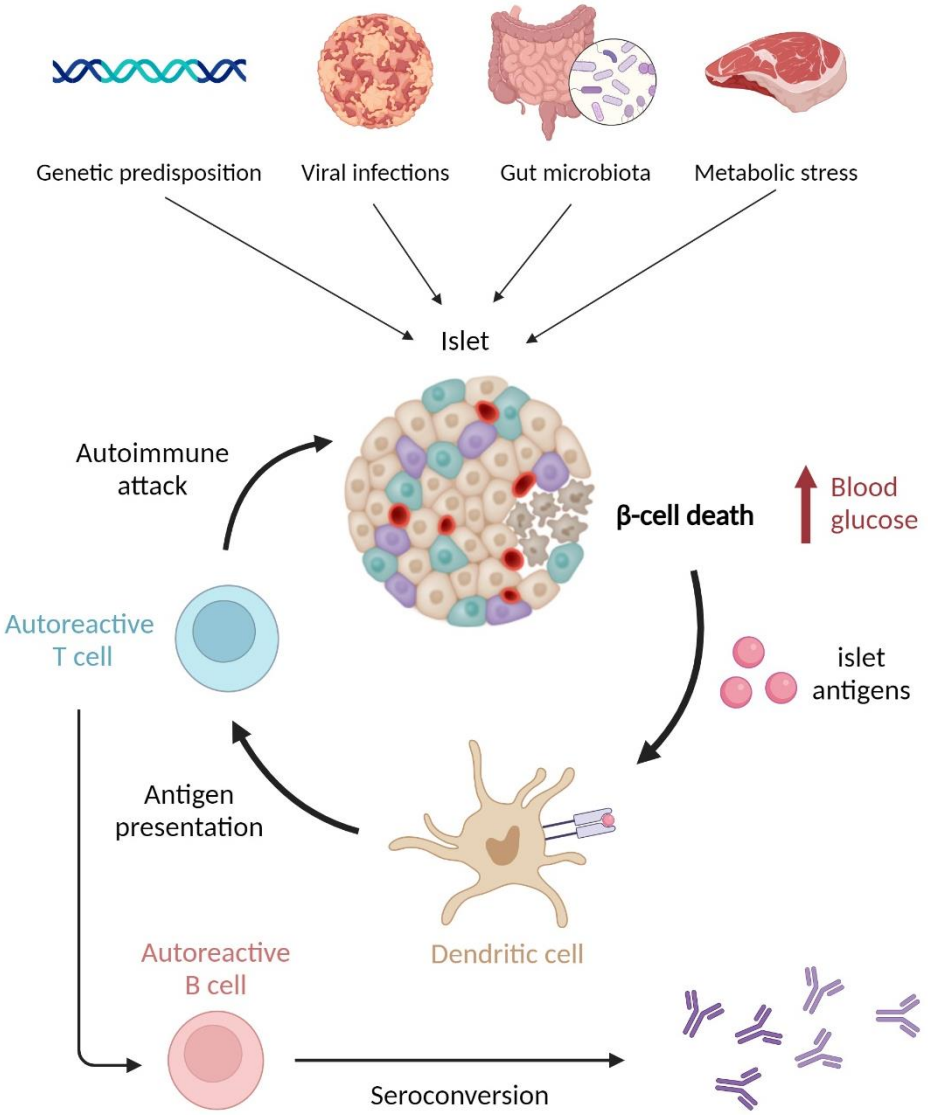

Figure 2. ***Proposed model for type 1 diabetes development.*** *New models of T1D initiation propose that the development of β-cell autoimmunity is the consequence of another as-yet-unidentified cause of β-cell death. Various factors may drive β-cell damage, such as genetic predisposition, viral infections, changes in gut microbiota, or metabolic stress (diet). These insults could lead to β-cell death and islet antigen presentation by immunogenic dendritic cells capable of activating the adaptive immune system. At this point, increased blood glucose levels can be detected before the appearance of islet autoantibodies. Then, an autoreactive immune response due to a genetic predisposition may cause T1D and precipitate total β-cell demise. Figure created using BioRender and adapted from [34].*

Finally, in **stage 4**, patients present a chronic and established T1D. While insulin treatment has enabled many patients to lead relatively healthy lives, it does not alleviate the disease burden and merely postpones the onset of long-term secondary complications. The high glucose levels in the blood can harm nerves and large and small blood vessels of the eyes, kidneys, and heart which can lead to neuropathy, retinopathy, nephropathy or cardiovascular diseases. Patients also exhibit an increased risk of other autoimmune disorders such as celiac disease or autoimmune thyroid diseases [35,36]. In individuals with long-standing T1D, the loss of β-cells persists for months to years following, yet they still manage to produce limited quantities of insulin [37]. The rate of β-cell function decline in the initial year following diagnosis is highly variable, ranging from 0% to 58%, and older age is associated with slower loss of C-peptide [38,39]. Furthermore, the entire pancreas is smaller in individuals with long-standing T1D, suggesting that the exocrine compartment of the pancreas must also be affected [40,41].

Maintaining this residual β-cell function has been demonstrated to be clinically important because it reduces the prevalence of severe hypoglycemia and has long-lasting clinical benefits [42,43]. In fact, the remaining β-cells are able to partially recover, and an increased proliferation occurs in humans during the progression of T1D [44]. Immunoregulatory events would also allow this proliferation; however, the result of this regeneration could be associated with an increase in neoantigens and cyclic destruction of islets, generating a relapsing-remitting profile in this disease [45]. The only clinically detectable period of β-cell recovery throughout the natural history of T1D is called **partial remission** (PR). This thesis presents a focus on the immunological and epigenetic study of this period, which is thought to be linked not only to metabolic changes but also to immune regulation (explained in ***section 2***).

Despite recent advances in understanding the natural history of T1D, many questions remain unanswered. It is still unclear what triggers autoimmunity towards the β-cell and whether these triggers are consistent across all individuals. Additionally, the β-cell mass at each stage of the disease, the progression of its loss, and the potential for regeneration of the remaining ones are still unknown. Furthermore, it is unclear whether autoimmunity fluctuates over time. What seems rather clear is that T1D has no single pathway and is a diverse disease in terms of genetics, immunology, environmental influences, and metabolic characteristics. Age also plays a significant role in defining heterogeneity, since a younger age is associated with an increased risk and accelerated progression through the stages of the disease, along with unique histological characteristics and genetic and immunological patterns [46].

1.2. Etiology

The etiology of T1D, like most common chronic diseases, is complex and multifactorial, resulting from the interplay between genetic, epigenetic, environmental and immunological factors, which are delineated below.

1.2.1. Genetic factors

T1D is a complex disorder with a strong genetic component evidenced by the fact that the risk of developing the disease can be greater than 70% in identical twins [47]. The progression to T1D in monozygotic twins is also age-related, with a higher susceptibility to progression to diabetes in those diagnosed at a younger age, which can reflect a lower genetic impact in adult-onset T1D [48]. Although over 85% of patients do not have a positive family history of the disease, the risk for children who have a parent with T1D is 1-9% and for siblings of patients is 5-10%, compared to the 0.5% risk of the general population [49,50]. The **HLA region** on chromosome 6p21 is reported to confer 40–50% of the genetic susceptibility, which encodes cell surface molecules specialized to present antigenic peptides at the T–cell receptor (TCR) of T lymphocytes [51]. Specifically, polymorphisms of class II HLA genes encoding DQ and DR molecules show the strongest association with T1D. Both DR and DQ are αβ heterodimers. The DRα chain is encoded by the DRA locus, and the DRβ chain is encoded by the DRB locus. Similarly, the α and β chains of the DQ molecules are encoded by the DQA1 and DQB1 loci, respectively [52]. Although HLA alleles are very common in the general population, the HLA haplotype, constituted by a composite of alleles inherited from both parental sources, is key for the development of T1D. In this sense, the most T1D predisposing haplotypes are combinations of HLA-DRB1, HLA-DQA1 and HLA-DQB1 alleles, such as DR4-DQ8 haplotypes (*DRB1*04:01 or DRB1*04:02-DQA1*03:01-DQB1*03:02*) and DR3-DQ2 haplotypes (*DRB1*03:01-DQA1*05:01-DQB1*02:01*), which are present in up to 90% of patients [50,51]. Other haplotypes are known to confer protection against the disease, such as DR15-DQ6 (*DRB1*15:01-DQA1*01:02-DQB1*06:02*) [53]. It is thought that the high-risk HLA–peptide complex is responsible for the display of antigenic peptides that trigger autoreactive diabetogenic T-cell responses.

One of the most consistently replicated regions associated with T1D is the **insulin** gene, located on chromosome 11p15.5. The marker in this case consists of a variable number of tandem repeats (VNTRs) located upstream of the *INS* locus. If the allele contains a low number of VNTRs (26 to 63 repetitions), it is classified as a class I allele and is associated with low expression of insulin in the thymus. This, in turn, leads to a higher susceptibility

to T1D since autoreactive insulin-specific T cells are not destroyed during thymic education. Contrarily, if the allele presents a high number of VNTRs (140 to 210 repetitions), it is classified as a class III allele and is associated with a high ectopic expression of insulin in the thymus. This confers a protective effect by enhancing T-cell tolerance [54,55].

Additionally, genome-wide association studies (GWAS) have identified nearly 60 **independent candidate genes** conferring also susceptibility to T1D, which mainly affects T-cell responses [56–58] (**Figure 3**). Among these genes, some with confirmed established associations are *PTPN22*, *IL2RA, IL10, IFIH1* and *CTLA4* [59,60]. For example, cytotoxic T lymphocyte-associated protein 4 (CTLA-4) is a vital negative regulator of T cell activation since it binds to CD80 and CD86 and prevents their interaction with CD28, impairing T cell stimulation [61]. Thus, *CTLA4* polymorphisms that lead to a decreased expression of this molecule are related to enhanced T cell activation and increased risk for T1D. Moreover, T1D-associated gene variants are enriched in the open chromatin of specific cell types, including activated and cytotoxic T cells, plasmacytoid dendritic cells (pDCs), classical monocytes, insulin$^+$ β-cells, acinar cells and ductal cells [62], suggesting that they may impact their functionality.

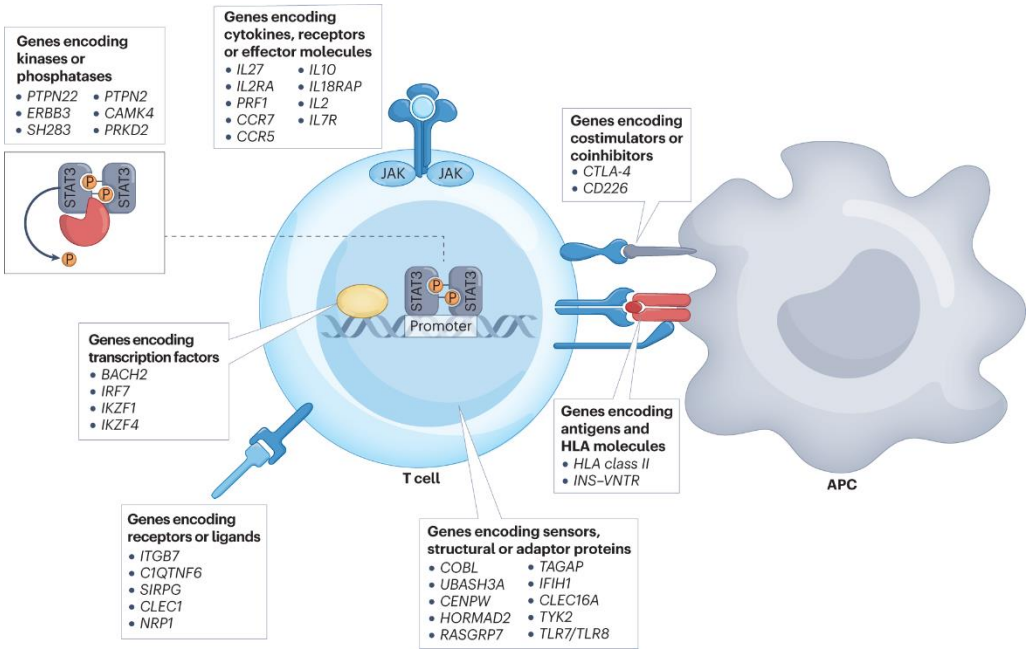

Figure 3. ***Risk genes for type 1 diabetes encode proteins that impact T cell development and function.*** *Specific haplotypes within the human HLA class II locus, along with a reduced number of repeats in the insulin variable number of tandem repeat (VNTR) region, have been associated with*

autoimmune responses targeting pancreatic islets in individuals with type 1 diabetes. Furthermore, approximately 50 other candidate risk genes have been identified, encompassing a diverse array of proteins implicated in T cell functionality, activation, and differentiation. These genes include kinases, phosphatases, transcription factors, receptors, ligands, cytokines, cytokine receptors, T cell effector molecules, structural and adaptor proteins, as well as co-stimulatory or co-inhibitory proteins. Figure adapted from [63].

1.2.2. Environmental factors

There is mounting evidence that **environmental** and **lifestyle factors** are significant contributors to the development of T1D. First, this is supported by the fact that T1D shows around 50% concordance rate in identical twins [64]. Secondly, the rapid increase in the incidence of T1D in recent decades cannot be solely attributed to genetic changes, as the gene pool has remained stable over this period [65]. Third, the incidence of the disease varies significantly by geography and latitude, with higher rates observed in nordic countries [66–68]. Moreover, migration studies also suggest that the risk of incidence in a new location is assumed [69]. Fourth, T1D incidence is increasing by 2–3% each year in all age groups, particularly in young children, despite a decline in the highest-risk genotypes over the past 40 years in this population group [70,71]. Therefore, a number of large observational and longitudinal studies, such as The Environmental Determinants of Diabetes in the Young (TEDDY) or the Diabetes Autoimmunity Study in the Young (DAISY), are currently underway to explore environmental triggers in genetically predisposed children.

One of the most well-established environmental factors associated with T1D is exposure to **viral infections**, which can induce β-cell damage. Different viruses have been related to the onset of the disease, including coxsackievirus B, rotavirus, mumps virus and cytomegalovirus [72], which can accelerate it by increasing the insulin demand [73]. In addition to the cytolysis of β-cells by productive infection, the associated inflammation and the release of β-cell autoantigens to the nearby inflammatory microenvironment could accelerate the disease. Viral infection of β-cells also results in over-expression of major histocompatibility complex (MHC) class I molecules, resulting in the presentation of self-antigens and perpetuation of further autoimmunity [74]. Histological analysis of donor pancreas and experimental data has provided sufficient evidence to support the involvement of *Enteroviruses*, and in particular *Coxsackievirus B4*, in the pathogenesis of T1D. This virus is present in most pancreatic biopsies from patients with T1D compared to its absence in samples from control subjects [75,76], and is capable of infecting β-cells and destroying them [72,77–79]. Furthermore, there are studies demonstrating the appearance of antibodies as a result of *Enterovirus* infection that recognize islet antigen epitopes [80], as well as a $CD4^+$ T cell cross-reactivity between the IA-2 islet antigen

epitope and rotavirus VP7 peptide [81]. In this sense, some viral infections probably trigger an immune response that mistakes β-cells for foreign invaders by a process named molecular mimicry, leading to their destruction and functional impairment. However, establishing a causal relationship between viral infections and T1D is complicated, as sampling over long periods of time would be required. As an example, the DAISY study showed that the presence of *Enterovirus* in serum can predict an increased rate of progression from islet autoimmunity to T1D [82], and the TEDDY study showed that prolonged enterovirus B infections may be involved in the development of islet autoimmunity in some young children [83].

On the other hand, early exposure to microbial products and infections is hypothesized to train and stimulate the immune system, lowering the risk for autoimmune diseases. The **hygiene hypothesis** states that the lack of infectious disease rates in industrialized countries by the usage of antibiotics or vaccines and having better hygiene could impact negatively the maturation of the immune system, which could lead to defects in the establishment of immune tolerance [84].

The **gut microbiome** plays also a key role in shaping and training the innate and adaptive immune system and in maintaining immune homeostasis [85]. Many factors can influence the gut microbiota composition and diversity, such as perinatal factors, the birthing process, diet, use of antibiotics, viral infections, geographic residence or physiological stress. Recently, its perturbation has been associated with T1D both in human and animal models [86,87]. A recent study demonstrated a different microbial composition in the gut of children who later developed T1D as early as 1 year of age, serving as a possible biomarker for T1D. These children presented an enrichment for *Bacteroides* and decreased butyrate production [88]. Moreover, the hallmark characteristics of genetically predisposed people or patients with recent onset T1D are decreased bacterial diversity, reduced community stability, increased gut permeability and inflammation, increased frequency of *Bacterioides* species and decreased frequency of *Prevotella*, *Bifidobacteria*, and *Lactobacillus* [89]. Species like *Lactobacillus* are crucial to maintaining homeostasis since they confer immunomodulatory and anti-inflammatory properties by producing short-chain fatty acids, like butyrate [90,91]. Therefore, loss of barrier function and altered gut mucosal immune responses can influence the development of T1D [92]. In fact, fecal microbiota transplantation in humans has highlighted the critical role of the microbiota in the development of autoimmune diseases such as T1D, as it was able to slow the decline in endogenous insulin production in newly diagnosed patients, and many of the microbiota-derived metabolites were associated with the preservation of β-cell function [93]. Furthermore,

HLA gene alleles appear to have a significant effect on the bacterial composition of the gut, which highlights the importance of understanding the interaction between host genetics and microbiome [94]. Interestingly, high-risk HLA haplotypes were associated with antibody development to host commensal microorganisms and future diagnosis of T1D [95].

Finally, dietary factors such as breastfeeding and the introduction of cow's milk, gluten and solid foods, low vitamin D concentrations, childhood obesity or gestational events have been also proposed as candidate etiological factors, although the effects of most of them are inconclusive and require further study [96,97]

1.2.3. Epigenetic factors: emphasis on microRNAs

Epigenetic variation could also explain part of the non-genetic component of T1D etiology. **Epigenetic changes**, defined as stable and heritable changes in gene expression that do not involve alterations in the DNA sequence, can link the effect of external surrounding environments with changes in gene expression by regulating DNA accessibility or repressing gene expression. The main epigenetic mechanisms involve DNA methylation, post-translational histone modifications and microRNA (miRNA) regulation, and their dysregulation can lead to autoimmune disorders, including T1D [98]. Indeed, epigenetic mechanisms play a role in the aberrant activation of the immune system triggered by environmental factors, such as changes in the composition of the gut microbiota [99].

One of the most well-studied epigenetic modifications is **DNA methylation**, which occurs when a methyl group is added to the fifth carbon of a cytosine, usually at CpG sites. It is typically associated with gene expression silencing by impeding the binding of transcription factors [100]. Circulating immune cells of T1D-discordant monozygotic twins presented an overall increase in DNA methylation in T1D twins relative to their healthy co-twins, which was located at genes involved in immune cell metabolism or T1D susceptibility genes, such as *HLA* or *IL2RA* [101–103]. Moreover, analysis of the temporal origins of T1D-associated epigenetic changes revealed that a different DNA methylation pattern in circulating immune cells in comparison to controls or healthy co-twins arises very early in the etiological process leading to overt T1D, even before seroconversion [104–106]. Both in animals and humans, it was also found that an inflammatory environment induces increased DNA methylation and decreased expression levels of insulin in islets [107]. Altogether, it is likely that epigenetic changes affect the natural history of the disease.

Histones are nuclear proteins that allow DNA condensation through the formation of nucleosomes. These proteins undergo **post-translational modifications** such as methylation or acetylation on the specific amino acid residues in the N-terminal part, which can affect gene expression by regulating chromatin accessibility. Similarly, altered histone methylation patterns in key genes related to the immune system function, including *CTLA4*, have been found in lymphocytes from patients with T1D [108]. The repressive mark found could imply lower *CTLA4* expression and enhanced T-cell activation, compatible with dysregulated T-cell activation in T1D.

Last but not least, **miRNAs** are the most abundant and functionally dominant small RNA class. MiRNAs are small non-coding RNA molecules of 18–25 nucleotides that regulate gene expression at the post-transcriptional level and in a sequence-specific manner. They were first discovered in the early 1990s, yet nearly a decade passed before their pivotal roles in gene regulation were fully appreciated. Presently, it is widely acknowledged that miRNAs are present across nearly all eukaryotic organisms and even some viruses, which highlights the significant regulatory capability of these small RNAs.

The biogenesis of miRNAs is under tight temporal and spatial control. The majority of canonical miRNAs are encoded by introns of non-coding or coding transcripts, but some miRNAs are encoded by exonic regions [109]. Moreover, miRNAs are often found in clusters within genomes and transcribed as a single unit. As a result, multiple miRNAs can be produced from the same primary transcript [110]. In the canonical pathway, the miRNA gene (located in intergenic regions) is transcribed as an independent transcription unit by RNA polymerase II in the nucleus to produce a long primary miRNA hairpin (pri-miRNA) where miRNA sequences are embedded (**Figure 4**). Next, the nuclear Drosha (RNase III enzyme) complex cleaves the pri-miRNAs to release hairpin-shaped precursor miRNAs (pre-miRNAs). On the other hand, in the non-canonical pathway, intronic miRNAs (called mirtrons) are believed to be processed from the introns of their hosting mRNA-encoding gene. Here, the Drosha-mediated processing step is bypassed and a pre-miRNA is instead generated through mRNA splicing [111]. Then, the resulting pre-miRNAs are translocated to the cytoplasm. There, it is processed by the RNase III endonuclease Dicer, which cleaves the terminal loop. This results in a miRNA duplex of approximately 22 nucleotides. The mature double-stranded miRNA is loaded into a ribonucleoprotein complex called the RNA-induced silencing complex (RISC). The pre-RISC quickly removes the passenger strand to generate a mature RISC containing only the guide strand. The mature RISC serves as the catalytic engine for miRNA-mediated post-transcriptional gene silencing and involves P-body proteins [112]. P bodies are cytoplasmatic bodies enriched with enzymes and other proteins involved in mRNA

degradation and sequestration from translational machinery. mRNA degradation usually occurs when the miRNA-mRNA duplex presents a perfect complementarity via limited base-pairing interactions and, while it is a terminal process, translational repression —which usually involves an imperfect binding— is reversible and can be used to swiftly respond to internal or external stimuli. Partially complementary miRNAs can also accelerate deadenylation, causing mRNAs to be degraded earlier [113].

Even though the base pairing between the miRNA and its target mRNA is not always perfectly matched, the "seed sequence" (first 2–8 nucleotides starting at the 5′ end) has to be perfectly complementary [114]. Typically, the seed sequence of a miRNA interacts with target sites located in 3′ untranslated regions (3′UTR) of protein-coding genes [115]. This allows miRNAs to regulate a large number of target genes (an average of 300 conserved targets), which at the same time can be regulated by multiple miRNAs simultaneously [116]. Thus, miRNAs are known to modulate many biological processes, such as immune regulation or cellular differentiation, proliferation, metabolism, and apoptosis. Also, miRNAs are grouped into families that incorporate similar mature miRNA sequences and complete identical seed regions, presenting therefore similar functions [117].

Due to their ability to regulate a wide range of cellular developmental processes such as cellular proliferation, metabolism, cell death, and intracellular communication, excess or deficiency of miRNAs has been associated with numerous diseases, including cancer, neurodegenerative, cardiovascular or autoimmune diseases [118]. Indeed, some differentially expressed miRNAs (DEMs) have been linked to an aberrant T lymphocyte activation, differentiation, and function as well as β-cell apoptosis, insulin secretion and endoplasmic reticulum (ER) stress, which suggests a direct role of these molecules in regulating the onset of islet autoimmunity [119–121].

For instance, overexpression of miR-92a-3p, miR-181a-5p and miR-142-3p in T cells during islet autoimmunity is related to impaired regulatory T cell (Treg) induction and stability [122–124], which favors disease progression. Moreover, miR-15, miR-26 and miR-31 are also believed to compromise Treg survival in pre-T1D stages, thus contributing to the onset of the disease. During this prediabetic stage, miRNA transcriptome of $CD4^+$ T cell subsets is altered compared to healthy individuals and suggests an intrinsic predisposition to T helper (Th)1-type immunity and defects in Treg suppressor functions [125]. In addition, the levels of T1D autoantigens can also be modified by multiple miRNAs within the 14q32 cluster targeting their mRNA transcripts [126].

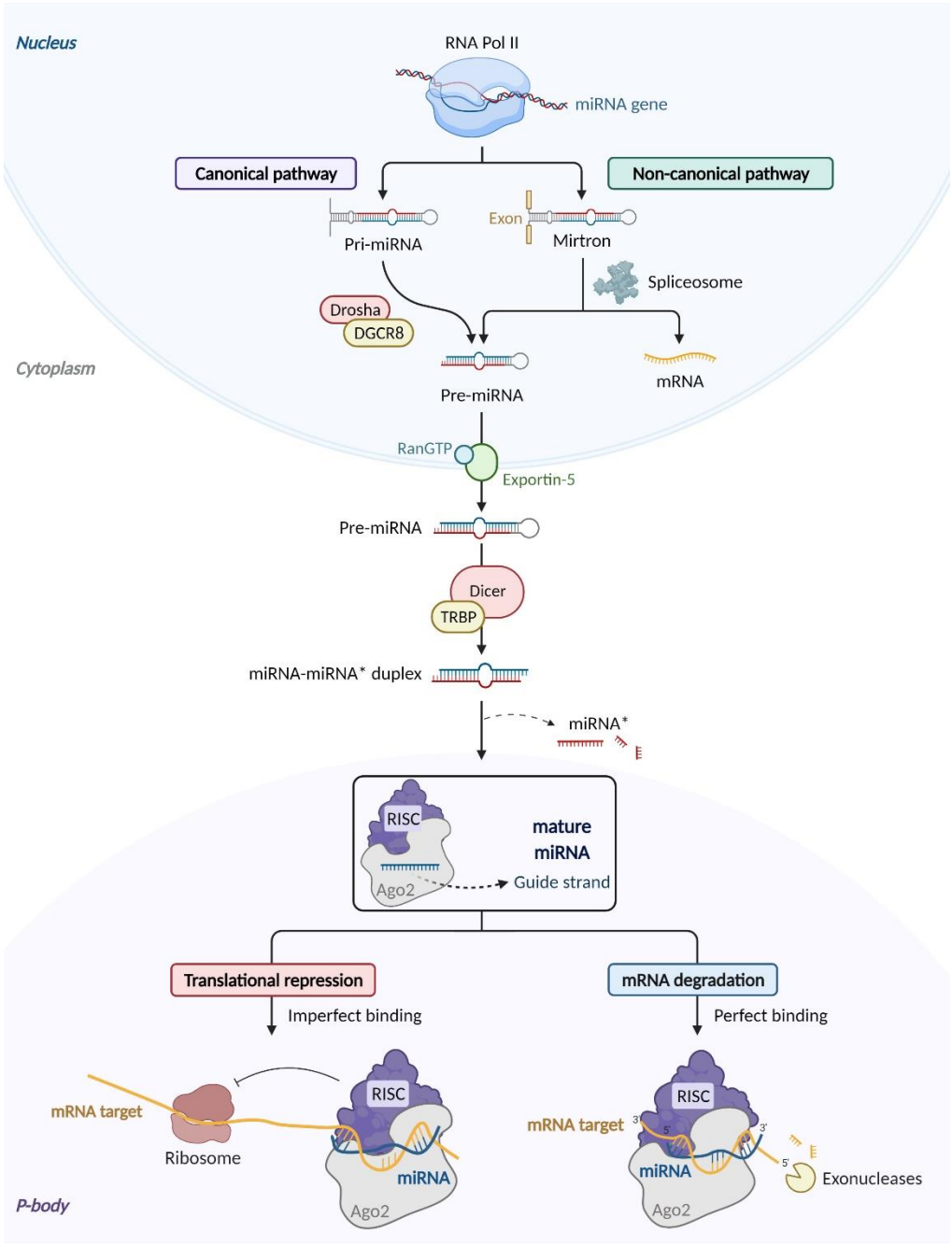

Figure 4. ***MicroRNA canonical and non-canonical biogenesis pathways and function.*** *In the canonical pathway, the miRNA gene (located in intergenic regions) is transcribed as an independent transcription unit by RNA polymerase II in the nucleus to produce a long primary miRNA hairpin (pri-miRNA) where miRNA sequences are embedded. Next, the nuclear Drosha (RNase III enzyme)-DGCR8 complex cleaves the pri-miRNAs to release hairpin-shaped precursor miRNAs (pre-miRNAs). On the other hand, in the non-canonical pathway, intronic miRNAs (called mirtrons) are believed to*

be processed from the introns of their hosting mRNA-encoding gene. Here, the Drosha-mediated processing step is bypassed and a pre-miRNA is instead generated through mRNA splicing. Then, the resulting pre-miRNAs are translocated to the cytoplasm by Exportin5/RanGTP. There, it is processed by the RNase III endonuclease Dicer, which is bound to TRBP (RNA-binding protein). This processing involves the binding of TRBP to the pre-miRNA and the cleavage of the terminal loop by Dicer, which results in a miRNA duplex of approximately 22 nucleotides. The mature double-stranded miRNA is loaded into a functional ribonucleoprotein complex called the RNA-induced silencing complex (RISC). The pre-RISC (in which Argonaute 2 proteins associate with RNA duplexes) quickly removes the passenger strand to generate a mature RISC containing only the guide strand. Figure created using BioRender and adapted from [127].

Besides that, proinflammatory cytokines secreted by infiltrating immune cells are believed to promote autoimmunity by inducing ER stress in β-cells. Under conditions of stress, human β-cells decrease miR-17 levels, a fact related to enhanced presentation of insulin-derived HLA class I epitopes and increased β-cell visibility to the immune system [128]. Conversely, stressed β-cells overexpress miR-155-5p, miR-21-5p and miR-146a-5p, which are associated with apoptosis, mitochondrial dysfunction and impaired insulin secretion [129–132]. Pancreatic islets under stress are also enriched in miR-101-3p, which participates in cytokine-mediated β-cell dysfunction and death [133]. Furthermore, the gradual increase in serum miR-375 levels —an abundant miRNA originating from islet cells— observed prior to the onset of hyperglycemia in the non-obese diabetic (NOD) mice suggests its potential utility as a circulating biomarker for β-cell death [134]. Moreover, newly diagnosed T1D patients present a different peripheral miRNA signature when compared to control subjects or patients with long-standing disease [135–141], indicating that these miRNAs may reflect different stages of the disease and serve both as diagnostic and prognostic biomarkers.

1.2.4. Failure of control checkpoints and immunosuppressive mechanisms

Additionally, stochastic factors such as random rearrangements of the TCR and B-cell receptor (BCR) genes and the failure of control checkpoints present in central and peripheral tolerance are also decisive in driving β-cell autoimmunity. In fact, the existence of autoreactive T lymphocytes in peripheral blood, both in healthy individuals and those with the disease, suggests that T lymphocytes may not have undergone complete thymic education and have evaded negative selection [142]. Nonetheless, the mere presence of these autoreactive T cells is not sufficient to trigger T1D. Additional factors, such as defects on Treg suppressive function, stress on β-cells that can increase their antigenicity (e.g., by upregulating HLA class I molecules for antigen presentation) or trigger epitope spreading may also be crucial in the development of the disease [20,143].

Growing evidence shows that impaired function of different immunosuppressive axes may play an important role in the development of autoimmune diseases such as T1D [144]. Indeed, maintenance of **peripheral tolerance** is critical for regulating autoreactive diabetogenic T cells. The mechanisms that mediate peripheral tolerance include: **1)** the induction of anergic T cells, which are functionally inactivated and unable to respond to antigens, **2)** deletion of T cells that recognize self-antigens with high affinity in the absence of co-stimulatory signals or undergo repeated stimulation, and **3)** suppression of autoreactive T cells by Tregs, which for example can produce anti-inflammatory cytokines like interleukin (IL)-10 or transforming growth factor (TGF)-β. T1D is associated with several functional defects in Tregs. Research has shown that Tregs from patients have a reduced ability to suppress T cell proliferation, reduced stability, a higher pro-inflammatory cytokine profile, and impairments in IL-2 receptor signaling [124,145–147]. One of the mechanisms that maintain anergy in T cells or that Tregs use as a suppressive mechanism is the recruitment of inhibitory molecules (**Figure 5**).

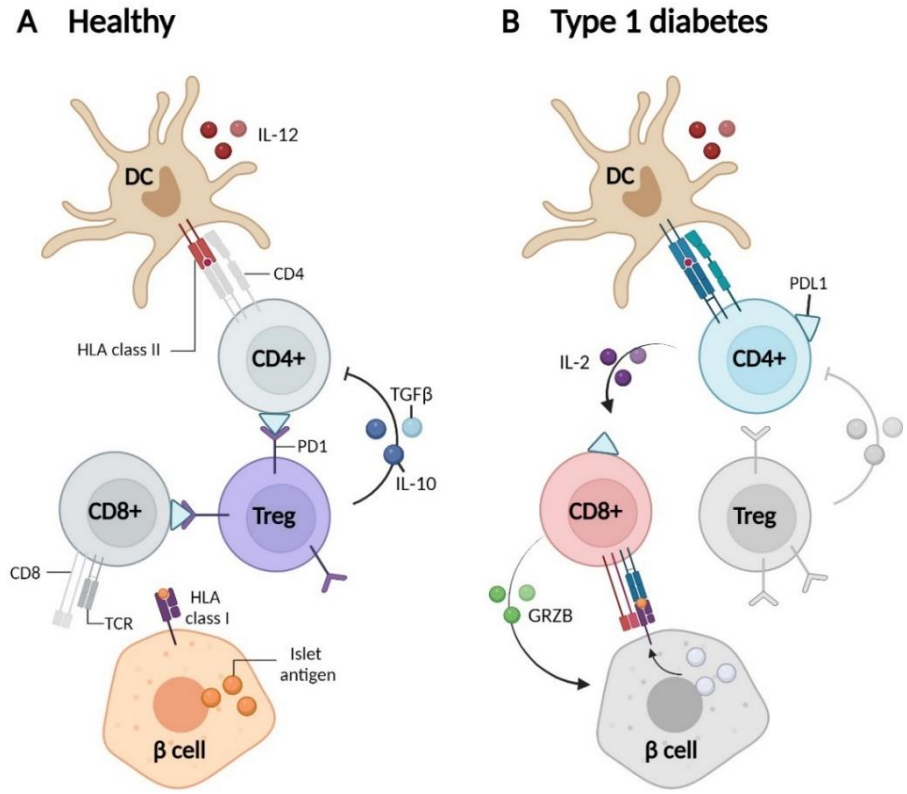

Figure 5. ***Peripheral immune regulation in healthy subjects or with type 1 diabetes. (A)*** *In healthy individuals, β-cells are protected from autoimmune β-cell destruction by immune regulation exerted by regulatory T (Treg) cells and PD-1/PD-L1 ligation.* ***(B)*** *In T1D, insufficient immune regulation caused by impaired Treg or PD-1/PD-L1 immunosuppressive axis function can result in*

an autoimmune response by autoreactive T cells, particularly if these cells are provoked by β-cells. GRZB, granzyme B; TCR, T cell receptor. Figure created using BioRender and adapted from [20].

In this sense, immune checkpoints are a group of proteins and ligands that regulate the immune response and maintain tolerance to self. Programmed cell death protein 1 (PD-1) is one such protein, expressed primarily in activated T lymphocytes, which maintain self-tolerance by binding to its ligand, the programmed cell death ligand 1 (PD-L1) molecule [148,149]. This immunosuppressive axis has been extensively explored in cancer as it represents a mechanism of resistance by tumor cells, which express abundant PD-L1 in response to antitumor immune activity [150,151]. The inhibition of PD-1 or PD-L1 by monoclonal antibodies promotes functional activation of cytotoxic T lymphocytes against cancer cells and represents a very effective immunotherapy for some tumor types [152]. However, it can induce autoimmune side effects, such as diabetes mellitus in genetically susceptible individuals [153].

1.3. Partners in crime: the immune system and β-cells

A conflicting bidirectional dialogue between β-cells and the immune system is increasingly recognized as a key player in the pathogenesis of T1D [154]. To gain a thorough understanding of these interactions, it is crucial to examine the conditions facilitating physical interactions between β-cells and immune cells, as well as exposure to soluble factors secreted by either cell type.

1.3.1. The role of pancreatic β-cells

T1D is a disease mediated by T lymphocytes and other cells of the immune system. However, β-cells also play a role in the pathogenesis of the disease, being more than just victims [20]. This "homicidal" view, in which β-cells contribute to their own destruction, was first proposed by Prof GF Bottazzo in the 1980s [155].

The role of the β-cell in T1D pathogenesis is rooted in the biology of these cells since they present vulnerabilities that make them attractive to be recognized by the immune system. First of all, insulin synthesis by β-cells is increased by more than ten-fold following nutrient stimulation, representing nearly 50% of total β-cell protein production. This can induce a state of cellular stress that, when poorly resolved, can lead to inflammation and cell death. Next, islets are highly vascularized which favors the encounter between β-cells and cells of the immune system. Finally, β-cells secrete insulin and other granular proteins directly into the bloodstream, which may favor the initiation of an autoimmune response beyond the pancreatic lymph nodes (PLN) [156].

As mentioned before, β-cells may be vulnerable to **stress-induced changes** that occur after an environmental insult, such as local infections, metabolic stress or the release of inflammatory agents from the intestines (**Figure 6**). Stress in β-cells can affect normal transcription, translation, and protein degradation, resulting in alternative RNA splicing, defective ribosomal products, and the synthesis of hybrid peptides or neoantigens, which in turn can activate pathogenic T cells [157–160]. For example, hybrid insulin peptides have been identified as targets for autoreactive T cells [161].

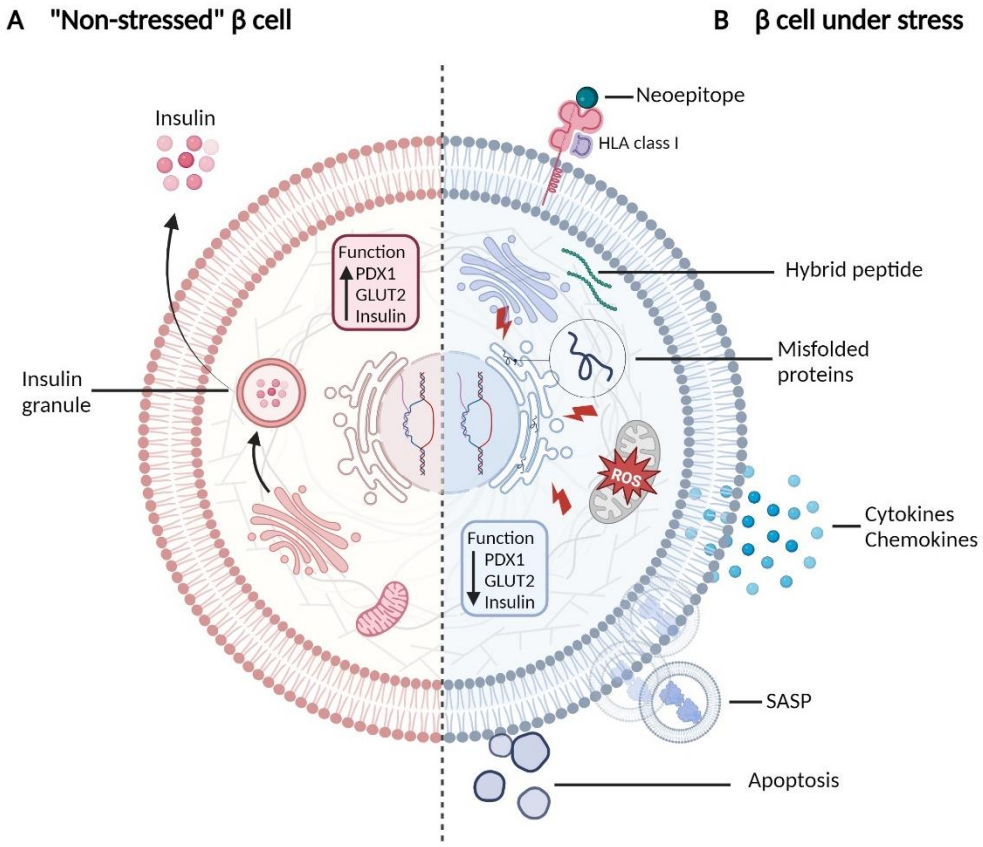

Figure 6. ***The effects of stress on β-cell function and immunogenicity.*** *(**A**) In normal or "non-stressed" conditions, β-cells function by synthesizing and secreting insulin into the bloodstream. (**B**) In the stress condition, transcription, translation and protein degradation are affected, which results in the synthesis of neoepitopes and hybrid peptides that are loaded into HLA class I molecules and presented to pathogenic T lymphocytes. Long-term exposure to inflammatory stress also results in profound changes in gene and protein expression, leading for example to the production of reactive oxygen species (ROS) or the downregulation of key β-cell transcription factors (PDX1) and insulin production. The accumulation of misfolded proteins in the endoplasmic reticulum (ER) and their aggregation can impair normal cellular function and be toxic, ultimately leading to cell death. Also, it triggers the unfolded protein response, which upregulates HLA class I and II expression, alters*

antigen presentation and drives apoptosis when it fails to reduce ER stress. Another type of stress response is senescence. β-cells can acquire a senescence-associated secretory phenotype (SASP), characterized by the production and secretion of diverse pro-inflammatory cytokines, chemokines, growth factors, and proteases. Figure created using BioRender.

Moreover, β-cells are poorly equipped to survive in an inflammatory environment and are highly sensitive to cytokine-mediated killing. Indeed, cytokines cause profound genetic, epigenetic and transcriptional changes, leading to the loss of the differentiated β-cell phenotype, the production of reactive oxygen species (ROS) and chemokines and the initiation of proapoptotic machinery [162–164]. The inflammatory signaling within β-cells also exerts deleterious effects on mitochondria, leading to compromised bioenergetic function and attenuated responsiveness to glucose-induced insulin secretion [165]. Additionally, β-cells are highly sensitive to various forms of ER stress [166,167]. For instance, both the proinflammatory cytokines and the progressive accumulation of misfolded proteins within the ER activate ER stress sensors and the unfolded protein response (UPR). If the adaptive UPR is unable to alleviate chronic ER stress, a terminal UPR is activated, leading to apoptosis [168]. Alternatively, β-cells can become senescent cells, a stable anti-apoptotic state that involves growth arrest and a proinflammatory secretome. Indeed, the induction of stress-related senescence in β-cells leads to the acquisition of a senescence-associated secretory phenotype (SASP), characterized by the production and secretion of diverse pro-inflammatory cytokines, chemokines, growth factors, and proteases. This phenotype is correlated with intra-islet infiltration of $CD45^+$ immune cells in patients with T1D [169]. Studies of human insulitis have revealed that 'danger signals' from stressed β-cells may precede insulitis. For example, hyper-expression of HLA class I and II molecules were noted in the pancreata of patients with newly diagnosed T1D, which enhances β-cell visibility to immune surveillance [170,171]. Islets also secrete the CXC chemokine ligand (CXCL)10, which attracts leukocytes expressing the CXC chemokine receptor (CXCR)3 to the lesion [172].

Ultimately, stress-induced changes may contribute to the exacerbation of inflammation and destruction of β-cells by initiating communication with other immune cells and triggering pathways leading to β-cell apoptosis and antigenicity. Over time, the reduction in β-cell mass will increase the secretory demand on the remaining β-cells to cope with glycemic control, thereby disturbing β-cell function.

1.3.2. The role of the immune system

The study of the pathogenic processes in T1D is hampered by the lack of access to pancreatic tissue and the delay of the symptomatology regarding the start of the autoimmune attack. Most data about the pathogenic role of the immune system have been obtained from peripheral blood samples; however, our knowledge about the composition of the autoimmune insulitis has been greatly expanded with the availability of pancreases from deceased donors obtained by the Network for Pancreatic Organ Donors with Diabetes program (nPOD; www.jdrfnpod.org), as well as from pancreatic biopsies from prediabetic subjects and living individuals with T1D. Furthermore, studies in spontaneous animal models of diabetes, such as the NOD mouse, have identified roles for different immune cell types in β-cell destruction.

The development of T1D involves complex interactions between cells of both the innate and adaptive immune systems and pancreatic β-cells. Initial events comprehend the generation of **autoantigen-specific $CD4^+$ and $CD8^+$ T cells** that escape the mechanisms of self-tolerance and stay in the periphery carrying an islet antigen-specific TCR. Then, a mild cell infiltrate (predominantly lymphocytic) starts surrounding and invading the islets of Langerhans [173]. Tissue imaging mass cytometry of pancreatic tissue from individuals with T1D unveiled concurrent recruitment of $CD4^+$ and $CD8^+$ T cells to the islets, suggestive of a correlation between insulitis and the presence of insulin-containing β-cells [174]. Indeed, $CD4^+$ T cells specific to different autoantigens have been isolated from the pancreatic islets of organ donors who had T1D [175]. Moreover, expanded clones of islet antigen-reactive $CD4^+$ memory T cells in the periphery can be detected during disease progression [176]. Although non-diabetic controls and individuals with T1D exhibit comparable frequencies of autoantigen-reactive $CD8^+$ T cells in peripheral blood, there is a notable accumulation of these cells within the pancreas of T1D donors [142]. Also, cytotoxic $CD8^+$ T cells reactive against preproinsulin epitopes were increased in T1D individuals and showed a potent autoreactivity, capable of killing β-cells [177,178]. However, autoreactive T cells are also present in pancreatic tissue of non-diabetic individuals, suggesting that an islet-specific trigger such as up-regulation of HLA class I might be essential to unmask β-cells to the immune system [179].

To be able to perform their function, autoreactive T cells first need to be primed (**Figure 7**). In this sense, cells of the innate immune system, in particular antigen-presenting cells (APCs), such as macrophages or dendritic cells (DCs), can provide a link between stressed β-cells and the adaptive immune response. APCs characteristically infiltrate and monitor different tissues, and become activated and fully mature upon recognition of pathogen-

or danger-associated molecular patterns through pattern-recognition receptors. As previously stated, stressed β-cells produce chemokines (e.g., CXCL10, chemokine ligand (CCL)2, CCL20, and IL-15) capable of attracting cells of the innate immune system, such as monocytes or DCs [180], and also of the adaptive immune system. Under conditions of stress and inflammation, the β-cell will release immunogenic autoantigens that will be captured and processed by inflammatory **conventional DCs** (cDCs) [181]. These DCs migrate then to the draining lymph nodes where they present autoantigens through HLA class I or class II molecules to naïve autoreactive cytotoxic ($CD8^+$) or helper ($CD4^+$) T cells, respectively. Then, T cells undergo activation upon receiving both a signal from the TCR and a co-stimulatory signal by CD28 binding to CD80 and CD86 molecules on APCs.

On the other hand, the circulating **monocytes** already possess functional properties before reaching the inflamed tissue. For instance, classical monocytes ($CD14^+CD16^-$) are pivotal in starting innate immune responses and engaging in phagocytosis, but they present no inflammatory attributes. Contrarily, non-classical monocytes ($CD14^{dim}CD16^+$) display inflammatory signatures on activation and exhibit properties for antigen presentation [182]. Once circulating monocytes reach the tissue, they differentiate into **macrophages** or monocyte-derived DCs, being among the first cells to infiltrate the islets. However, the pancreas itself already contains resident macrophages with an immunoregulatory phenotype responsible for silently clearing apoptotic cells, which is disrupted during the pathogenesis of T1D [183,184]. Depending on the local microenvironment, macrophages possess the ability to acquire different phenotypes, spanning from the classical M1 phenotype (inflammatory) to the M2 phenotype (anti-inflammatory). In the context of T1D, macrophages tend to adopt a proinflammatory phenotype, releasing significant levels of proinflammatory cytokines such as tumor necrosis factor (TNF)-α, IL-1β and IL-6. These cytokines have been reported to trigger nuclear factor kappa B (NF-κB)-dependent pathways in β-cells, leading to apoptosis [185–187]. Moreover, macrophages uptake and process the β-cell-derived antigens to prime the autoreactive diabetogenic $CD4^+$ T cells through HLA class II molecules and promote its differentiation towards a Th1 phenotype through the production of IL-12 [188].

In fact, during the immunological synapse, the DC will also secrete different cytokines that will determine the final differentiation of the T lymphocyte towards a particular functional phenotype. DCs promote the activation and differentiation of naïve $CD4^+$ T cells into effector Th1 or Th17 cells through IL-12 or IL-6 and IL-23 secretion, respectively. Depending on their phenotype, diabetogenic $CD4^+$ T cells secret in turn different pro-inflammatory cytokines that influence β-cells and contribute to their death. Traditionally,

T1D has been perceived as a condition primarily driven by **Th1** cells, while Th2 cells have been seen to offer a protective function. Th1 cells can secret IFN-γ, which in turn activates macrophages and induces them to secret ROS and the proinflammatory cytokines IL-1β and TNF-α [189]. Furthermore, the production of IFN-γ within the islet creates an inflammatory milieu that causes up-regulation of vascular adhesion molecules on the islet endothelium and increased chemokine production, which will contribute to the further recruitment of immune cells [190]. On the other hand, the role of effector **Th17** cells in T1D remains unclear, although some evidence suggests a pathogenic Th17 response where IL-17 promotes β-cell apoptosis [191,192]. Recently, it has been demonstrated that individuals with T1D exhibit elevated frequencies of circulating T cells displaying a follicular helper (**T_{FH}**) phenotype, which secrete the pleiotropic cytokine IL-21 [193]. This subset initiates the formation of germinal centers and provides help for B cell antibody production. In mouse models of diabetes, insulin-specific T cells can exhibit a T_{FH} phenotype and provide help to B cells that mount insulin-specific antibody responses [194].

Additionally, $CD4^+$ T cells provide help for the complete activation of $CD8^+$ T cells through the release of cytokines like IL-2 or IL-21. These activated and differentiated **cytotoxic $CD8^+$ T cells** can directly kill β-cells through HLA class I-mediated cytotoxicity (secretion of perforin and granzyme B) and Fas pathways [195]. One notable aspect emphasizing the functional interplay between infiltrating T cells and the islet microenvironment is the elicitation of an effector memory (EM) phenotype *in situ* [196,197]. Moreover, in contrast to responses towards conventional antigens such as viral antigens, the interactions of $CD8^+$ T cells with autoantigens demonstrate lower avidity but prolonged persistence. An examination of the epigenome of T1D-specific autoantigen-reactive $CD8^+$ T cells in the periphery unveiled stem-like epigenetic characteristics, hypothesized to explain the longevity of these cells despite continuous exposure to autoantigens [198]. Correspondingly, autoantigen-reactive $CD8^+$ T cells found within the pancreatic draining lymph nodes of NOD mice exhibited an increased self-renewal capacity, enabling their differentiation into short-lived effector cells that cause β-cell destruction [199].

While conventionally regarded as a T cell-mediated disorder, emerging evidence challenges the dogma surrounding T1D by implicating **B lymphocytes** as potentially significant contributors to its pathogenesis, likely through antigen presentation to T cells. Disease-related B cells in T1D subjects show loss of anergy [200] and defective central and peripheral tolerance [201], leading to increased frequencies of autoreactive cells.

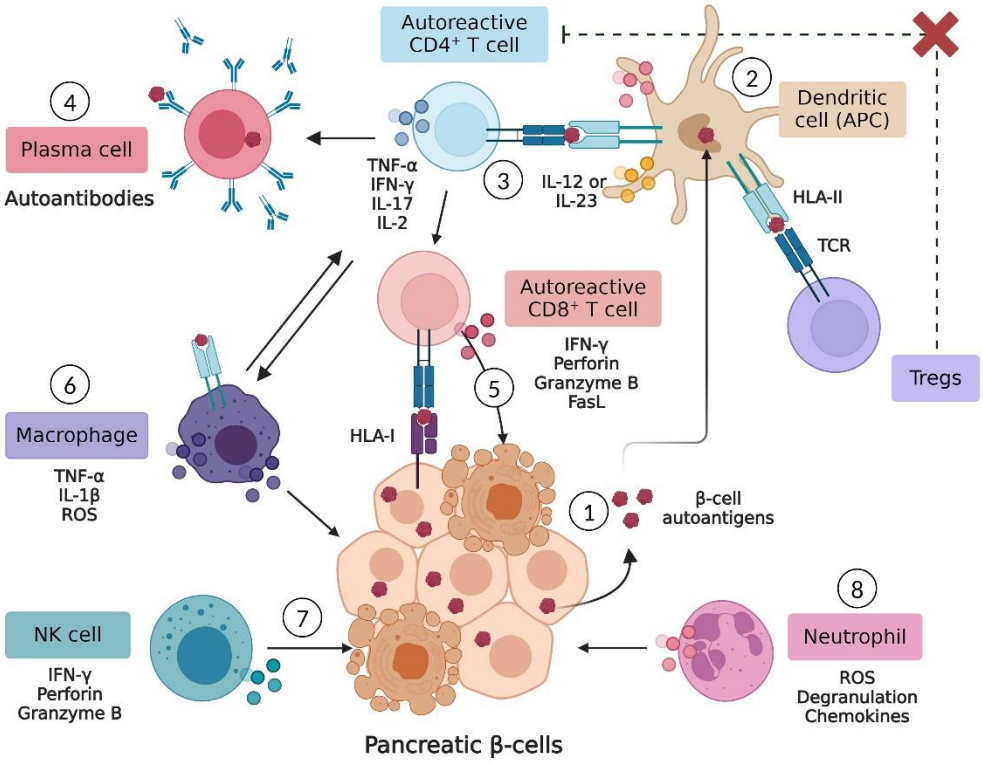

Figure 7. ***Immune mechanisms in type 1 diabetes.*** *(**1**) Due to an unknown trigger, inflammation occurs in the pancreas together with β-cell stress and death, and β-cell autoantigens and neoantigens are released and captured by DCs. (**2**) Autoantigens are presented to naïve autoreactive cytotoxic ($CD8^+$) or helper ($CD4^+$) T cells, generating at the end memory and effector T cells. Also, Tregs cannot effectively suppress autoreactive T cells. (**3**) Activated effector $CD4^+$ T cells (mainly Th1) are needed for the complete activation of $CD8^+$ T cells and (**4**) for the stimulation and differentiation of B lymphocytes exposed to β-cell autoantigens into plasma cells that produce autoantibodies. (**5**) $CD8^+$ T lymphocytes directly kill β-cells through HLA class I-mediated cytotoxicity and FasL/Fas interactions. (**6**) Other innate myeloid cells like macrophages are polarized towards a pro-inflammatory phenotype, thus secret pro-inflammatory cytokines targeting β-cells (IL-1β, TNF-α) and ROS. Macrophages also mediate T-cell recruitment via antigen presentation. (**7**) NK cells may also have potent cytotoxic activity against β-cells and secret high amounts of IFN-γ. (**8**) Chemokines, ROS, and proinflammatory cytokines produced by neutrophils also promote β-cell apoptosis and the generation of neoantigens, amplifying the inflammatory network and driving to the chronic autoimmune state. Figure created using BioRender.*

Autoreactive B cells can recognize autoantigens directly through their BCR in the secondary lymphoid organs, process them and present them via HLA class II molecules. In this way, B lymphocytes create an immunological synapse with the T_{FH} lymphocyte that recognizes just the same antigen through its TCR, and the two cells co-stimulate

each other. Autoreactive B cells become activated, proliferate and differentiate into memory cells or autoantibody-producing **plasma cells**. Furthermore, in the germinal center, B lymphocytes undergo somatic hypermutation in the complementarity-determining regions of BCRs (areas that recognize the autoantigen) to create autoantibodies that are more affine than the original BCR. These B cells also infiltrate the pancreas and are significantly enriched in the islet proximal area, together with $CD8^+$ T cells [184]. It has been postulated that infiltrating autoreactive B cells might possess superior efficiency in processing and presenting antigens to $CD4^+$ T cells compared to other APCs, which is attributed to their high-affinity antigen uptake through their BCR [202]. Moreover, B cells are able to accelerate diabetes in animal models by cross-presentation of antigens to $CD8^+$ T cells on MHC class I molecules [203], and the loss of their ability to present antigens —but not their loss of antibody secretion— is sufficient to prevent the disease [204]. Recently, it has been demonstrated that increased numbers of B cells in the peripheral blood and within the islets from individuals who develop T1D at an early age correlate with an accelerated disease trajectory [31,205]. Clear evidence of the contribution of B lymphocytes to the development of the disease is that the B cell depletion therapy Rituximab (anti-CD20) partially preserves β-cell function in recent-onset T1D [206]. Interestingly, post-analysis work showed a split between 'responders' and 'non-responders' of the therapy [207], which may be linked with patients having high or low numbers of B cells, as the former (younger patients) may benefit more from B cell depletion.

Finally, other cells present in the infiltrate such as neutrophils and natural killer (NK) cells can precipitate the autoimmune reaction. On one hand, **neutrophils** infiltrate mainly the exocrine pancreas [208] and can contribute to the onset of T1D by releasing cytokines and chemotactic factors that affect other immune cells, including macrophages and DCs. Of interest, a fraction of these neutrophils infiltrating the pancreas also extrude neutrophil extracellular traps (NETs), which consist of modified chromatin decorated with granules of degradative enzymes, indicating a potential tissue-specific pathogenic role [209]. Indeed, NETs can activate other innate effector cells, such as pDCs, which secret large amounts of proinflammatory IFN-α [210]. IFN-α induces the secretion of several chemokines by β-cells that are involved in the recruitment of immune cells [211], and promote an IFN-responsive gene signature in islets that is involved in antigen presentation, ER stress and apoptosis [212]. On the other hand, **NK cells** are effector lymphocytes characterized by being somewhat of a hybrid between the innate and adaptive arms of the immune system, since they express many lymphocyte markers but lack antigen-specific cell surface receptors. These cells are primed for rapid and potent cytolytic activity, as they are equipped with cytotoxic granules containing perforin and

granzymes. Moreover, their activation depends on the balance between the activating and inhibitory signals they receive. For example, NK cells express inhibitory receptors that recognize HLA class I molecules which prevent them from attacking self-healthy cells. In the context of T1D, stressed and/or infected β-cells present many activating ligands that together with the secretion of cytokines such as IL-15 or IL-12 will ultimately promote the activation of effector NK cells (NKeffs). Then, these cells induce β-cell apoptosis by secreting their granules and boosting autoreactive T-cell responses through IFN-γ secretion [213]. Indeed, studies in experimental models support an active role of NK cells in T1D pathogenesis [213,214], and most data point to NK's contribution to the aggressivity of insulitis and the acceleration of the disease [215]. However, their role in human disease pathogenesis is controversial with both protective and destructive functions, as these cells may also exhibit an immunoregulatory phenotype and secrete anti-inflammatory cytokines such as IL-10 or IL-4 that limit autoreactive T and B responses [216,217].

Following the establishment of islet inflammation, islet infiltration and destruction are self-sustaining and the induction of neoantigen generation activates additional autoreactive memory and effector T cells, which leads to chronic islet inflammation and gradual loss of functional β-cell mass.

1.4. Current therapies and future strategies

Since 1992, the standard-of-care for T1D has been **exogenous insulin** replacement therapy, along with daily glucose monitoring and a healthy lifestyle. In fact, T1D was transformed from a fatal to a chronic disease thanks to the discovery and use of insulin. Research conducted on the prediction and prevention of complications linked to diabetes has highlighted the significance of initiating treatment promptly and managing glucose levels effectively to minimize the likelihood of experiencing diabetic complications [218]. Insulin can be injected subcutaneously by syringes and pens or continually infused with the use of an insulin pump. In 2016, the Food and Drug Administration (FDA) approved the first largely automated insulin dosing system known as an artificial pancreas system. It is a hybrid closed-loop system that combines the technology of a pump with that of a continuous glucose monitor. Through this mechanism, the computer program improves blood glucose control by autonomously adjusting the insulin dosage it administers to maintain the blood glucose levels in range for longer periods [219].

On the other hand, many **immunomodulatory strategies** have been tested in several clinical trials to mitigate the autoimmune attack and preserve β-cell function. However, these strategies have had limited success, which highlights a gap in knowledge regarding the efficient translation of immunotherapies to provide benefits for individuals with T1D. Various immunomodulatory agents, such as monoclonal antibodies targeting specific immune cells or cytokines involved in the autoimmune response, are being investigated in clinical trials with the goal of preserving β-cell function and achieving sustained glycemic control without the need for exogenous insulin [220–228]. Encouraging, in 2022, the FDA approved *Teplizumab* as the first immunotherapy for T1D. It is a humanized non-Fc receptor (FcR)-binding anti-CD3 antibody able to delay the onset of T1D in adults and children older than 8 years who are at risk for developing stage 3 T1D [229]. Moreover, immune cell-based strategies are making their way into clinical trials, such as autologous *ex vivo*-expanded polyclonal Tregs [230] and autologous tolerogenic DCs [231], showing so far promising results. Recently, a randomized controlled trial with fecal microbiota transplantation was able to preserve stimulated C-peptide levels up to 12 months after the onset [232].

Although these strategies demonstrate good tolerability and safety, their effect on the immune system is broad and not directed toward the root cause of the disease, which is the specific autoimmune attack on the β-cell. For this reason, various **antigen-specific immunotherapies** have been tested in clinical trials to assess their safety, feasibility, and efficacy using different delivery methods. Indeed, there are multiple approaches to peptide presentation in antigen-specific immunotherapies, including unencapsulated, protein- or epitope-based vaccines, DNA-based vaccines, and antigens loaded into DCs or nanoparticles [233]. However, peptide and protein-based immunotherapies have shown mixed outcomes in clinical trials, with the majority of them failing to improve or maintain β-cell function. Alternatively, several platforms are developing different nanocarriers, such as nanoparticles displaying a large density of autoantigenic peptide-MHC complexes in the absence of co-stimulatory signals [234] or peptide-encapsulating phosphatidylserine-rich liposomes that induce tolerance through efferocytosis [235]. These approaches have shown good results in preclinical phases and are rapidly working their way to clinical trials.

Another area of research focuses on **β-cell replacement or regeneration** therapies. Islet transplantation, which involves transplanting insulin-producing islet cells from donor pancreases into recipients with T1D, has shown promise in restoring endogenous insulin secretion and achieving insulin independence [236,237]. However, challenges such as the limited availability of donor islets, and the need for immunosuppressive therapy to

prevent graft rejection remain significant hurdles to widespread adoption of this approach. In 2023, the FDA approved *Lantidra* as the first cellular therapy for adult T1D, which consists of a single infusion of allogeneic islet β-cells into the hepatic (liver) portal vein [238]. To address the shortage of islet material, several protocols have been developed to direct the *in vitro* differentiation process of human induced pluripotent stem cells towards the generation of functional stem cell-derived islets (SC-islets), comprising glucose-responsive β-cells [239,240]. Currently, alternative strategies for β-cell replacement without the usage of immunosuppression, such as encapsulated SC-islets or engineered SC-islets that evade immune rejection are also being explored as potential long-term solutions for T1D [241,242]. However, combining safe and efficient antigen-specific immunotherapy with a regenerative approach aimed at restoring β-cell function and mass may represent the best viable avenue for achieving normoglycemia.

Another aspect to consider is that there is a significant lack of information regarding the optimal immunointervention checkpoint for T1D once diagnosed. Unlike some autoimmune diseases such as multiple sclerosis, which exhibit recurring flares followed by periods of remission indicating a potential optimal time for immune intervention, T1D typically lacks clinical evidence of a relapsing-remitting behavior, except for the sporadic *honeymoon* or PR phase. Enhancing our comprehension of the underlying mechanisms orchestrating this phase, as well as finding specific biomarkers indicative of immunoregulatory and/or β-cell regeneration and recovery attempts would facilitate pinpointing the most opportune time for successful modulatory immunointervention.

2. THERE IS HOPE AFTER ALL: THE SPONTANEOUS PARTIAL REMISSION PHASE

2.1. Definitions and main features

After the diagnosis of T1D and within 2–6 months of the start of insulin therapy, up to 80% of patients experience a partial, transitory and spontaneous remission phase also called the ***honeymoon phase*** [243]. During this phase, patients recover partially from exogenous insulin, with hormone levels that may decrease to as low as half the initial dose or even be interrupted completely (**Figure 1**). The term '*honeymoon*' was first proposed during the 1940s [244] and has been corroborated over the years by the observation that a few patients maintain both excellent blood glucose control and increased C-peptide levels after insulin treatment and experience milder forms of the disease. Thus, during this phase, there is a temporary restoration of β-cell function.

The prevalence of the PR phase in T1D detected in different studies varies widely (30–80%), which partly reflects the use of different definitions. Traditional descriptions of this phase include insulin requirements <0.5 units (U)/kg of body weight per day and HbA1c <7% or stimulated C-peptide >300 pmol/L [245]. According to Mortensen et al., the definition of PR is based on the insulin dose-adjusted glycated hemoglobin (IDAA1c) index, where a value of HbA1c (%) + [4 × insulin dose (U/kg/day)] ≤9 indicates PR [246]. This formula reflects both residual β-cell function and insulin treatment efficiency and correlates well with stimulated C-peptide levels of >300 pmol/L, being validated in large cohorts of patients [247,248]. In accordance with this definition, the phase of PR can be predicted to manifest in ~61% of cases after a period of 3 months after diagnosis, 44% after 6 months, and 18% following a span of 12 months. Given that IDAA1c does not discriminate between insulin secretion and sensitivity, studies suggest using this formula in conjunction with the insulin sensitivity score to better capture the residual capacity of the pancreas to produce insulin during the honeymoon phase [249]. In addition, because estimated C-peptide emerges as an improved surrogate for tracking residual β-cell function [250], it could be a valuable tool for future PR monitoring.

This phase is significantly influenced by sex and age at diagnosis, with male patients diagnosed at the age of five or older exhibiting a higher likelihood of detection [247,251–254]. In fact, it is uncommon to find patients under the age of two experiencing the PR phase. Moreover, variations in the duration and strength of this phase are evident across individuals. While some patients may undergo a transient and moderate honeymoon stage, which usually lasts 7–9 months [243,247,253], others may experience a more

prolonged and striking period. However, both have similar factors influencing their onset, which are related to early diagnosis, strict glycemic control and better residual pancreatic β-cell secretory function [255,256]. In this regard, cases of long-lasting remission periods have been reported, although very rarely in children and adolescents (2.8% of patients) [255,257–259]. In these studies, complete remission has been associated with reduced levels of Tregs in peripheral blood, IL-10-dependent pathways in response to insulin antigens, and increased levels of stimulated C-peptide. A deeper understanding of the immunological and metabolic mechanisms underlying these episodes of remission could provide valuable insights into the progression of T1D and the pathways leading to β-cell protection and immune modulation.

2.2. Proposed mechanisms of partial remission

Behind this phase of spontaneous improvement, it has been hypothesized that early correction of hyperglycemia by exogenous insulin may lead to **β-cell resting** (non-stressed state), increased β-cell viability, the recovery of insulin synthesis and secretion, and improved insulin sensitivity [256,260]. It has also been postulated that **immunoregulatory processes** and the downmodulation of inflammation ensue as a result of the early correction of hyperglycemia, which could promote the regeneration (proliferation, neogenesis or α-to-β transdifferentiation) and recovery of β-cells [261,262] (**Figure 8**). In this sense, some pathways can control autoimmunity and extend this period, such as IL-10-dependent regulatory $CD4^+$ T cell responses or the enhanced PD-1/PD-L1 expression on T cells [263,264]. In mice, it is clear that β-cell proliferation is linked to islet inflammation, so it increases as inflammation becomes more severe. Then, there may be spontaneous recovery of β-cell mass and function if autoimmunity and islet inflammation are arrested [265]. Rui et al. identified a mechanism of cell protection from the immune attack during T1D progression in the NOD mouse in which β-cells lose granularity and β-cell markers and increase features of stemness, proliferation and immune inhibitory markers. This process might cause a continuous cycle where new β-cells are generated but then destroyed by an immune reaction, or it could result in a subset of β-cells surviving over the long term, which has been observed in people with chronic T1D [266]. Interestingly, a recent study of single-cell multi-omics of human pancreatic islets revealed the presence of a novel subset of exocrine ductal cells that acquire a signature of tolerogenic DCs in an attempt at immune suppression in T1D [267]. Although the degree to which β-cell regeneration occurs is still a subject of ongoing discussion [37], individuals in the honeymoon phase have higher β-cell mass than those with long-standing T1D [268]. In a recent study, Doke et al. employed single-cell RNA sequencing (RNA-seq) to demonstrate, for the first time, that β-cell regeneration can

occur in human pancreatic tissue through a ducto-acinar-endocrine differentiation axis, ultimately leading to the formation of functional β-cells [269]. One potential drawback of β-cell regeneration without lasting tolerance to islet antigens is that it can expose autoantigens and neoantigens to the extracellular media, which may act as a trigger for autoimmunity against both newly formed and functionally improved β-cells. This could result in insulin production declining and the patient becoming dependent on exogenous insulin administration again, which would put an end to the PR phase. Consequently, a vicious circle of regeneration and autoimmunity would be perpetuated. In accordance with this hypothesis, it can be postulated that distinct episodes of remission may exist throughout the course of the disease —although currently undetectable—, implying its chronicity. However, there are currently no studies supporting this hypothesis.

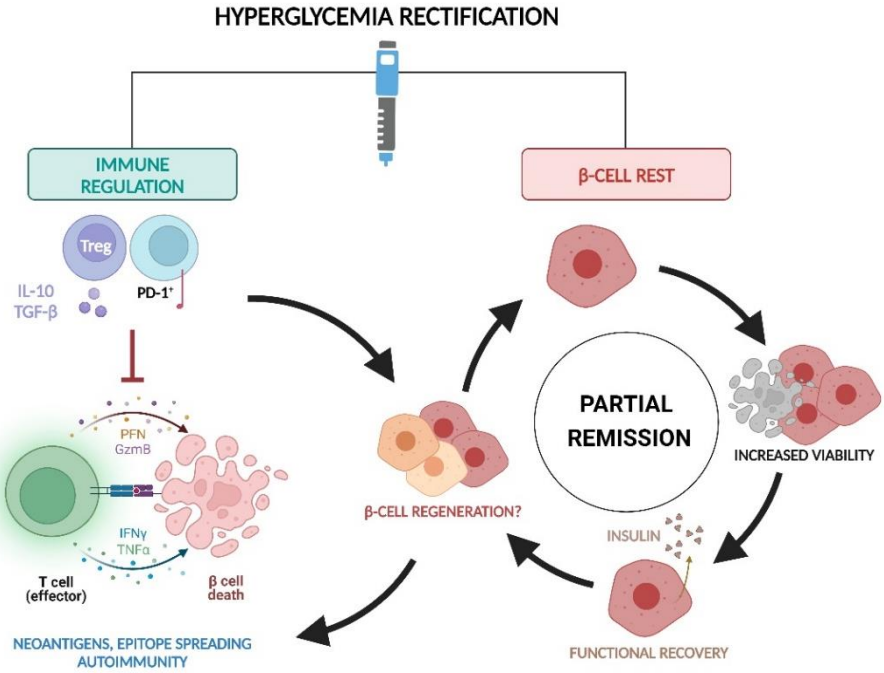

Figure 8. ***Mechanisms underlying the partial remission phase in type 1 diabetes.*** *Early correction of hyperglycemia by exogenous insulin administration initiates a phase of spontaneous partial remission. This correction may induce a relief in β-cells from the stress of controlling glycemia, enhancing their viability, insulin synthesis and secretion, as well as improving insulin sensitivity. Additionally, it is suggested that immunoregulatory mechanisms such as PD-1 expression on T cells or Treg suppressive functions could facilitate β-cell recovery and regeneration. Then, β-cell regeneration-introducing auto- and neoantigens might be a trigger for autoimmunity, potentially bringing an end to this favorable remission phase. In fact, the unabated autoimmune attack would gradually destroy both newly formed and existing β-cells so that insulin production would eventually decline again. This perpetuates a cycle of regeneration and autoimmunity, implying the chronicity of the disease. Figure created using BioRender.*

2.3. Clinical implications

The PR phase is linked not only to metabolic changes but also to immune regulation. These alterations can be reflected in the form of reliable blood biomarkers, providing valuable insights into the pathways leading to β-cell protection and immune modulation [270]. The discovery of these novel biomarkers holds great potential for physicians, because they enable the prediction and detection of subsequent remission stages that might otherwise go unnoticed. Prolonging the honeymoon phase as much as possible, or even inducing it, becomes highly pertinent for patients given the association between residual β-cell function and reduction of both long-term complications (e.g., atherosclerotic cardiovascular disease) and other autoimmune diseases [271–273]. Preserving the function of remaining β-cells beyond the honeymoon stage, alongside halting the autoimmune assault, is a promising strategy.

Since PR is a stage of partial recovery of β-cell function [256], it offers a unique therapeutic window to rebalance the immune system through immunotherapies. The concept of immunointervention during this stage has strongly evolved over the past few years, with the success of clinical trials being influenced not only by the efficacy of the therapy but also by the appropriate timing of intervention [274]. By targeting these interventions during periods of reduced inflammation or heightened immunoregulatory activity, the outcomes of clinical trials may be favorably influenced. Currently, no clinical trials are being conducted during the PR phase. Nevertheless, the potential for monitoring the outcomes of interventional studies in stages 2 and 3 of T1D seems encouraging through the utilization of distinct biomarkers associated with this stage. Moreover, identifying suitable individuals for enrollment in clinical trials poses challenges. Patient stratification based on the presence or absence of remission can not only enhance their selection for clinical trials but also enable a more precise therapeutic approach.

Given the current lack of large longitudinal studies aimed at studying the PR phase, there is an urgent need to identify biomarkers that reflect the state of remission, whether at the metabolic, immunological, or even epigenetic level. This will enable a better understanding of the progression of the disease and the development of tools to manage and modulate the natural history of T1D once diagnosed.

3. UNVEILING DISEASE PROGRESSION THROUGH BIOMARKERS

Biomarkers are indicators of both normal and abnormal physiological or pathological processes, playing crucial roles in clinical diagnosis, prognosis, and the monitoring of therapeutic responses. Any indicator that can be measured accurately and reproducibly —for instance, cells, proteins, lipids, hormones, genes or imaging methods— may serve as a biomarker. The development of specific blood serum or plasma biomarkers holds particular interest across various diseases due to the systemic circulation of blood throughout the entire body, which serves as a carrier of molecules that are altered at localized pathological sites. Moreover, blood biomarkers can be obtained with minimal discomfort for the patients and are relatively easy to access compared to other biological fluids or pathological tissues.

While there have been advances in our understanding of the pathogenesis of T1D, we still do not have effective serum or plasma biomarkers that reflect immunoregulatory processes or β-cell function and mass. So far, a combination of serum biomarkers has been well established for the diagnosis of the disease, including high levels of glucose, HbA1c, C-peptide and autoantibodies. Unfortunately, nowadays it is not only difficult and inaccurate to predict the onset of the disease, but it is still unrealistic to distinguish between different stages of diabetes progression once diagnosed [275].

Nonetheless, the development of biomarkers is a long process encompassing candidate identification, validation, and clinical assay development. Despite extensive efforts within the field, our current knowledge primarily remains focused on the initial step of identifying biomarker candidates. In the following sections, we will discuss the latest advances in the discovery of biomarkers that can predict T1D onset and remission, as well as those that can reflect changes during the honeymoon period.

3.1. Biomarkers of progression: from prediabetes to overt type 1 diabetes

After a triggering event, genetically susceptible individuals with normal glucose levels test positive for two or more autoantibodies to β-cells. The number of different islet autoantibodies identifies those patients with a higher risk of developing T1D. In this sense, whereas only 15% of children with one autoantibody eventually develop T1D within 10 years, 70% do so if they present at least two autoantibodies [276]. However, this risk can be modified by several factors such as autoantibody titer, order and age of seroconversion, genotype, or specific antibody combinations, highlighting the great heterogeneity entailed with the disease [277]. In the TEDDY Study it was determined that

younger individuals tend to present IAA first, related to DR4-DQ8 haplotype, thus being more prone to develop multiple autoantibodies and to experience an accelerated β-cell loss [278]. The Type 1 Diabetes Prediction and Prevention (DIPP) Study explored autoantibody appearance from birth, finding that progressors peaked seroconversion at one-year-old [279].

Apart from autoantibodies, immunological and molecular changes have been found in stages 1 and 2 of T1D. In fact, a comprehensive transcriptomics study analyzing RNA from whole blood samples found that a type I IFN signature could be identified in children at a higher risk of developing T1D even before the detection of disease-associated autoantibodies [280]. A highly reported circulating biomarker that can predict T1D is the increased number of Tregs together with a decreased suppressive capacity [281–283]. It was recently described a specific miRNA signature in those islet autoantibody-positive individuals who progressed to T1D [284]. Also, the decrease in phosphatidylcholine, the differential expression of certain genes in immune system cells (e.g., low levels of CTLA-4), or increased complement factor H have been found in individuals progressing to T1D [285]. Furthermore, pre-T1D stages are characterized by an increased ratio of proinsulin to C-peptide, which suggests β-cell dysfunction [286]. As T1D progresses, the loss of β-cells causes fragments of unmethylated insulin DNA to enter the bloodstream, where they can be detected. Thus, measuring the levels of unmethylated insulin DNA in the blood may indicate the extent of β-cell death and could be used for the early detection of T1D [287].

While these biomarkers need to be validated in larger cohorts of individuals, they may be useful together with the number and levels of autoantibodies to detect subjects at high risk of developing T1D. Indeed, the TEDDY study group has developed a combined risk score incorporating both fixed and variable factors (genetic, clinical, and immunological) that is able to significantly improve T1D prediction in susceptible children [288].

3.2. Predictive biomarkers of partial remission

One of the primary considerations following the diagnosis of T1D pertains to the understanding of its progression and prospective metabolic control. In this context, gaining knowledge of the likelihood of a PR subsequent to diagnosis would facilitate a more individualized approach to disease management. In addition, predicting disease progression and PR may be important to improve therapeutic strategies, since, for instance, the efficacy of immunotherapies depends on the time of intervention [274]. In

this regard, a gene signature comprising IFN-γ signaling pathways, increased B lymphocyte levels, and decreased neutrophil-mediated responses has been associated with a rapid progression of the disease [289]. Moreover, circulating miRNAs near T1D diagnosis also predict future stimulated insulin secretion. Specifically, the combination of the circulating miR-3187-3p/miR-103a-3p predicts C-peptide decline efficiently [290]. Consequently, various investigations have been conducted to predict the occurrence of PR at the time of diagnosis. However, most of these studies primarily focus on anthropometric, clinical, or metabolic factors.

At the clinical level, numerous studies in children and adolescents show that age is a key factor in the presentation of PR, and agree that a diagnosis over the age of 5 years is associated with a higher probability of presenting this phase [251]. Typically, children exhibit a higher likelihood of experiencing remission compared with adults and, within the former group, the probability of sustained remission tends to increase with higher onset age [291]. Other factors that predispose to PR include bicarbonate concentrations >15 mg/dl, male sex, higher body mass index (BMI) and pH values, lower HbA1c levels, and less than three diabetes-associated autoantibodies [243,247,252,253,292]. Moreover, other lifestyle factors, such as exercise, can reduce insulin needs [293], preserve β-cell mass [294], and increase the occurrence and length of the PR phase [295].

As mentioned previously, the immunomodulatory changes demonstrate nonlinear mechanisms of immune regulation in T1D, particularly during the PR phase. In this context, only a few studies have investigated the immunological factors that are associated with the occurrence or duration of PR (**Table 1**). Elevated levels of IL-6, IL-10, and anti-inflammatory IL-1 receptor antagonist (IL-1Ra) have been positively associated with PR or with higher levels of C-peptide 1 year after diagnosis, contrary to IFN-γ levels [296–298]. Moreover, low cytokine responders at disease onset and those with a higher frequency of $CD4^+CD25^+CD127^{hi}$ lymphocytes, which display a Th2 bias but are neither Treg nor type 1 regulatory cells, are more prone to experience longer remission periods [299,300].

Other cells, such as $CD4^+CD45RO^+$ (memory) T cells or apoptotic Tregs, are also associated with pediatric remission [301,302]. These apoptotic $CD4^+CD25^{hi}$ Tregs detected after metabolic stabilization inversely correlate with insulin doses, and low levels of total Tregs are associated with increased C-peptide levels [282]. Both correlations show that patients with worse metabolic control tend to present higher levels of total Tregs, which can be evidenced by their reduced apoptosis, highlighting the intersection between metabolism and the immune system.

Table 1. ***Biomarkers predicting partial remission at type 1 diabetes diagnosis***

Predictive biomarkers of PR	Association	Reference number
Anthropometric, clinical, or metabolic		
Children	Positive	[251,291]
>5 years old	Positive	[243,247,251,252]
Male sex	Positive	[247,252,253]
Increased BMI*	Positive	[292]
Bicarbonate concentrations >15 mg/dl	Positive	[252]
>pH values	Positive	[243,292]
Decreased HbA1c	Positive	[247,253]
<3 diabetes-associated autoantibodies	Positive	[247,252]
Exercise	Positive	[295]
Immunological		
IL-6, IL-10, IL-1Ra	Positive	[296–298]
IFN-γ	Negative	[297]
$CD4^+CD25^+CD127^{hi}$	Positive	[299]
Activated Tregs	Positive	[303]
Apoptotic Tregs	Positive	[302]
$CD4^+CD45RO^+$	Positive	[301]
$CD4^+$ T cells responses to proinsulin peptides	Positive	[304]
Low cytokine profile (undetectable IL-4, IL-10, IL-13 and TNF-α)	Positive	[300]

*BMI, body mass index

By contrast, having increased levels of circulating activated Tregs ($CD4^+/CD45RA^-$/Forkhead box protein 3 $(FoxP3)^{hi}$) is positively associated with persistent insulin secretion [303]. It is noteworthy that the proliferative responses of $CD4^+$ T cells to proinsulin peptides decrease following diagnosis. However, maintaining a robust response in these cells is indicative of a prolonged period of PR in children and is linked to β-cell function [304]. Nonetheless, additional investigations are required to ascertain whether these proliferative cells have a regulatory function. Overall, these collective studies suggest that the lower severity of the underlying inflammation at diagnosis explains PR occurrence and length. However, many of these studies have been conducted with small patient cohorts and have focused on studying only a few specific cellular or molecular parameters. This limited approach does not provide a comprehensive view of the immunological changes that can predict this phase and does not apply to clinical practice.

3.3. Emerging monitoring biomarkers of partial remission

In recent years, small longitudinal studies have been conducted to identify differences in the progression of T1D. However, these studies do not detect the PR phase per se, as indicated by indices such as IDAA1c. Instead, they merely associate the potential changes observed 3–6 months after diagnosis with the possibility of presenting this phase. Consequently, although there has been notable advancement in elucidating the heterogeneity of the disease once diagnosed, studies comparing remitters and non-remitters remain scarce. Consequently, there is a pressing need to identify specific biomarkers of the PR phase.

3.3.1. Immune populations

Different peripheral immune cell subpopulations have been proposed as biomarkers to follow the progression of many autoimmune diseases such as systemic lupus erythematosus, rheumatoid arthritis, grave's disease and psoriasis [305–308], since these cells can reflect variations of the autoimmune response. In addition, immune cell subpopulations have shown their usefulness as biomarkers of response to treatments and efficacy of immunotherapies [309,310]. Therefore, it would be interesting to analyze changes in different leukocyte subsets to detect periods of remission.

It has been proposed that immunoregulatory mechanisms or transient immune tolerance are associated with PR. Indeed, homeostasis between Tregs and effector T lymphocytes has an important role in the regulation of autoimmunity. Different studies coincide in finding a higher number of Tregs at T1D diagnosis or during the prediabetes period compared with non-diabetic controls, which may reflect their impaired functionality in the context of hyperglycemia and the need to constantly generate new cells to cope with the autoimmune attack [282,311]. Indeed, the first longitudinal study regarding PR in children observed increased levels of Th1, Th17, and $CD8^+$ cytotoxic T cells during this phase compared with disease diagnosis, along with increasing Th1/Treg and Th17/Treg ratios throughout progression [300]. It should be noted that the study did not include patients who had not achieved remission. Contrarily, Tregs with an activated phenotype were increased during the first year post-diagnosis [312]. Another study also found that patients with higher levels of both Tregs and Th17 showed higher remission rates [282], while presenting diminished peripheral antigen-specific Tregs was also a feature of remission compared with the diagnosis time-point [298]. These collective findings may reflect the recovered functionality in Tregs and the reduction in their numbers after the rapid rectification of hyperglycemia, thereby enabling enhanced activity in the target

organ and secondary lymphoid organs. Nonetheless, further research that dissects the exact mechanisms explaining these differences should be conducted.

Other immune cells are also altered during disease progression. Longitudinal studies analyzing samples up to 2 years after diagnosis in children and adolescents identified decreased levels of total B cells and increased levels of both regulatory B (Breg) and NK (NKreg) cells, which may coincide with the remission stage and may reflect immunoregulatory attempts [300,312]. B lymphocytes have a clear role in the autoimmune process, evidenced by the extension of the remission phase for 2 years after their depletion with rituximab [313]. Even the combined therapy of autologous expanded Tregs and rituximab increased the proportion of patients going into remission compared with the control treatment group [314]. Therefore, it would be interesting to assess specific molecular changes in B lymphocytes to better understand their relationship with the remission phase.

Not only can the percentages or the total number of immune system cells be biomarkers of immunomodulation during this phase, but their phenotype or functionality can also provide information on the exact mechanisms that occur behind it. For example, islet-specific $CD8^+$ T cells with an exhaustion-like profile identify patients with slow T1D progression after onset [315]. In addition, much effort and emphasis are being placed on the study of inhibitory molecules or immune checkpoints during PR. Several studies have reported the association of the PD-1/PD-L1 axis with T1D pathogenesis [316]. Inhibition of PD-1 and PD-L1 in the NOD mouse induces the disease, while the overexpression of these molecules inhibits the autoreactive T lymphocyte response and reverses diabetes [317]. Interestingly, both pediatric and adult patients in PR show a higher percentage of peripheral T lymphocytes positive for both PD-1 and PD-L1, thus recovering the low levels reached during the diagnosis of the disease [263]. However, the recovery of the PD-1/PD-L1 axis is not observed in non-remitters.

3.3.2. Cytokines and chemokines

Cytokines orchestrate multiple interactions between β-cells and immune cells and can serve as biomarkers reflecting the inflammatory status of the patients. While published data are sometimes contradictory, PR tends to be associated with decreased levels of proinflammatory cytokines. For instance, some studies suggest that low levels of circulating TGF-β and IFN-γ are distinct features of PR [297,312]. Unexpectedly, it was found that the concentration of adiponectin, an anti-inflammatory cytokine expressed by adipocytes, was lower in pediatric remitters than in non-remitters, but it was also

negatively correlated with C-peptide levels [296]. Furthermore, chemokines involved in the recruitment of lymphocytes into the islets, such as CCL5, show decreased concentrations in pediatric remitter patients compared with non-remitters [318].

3.3.3. Immune metabolism

Metabolism has a key role in regulating T cell functions. Activation of T cells rapidly implies metabolic reprogramming toward anabolism and increases their glucose metabolism to build biomass [319]. Therefore, it is conceivable that a reduction of the glucotoxic environment during PR would have an impact on T cell function; indeed, intracellular glucose uptake of circulating $CD4^+$ and $CD8^+$ T cells is enhanced in T1D compared with healthy controls, and is positively associated with HbA1c and negatively associated with C-peptide levels [320]. In addition, patients progressing to T1D show a distinct metabolic pattern in peripheral blood mononuclear cells with increasing levels of lipids and amino acids [321]. However, there are few studies on the intersection of metabolism and the immune system during PR as a possible target for therapeutic interventions.

Recently, it was described that T lymphocytes show decreased glucose uptake during the remission phase in both children and adults compared with the time of diagnosis, reaching the values presented by non-diabetic controls [322]. Moreover, at the end of PR, glucose uptake by T lymphocytes increases again. However, these fluctuations in T cell metabolism were not detected in non-remitters, in whom there appears to be an increase in glucose uptake during the first 12 months after diagnosis. These results, not found in type 2 diabetes (T2D), suggest a T cell metabolism unique for remitters, which can affect the immune balance and may be autoimmune driven. In addition, a negative relationship between the expression of the exhaustion marker PD-1 and glucose uptake was observed in $CD8^+$ T lymphocytes. This observation holds significant importance since the presence of pathways that counteract co-stimulation, such as the signaling pathways associated with CTLA-4 and PD-1, negatively impact glucose metabolism [323]. The inhibition of glycolysis, the main metabolic pathway for T cell activation and proliferation, also leads to exhausted diabetogenic $CD4^+$ T cells, and, thus, could be exploited as a novel therapeutic strategy for T1D [324].

Furthermore, it was observed that the length of PR can be modified by metabolic interventions, such as by the dipeptidyl peptidase 4 inhibitor sitagliptin plus vitamin D3 in patients with new-onset T1D, which increases insulin synthesis and secretion [325,326]. Interestingly, this combined therapy presents synergistic anti-inflammatory and

immunomodulatory properties. While vitamin D3 activates $CD4^+CD25^+FoxP3^+$ Tregs, sitagliptin deregulates Th1/Th17 differentiation and reduces pancreatic inflammation [327,328]. Altogether, metabolic reprogramming on T cells is a promising intervention to control aberrant T cell responses.

3.3.4. Systemic metabolism

PR is characterized by increased levels of basal and stimulated C-peptide, decreased HbA1c, and reduced requirements of exogenous insulin, with a direct impact on β-cell function. In a follow-up study of children and adult patients with newly diagnosed T1D, a three-phasic pattern of C-peptide decline was observed for remitters. While non-remitters presented an initial fast fall of C-peptide levels followed by a slower decrease, remitters presented a rapid increase of C-peptide during the first 2 months after diagnosis, non-observable in non-remitters, followed by a continuous fall for up to 3 years and a slower decrease thereafter. Therefore, while recovery of β-cell function can be detected during PR, non-remitters present a continuous β-cell mass decline [329]. Glucose variability parameters (e.g., coefficient of variation and time in hypoglycemia) also differentiate the remission status in children and can identify different glucotypes that reflect the different patterns of loss of glucose homeostasis during the first year after T1D onset [330].

Whereas the recovery of β-cell function with improved endogenous insulin production during this phase is well established, little is known about insulin sensitivity. A year after diagnosis, non-remitters showed lower insulin sensitivity compared with remitters, while exhibiting similar C-peptide levels [331]. However, differences in insulin sensitivity within the PR group were found, and those children with lower insulin sensitivity presented a shorter PR phase. Due to these discrepancies, a suggestion of combining IDAA1c with insulin sensitivity score to define PR has been proposed, as mentioned before [249].

Moreover, remitter children, unlike non-remitters, have puberty-related reductions in low-density lipoprotein and total cholesterol even 5 years after T1D diagnosis. By contrast, non-remitters present increased lipid-based cardiovascular risk similar to that seen in T2D [271,332–334].

3.3.5. Genetic and epigenetic biomarkers

Unveiling the genetic risk alleles that contribute to the appearance and duration of the PR phase can shed light on its mechanistic pathways. A single nucleotide polymorphism on the *EP4* gene was found to be positively associated with remission occurrence and extension [335]. This gene encodes a receptor for prostaglandin E2, a ligand related to immunoregulatory mechanisms in the context of T1D [336]. Moreover, the relationship between HLA class II genes and remission has also been investigated. Both children and adults carrying DR9/DR9, a high-risk T1D genotype in Chinese individuals, were less likely to experience PR, which could be explained by the relation between this haplotype and both limited recovery of β-cell function and acute disease onset [337,338]. Given its predictive capacity, patients carrying DR9/DR9 can be chosen for intensive insulin intervention as early as possible to increase their odds of experiencing PR.

Another point to consider is that alterations in metabolite concentrations can impact the epigenetic profile of T lymphocytes, thereby affecting their differentiation, proliferation, and functionality. As epigenetic modulators, miRNAs have been proposed as potential blood biomarkers for autoimmunity [339]. Although many studies have described several DEMs in T1D diagnosis compared with healthy subjects or those with long-standing disease [135,140,141], there is a dearth of information regarding PR. Altogether, exploring the epigenetic landscape during PR could elucidate the processes driving this phase and the link between metabolism and the immune system.

2

HYPOTHESIS & OBJECTIVES

1. HYPOTHESIS

In T1D, the loss of β-cell mass due to the autoimmune attack is not linear; rather, it follows an immunologically relapsing-remitting pattern. In this sense, the persistence of residual β-cells and increased immune tolerance alternate with periods of destruction. However, these oscillations are only clinically reflected during the PR phase after diagnosis, during which insulin requirements decrease and glycemic control improves due to temporary β-cell function recovery. The precise mechanisms underlying this phase remain unclear; however, it is thought to result from a reduction in β-cell stress due to corrected hyperglycemia, as well as improvements in β-cell viability, insulin sensitivity, regeneration, and immune regulation. Although all patients receive exogenous insulin and experience a reduction in glucotoxicity, not all undergo this phase, and only a few achieve complete remission. It is therefore of great importance to gain an understanding of not only the immunological fluctuations preceding the diagnosis of the disease but also those occurring subsequent to it. This can provide valuable insights into the pathways leading to β-cell protection and immune modulation, which can have important clinical implications for patient stratification in clinical trials, the identification of optimal stages for immune interventions, and the enablement of a more precise therapeutic approach.

The hypothesis of this work is that the identification and characterization of metabolic, immunological, and epigenetic changes can lead to the development of predictive algorithms and monitoring biomarkers of the PR phase in T1D. Furthermore, the miRNA epigenetic signature during this period may have the potential to regulate T lymphocyte activity, promote β-cell recovery and regeneration, and influence the progression of islet autoimmunity.

2. OBJECTIVES

The main aim of the present work is to identify novel immunological and epigenetic biomarkers of PR in pediatric patients with T1D and elucidate the mechanisms underlying the intersection of immunometabolism and epigenetic regulation, with the potential to provide insights into β-cell protective pathways.

To accomplish the main aim, specific objectives were set as follows:

1. To implement a predictive algorithm for PR at the time of T1D diagnosis based on metabolic and immunological parameters as a tool with potential clinical use.

2. To characterize peripheral blood leukocyte subpopulations and the concentration of inflammatory and anti-inflammatory cytokines in plasma at different phases of T1D progression as monitoring biomarkers of PR.

3. To determine the specific profile of miRNAs as new epigenetic biomarkers of PR.

4. To demonstrate the immunoregulatory potential on T lymphocytes of the most differentially expressed miRNA during PR.

5. To demonstrate the effect on the functional recovery and regeneration of β-cells of the most differentially expressed miRNA during PR.

6. To ascertain the pathological implications of the modulation of the most differentially expressed miRNA during the progression of islet autoimmunity.

3

MATERIAL & METHODS

1. HUMAN SAMPLES

To identify biomarkers of PR and to characterize the effects of miRNAs on T lymphocytes, venous peripheral blood samples of pediatric patients with T1D and from control subjects were obtained. To dissect the effect of upregulated miRNAs during the PR phase on β-cell functionality and neogenesis, human pancreatic tissue of non-diabetic deceased donors was obtained.

1.1. Ethics statement

All the experiments were carried out in strict accordance with the principles outlined in the Declaration of Helsinki for human research and after the approval of the Committee on the Ethics of Research of the Germans Trias i Pujol University Hospital (protocol codes PI-19-010 and PI-23-128) and Parc Taulí University Hospital (2019/583 and 2023/6028). All individuals or their legal representatives gave written informed consent to donate blood for research. Human pancreatic tissue biopsies were obtained from the cGMP facility at the Diabetes Research Institute (DRI), University of Miami. Human pancreatic slices (HPSs) were also obtained from the nPOD program at the University of Florida or Prodo Labs (Aliso Viejo, CA). All procedures were performed according to the established SOPs by the nPOD/OPPC and approved by the University of Florida Institutional Review Board (IRB201600029) and the United Network for Organ Sharing (UNOS) according to federal guidelines, with informed consent obtained from each donor's legal representative. The collection and processing of personal and clinical data were confined to the essential information required to fulfill the study's objectives, conducted with adequate precautions to ensure confidentiality, and adhered to the pertinent data privacy protection laws and regulations.

1.2. Participants

Samples of peripheral blood were collected from 88 pediatric patients with T1D and 38 age- and sex-related control subjects. Pancreatic tissue samples were obtained from 6 deceased control donors. Different groups of patients and controls were generated according to the objective (**Figure 9**):

1. For the prediction of PR, a sample of 56 pediatric patients with new-onset T1D was obtained only at the time of diagnosis.

2. For the discovery of specific immunological and epigenetic biomarkers of PR, a sample was obtained from 17 pediatric patients with new-onset T1D at 3 different times (diagnosis, PR or non-PR and after 12 months of evolution) and from 17 age- and sex-matched non-diabetic control subjects. For the validation of miRNAs as

biomarkers of PR, a validation cohort was generated composed of non-paired samples that included 8 pediatric patients with new-onset T1D, 10 remitters, 9 non-remitters (5 of them also included in the discovery cohort), and 15 age- and sex-matched control subjects.

3. For the identification of the effect of miRNAs on primary human T lymphocytes, unpaired samples were obtained from 7 pediatric patients with new-onset T1D and 6 age- and sex-matched non-diabetic control subjects.

4. For the study of the effect of miRNAs on β-cell functionality and neogenesis, pancreatic tissue was obtained from 6 non-diabetic control donors.

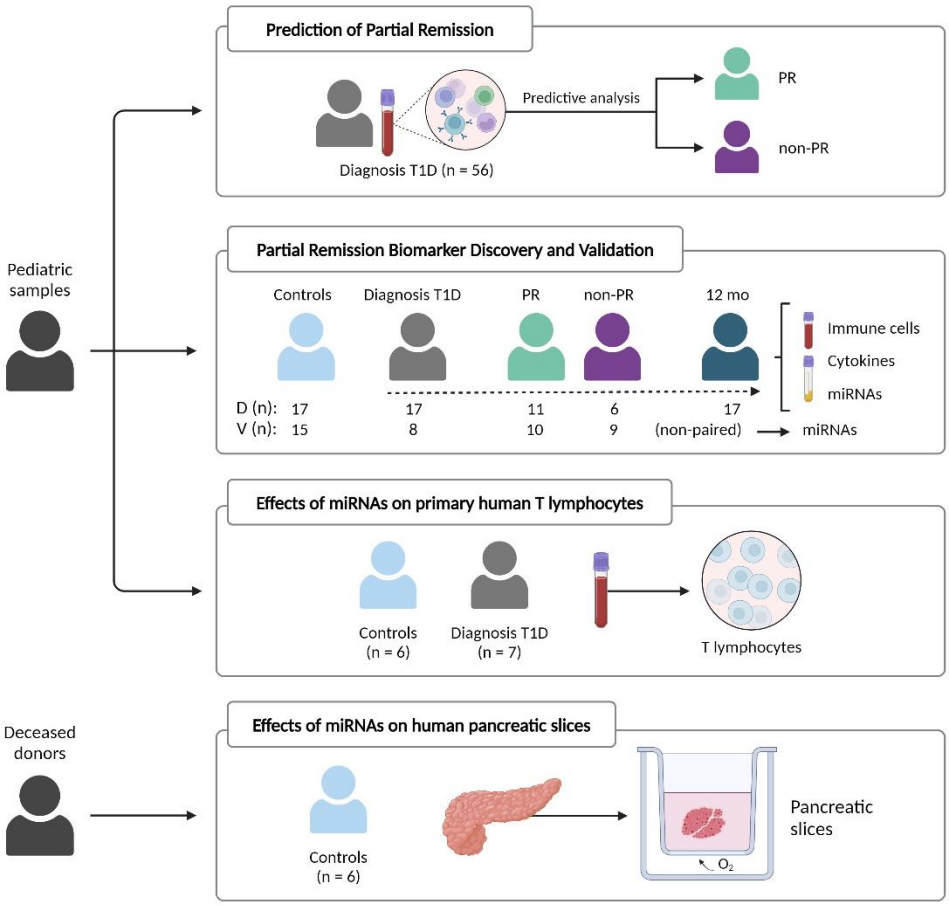

Figure 9. ***Diagram of the distribution of the samples for each experimental objective***. *Samples were collected from non-diabetic children and adolescents (controls) or patients with T1D, who were followed up to detect partial remission (PR). For the predictive study of partial remission, whole blood samples were collected from patients at the time of diagnosis. For the study of new biomarkers, peripheral whole blood and plasma samples were collected from patients with T1D longitudinally at*

different times (diagnosis, PR or non-PR and at 12 months) and from controls. For the validation of miRNAs, plasma samples were collected from unpaired T1D patients at 2 time points (diagnostic and PR or non-PR) and from controls. To observe the effect of miRNAs on the primary culture of human T lymphocytes, peripheral blood samples were obtained from controls and newly diagnosed patients. Finally, for the study of miRNAs on β-cell functionality, pancreatic samples were obtained from deceased control donors. Figure created using BioRender.

1.3. Blood collection, longitudinal T1D follow-up and detection of PR

All patients fulfilled the American Diabetes Association classification criteria for T1D [16], with at least one positive anti-islet autoantibody at disease onset (to IA-2 or GAD65). Inclusion criteria were 1–18 years of age and normal BMI according to the Spanish BMI pediatric cohort growth chart [340]. Exclusion criteria were being under immunosuppressive or anti-inflammatory treatment, T2D, other autoimmune diseases, pregnancy, compromised kidney function, or liver diseases. The same inclusion/exclusion criteria were used for non-diabetic controls.

T1D data collection occurred for over a year in two University Hospitals of our geographical area, Germans Trias i Pujol (Badalona) and Parc Taulí (Sabadell). Blood samples of 6–10 mL were obtained at disease onset, PR (2–7 months after diagnosis) or non-PR (8 months after diagnosis), and after 12 months in EDTA tubes (BD Biosciences, San Jose, CA, USA) and processed immediately. Blood samples from control subjects without T1D were acquired once following the same protocol.

At disease onset, all samples were collected between 1 and 14 days after diagnosis. To measure PR, we calculated the IDAA1c using both the HbA1c value and the insulin requirement as HbA1c (%) + [4 × insulin dose (U/kg/day)]. An IDAA1c equal to or lower than 9 indicated the PR phase [246]. Given that the highest percentage of patients in PR is detected within the first 2–7 months after diagnosis, those who did not meet the criteria of PR after 8 months were defined as non-remitters.

1.4. Clinical and laboratory testing

Clinical descriptors on each patient and control subject were collected, including age, sex, and BMI. Blood samples from patients with T1D were obtained for centralized measurement of HbA1c, basal non-fasting C-peptide (which reflects residual insulin storage), and islet autoantibodies (to IA-2 or GAD65). Insulin requirements were also recorded. HbA1c was determined by high-performance liquid chromatography (ADAMS A1c HA-8180V, Arkray, MN, USA) in all patients at each time point. Basal non-fasting C-peptide was determined by enzyme-linked immunosorbent assay (ELISA) (Architect i2000, Abbott, IL, USA) in both controls and patients at each time point. For the discovery cohort, HLA typing of DRB1 alleles was determined at the Immunology Service by

hybridization with sequence-specific oligonucleotide probes (LABType SSO, One Lambda, CA, USA), following the manufacturer's instructions. According to HLA-DRB1 allele combinations, three groups of HLA-DRB1 genotypes were formed: high-risk (positive for both HLA-DRB1*03 and HLA-DRB1*04 or homozygous for these alleles), moderate risk (positive for HLA-DRB1*03 or HLA-DRB1*04), and neutral risk (negative for HLA-DRB1*03 and HLA-DRB1*04).

2. HUMAN PERIPHERAL BIOMARKER DISCOVERY

In the pursuit of a comprehensive understanding of the PR phase in pediatric patients, we focused first on the determination of leukocyte subsets, cytokines, and miRNAs as potential biomarkers by utilizing a minimally invasive approach through the analysis of a singular blood sample from the discovery cohort.

2.1. Whole blood immunophenotyping by flow cytometry

Initially, seven flow cytometry panels were employed to phenotype up to 55 distinct immune cell subpopulations. Phenotypic analysis of cellular subpopulations was performed in control subjects and patients with T1D at each time point. To that end, fresh venous blood samples of 1–2 mL were washed with 15 mL of FACSFlow Sheath Fluid (ThermoFisher Scientific, Waltham, MA, USA), and 100 µL were stained with specific monoclonal antibodies for 20 min at room temperature and protected from light. The panels of antibodies and the specific markers used to detect each immune cell type can be found in **Tables 2, 3**. After incubation, erythrocytes were lysed for 7 min (Lysing Buffer, BD Biosciences). Samples were then washed and resuspended in FACSFlow Sheath Fluid (ThermoFisher Scientific).

Absolute counts (cells/µL) of leukocytes and lymphocytes were calculated using Perfect Count Microspheres of known concentration (Cytognos SL, Salamanca, Spain) as: $\frac{Number\ of\ cell\ events}{(\text{Bead A events}+\text{Bead B events})} \times \frac{beads}{\mu L}$.

A minimum of 10,000 events per sample and 5,000 beads were acquired using a 3-laser FACS Canto II and a 4-laser LSR Fortessa Flow Cytometers (BD Biosciences) and analyzed using FACSDiva software (BD Biosciences). Necrotic and apoptotic cells were excluded from the analysis based on their forward scatter (FSC)-A/side scatter (SSC)-A properties and doublets were excluded by FSC-A/FSC-H. The gating strategy to analyze specific leukocyte subsets was based on international consensus [341,342] (**Supplementary Figures 1-7**). Fluorescence minus one (FMO) controls were used to define chemokine receptor (CCR)7 expression on Th17 lymphocytes and PTK7 expression on recent thymic

emigrants (RTEs). Furthermore, internal reference populations were used as positivity controls in the analysis of CCR7 vs. CD45RA in panel 1, CD27 vs. CD24 in panel 2, CD19 vs. CD21 in panel 3, CCR4 vs. CCR7 in panel 4, and CD45RO vs. CCR4 plus CD45RO vs. HLA-DR in panel 5. Absolute counts were calculated as follows: (%subset/100) × counts of the main subpopulation.

2.1.1. Predictive analysis of partial remission

To establish associations between immunological (immune cell subset percentages), clinical, and metabolic variables at disease onset and the occurrence of PR, simple logistic regressions were developed. The OR with the 95% CI was reported as a probability measure. Receiver-operating characteristic (ROC) curves were generated from the logistic regressions to obtain the area under the curve (AUC), which is useful for assessing the discrimination ability of the variables. To find statistically significant correlations between different parameters, a two-tailed Pearson's test was used. To create a comprehensive model incorporating the statistically significant immunological variables, an index was constructed using the optimal cut-off values derived from the ROC curves for each variable. A machine learning logistic regression was performed to construct the predictive model, with the sample divided into two parts: 70% was used to obtain the estimates of the index by multiple logistic regressions, while the remaining 30% was used to assess its performance through a confusion matrix. A decision tree was generated to classify patients as remitters or non-remitters, giving as an input the index, age and BMI.

Table 2. ***Monoclonal antibodies used for the immunophenotyping***

	Target	Fluorochrome	Species/Isotype	Clone	Use*	Company
PANEL 1	CD3	Violet 500	Mouse BALB/c IgG_1, κ	UCHT1	2.5 µL	BD Horizon
	CD4	PerCP-Cy5.5	Mouse IgG_1, κ	RPA-T4	1.25 µL	BD Pharmingen
	CD8	APC-H7	Mouse BALB/c IgG_1, κ	SK1	2.5 µL	BD Biosciences
	CD27	Brilliant Violet 421	Mouse IgG_1, κ	0323	2.5 µL	BioLegend
	CD45RA	FITC	Mouse BALB/c IgG_1, κ	L48	5 µL	BD Biosciences
	CCR7	PE-Cy7	Rat IgG_{2a}, κ	3D12	5 µL	BD Pharmingen
	CD31	Alexa Fluor 647	Mouse IgG_{2a}	M89D3	2 µL	BD Pharmingen
	PTK7	PE	Mouse IgG_{2a}, κ	188B	5 µL	Miltenyi Biotec
PANEL 2	CD19	PerCP-Cy5.5	Mouse IgG_1, κ	HIB19	5 µL	BD Pharmingen
	CD24	FITC	Mouse IgG_{2a}, κ	ML5	5 µL	BD Pharmingen
	CD38	PE	Mouse IgG_1, κ	HIT2	5 µL	BD Pharmingen
	CD27	APC	Mouse BALB/c IgG_1	L128	2 µL	BD Biosciences

Continue on next page

	Target	Fluorochrome	Species/Isotype	Clone	Use*	Company
PANEL 3	CD3	Violet 450	Mouse BALB/c IgG_1, κ	UCHT1	2.5 µL	BD Horizon
	CD19	Violet 500	Mouse IgG_1, κ	HIB19	1 µL	BD Horizon
	CD27	APC	Mouse BALB/c IgG_1	L128	2 µL	BD Biosciences
	IgD	FITC	Mouse BALB/c IgG_{2a}, κ	IA6-2	10 µL	BD Pharmingen
	IgM	PerCP-Cy5.5	Mouse IgG_1, κ	G20-127	5 µL	BD Pharmingen
	CD21	PE	Mouse IgG_1, κ	B-ly4	5 µL	BD Pharmingen
PANEL 4	CD4	Violet 450	Mouse IgG_1, κ	RPA-T4	5 µL	BD Horizon
	CCR7	PE-Cy7	Rat IgG_{2a}, κ	3D12	5 µL	BD Pharmingen
	CCR4	Alexa Fluor 647	Mouse C57BL/6 IgG_1, κ	1G1	2 µL	BD Pharmingen
	CCR6	PE	Mouse IgG_1, κ	11A9	1 µL	BD Pharmingen
PANEL 5	CD45	FITC	Mouse IgG_1, κ	HI30	2.5 µL	BD Pharmingen
	CD3	Violet 450	Mouse BALB/c IgG_1, κ	UCHT1	2.5 µL	BD Horizon
	CD4	PerCP-Cy5.5	Mouse IgG_1, κ	RPA-T4	1.25 µL	BD Pharmingen
	CD25	PE	Mouse BALB/c IgG_1, κ	M-A251	5 µL	BD Pharmingen
	CD127	Alexa Fluor 647	Mouse IgG_1, κ	HIL7R-M21	10 µL	BD Pharmingen
	CD45RO	APC-H7	Mouse BALB/c IgG_{2a}, κ	UCHL1	2.5 µL	BD Pharmingen
	CCR4	PE-Cy7	Mouse C57BL/6 IgG_1, κ	1G1	2.5 µL	BD Pharmingen
	HLA-DR	Violet 500	Mouse IgG_{2a}, κ	G46-6	2.5 µL	BD Horizon
PANEL 6	CD3	PerCP	Mouse BALB/c IgG_1, κ	SK7	8 µL	BD Biosciences
	CD4	Violet 450	Mouse IgG_1, κ	RPA-T4	5 µL	BD Horizon
	CD8	APC-H7	Mouse BALB/c IgG_1, κ	SK1	2.5 µL	BD Biosciences
	αβ TCR	FITC	Mouse BALB/c IgM, κ	T10B9	10 µL	BD Pharmingen
	γδ TCR	PE	Mouse IgG_1, κ	B1	10 µL	BD Pharmingen
PANEL 7	CD45	Alexa Fluor 700	Mouse IgG_1, κ	HI30	0.5 µL	BioLegend
	CD19	APC-H7	Mouse IgG_1, κ	HIB19	2.5 µL	BD Pharmingen
	CD3	APC-H7	Mouse BALB/c IgG_1, κ	SK7	2.5 µL	BD Biosciences
	CD14	Violet 450	Mouse BALB/c IgG_{2b}, κ	MφP9	2.5 µL	BD Horizon
	CD16	APC	Mouse BALB/c IgG_1, κ	B73.1	5 µL	BD Pharmingen
	Slan	FITC	Mouse IgM, κ	DD-1	2 µL	Miltenyi Biotec
	HLA-DR	Violet 500	Mouse IgG2a, κ	G46-6	2.5 µL	BD Horizon
	CD11c	PE-Cy7	Mouse BALB/c IgG_1, κ	B-ly6	2.5 µL	BD Pharmingen
	CD123	PerCP-Cy5.5	Mouse IgG_{2a}, κ	7G3	2.5 µL	BD Pharmingen
	CD56	PE	Mouse IgG_1, κ	MY31	5 µL	BD Biosciences

*Use/100µL

PerCP-Cy5.5: peridinin-chlorophyll-cyanine 5.5; APC-H7: allophycocyanin-hilite 7; FITC: fluorescein isothiocyanate; PE-Cy7: phycoerythrin-cyanine 7; PE: phycoerythrin; APC: allophycocyanin; PerCP: peridinin-chlorophyll-protein

Table 3. ***Specific markers for phenotypic characterization of immune cell subpopulations***

Immune cell subsets	Phenotype	Immune cell subsets	Phenotype
T lymphocytes		**B lymphocytes**	
CD4⁺ T cells	**CD3⁺CD4⁺**	**B cells**	**CD3⁻CD19⁺**
CD127⁻CD25⁺ T_{reg} cells	CD3⁺CD4⁺CD127$^{-/low}$ CD25^{hi}	Naïve B cells	CD3⁻CD19⁺CD27⁻IgD⁺ IgM⁺
Memory T_{reg} cells	CD3⁺CD4⁺CD127$^{-/low}$ CD25^{hi}CD45RO⁺CCR4⁺	Immature naïve B cells	CD3⁻CD19⁺CD27⁻IgD⁺ IgM⁺CD21⁻
Activated T_{reg} cells	CD3⁺CD4⁺CD127$^{-/low}$ CD25^{hi}CD45RO⁺CCR4⁺HLA-DR⁺	CD21$^{-/low}$ naïve B cells	CD3⁻CD19⁺CD27⁻IgD⁺ IgM⁺CD21^{low}
Naïve CD4⁺ T cells	CD3⁺CD4⁺CCR7⁺CD45RA⁺ CD27⁺	Mature naïve B cells	CD3⁻CD19⁺CD27⁻ IgD⁺IgM⁺CD21⁺
RTEs	CD3⁺CD4⁺CCR7⁺CD45RA⁺ CD27⁺CD31⁺PTK7⁺	Exhausted memory B cells	CD3⁻CD19⁺CD27⁻IgD⁻ IgM⁻
CM CD4⁺ T cells	CD3⁺CD4⁺CCR7⁺CD45RA⁻ CD27⁺	Unswitched memory B cells	CD3⁻CD19⁺CD27⁺IgD⁺ IgM⁺
Late EM CD4⁺ T cells	CD3⁺CD4⁺CCR7⁻CD45RA⁻ CD27⁻	IgM memory B cells	CD3⁻CD19⁺CD27⁺IgD⁻ IgM⁺
Early EM CD4⁺ T cells	CD3⁺CD4⁺CCR7⁻CD45RA⁻ CD27⁺	Switched memory B cells	CD3⁻CD19⁺CD27⁺IgD⁻ IgM⁻
CD4⁺ T_{EMRA} cells	CD3⁺CD4⁺CCR7⁻CD45RA⁺ CD27⁻	Plasmablasts	CD19⁺CD27^{hi}CD38^{hi}
Th17	CD4⁺CCR7⁻CCR4⁺CCR6⁺	B_{reg} cells	CD19⁺CD27⁺CD24^{hi}
CD8⁺ T cells	**CD3⁺CD8⁺**	Total transitional B cells	CD19⁺CD27⁻CD38^{hi} CD24^{hi}
Naïve CD8⁺ T cells	CD3⁺CD8⁺CCR7⁺CD45RA⁺ CD27⁺	Transitional T1 B cells	CD19⁺CD27⁻CD38^{hi} CD24^{hi}
CM CD8⁺ T cells	CD3⁺CD8⁺CCR7⁺CD45RA⁻ CD27⁺	Transitional T2 B cells	CD19⁺CD27⁻CD38^{hihi} CD24^{hihi}
Late EM CD8⁺ T cells	CD3⁺CD8⁺CCR7⁻CD45RA⁻ CD27⁻		
Early EM CD8⁺ T cells	CD3⁺CD8⁺CCR7⁻CD45RA⁻ CD27⁺		
CD8⁺ T_{EMRA} cells	CD3⁺CD8⁺CCR7⁻CD45RA⁺ CD27⁻		
αβ TCR cells	**CD3⁺αβ⁺**		
αβ TCR CD4⁺ cells	CD3⁺αβ⁺CD4⁺		
αβ TCR CD8⁺ cells	CD3⁺αβ⁺CD8⁺		
αβ TCR DP cells	CD3⁺αβ⁺CD4⁺CD8⁺		
αβ TCR DN cells	CD3⁺αβ⁺CD4⁻CD8⁻		
γδ TCR cells	**CD3⁺γδ⁺**		
γδ TCR CD4⁺ cells	CD3⁺γδ⁺CD4⁺		
γδ TCR CD8⁺ cells	CD3⁺γδ⁺CD8⁺		
γδ TCR DP cells	CD3⁺γδ⁺CD4⁺CD8⁺		
γδ TCR DN cells	CD3⁺γδ⁺CD4⁻CD8⁻		
		NK cells	
		NK cells	**CD3⁻CD19⁻CD14⁻CD56⁺**
		NK_{reg} cells	CD3⁻CD19⁻CD14⁻CD56^{bri} CD16⁻
		NK_{eff} cells	CD3⁻CD19⁻CD14⁻CD56^{dim} CD16⁺
		Intermediate NK cells	CD3⁻CD19⁻CD14⁻CD56^{bri} CD16⁺
		CD56^{dim}CD16⁻ NK cells	CD3⁻CD19⁻CD14⁻CD56^{dim} CD16⁻
Monocytes		**DCs**	
Monocytes	**CD3⁻CD19⁻CD14⁺**	**DCs**	**CD3⁻CD19⁻CD14⁻CD56⁻ HLA-DR⁺**
Non-classical CD16⁺ monocytes	CD3⁻CD19⁻CD14⁺CD16⁺	pDCs	CD3⁻CD19⁻CD14⁻CD56⁻ HLA-DR⁺CD123⁺CD11c⁻
Classical monocytes	CD3⁻CD19⁻CD14⁺CD16⁻	mDCs	CD3⁻CD19⁻CD14⁻CD56⁻ HLA-DR⁺CD123⁻CD11c⁺
		Slan⁻CD16⁻ mDCs	CD3⁻CD19⁻CD14⁻CD56⁻ HLA-DR⁺CD123⁻ CD11c⁺slan⁻CD16⁻
		Slan⁻CD16⁺ mDCs	CD3⁻CD19⁻CD14⁻CD56⁻ HLA-DR⁺CD123⁻CD11c⁺ slan⁻CD16⁺
		Slan⁺CD16⁺ mDCs	CD3⁻CD19⁻CD14⁻CD56⁻ HLA-DR⁺CD123⁻CD11c⁺ slan⁺CD16⁺

2.2. Plasma cytokine quantification

Cytokines are low molecular weight (<30 kDa) proteins secreted by leukocytes and other cells that play a very prominent role in regulating the immune system. Aside from immune cell variations along T1D natural history and PR, cytokines can also inform us about the inflammatory status of the patient and serve as biomarkers of disease progression. Here, we decided to analyze the concentration of some inflammatory (IL-2, IL-6, and IL-17A) and anti-inflammatory (IL-10, TGF-β) cytokines.

2.2.1. Plasma isolation

Plasma samples were always obtained within the first hour after venipuncture. The tube containing 4–5 mL of blood was centrifuged at 1900×g at 4°C for 10 min. The plasma was then transferred to a 1.5 mL Eppendorf (without disturbing the intermediate layer containing white blood cells and platelets) and centrifuged at 16,000×g at 4°C for another 10 min to remove additional cellular nucleic acids bound to cellular debris. Finally, 250 µL of clear plasma was pipetted into a 1.5 mL Eppendorf and stored at −80°C.

2.2.2. Cytometric Bead Array

To measure the concentration of IL-2, IL-6, IL-10, and IL-17A in plasma samples, the BD Cytometric Bead Array Human Enhanced Sensitivity Flex Sets (BD Biosciences) was used. This is a flow cytometry-based assay used for the simultaneous detection of multiple analytes in a single sample. The assay is based on four capture beads with distinct fluorescence intensities (read in a red channel of a flow cytometer), each coated with specific antibodies for a single targeting cytokine. These beads are mixed with the samples and incubated with PE-conjugated detection antibodies, which recognize different epitopes on the cytokines, to form sandwiched complexes. By measuring the intensity of PE fluorescence, the concentration of each analyte in the sample can be quantified. Briefly, human cytokine standards were reconstituted (200,000 fg/mL) and diluted serially in three-fold steps to 1:729 dilution (274 fg/mL), and the four capture beads were thoroughly vortexed and mixed. Then, standards or samples, the pooled capture beads and detection reagents were added to 96-well round bottom plates (Labclinics, Barcelona, Spain). After appropriate incubations at room temperature, wash buffer was added to wash the plate once (400×g, 5 min at room temperature), the supernatant was discarded and 150 µL of wash buffer was added to resuspend beads and cells before acquisition. Samples were acquired with FACS LSR Fortessa (BD Biosciences). The theoretical limit of detection was 13.7 fg/mL for IL-10, 26.1 fg/mL for IL-17A, 88.9 fg/mL for IL-2 and 68.4 fg/mL for IL-6. Data were analyzed using FCAP Array software.

2.2.3. Enzyme-linked immunosorbent assay

To measure the concentration of TGF-β1 in plasma samples, the Human TGF-β1 ELISA Kit (FineTest, Wuhan Fine Biotech, Wuhan, China) was used. Briefly, anti TGF-β1 antibody was pre-coated onto the 96-well plate. Then, the standards and samples were added to the wells. After 90 min incubation, unbound conjugates were removed by wash buffer. Then, a biotinylated detection antibody for TGF-β1 was added to bind with TGF-β1 conjugated on coated antibody, forming a sandwich complex. After washing off unbound conjugates, horseradish peroxidase (HRP)-streptavidin was added. After a third washing, 3,3′,5,5′-tetramethylbenzidine (TMB) substrates were added since they are catalyzed by HRP to produce a blue color product that turned yellow after adding a stop solution. Finally, the optical density (OD) absorbance was read at 450 nm in a microplate reader. The concentration of TGF-β1 in the sample was calculated by drawing a standard curve, being the concentration of the target substance proportional to the OD_{450} value. The theoretical detection range was 31.25–2,000 pg/mL.

2.3. Plasma microRNA expression profile through small RNA-seq

To elucidate the differential plasmatic miRNA profile during the PR phase, RNA extracted from the discovery cohort was used to prepare sequencing libraries. Small RNA-seq was then executed, revealing a signature of DEMs, along with their respective targets and associated biological processes and pathways. In this way, genes with key activities in the metabolic and immunological processes associated with T1D can be identified. Thereafter, the differential expression of some miRNAs was validated using reverse transcription–quantitative polymerase chain reaction (RT-qPCR) in a validation cohort (**Figure 10**).

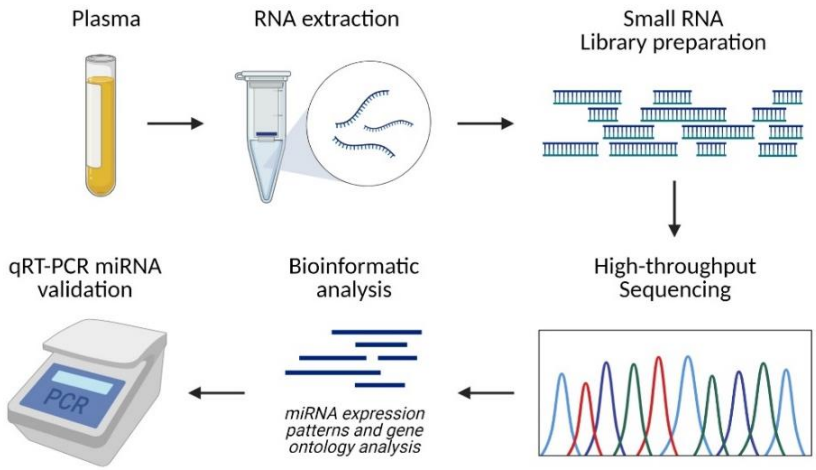

Figure legend on next page

Figure 10. ***Workflow for small RNA-seq and its validation***. *From the plasma samples of the discovery cohort, total RNA, including miRNAs, was extracted and a library of small RNAs was prepared. The libraries were then sequenced on the Illumina® platform and bioinformatics analysis was performed to see the differentially expressed miRNAs (DEMs) during the PR phase. The target genes of these miRNAs and the biological processes and pathways associated with them were analyzed. Finally, the differential expression of some of these miRNAs was confirmed by RT-PCR on plasma samples from the validation cohort. Figure created using BioRender.*

2.3.1. Total RNA isolation from plasma

Total cell-free and exosomal RNA, including miRNA, was isolated from 200 µL of plasma using the miRNeasy Serum/Plasma Advanced Kit (Qiagen, Hilden, Germany), according to the manufacturer's instructions. Briefly, 200 µL of plasma were mixed with a lysis buffer to release and stabilize RNA from plasma proteins and extracellular vesicles. The sample was next mixed with a protein precipitation buffer and incubated for 3 min at room temperature. Then, the precipitate is pelleted by centrifuging at 12,000×g for 3 min at room temperature and isopropanol is added to the supernatant to provide the appropriate conditions for RNA molecules to bind to the silica membrane. The sample is transferred to the RNeasy UCP MinElute spin column, where RNA binds to the membrane and other contaminants are washed away in subsequent wash steps. After drying the membrane by centrifugation at full speed, RNase-free water was added to recover RNA. RNA purity, integrity and concentration were determined using TapeStation 2200 (Agilent High Sensitivity Screen Tape, Agilent Technologies Inc., Santa Clara, CA, USA). RNA was stored at −80°C until use.

2.3.2. Small RNA library preparation, sequencing and data analysis

After the isolation of RNA, 1 µg was used to prepare RNA libraries by D-Plex Small RNA-seq Kit (Diagenode, Liege, Belgium), following the manufacturer's instructions. After PCR amplification, size selection of fragments and adapter dimer removal were conducted in a 6% polyacrylamide gel (Invitrogen, Carlsbad, CA, USA), and library quality controls were assessed with a TapeStation 2200 using a High Sensitivity D1000 Screen Tape (Agilent Technologies Inc). Then, small RNA libraries were sequenced on the Illumina® NextSeq 1000 System (SBS-based sequencing technology, Illumina, San Diego, CA, USA) in a run of 92 and 2×71 cycles and a high output sequencing mode. Data were retrieved from the sequencer in the form of fastq files. The fastq files of the same sample corresponded to different runs of the same library. In this study, up to six runs were performed for each sample to achieve the desired sequencing depth (ranging from 1.6 to 35.1 million reads depending on the sample). Samples were randomly distributed among the six sequencing runs regardless of the group to which they belong.

Trimming steps were further conducted using the Cutadapt tool. This trimming included the removal of the first 16 bp of each read (corresponding to unique molecular identifiers), the polyA tail, and Illumina® adapter sequences. Additionally, trimmed sequences of less than 18 bp in length were discarded. After trimming, the quality of the reads (Fastq files) was assessed with FastQC. All the reads were treated as single-end reads, a fact that allowed merging the reads from different runs according to their sample of origin with the multiQC tool. Next, the Subread/Rsubread package was used to map the sequencing reads to the genome of reference (hg38) and quantify the aligned reads. For the read summarization/quantification step, annotations for precursor and mature miRNAs were obtained from the miRBase v22 database. First, mapped reads were quantified using the mature miRNA annotations contained in miRBase only. Then, unassigned reads were further quantified using the remaining small RNA annotations from miRBase (for pre-miRNA) and Gencode (for other small non-coding RNAs) databases. Filtering and normalization steps were performed using *edgeR* 3.34.1 and *Limma* v.3.48.3 packages from Bioconductor in R. Here, a minimal rule was applied to keep only transcripts that had at least one count per million in at least five samples, and the trimmed mean of M-values normalization method was performed to eliminate composition biases between libraries. Different types of quality controls were also performed (multi-dimensional scaling plot analysis, Euclidean distances between samples) to check that the normalized data were appropriate for the differential expression analysis; by doing so, no outliers or batch effects were detected.

For differential expression testing, the *Limma's* package v.3.48.3 was used, specifically the limma-voom pipeline. Normalized data were transformed to log2, and DEMs were selected by adjusting a linear model with empirical Bayes moderation of the variance and, in the case of paired samples, a paired design was considered. Data were adjusted for multiple testing to obtain strong control over the false discovery rate (FDR) using the Benjamini and Hochberg method; however, since these criteria yield too few small RNAs, unadjusted p-values of ≤0.05 were considered for the significance criteria. Therefore, miRNAs with a p-value ≤0.05 and $\log_2$(fold change(FC)) >1 were considered upregulated, whereas those with $\log_2$(FC) <1 were considered downregulated. The data for this study were deposited in the European Nucleotide Archive at EMBL-EBI under accession number PRJEB58187 (https://www.ebi.ac.uk/ena/browser/view/PRJEB58187, accessed on 22 December 2022).

2.3.3. Gene targets for microRNAs

In this study, the multiMiR Bioconductor's package was used to identify miRNA target sites in different databases (miRecords, miRTarBase, and TarBase for validated targets; DIANA-microT, ElMMo, MicroCosm, miRanda, miRDB, PicTar, PITA, and TargetScan for predicted targets). In order to classify the vast number of gene targets for each miRNA, a list of keywords was generated and distributed in three different groups: metabolism, regeneration, and immune system. In this way, the metabolism group was composed of keywords like "mTOR signaling" or "insulin signaling pathway", while the immune system group was composed of words such as "T cell activation" or "dendritic cell" (**Supplementary Table 1**). Then, using a computer logarithm, the Entrez summary of each gene was searched for those keywords, and the genes were consequently classified into one group or another.

2.3.4. Gene ontology and Pathway analysis

miRNA gene ontology (GO) and pathway analysis were performed using the open-access web server DIANA-miRPath v3.0 (http://www.microrna.gr/miRPathv3, accessed on 13 September 2022) [343] using the DEMs with validated target genes between PR and non-PR groups to search for potential biological pathways under their regulation. Biological processes and enriched pathways were investigated using the DIANA-TarBase v7.0 [344], a database that provides high-quality, manually curated and experimentally validated miRNA–target interactions. Significance levels were calculated by using Fisher's exact test meta-analysis method with Benjamini–Hochberg's FDR correction (q-value ≤0.05). The statistically significant biological processes and their corresponding q-values were introduced in the web server REVIGO (http://revigo.irb.hr/) [345], which takes long lists of GO terms and summarizes them by removing the redundant ones. Interactive graphs showing the relationship between biological processes link highly similar GO terms by edges (using the SimRel semantic similarity measure), where the line width indicates the degree of similarity, and the color of the bubbles is the user-provided p-value.

Functional enrichment analysis of miRNA target genes was performed using pathway annotation from the Kyoto Encyclopedia of Genes and Genomes (KEGG) database and a posteriori of the statistical analysis. In this mode, the server identifies all the significantly targeted pathways by the selected miRNAs. The enrichment analysis is first carried out by the server, and the significance levels (p-values) between each miRNA and each pathway are computed. Subsequently, for each pathway a merged p-value is extracted by combining the previously calculated significance levels using the Fisher's exact test meta-analysis method and Benjamini–Hochberg's FDR (q-value) to compensate for

multiple testing. Since comparable miRNAs are clustered together, the heatmap makes it possible to identify miRNA subclasses or pathways that define them.

2.3.5. Validation of microRNAs by RT-qPCR

To validate the small RNA-seq results, a RT–qPCR was performed on human plasma samples from the validation cohort. Because plasma samples hemolyzed during acquisition can be contaminated by erythrocyte miRNAs [346], the degree of hemolysis was determined based on the optical density at 414 nm (absorbance peak of free hemoglobin) by spectrophotometry (Nanodrop 1000 Spectrophotometer, ThermoFisher Scientific), and the severely hemolyzed samples (OD_{414} >0.3) were discarded (**Supplementary Figure 8**). Then, RNA isolation was conducted as described above. RNA was reverse transcribed to complementary DNA (cDNA) with the TaqMan™ Advanced miRNA cDNA Synthesis Kit (ThermoFisher Scientific) following the manufacturer's instructions and by using the Veriti® Thermal Cycler (ThermoFisher Scientific). To monitor retrotranscription reproducibility, we spiked in 5'-phosphorylated Arabidopsis thaliana miR-159a (ath-miR-159a, uuuggauugaagggagcucua), a synthetic oligonucleotide for exogenous control (ThermoFisher Scientific), to cDNA synthesis. Briefly, poly(A) polymerase was used to add a 3'-adenosine tail to the miRNA, which underwent adaptor ligation at the 5' end. Then, a Universal RT primer (which also incorporates an adaptor) bound to the 3' poly(A) tail and the miRNA was reverse transcribed. To improve the detection of low-expressing miRNA targets, the cDNA was next pre-amplified using the Universal forward and reverse miR-Amp Primers (which bind to the adaptors) and miR-Amp Master Mix (ThermoFisher Scientific). The 50 µL miR-Amp reaction product was stored at −20°C until use. Amplified cDNA was 1:10 diluted, and miRNAs were profiled by RT-qPCR using the TaqMan™ Fast Advanced Master Mix (Applied Biosystems, Waltham, MA, USA) with TaqMan Advanced miRNA Assays (ThermoFisher Scientific) in 15 µL PCR reactions in triplicate. In detail, each well from the 96-well plate (96 Well Lightcycler plate, Sarstedt, Nümbrecht, Germany) contained 3.75 µL of the diluted cDNA and a PCR reaction mixture prepared with 0.75 µL of the TaqMan probe, 7.5 µL of the TaqMan Master Mix and 3 µL of RNase-free water. **Table 4** shows the list of the TaqMan Assays used. MiRNAs to validate were chosen based on (1) the number of reads obtained in the small RNA-seq and their wide expression in most of the samples (>70%), (2) miRNAs most differentially expressed between PR and non-PR patients, and (3) target genes involved in immune system functions.

Table 4. ***List of TaqMan Assays used for analyzing miRNA expression in plasma***

Gene	Assay ID
hsa-miR-142-3p	477910_mir
hsa-miR-20b-5p	477804_mir
hsa-miR-17-5p	478447_mir
hsa-let-7b-5p	478576_mir
hsa-let-7c-5p	478577_mir
hsa-miR-106b-5p	478412_mir
ath-miR159a	478411_mir
hsa-miR-16-1-3p	478727_mir

Plates were centrifuged at 1000 rpm for 1 minute and run on a LightCycler®480 RT-PCR machine (Roche, Mannheim, Germany) following these settings (**Table 5**):

Table 5. ***Thermal cycling conditions for the PCR reaction to detect miRNA expression***

Step	Temperature	Time	Cycles
Enzyme activation	95°C	20 seconds	1
Denature	95°C	3 seconds	40
Anneal / Extend	60°C	30 seconds	

All analyzed miRNAs showed a cycle threshold (C_t) <30. Relative values were calculated with the $2^{-\Delta Ct}$ method [347], and results are given as arbitrary units. Currently, a universally accepted normalization strategy based on endogenous miRNAs is still lacking. NormFinder, an algorithm for identifying the optimal normalization gene among a set of candidates [348], was used to identify the most stable miRNA within our normalized small RNA-seq data to be used as an endogenous control. In our case, the miRNA with the best stability value was miR-16-1-3p. Raw Ct of miR-16-1-3p in samples from the validation cohort can be found in **Supplementary Figure 9**.

3. MIRNA-MEDIATED IMMUNE REGULATION AND β-CELL NEOGENESIS

Based on the bioinformatic results and considering that it is the most differentially expressed miRNA during the PR phase in comparison to the non-remission, miR-30d-5p was chosen to study its role in regulating both immune system responses and β-cell recovery using *in vitro* methodologies.

3.1. Effect of microRNAs on primary human T lymphocytes

To evaluate the immunoregulatory effect of miRNAs on the immune system, an electroporation protocol was set up. Briefly, T lymphocytes were isolated from peripheral blood mononuclear cells (PBMCs) obtained from venous blood samples and activated for 3 days. After being stimulated, electroporation of the miR-30d-5p inhibitor was performed. After one day of incubation, the phenotype of these cells was analyzed and a restimulation was carried out with the remaining cells to evaluate their proliferative and cytokine secretion capacity after two more days of culture (**Figure 11**).

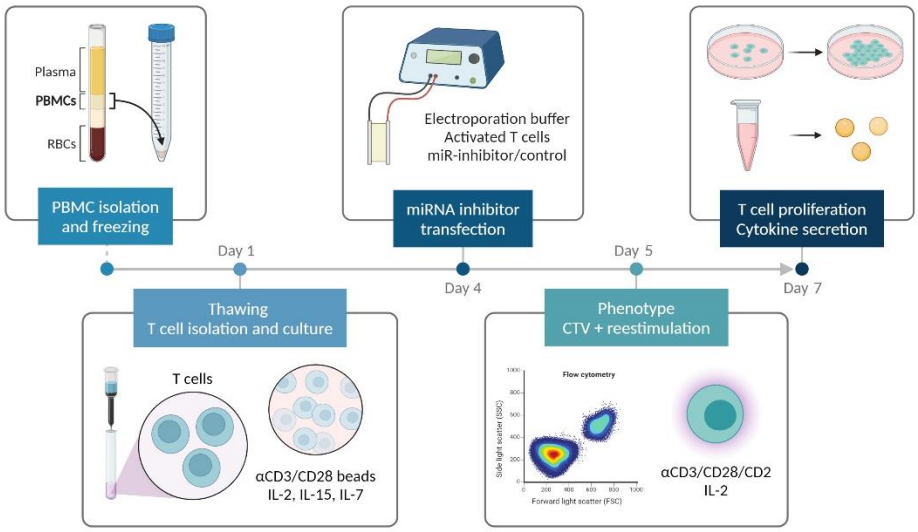

Figure 11. ***Workflow for electroporation of T lymphocytes and subsequent analysis of their phenotype, molecule secretion and proliferation.*** *PBMCs were isolated from the whole peripheral blood sample and frozen until use. On the first day of the protocol, T cells were isolated by negative magnetic sorting from PBMCs and cultured for three days in the presence of activation beads (anti-CD3/CD28), IL-2, IL-7 and IL-15. After activation, electroporation with miRNA inhibitor or inhibitor control was performed. One day after electroporation, their phenotype was analyzed and the remaining T cells were restimulated with soluble anti-CD3/CD28/CD2 antibodies for another two days. Finally, the non-specific proliferation was analyzed along with the cytokine secretion in the supernatant. Figure created using BioRender.*

3.1.1. PBMC isolation and freezing

PBMCs were obtained from up to 10 mL blood samples through Ficoll Paque (GE Healthcare Life Sciences, Marlborough, MA, USA) density gradient centrifugation. First, whole blood was 1:1 diluted with sterile phosphate buffered saline (PBS) 1X (Oxoid Limited, Hampshire, UK), and two volumes of the diluted blood were layered gently on top of one volume of density gradient medium. The tubes were centrifuged at 700×g without brake for 30 min at room temperature. Carefully, cells were harvested by inserting the Pasteur pipette directly through the upper plasma layer to the mononuclear cells at the interface. Cells were washed and then platelets were further removed by centrifugation at 200×g for 15 min at room temperature. The pelleted cells were suspended in PBS+2% fetal bovine serum (FBS) media, and cell viability and number were determined (see next point). The PBMCs obtained were next frozen at 10-20×10^6 cells/mL in a cryopreservation medium prepared with cold FBS+10% dimethyl sulfoxide (DMSO, Sigma-Aldrich, St. Louis, Missouri, USA) for later use. Each cryotube was placed inside a tube filled with cold isopropanol. After 24 hours at -80°C, the samples were kept in liquid nitrogen tanks.

3.1.2. Viability and cell counting

To assess cell viability and counting, 10 µL of cells were incubated with 2 µL of 7-aminoactinomicina D (7-AAD, BD Biosciences) in 50 µL of PBS for 10 min at room temperature and protected from light. Then, 10 µL of Perfect Count Microspheres (Cytognos SL) were added to perform cell counting. Cells were acquired by FACSCanto II flow cytometer (BD Biosciences) using the FACSDiva software (BD Biosciences).

3.1.3. T lymphocyte isolation and culture

First, PBMCs were thawed in pre-warmed RPMI-1640 (Biowest, Nuaille, France) + 10% FBS (Gibco, Invitrogen) (R-10) media and washed twice in PBS+2% FBS by centrifugation at 400×g 5 min at room temperature. Viability and cell number were determined as previously detailed. Then, the human Pan T Cell Isolation Kit (Miltenyi Biotech, Bergisch Gladbach, Germany) was used to collect T cells by negative magnetic isolation. First, the cell pellet is resuspended in 40 µL of cold MACS buffer (PBS+0.5% bovine serum albumin (BSA)) per a maximum of 10^7 total cells. Cells were mixed with 10 µL of biotin-antibody cocktail against CD14, CD15, CD16, CD19, CD34, CD36, CD56, CD123, and CD235a to label all non-T cells. After a 5-minute incubation at 4°C, 30 µL of cold MACS buffer and 20 µL of the microbead cocktail were added in order to magnetically label all non-target cells, which were incubated for 10 min at 4°C. Thereafter, the LS columns were placed in the magnetic field of a QuadroMACS Separator (Miltenyi Biotech) and rinsed with 3 mL

of cold MACS buffer. After hydrating the columns, a minimum of 500 µL of the prepared cell suspension in cold MACS buffer was applied onto the column. The flow-through containing the enriched unlabeled T cells was collected in a 15 mL falcon tube. Next, the column was washed twice with 3 mL each time and the unlabeled T cells were further collected in the same tube.

T lymphocytes were washed at 400×g for 5 min at room temperature and resuspended in 500 µL of complete medium [RPMI-1640 media (Biowest) supplemented with 2 mM L-Glutamine (Sigma), 1 mM sodium pyruvate (ThermoFisher Scientific), 5% male human AB serum (Biowest), 100 IU/mL penicillin (Normon SA, Madrid, Spain), 100 µg/mL streptomycin (Laboratorio Reig Jofré, Sant Joan Despí, Spain) and 0.025 mM of 2-Mercaptoethanol (Sigma)]. Cell number and viability were determined as aforementioned but adding this time 1.5 µL CD3 PE, 0.5 µL CD4 APC, 0.5 µL CD8 FITC to the mix (**Table 6**). CD3 purity was >70% in all cases. T lymphocytes were cultured in 24- or 6-U-bottom well plates (Labclinics) at a concentration of $0.5\text{-}1\times10^6$ cells/mL in complete medium with 100U/mL of IL-2 (PeproTech, Cranbury, NJ, USA), 5 ng/mL of IL-7 (PeproTech), and 5 ng/mL of IL-15 (PeproTech). Moreover, T lymphocytes were stimulated with Dynabeads™ Human T-Activator CD3/CD28 beads (ThermoFisher Scientific) at a concentration of 1:1 (bead:cell). Before adding them, beads were resuspended by vortex for more than 30 seconds and the corresponding volume of beads was washed with at least 1 mL of PBS+0.1% BSA. The tube containing the beads was placed on a magnet for one minute and the supernatant was discarded with a pipette. Finally, the tube was removed from the magnet and the beads were resuspended in the same volume of complete culture medium as the initial volume of beads taken from the vial. T lymphocytes were then incubated in a humidified 5% CO_2 incubator at 37°C for three days.

Table 6. ***Monoclonal antibodies used for viability and T cell proliferation assessment***

Target	Fluorophore	Species/Isotype	Clone	Use/100µL	Company
CD3	PE	Mouse IgG_1, κ	UCHT-1	1	Immunotools
CD4	APC	Mouse IgG_{2a}	EDU-2	1	Immunotools
CD8	FITC	Mouse IgG_1, κ	HIT8a	1	Immunotools

3.1.4. Electroporation of T lymphocytes with miR-30d-5p inhibitor

As T lymphocytes are suspension-grown cells, the best way to ensure transfection of small RNA molecules is by electroporation [349]. Thus, a protocol for electroporation of T lymphocytes was fine-tuned to see the effect of miR-30d-5p on their phenotype, proliferation and cytokine secretion. The first thing to keep in mind is that electroporation is a very aggressive process for the cells, so it is important to ensure good transfection efficiency without impairing viability too much.

After three days of culture, we checked cells noting cell size and shape to make sure that they were not exhausted. T lymphocytes were collected from cultures and the bead/cell suspension was resuspended thoroughly by pipetting to increase cell recovery. After that, the suspension was added to a sterile flow cytometry tube placed inside an EasySep Cell Separation Magnet (STEMCELL Technologies, Vancouver, Canada) for 2 min to separate the beads from the cells. The supernatant containing only the cells was transferred to a new 15 mL falcon tube with the pipette without taking out the tube from the magnet. After collecting all the cells, wells were washed with 1 mL of R-10 and the process was repeated. Subsequently, cells were washed at 400×g for 5 min at room temperature and the supernatant containing the medium with antibiotics was completely removed, since the incorporation of some antibiotics into the cells during the electroporation process can be toxic. The pelleted cells were resuspended in 500 µL – 1 mL of PBS+2% FBS and cell number and viability were determined as aforementioned but adding this time 1.5 µL CD3 PE, 0.5 µL CD4 APC and 0.5 µL CD8 FITC to the mix.

Next, the appropriate volume of cells was taken in order to electroporate cells at a concentration of 5–10×10^6 cells/mL, washed at 400×g for 5 min at room temperature and resuspended in 150-200 µL of Gene Pulser Electroporation Buffer (Bio-rad, Hercules, California, USA). Moreover, when corresponding, 500 nM of miRNA-inhibitor (inhibitor probe hsa-miR-30d-5p, Exiqon Co., Copenhagen, Denmark) or miRNA-inhibitor control (negative control A probe, Exiqon) was added. The mixture is homogenized by pipetting gently up and down and loaded into 0.2 cm gap cuvettes (Bio-rad), which were kept on ice. At this point, it is important to point out that the electroporation is carried out one by one, meaning that cells of one condition are resuspended in the electroporation buffer with the oligonucleotides —if appropriated—, and electroporated before doing the same for other conditions, since 1-minute delay can cause 3-fold reduction in efficiency.

Cuvettes are shacked gently to evenly distribute the cell suspension and the metallic part is cleaned with a paper to remove possible oil stains on the electrodes. Then, cuvettes are placed in the shockpod cuvette chamber of the Gene Pulser Xcell System (Bio-rad).

Cells were electroporated according to the following conditions: square wave protocol, 220 V, 2 ms pulse length, 1 pulse. Immediately after electroporation, T cells were transferred by using a glass Pasteur pipette to the pre-heated recovery medium without antibiotics [RPMI-1640 media (Biowest) supplemented with 2 mM L-Glutamine (Sigma), 1 mM sodium pyruvate (ThermoFisher Scientific), 10% male human AB serum (Biowest), and 0.025 mM of 2-Mercaptoethanol (Sigma)]. T cells were rested for at least 4 hours at 37°C in a humidified 5% CO_2 incubator.

After incubation, cells were washed at 400×g for 5 min at room temperature and the supernatant was completely removed. The pelleted cells were resuspended in 1 mL of complete medium and cell number and viability were determined. Finally, T lymphocytes were cultured in 24 U-bottom well plates (Labclinics) in complete medium with 100U/mL of IL-2 (PeproTech) for one day.

3.1.5. Transfection efficiency measurement

In order to evaluate the transfection efficiency and the functionality of the inhibitor, T cells were transfected as explained above using a miR-30d-5p inhibitor conjugated with 6-Carboxyfluorescein (6-FAM, Exiqon). In this way, both the percentage of T lymphocytes positive for this fluorescent dye and the expression of miR-30d-5p could be assessed by flow cytometry and RT-qPCR, respectively, 4 and 24 hours after electroporation.

For the first point, cells were collected at the corresponding times and centrifuged at 400×g for 5 min at room temperature. The pellet was resuspended in 100 µL of PBS containing 1 µL of CD3 PE (Immunotools) and 4 µL of 7-AAD (BD Biosciences). After incubation at 4°C for 15 min and protected from light, the percentage of 6-FAM positive cells was evaluated using a 3-laser FACS Canto II (BD Biosciences). Cells subjected to electroporation, but without any oligonucleotide in the medium, were used as a negative control (mock).

For the second point, the cells were harvested and pelleted at 400×g for 5 min at room temperature and total RNA, including miRNA, was isolated using the miRNeasy Tissue/Cells Advanced Mini Kit (Qiagen), according to the manufacturer's instructions. Briefly, cells were disrupted by adding a lysis buffer and homogenized by vortexing for 1 minute. Then, the appropriate volume of another lysis buffer was added and mixed thoroughly. After three min of incubation, the homogenized lysate was transferred to a gDNA eliminator spin column to remove genomic DNA by centrifugation. The flow-through containing the RNA was mixed with 1 volume of isopropanol and the sample was transferred to an RNeasy mini column. Four consecutive centrifugations were then carried out, subsequently adding to the column washing buffer, a buffer to precipitate

the proteins and other contaminants, and 80% ethanol to dissolve and wash away the salts. After drying the membrane by centrifugation at full speed, RNase-free water was added to recover RNA. RNA purity, integrity and concentration were determined using TapeStation 2200 (Agilent Technologies Inc). RNA was next reverse transcribed to cDNA with the TaqMan™ Advanced miRNA cDNA Synthesis Kit (ThermoFisher Scientific) following the manufacturer's instructions and by using the Veriti® Thermal Cycler (ThermoFisher Scientific). **Table 7** shows the list of the TaqMan Assays used. Amplified cDNA was 1:5 diluted, and miRNAs were profiled by RT-qPCR using the TaqMan™ Fast Advanced Master Mix (Applied Biosystems) with TaqMan Advanced miRNA Assays (ThermoFisher Scientific) in 15 µL PCR reactions in triplicate (see ***section 2.3.5***.). Relative values were calculated with the $2^{-\Delta\Delta Ct}$ method and gene expression was normalized to the housekeeping gene *5S rRNA*.

Table 7. ***TaqMan Assays used for miRNA expression analysis in human T cells***

Gene	Assay ID
hsa-miR-30d-5p	478606_mir
RNA, 5S ribosomal 1	Hs03682751_Gh

3.1.6. T cell phenotype

After one day of incubation, the activation and maturation status of T cells (**panel 1**) and T cells positive for different immune checkpoint molecules (**panel 2**) were assessed by flow cytometry for each transfection condition. Cells were first collected from the wells, washed, and resuspended in 1–2 mL of PBS to subsequently determine their viability and number (***section 3.1.2***). For phenotype labeling, 0.2×10^6 cells per panel were used. For panel 1, surface staining was carried out with CD3 V500, CD4 V450, CD8 APC-H7, CD25 PE, CD69 BV711, CCR7 PECy7 and CD45RA BV605, and intracellular staining was carried out with FoxP3 FITC. For panel 2, surface staining was carried out with CD3 V500, CD4 APC, CD8 APC-H7, CD200 PE, T cell immunoreceptor with Ig and ITIM domains (TIGIT) BV605, T cell immunoglobulin and mucin domain containing-3 (TIM-3) PECy7, lymphocyte activation gene 3 (LAG-3) PECy5, PD-1 BV711 and CD226 FITC, and intracellular staining was carried out with CTLA-4 BV421. Further information on antibodies used can be found in **Table 8**.

First, the desired number of cells were pelleted and resuspended in 100 µL of 1:1000 times diluted Fixable Viability Stain 575V (BD Biosciences) with PBS. After 15 min of incubation at room temperature and protection from light, cells were washed twice with 1 mL of PBS+2%FBS (400×g, 5 min, at room temperature). Next, surface staining was

performed. Cells were incubated with 100 µL of the appropriate monoclonal antibody mix for 20 min at 4°C in the dark. After incubation, cells were washed twice with 3 mL of PBS (400×g, 5 min, at room temperature). For the intracellular staining, cells were fixed and permeabilized using the True-Nuclear™ Transcription Factor Buffer Set (BioLegend, San Diego, CA, USA).

To do so, pelleted cells were resuspended in 500 µL of Fixation solution (1 fix concentrate: 4 fix diluent) for 1 hour at 4°C in the dark. After the incubation, cells were washed twice with 1 mL of 1X Permeabilization buffer (400×g, 5 min, at room temperature), and the supernatant was discarded. Then, fixed and permeabilized cells were incubated with 1.25 µL of Human TruStain FcX Fc Receptor Blocking Solution (BioLegend) for 15 min at 4°C in the dark followed by another incubation with the corresponding monoclonal antibody (FOXP3 FITC or CTLA-4 BV421) for 40 min at 4°C and protected from light. After that, cells were washed twice with 1 mL 1X Permeabilization buffer at 400×g for 5 min and suspended in 200 µL FACSFlow™ Sheath Fluid. At least 100.000 $CD3^+$ events per sample were acquired using LSR Fortessa flow cytometer (BD Biosciences). Doublets were excluded by FSC-A/FSC-H. FMO controls were used to assess CD25, CD69, FoxP3, CD200, TIGIT, TIM-3, LAG-3, CTLA-4, PD-1, and CD226 staining positivity. The gating strategy can be found in **Supplementary Figures 10-11**. Data were analyzed using FlowJo software (Tree Star Inc., Ashland, OR, USA).

3.1.7. T cell proliferation

The rest of the cells were taken to a final concentration of 2×10^6 cells/mL in pre-warmed PBS and stained with CellTrace Violet (CTV, ThermoFisher Scientific). CTV is used to track cell proliferation by permanently binding cellular proteins and rendering the cell fluorescent. Upon cell division, the dye is evenly distributed between daughter cells, enabling quantification of proliferation through flow cytometry.

Briefly, 1 µL 5 mM CTV stock solution was diluted to 0.62 µM in 8,000 µL PBS and then combined with the cell suspension at a 1:1 volume ratio, resulting in a final working concentration of 0.31 µM CTV and a cell concentration of 1×10^6 cells/mL. After incubation for 20 min at 37°C, any unbound dye was quenched with R-10 medium. Cells were centrifuged at 400×g, 5 min, at room temperature, resuspended in 5 mL of pre-warmed R-10, and incubated for at least 10 min at 37°C to allow ester hydrolysis. T cells were washed in PBS at 400×g for 5 min at room temperature and resuspended in 2 mL of complete medium prior to assessing viability and cell number as abovementioned. Finally, T lymphocytes were cultured per triplicates in 96-well flat-bottom culture plates (Labclinics) at a final concentration of 2.5×10^5 cells/mL in 200 µL of complete medium as a negative control, with 100 U/mL of IL-2 as a basal stimulation condition, or with 12.5

µL/mL of ImmunoCult™ Human CD3/CD28/CD2 T Cell Activator (STEMCELL Technologies) as a second TCR stimulus to further expand them.

Table 8. ***List of antibodies used for T cell immunophenotyping***

	Target	Fluorophore	Species/Isotype	Clone	Use*	Company
PANEL 1	CD3	Violet 500	Mouse BALB/c IgG1, κ	UCHT1	2	BD Biosciences
	CD4	Violet 450	Mouse IgG1, κ	RPA-T4	5	BD Biosciences
	CD8	APC-H7	Mouse BALB/c IgG1, κ	SK1	5	BD Biosciences
	CD25	PE	Mouse BALB/c IgG1, κ	M-A251	1	BD Biosciences
	CD69	BV711	Mouse IgG1, κ	FN50	1	BioLegend
	FOXP3	FITC	Mouse IgG1, κ	206D	2.5	BioLegend
	CCR7	PE-Cy7	Rat IgG2a, κ	3D12	1	BD Biosciences
	CD45RA	BV605	Mouse IgG2b, κ	HI100	1	BD Biosciences
PANEL 2	CD3	Violet 500	Mouse BALB/c IgG1, κ	UCHT1	2	BD Biosciences
	CD4	APC	Mouse IgG2a	EDU-2	5	Immunotools
	CD8	APC-H7	Mouse BALB/c IgG1, κ	SK1	5	BD Biosciences
	CD200	PE	Mouse IgG1, κ	MRC OX-104	5	BD Biosciences
	TIGIT	BV605	Mouse IgG2a, κ	A15153G	1	BioLegend
	TIM-3	PE-Cy7	Mouse IgG1, κ	F38-2E2	5	BioLegend
	LAG-3	PE-Cy5	Mouse IgG1, κ	11C3C65	1	BioLegend
	CTLA-4	BV421	Mouse IgG2a, κ	BNI3	5	BioLegend
	PD-1	BV711	Mouse IgG1, κ	EH12.1	1	BD Biosciences
	CD226	FITC	Mouse IgG1, κ	11A8	1	BioLegend

*Use/100µL. BV: Brillian Violet; PE-Cy5: Phycoerythrin-cyanine 5.

After two more days of expansion in the incubator at 37°C and 5% CO_2, T cell proliferation was assessed in both CD4 and CD8 compartments. After centrifuging the plate at 400×g, 5 min, at room temperature, supernatants of each well were collected and stored at -20°C for further analysis. Cells were then resuspended in 25 µL of the staining mix containing 7-AAD (BD Biosciences), CD3 PE, CD4 APC and CD8 FITC monoclonal antibodies (**Table 6**). After 20-minute incubation at 4°C in the dark, cells were washed as abovementioned in 150 µL of PBS per well and resuspended in 150 µL of PBS. Samples were acquired with FACS LSR Fortessa. Data were analyzed using FlowJo software (Tree Star).

3.1.8. T cell secretion of soluble molecules

Supernatants from re-stimulated T lymphocytes with ImmunoCult™ Human CD3/CD28/CD2 T Cell Activator (STEMCELL Technologies) were collected after the different electroporation conditions (mock, control inhibitor or miR-30d-5p inhibitor) and frozen at −20°C until use. IFN-γ, IL-1β, IL-10, IL-17A, IL-21, IL-4, IL-6, IL-8, CCL5 and TNF-α were quantified using Luminex® multiplex kit (ThermoFisher Scientific). Briefly, antigen standard vials were reconstituted, mixed and diluted serially in four-fold steps. Then, the capture bead mix was added to 96-well round bottom plate and washed, followed by an overnight incubation with the standards or the corresponding samples. The next day, the plate was washed and the detection reagents were added to the plate. After appropriate incubations at room temperature and washing steps, the reading buffer was added before acquisition. TGF-β1 was measured using Luminex® simplex kit (ThermoFisher Scientific) following the manufacturer's instructions. In this case, samples were pre-treated with 1N HCl and 1.2N NaOH/0.5M HEPES to obtain the immunoreactive form of mature TGF-β1. Samples were analyzed using Luminex® 200.

3.2. Effect of miRNAs on human pancreatic slices

To evaluate the effect of miRNAs on β-cell functionality and regeneration, a transfection protocol was set up. Briefly, HPSs were obtained or cut from non-diabetic deceased donor's pancreatic tissue. HPSs were transfected with miR-30d-5p inhibitor/mimic to see changes in gene expression and C-peptide secretion. To track β-cell neogenesis, transfected slices were first cotransduced with recombinant adenoviruses to tag β-cells in blue and non-β-cells in red, and treated or not for 5 days with bone morphogenetic protein (BMP)-7, a TGF-β family member associated with regeneration in multiple organs [350–352] (**Figure 12**).

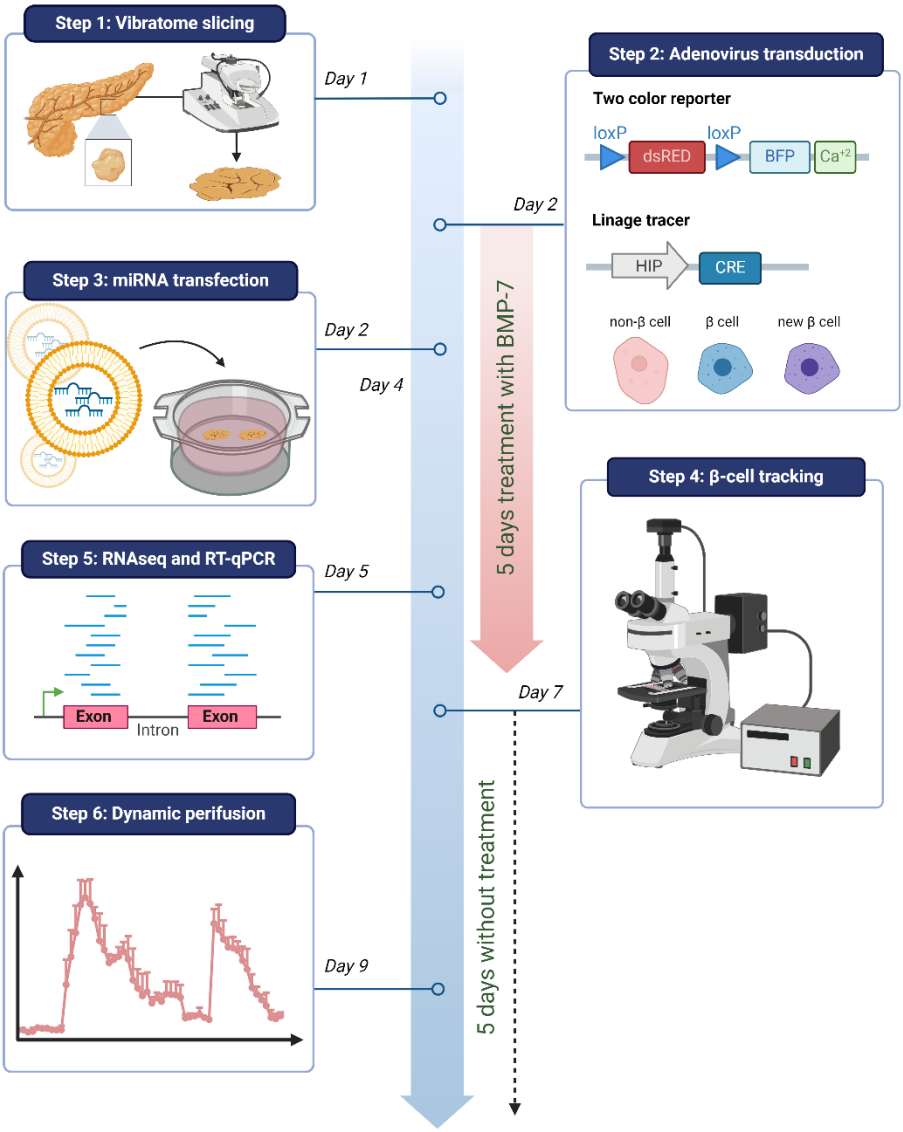

Figure 12. ***Workflow of the different experiments with human pancreatic slices.*** *Human pancreatic slices (HPSs) are obtained by making 120 µm slices from a small piece of agarose-embedded pancreas with a vibratome. For β-cell neogenesis experiments, the slices were transduced with reporter and lineage tracer adenoviruses. As a positive control, slices were treated for five consecutive days with BMP-7. Two days after transduction, when appropriate, slices were transfected with the miRNA mimic or inhibitor or their corresponding controls (day 4). On the seventh day, the appearance of new β-cells was followed by microscopy, taking pictures every day for five more days. For bulk RNA-seq experiments, the slices were transfected and after three days the RNA was extracted. For the dynamic perifusion experiments, they were transfected and kept in culture for one week and after the perifusion, the fluid with the analyte of interest (C-peptide) was collected for ELISA analysis. Figure created using BioRender.*

3.2.1. Human pancreatic tissue slicing and culture

Tissue pieces of approximately 2 g were obtained from the pancreas body-tail juncture and placed into cold Euro-Collins Solution (ECS: 125 mM NaCl, 2.5 mM KCl, 26 mM NaHCO3, 1.25 mM NaH2PO4, 1 mM MgCl2, 2 mM CaCl2, 10 mM HEPES, 3 mM glucose, pH 7.4), supplemented with 0.5 g BSA (Sigma Aldrich), 10 µg/mL aprotinin (Sigma Aldrich, St. Louis, MO), 100 µg/mL trypsin inhibitor from *Glycine max* (Sigma Aldrich), 10 µg/mL chymostatin (solubilized initially in DMSO; Sigma Aldrich) and 1% penicillin-Streptomycin-Amphotericin B solution (Sigma Aldrich). Tissue pieces were cut into smaller tissue blocks and fibrotic, adipose and/or connective tissue were removed. Tissue blocks of approximately 5 mm^3 were then embedded in warm low-melting-point agarose (3%, Sigma Aldrich). After allowing to set in a refrigerator for 5-10 min, cubes with the embedded tissue were cut and mounted on a vibratome holder using superglue. Then, the holder was connected to the tray of a semiautomatic vibratome (Leica VT1200S, Leica Biosystems, Wetzlar, Germany) and filled with cold supplemented ECS solution. Tissue slicing was performed at a step size of 120 µm, speed of 0.1 mm/s, amplitude of 1 mm, and an angle of 15 degrees. Slices were placed using a brush into a 60-mm Petri dish containing washing medium [DPBS (Sigma Aldrich), 1X B27 supplement minus-insulin (Invitrogen, Carlsbad, CA), 1X penicillin-streptomycin-amphotericin B solution, 100 µg/mL trypsin inhibitor from *Glycine max*, 10 µg/mL aprotinin, 10 µg/mL chymostatin and 5.5 mM D-glucose (Sigma Aldrich)].

After slices were generated, they were cultured for up to 12 hours in human slice culture medium atop AirHive dishes (made to order by Biorep, Miami, FL) in an incubator at 30°C and 5% CO_2 atmosphere. This medium contains basal BrainPhys neuronal medium (Stemcell Technologies, Vancouver, BC) supplemented with 2% B27 supplement minus-insulin, 1% penicillin-Streptomycin-Amphotericin B solution, 1% Glutamax supplement (Invitrogen), L-Glutamic Acid 3.7 mg/mL (Sigma Aldrich), 5.5 mM final D-glucose concentration (of note, BrainPhys already contains 2.5 mM D-Glucose), 100 mg/mL trypsin inhibitor from *Glycine max*, 10 mg/mL aprotinin, 10 mg/mL chymostatin, and 1% HEPES buffer (Invitrogen). Dishes containing slices (maximum 3 slices per dish in 3 mL) were kept for a maximum of 2 weeks. The use of aprotinin (inhibits serine proteases) and chymostatin (inhibits a wide range of proteinases) was crucial for reducing degradation and maintaining the viability and function of tissue slices over the long term, compared to earlier medium formulations [353].

3.2.2. Tissue viability

Viability was assessed immediately after slicing, prior to RNA extraction and at the end of the culture. Cell viability within the tissue slices was evaluated by both live/dead immunofluorescence staining (Live/Dead Cell Imaging Kit [488/570], Thermo Fisher) and mitochondrial staining (BioTracker™ 633 Red Mitochondria Dye, Sigma-Aldrich). First, a 200 µM stock solution of the red mitochondria dye was generated by resuspending the powder in DMSO and keeping it at -20°C until use. Then, live green (Component A) and dead red (Component B) were mixed to create a 2X working solution. The solution was diluted to 1X with warm human slice culture medium containing 100 nM of the red mitochondria dye. After mixing, one slice was incubated in this staining solution for 15–20 min at 37°C. Slices were then transferred to 35 mm dishes containing a number-zero confocal grade crystal with PBS, and imaged using a fluorescent microscope (ApoTome Axiovert 200M, Zeiss).

3.2.3. Adenovirus transduction and BMP-7 treatment

Recombinant adenoviruses were constructed using the serotype 5 adenovirus with an E1/E3 deletion. Adenoviruses were stored at -80°C until use. After 24 hours of incubation and for the experiments aimed to fluorescently track new insulin-expressing cells, slices were cotransduced with 50 MOI/mL of the reporter Ad-(CMV)-loxP-dsRED-loxP-BFP-2A-GCaMP6 (Vector Biolab, Malvern, PA, USA) and a 10 MOI/mL of the insulin expression tracer Ad-HIP-Cre, where HIP is a human insulin promoter (Vector Biolab, Malvern, PA, USA). The promoter was cloned upstream of a codon-optimized Cre. This strategy was designed so that the expression of Cre driven by a human insulin promoter (tracer adenovirus) would elicit a recombination event in a second adenovirus (reporter), resulting in the excision of a red cassette (red fluorescent protein (dsRed)) and the consequent blue tagging (blue fluorescent protein; BFP) of the cell. Moreover, using a 2A self-cleaving peptide, the BFP tag would be co-expressed with GcAMP6s (green), a highly sensitive fluorescent calcium indicator that allows for the indirect measurement of insulin secretion in response to glucose stimulation.

To cotransduce the cells, viruses were thawed, diluted in human slice culture medium (2 µL/mL for the reporter adenovirus and 1 µL/mL for the tracer adenovirus), and filtered using a 50 mL 0.22 µm filter. Moreover, when appropriated, treatment with human BMP-7 (PeproTech) at a final concentration of 100 pg/mL was started as a positive control for regeneration. The medium was removed from the dishes containing the slices and 2 mL of the virus preparation (with or without BMP-7) was added into each dish and incubated for 24h at 30°C. The next day, the virus was removed by pipetting and treatment with BMP-7 was continued for four more days (5 days in total).

3.2.4. Transfection with miR-30d-5p inhibitor or mimic

Two days after transduction (or in case of no transduction, the next day after obtaining the slices for RNA-seq and perifusion experiments), HPSs were transfected with miRCURY Locked Nucleic Acid (LNA) miRNA mimics or inhibitors or the corresponding controls. First, 300 nM miRNA inhibitor (hsa-miR-30d-5p inhibitor probe, Exiqon) or miRNA inhibitor control (negative control probe A, Exiqon) or 200 nM miRNA mimic (hsa-miR-30d-5p mimic probe, Exiqon) or miRNA mimic control (mimic negative control probe, Exiqon) were prepared in a final volume of 200 µL of normal BrainPhys neuronal medium without serum and antibiotic supplementation in a sterile Eppendorf (tube 1). In addition, DharmaFECT 2 transfection reagent (Horizon, Cambridge, UK) was diluted 10-fold for the mimic/mimic control and 6.5-fold for the inhibitor/inhibitor control in another Eppendorf tube (tube 2) containing 200 µL of the media without serum or antibiotics. After 5 min incubation, tubes 1 and 2 were combined and mixed by gentle vortexing. The mixture was then incubated at room temperature for 30 min. After incubation, 400 µL of the lipid-oligonucleotide complex was mixed with 1,600 µL of complete human slice culture medium without antibiotics, serving as the new medium for the slices. When appropriated, BMP-7 was added as above specified. Slices were incubated for 24 hours at 30°C and 5% CO_2, and only half of the medium was changed the day following transfection to allow its success.

3.2.5. Transfection efficiency measurement

In order to evaluate the transfection efficiency and confirm the presence of the inhibitor in the islets of Langerhans, slices were transfected with different concentrations of a miR-30d-5p inhibitor conjugated with 6-FAM (Exiqon) and subjected to immunofluorescence staining. 24 hours after transfection, tissue slices were washed twice in 1X PBS for 5 min, and fixed in 4% paraformaldehyde solution for 1 hour at room temperature. Then, slices were washed 5X for 5 min in 1X PBS and kept covered at 4°C overnight. The next day, permeabilization was done by treating slices with 0.3% Triton (Sigma Aldrich) in 1X PBS for 30 min at room temperature. After this, blocking buffer [dH_2O, 5% normal donkey serum (Jackson Labs, Bar Harbor, ME, USA), 0.1% Triton and 1X power block (Biogenex, San Ramon, CA, USA)] was added and incubated for 1 hour at room temperature. A polyclonal guinea pig primary antibody against insulin (Dako/Agilent, Santa Clara, CA, USA, #IR00261-2) was diluted 1:3 in the blocking buffer and incubated for 48 hours at 4°C, gently agitated on the platform of a small rotator. The primary antibody was then removed, and sections were washed 7X for 5 min with 1X PBS, 0.01% Triton. Secondary antibody solutions (1:400) were made in blocking buffer with Alexa Fluor 647 donkey anti-guinea pig (Jackson Immuno Research Laboratories, #706-605-148) and 1:400 DAPI

(ThermoFisher/Life Technologies, Waltham, MA, USA). Slices were incubated with secondary antibodies for 24 hours at 4°C in the dark, gently agitated on the platform of a small rotator, followed by seven washes with 1× PBS, each lasting 5 min. To minimize background fluorescence, slices were washed for three additional days. Next, a drop of PBS is added to the slide (Fluoro Slides 25x75x1 with two 10 mm circles, ThermoFisher Scientific), and the tissue slice is carefully transferred, ensuring it is well-stretched. A Pasteur pipette is used to remove excess PBS and agarose. Once dry, a drop of mounting medium (ProLong Gold antifade reagent, ThermoFisher Scientific) is placed on top of each slice, and a coverslip (VWR, Radnor, Pennsylvania, USA) is added. The edges are sealed with nail polish, and the slide is kept covered and horizontal, away from light, for 1 hour at room temperature. Finally, slides are stored a 4°C until analysis.

Confocal images of randomly selected islets were acquired on a Leica SP5 confocal laser-scanning microscope with 20X magnification. Pancreatic tissue slices were reconstructed in Z-stacks of 15–30 confocal images (step size = 2.5–5.0 µm). By using ImageJ/FIJI, DAPI- and insulin- positive cells were counted to determine the total number of cells and β-cells, respectively, against which 6-FAM inhibitor was quantified.

Moreover, the expression of miR-30d-5p after the transfection of its inhibitor was assessed by RT-qPCR as explained in ***section 3.1.5***. **Table 9** shows the list of the TaqMan Assays used. Relative values were calculated with the $2^{-\Delta\Delta Ct}$ method and gene expression was normalized to the housekeeping gene *U6*.

Table 9. ***TaqMan Assays used for analyzing miRNA expression in human pancreatic slices***

Gene	Assay ID
hsa-miR-30d-5p	478606_mir
U6 snRNA	001973

3.2.6. Tracking β-cell neogenesis

After treatment (or no treatment) with BMP-7 for 5 consecutive days, the slices were kept in complete culture medium for another 5 days. Throughout this period, daily imaging was conducted at 10X magnification, focusing on specific regions of interest (ROIs). These ROIs were selected on the initial treatment day, using distinct topographical landmarks within the slice to ensure consistent and accurate imaging over time. Images were captured in bright field, red and blue channels using a fluorescent microscope (ApoTome Axiovert 200M, Zeiss).

The blue (BFP) signal, indicative of pre-existing β-cells in the HPSs, is generally detected between 72 and 96 hours, with these cells showing no red fluorescence at any stage. Neogenic insulin-producing cells, which are primarily observed after BMP-7 removal, are dsRED-labeled cells. At some point during treatment, these dsRED cells also begin to express BFP, suggesting a late recombination event associated with the onset of new insulin expression. Then, the transient violet (red+blue) color of these cells can be used to identify β-cell neogenesis [354].

3.2.7. Bulk RNA library preparation, sequencing and analysis

To assess if the global expression of genes was also altered after miR-30d-5p inhibition or upregulation, RNA was isolated from HPSs using the miRNeasy Tissue/Cells Advanced Mini Kit (Qiagen), according to the manufacturer's instructions (see ***section 3.1.5***). Total RNA was prepared with the NuGEN Universal Plus mRNA-Seq (M01442 v2) using 100 ng and 15 cycles PCR. Library quality control analyses were performed by using fluorometry Qubit and BioAnalyzer to determine the concentration and size bp. Libraries were sequenced at multiplex paired-end 150 bp on the Illumina Novaseq X, targeting more than 50 million reads per sample. Fastq files were aligned to the hg38 transcriptome using *kallisto* package [355]. Reads were assigned to genes with featureCounts. Differentially expressed genes (DEGs) were detected with DESeq2 [356]. To account for inter-donor variability, we employed the ComBat algorithm from the sva package in R. ComBat was used to adjust for batch effects by treating the donor as a covariate in the model. Only protein-coding genes with an absolute $\log_2$(FC) >0.5 and an FDR <0.05 were selected as DEGs. PCA projection matrices were calculated with R's prcomp function, and visual representations of PCs were plotted with the ggfortify package. GO analysis of DEGs was carried out using the online Enrichr tool (https://maayanlab.cloud/Enrichr/, accessed on 23 August 2024). GO categories with a p-value ≤0.05 were considered significantly enriched. To predict transcription factor (TF) involvement in transcriptomic changes, DoRothEA (Discriminant Regulon Expression Analysis) tool was used [357]. Regulons with a confidence score of A–C were analyzed, and cases with q-values ≤0.05 and a normalized enrichment score (NES) of ± 2 were considered significantly enriched. Statistical analyses were performed in R 4.3.2.

3.2.8. Dynamic glucose-stimulated insulin release

Continuous flow or dynamic perifusion of a glucose-containing solution through pancreatic tissue provides the most accurate *in vitro* assessment of regulated real-time insulin release [358]. The principle behind perifusion involves continuously flowing a nutrient-rich solution over the tissue, allowing researchers to monitor changes in insulin

release as a response to varying glucose concentrations over time. To assess glucose-stimulated insulin release 7 days after transfection, 5–6 viable tissue slices of the same condition were placed into a closed perifusion chamber (Warner Instruments, Holliston, MA, USA) and connected to a perifusion system with automated tray handling (PERI4-02-230-FA, Biorep Technologies, Miami, FL). Perifusion was done in Krebs buffer containing 125 mM NaCl, 5.9 mM KCl, 1.28 mM $CaCl_2$, 1.2 mM $MgCl_2$, 25 mM HEPES, and 0.1% BSA, pH 7.4 at 37°C. Tissue slices were perfused at a flow rate of 100 µL/minute, and samples were collected in 96-well plates with a 120-second interval and kept at 4°C.

First, slices were flushed for 60 min with Krebs buffer containing 3 mM glucose to wash out accumulated hormones and enzymes from the tissue. Then, slices were challenged with 3 mM glucose solution for 8 min, followed by 20 min in 16.7 mM glucose (high glucose), and 16 min with 1 mM glucose (low glucose). Perfusates with the secreted substances were stored at –80°C until C-peptide content was measured using a commercially available C-peptide kit (human C-peptide ELISA, Mercodia, Winston Salem, NC, USA), following the manufacturer's instructions. Briefly, standards and samples were added to the wells pre-coated with anti-C-peptide antibodies. After 60 min incubation at room temperature, unbound conjugates were removed by wash buffer. Then, peroxidase-conjugated anti-C-peptide antibodies were added to form a sandwich complex and incubated for 60 min at room temperature. After washing off unbound conjugates, TMB substrates were added since they are catalyzed by peroxidase to produce a blue color product that turned yellow after adding a stop solution. Finally, the OD absorbance was read at 450 nm in a microplate reader. The concentration of C-peptide in the sample was calculated by drawing a standard curve, being the concentration of the target substance proportional to the OD_{450} value.

4. MIRNA IMPLICATION ON THE ONGOING AUTOIMMUNE PROCESS IN MICE

The murine model NOD was employed to address the implication of miR-30d-5p in the development and progression of the autoimmune process in an *in vivo* setting. After the treatment with a miR-30d-5p inhibitor, and considering the obtained results *in vitro*, we expected to observe an acceleration of the autoimmune process.

4.1. Ethics statement

This study was carried out in strict accordance with the recommendations in the Guide for the Care and Use of Laboratory Animals of the Generalitat de Catalunya. The

procedures carried out with animal models were authorized by the Animal Experimentation Ethics Committee of the CMCiB and IGTP and by the Generalitat de Catalunya, and they followed the principles outlined in the Declaration of Helsinki for animal experimental investigation. All the conducted protocols followed the principles of the 3R, prioritizing the welfare of animals used in research. The animal study protocol was approved by the Ethics Committee of Germans Trias i Pujol Research Institute and Catalan Government (protocol code DMAH10030 approved on 6th June 2018).

4.2. NOD mice and monitoring of diabetes onset

Wild-type NOD mice were originally obtained from the Jackson Laboratory (Bar Harbor, ME, USA) and then kept in the Animal Facility of the Centre de Medicina Comparativa i Bioimatge de Catalunya (CMCiB) under specific pathogen-free conditions. The colony was subjected to a 12-hour dark/12-hour light cycle and controlled temperatures between 19-23°C with 40-60% humidity and fed with ad libitum access to acidic water at pH 5 and irradiated Teklad Global 18% Protein Rodent Diet (Harlan, Indianapolis, IN, USA). After 12 weeks of age, NOD mice spontaneously develop autoimmune diabetes with a higher incidence in females (60-80%) than in males (20-30%) [359]. Although asymptomatic, the autoimmune process starts at 3-4 weeks of age with an initial lymphocyte infiltration into the islets of Langerhans. In this study, only prediabetic NOD females of 9 weeks of age were used.

In order to detect and exclude mice with T1D, glycosuria levels were monitored weekly using urine test strips (Combiscreen, Analyticon Biotechnologies AG, Lichtenfels, Germany), and T1D was confirmed when glycemia rose above 300 mg/dL in one glucotest control (OneTouch Verio Reflect®, LifeScan IP Holdings, LLC., Zug, Switzerland).

4.3. *In vivo* miR-30d-5p inhibitor administration

The mature nucleotide sequence of mmu-miR-30d-5p (5'-UGUAAACAUCCCCGACUGGAAG-3') was obtained from www.mirbase.org (accessed on 3 May 2022), which is homologous between mice and man. Here, we used an antisense oligonucleotide LNA miRNA inhibitor for miR-30d-5p (LNA-anti-miR-30d-5p) and a miRNA inhibitor negative control A (scrambled LNA) (Exiqon), both modified for *in vivo* applications. This miRNA inhibitor has been shown to accumulate in tissues when applied systemically thereby facilitating miRNA silencing *in vivo*. Here, three groups composed of six prediabetic NOD mice of 9 weeks of age each were respectively treated with (1) miRNA-inhibitor (inhibitor probe mmu-miR-30d-5p, Exiqon), (2) miRNA-inhibitor control (negative control A probe, Exiqon), or (3) saline (PBS, sham). Mice received four

intraperitoneally (i.p.) doses every three days at 9 mg/kg (miRNA-inhibitor or miRNA-inhibitor control) in 200 µL saline solution (PBS, RNase free). Twenty-four hours after the last injection (or 10 days after the first one), mice were euthanized by i.p. ketamine (75 mg/kg)–xylazine (10 mg/kg) injection and blood collection via cardiac puncture. The spleen and PLN were harvested and processed to assess changes in the percentage of different immune cell subpopulations and gene expression. Pancreases were harvested, snap-frozen in an isopentane/cold acetone bath and stored at −80°C until use to assess changes in insulitis (**Figure 13**).

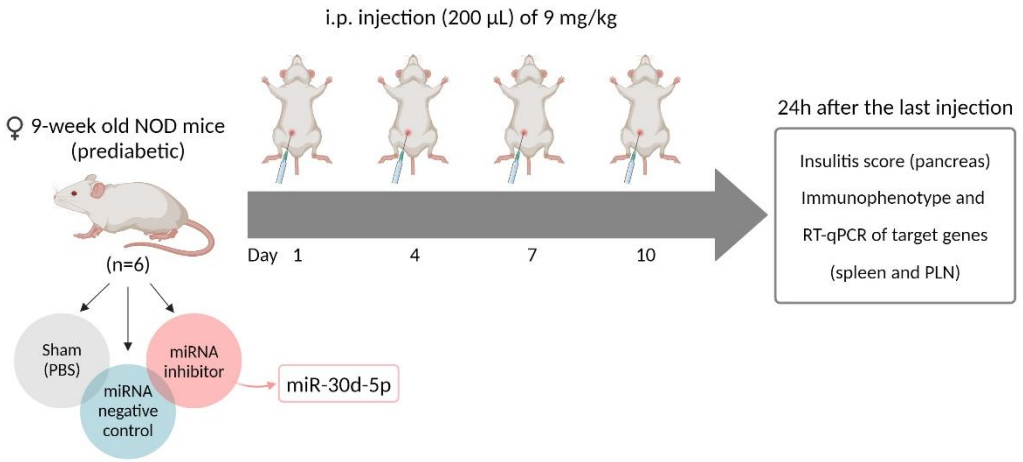

Figure 13. ***Mouse treatment protocol with miR-30d-5p inhibitor.*** *Three groups of six 9-week-old prediabetic NOD mice were treated with miR-30d-5p inhibitor, miRNA-inhibitor control, or saline. Mice received four intraperitoneal doses every three days at 9 mg/kg. Twenty-four hours after the final injection, spleen and pancreatic lymph nodes were harvested to assess immune cell and gene expression changes, and the pancreas to evaluate the degree of insulitis. Figure created using BioRender.*

4.4. Insulitis score

The degree of islet infiltration by leukocytes (insulitis) was determined in the pancreas of 6 mice per group at the end of the study. Briefly, non-overlapping cryosections of 6 µM were obtained, placed on a slide, and stored at -80°C. For the hematoxylin and eosin staining, slides were thawed and allowed to dry for 90 min. Then, cryosections were sequentially treated with hematoxylin for 3 min (Merck), water for 10 seconds (×2), eosin for 30 seconds (Merck), 70% ethanol (EtOH, Merck) for 10 seconds, 90% EtOH for 10 seconds, 100% EtOH for 2 min and xylene for 1 minute. Finally, the slides were covered with DPX mounting medium (Sigma-Aldrich) and a coverslip.

To score insulitis, a minimum of 40 islets per animal were analyzed under a light microscope, as previously described [360]: 0, intact islets/no insulitis; 1, peri-islet infiltrates; 2, < 25% islet infiltration; 3, 25%-75% islet infiltration; 4, >75% islet infiltration or complete islet destruction (**Figure 14**). The degree of insulitis was determined by a weighted average of the total number of islets analyzed according to the formula: $\frac{(0 \times A)+(1 \times B)+(2 \times C)+(3 \times D)+(4 \times E)}{number\ of\ islets\ counted}$, where A, B, C, D and E correspond to the number of islets assessed at the different degrees of infiltration. A double-blind analysis was performed by independent observers.

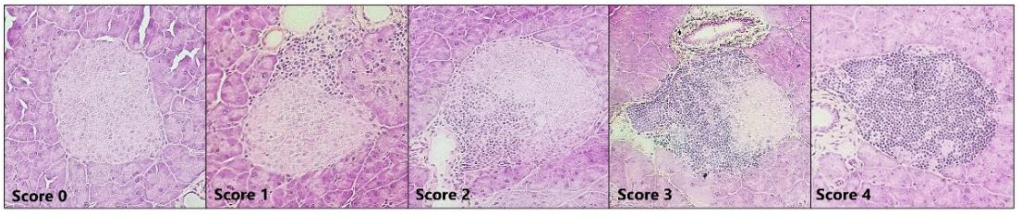

Figure 14. ***Degree of insulitis in the NOD mice***. *Images (10X) obtained by light microscopy showing the degree of leukocyte infiltration of the pancreatic islets of a 12-week-old female NOD mouse. From left to right: score 0, intact islets/no insulitis; 1, peri-islet infiltrates; 2, < 25% islet infiltration; 3, 25%–75% islet infiltration; 4, >75% islet infiltration or complete islet destruction. The images shown are a representative example of the criteria used to determine the degree of insulitis in this study.*

4.5. Flow cytometry

To determine changes in the percentage of different regulatory and effector immune cell subpopulations induced by miRNA blockade, the spleen and PLN of all mice were immunophenotyped by flow cytometry.

4.5.1. Leukocyte isolation from spleen and PLN

Splenocyte and leukocyte suspensions were obtained by the mechanical disruption of the spleen and PLN, respectively, and washed twice with R-10 in order to collect all the cells. The tissue remains were allowed to precipitate for 2 min, and the supernatant was obtained, which was then centrifuged at 400×g for 5 min at room temperature. Afterward, in the case of the splenocyte suspension, erythrocytes were lysed with 5 mL of hemolysis solution [500 mL deionized H_2O (Milli-Q Direct, Merck Millipore, Burlington, MA, USA) plus 1.0297 g Trizma Hydrochloride (Sigma-Aldrich) and 3.735 g NH4Cl (Probus, Badalona, Spain)] for 5 min at room temperature, which was next blocked by adding 5 mL of R-10. Cells were centrifuged again at 400×g for 5 min at room temperature and further washed with another 5 mL of R-10. Finally, leukocyte

suspensions from both spleen and PLN were resuspended in 1–3 mL and 200 µL of PBS+2% FBS, respectively. To assess cell viability and counting, we proceed as explained in ***section 3.1.2***.

4.5.2. Immunophenotype

Next, the percentages of T and B lymphocytes and DCs were assessed by flow cytometry. For phenotype labeling, 0.5×10^6 cells per panel were used; one of them was designed for the study of different T lymphocyte subpopulations (**panel 1**), and the other was designed for the detection of cDCs and B lymphocytes (**panel 2**). For the T lymphocyte panel, surface staining was carried out with CD3 PE, CD4 APC, CD8 V500, CD44 BV786, CD62L APC-Cy7, PD-1 PE-Cy7, and CD25 PerCP-Cy5.5, and intracellular staining was carried out with FoxP3 FITC. For the DC and B cell panels, surface staining was carried out with CD3 PE, CD19 V450, CD11c PE-Cy7, and MHC-II APC. Further information on antibodies can be found in **Table 10**.

First, a surface staining was performed. Cells were incubated with the appropriate monoclonal antibodies for 20 min at 4°C in the dark. If no intracellular staining was needed, cells were then washed with FACSFlow™ Sheath Fluid (ThermoFisher Scientific) and resuspended in the same solution for their acquisition or, for the DC panel, incubated with 4 µL of 7-AAD in 100 µL of PBS for 15 min at room temperature and protected from light.

In the case of the intracellular staining with FoxP3, cells were washed with cold FACSFlow™ Sheath Fluid (ThermoFisher Scientific) at 400×g for 5 min and fixed with 1 mL of Fixation/Permeabilization solution (1 Fix/Perm concentrate: 3 diluent solution, ThermoFisher Scientific) for 45 min at 4°C in the dark. After the incubation, cells were washed twice with 2 mL of 1X Permeabilization buffer (400×g, 5 min, at room temperature), and the supernatant was discarded. Then, fixed and permeabilized cells were stained with FoxP3 FITC for 40 min at 4°C in the dark. After that, cells were washed twice with 2 mL 1X Permeabilization buffer at 400×g for 5 min and suspended in 200 µL FACSFlow™ Sheath Fluid (ThermoFisher Scientific). At least 100.000 leukocyte events per sample were acquired using FACSCanto II and LSR Fortessa flow cytometers (BD Biosciences). Necrotic and apoptotic cells were excluded from the analysis based on their FSC-A/SSC-A properties and doublets were excluded by FSC-A/FSC-H. FMO controls were used to assess PD-1, CD25, and FoxP3 staining positivity. The gating strategy can be found in **Supplementary Figures 12 and 13**. Data were analyzed using FlowJo software (Tree Star Inc).

Table 10. ***List of monoclonal antibodies used for spleen and PLN immunophenotyping***

	Target	Fluorophore	Species/Isotype	Clone	Use*	Company
PANEL 1	CD3	PE	Hamster IgG2, κ	500A2	1	BD Biosciences
	CD4	APC	Rat IgG2a, κ	RM4-5	0.5	BD Biosciences
	CD8	Violet 500	Rat IgG2a, κ	53-6.7	0.4	BD Biosciences
	CD44	BV786	Rat IgG2b, κ	IM7	0.2	BD Biosciences
	CD62L	APC-Cy7	Rat IgG2a, κ	MEL-14	0.4	BioLegend
	PD-1	PE-Cy7	Rat IgG2a, κ	29F.1A12	2	BioLegend
	CD25	PerCP-Cy5.5	Rat / IgG1, λ	PC61.5	1	eBioscience
	FOXP3	FITC	Rat IgG2a, κ	FJK-16s	1.5	eBioscience
PANEL 2	CD3	PE	Hamster IgG2, κ	500A2	1	BD Biosciences
	CD19	Violet 450	Rat IgG2a, κ	1D3	1	BD Biosciences
	CD11c	PE-Cy7	Hamster IgG1, λ2	HL3	1	BD Biosciences
	MHC-II	APC	Rat IgG2b, κ	AMS-32.1	1	eBioscience

*Use/100µL

4.6. Gene expression profile through RT-qPCR

To assess if the expression of some target genes (*CD200*, *PRDM1*, *TGFBR2*) and *PDCD1* (gene coding for PD-1) were also altered after miR-30d-5p blockade, RNA was isolated from spleen and PLN samples using the RNeasy Micro Kit (Qiagen, Hilden, Germany), according to the manufacturer's instructions. This procedure allows for the purification of RNA molecules longer than 200 nucleotides, thus enriching for mRNA. Briefly, cells were disrupted by adding a lysis buffer mixed with β-mercaptoethanol (Sigma) and homogenized by vortexing for 1 minute. Then, 5 µL 4 ng/µL carrier RNA and one volume of 70% ethanol were added to the sample and the homogenized lysate was transferred to an RNeasy MinElute spin column for adsorption of RNA to the membrane. Samples were washed before and after incubation for 15 min with 80 µL 0.125X DNase I to eliminate DNA material that may have bound to the silica membrane. Two consecutive centrifugations were then carried out adding to the column a buffer to precipitate the proteins and other contaminants, and 80% ethanol to dissolve and wash away the salts. After drying the membrane by centrifugation at full speed, RNase-free water was added to recover RNA. Targets were selected based on the results of flow cytometry. In this sense, *CD200* and *TGFBR2* are related to the expansion and functional effect of FOXP3$^+$ Tregs, respectively, and *PRDM1* is a transcriptional repressor of PD-1.

After RNA isolation, the synthesis of cDNA was carried out by RT-qPCR. For all samples, a maximum of 500 ng of total RNA was reverse transcribed with a High Capacity cDNA Reverse Transcription Kit (ThermoFisher Scientific). The process of cDNA synthesis involved combining total RNA with 1 µL of 0.5 mg/mL random primers (BioTools, Valle de la Tobalina, Spain) and supplementing with RNase-free water to achieve a total volume of 13.75 µL. Subsequently, the samples were placed in a GeneAmp PCR System 9700 (ThermoFisher Scientific) and incubated for 5 min at 70°C. After cooling down at 4°C, 1.25 µL of 10 mM desxynucleosides (dNTPs, BioTools), 5 µL of 5X transcriptase buffer (Promega, Madison, WI, USA), 0.5 µL of 40 U/µL RNase Inhibitor (Promega), and 0.5 µL of 200U/µL reverse transcriptase Moloney Murine Leukaemia Virus (M-MLV, Promega) were added, along with 4 µL of RNase-free water to achieve a total volume of 25 µL. The samples underwent an additional incubation cycle at 37°C for 60 min. The copy of cDNA obtained was stored at -20°C until use.

cDNA was then thawed and 1:2 diluted and genes were profiled using the TaqMan™ Universal Master Mix II with UNG (Applied Biosystems) and TaqMan Gene Expression Assays (ThermoFisher Scientific) in 15 µL PCR reactions in triplicate. In detail, each well from the 96-well plate (96 Well Lightcycler plate, Sarstedt) contained 2 µL of the diluted DNA and a PCR reaction mixture prepared with 0.75 µL of the TaqMan probe, 7.5 µL of the TaqMan Master Mix and 4.75 µL of RNase-free water. **Table 11** shows the list of the TaqMan Assays used.

Table 11. ***List of TaqMan Assays used for the analysis of targeted genes in immune cells***

Gene	Assay ID
Cd200	Hs01033302_m1
Pdcd1	Hs01550088_m1
Prdm1	Hs00153357_m1
Tgfbr2	Hs00234253_m1
Gapdh	Hs02786624_g1

Plates were centrifuged at 1000 rpm for 1 minute and run on a LightCycler®480 RT-PCR machine (Roche) following the settings displayed in **Table 12**.

All analyzed genes showed a C_t <30. Relative values were calculated with the $2^{-\Delta Ct}$ method and gene expression was normalized to the housekeeping gene *GAPDH*.

Table 12. ***Thermal cycling conditions for the PCR reaction***

Step	Temperature	Time	Cycles
UNG activation	50°C	2 min	1
Polymerase activation	95°C	10 min	1
Denature	95°C	15 seconds	50
Anneal / Extend	60°C	1 minute	

5. STATISTICAL ANALYSIS

Data are presented as mean ± standard deviation (SD) or standard error of the mean (SEM), percentages, mean (min, max), or median and interquartile range, unless stated otherwise. For clinical parameters, a descriptive statistical analysis of the variables was performed. χ^2 test was used for categorical variables. The distribution of continuous variables was tested for normality by the Kolmogorov–Smirnov test. Differences between two groups were analyzed using the nonparametric 2-tailed Wilcoxon test for paired data and the nonparametric 2-tailed Mann–Whitney test for unpaired data. To test differences among longitudinal data, a mixed effects model was fit with condition as fixed effect, and individual and residual random variation as random effect covariates together with the Tukey's multiple comparisons test. Comparisons between three or more groups were performed by Kruskal–Wallis with Dunn's post hoc test. Samples from the same donors subjected to different treatments were analyzed by repeated measures two-way ANOVA with the Geisser-Greenhouse correction and Tukey's multiple comparisons test. Correlations between variables were tested by using a two-tailed Spearman's (nonparametric) or Pearson's (parametric) test. Simple and multiple logistic regressions were generated to assess the predictive value of the different variables. ROC curves were generated to assess their discrimination ability. Multivariate statistical analysis was performed using principal component analysis. A Fisher's exact test meta-analysis method with Benjamini–Hochberg's FDR correction was used to calculate the significant targeted biological processes and KEGG pathways. The complete linkage clustering method was used for the hierarchical clustering of pathways and miRNAs. Squared Euclidian distances were determined as distance measures, absolute p-values were used in all calculations, and the significance levels of the interaction were taken into consideration. Weight levels of mice throughout the study were compared using two-way ANOVA with Tukey's multiple comparisons test. For all tests, a two-tailed p-value of ≤ 0.05 was considered statistically significant. Levels of significance are indicated as: ns, $p > 0.05$; *, $p \leq 0.05$; **, $p \leq 0.01$; and ***, $p \leq 0.001$. Analyses were performed using the programs GraphPad Prism 9 (GraphPad Software Inc, San Diego, CA, USA) and R v4.3.2.

4

RESULTS

CHAPTER I. Predictive immunological biomarkers for partial remission in pediatric type 1 diabetes

The first chapter of this work presents a model for predicting PR from immunological data collected at the time of T1D diagnosis. The complete immunophenotyping of 56 pediatric patients has allowed us to know which cellular parameters could be related to future remission. Thus, using a logistic regression machine learning algorithm, we have been able to create an index-based model with a remission prediction capacity of 81%. Moreover, a decision tree was generated using this index and age to classify patients, which could serve as a guide in clinical practice.

1. Clinical features and metabolic data of pediatric patients with T1D at diagnosis

Table 13 summarizes the clinical features and metabolic data from 56 patients with T1D at the time of disease onset for the predictive study of the PR phase. Differences at T1D onset between future remitters and non-remitters were found in terms of age, BMI and stimulated C-peptide.

Table 13. ***Clinical features and metabolic data of patients with T1D at disease onset separated by future remitters and non-remitters***

	T1D dx		
	Future PR	**Future non-PR**	**P-value**
N (no. females)	37 (18)	19 (10)	0.78
Age (years)	10.6 ± 4.4	6.6 ± 3.9	**0.001*** **
BMI (kg/m^2)	18.2 ± 3.5	15.9 ± 2.1	**0.005** **
HbA1c (%)	11.4 ± 2.3	11.1 ± 1.9	0.51
Insulin dose (U/kg/day)	0.67 ± 0.2	0.74 ± 0.2	0.27
IDAA1c	14.1 ± 2.9	14 ± 2.3	0.85
Basal C-peptide (ng/mL)	0.4 ± 0.3	0.3 ± 0.2	0.07
Stimulated C-peptide (ng/mL)	1 ± 0.8	0.5 ± 0.4	**0.039***

Data presented as mean ± SD. P-value calculated from t-test when comparing baseline time-points (T1D dx) between future remitters and non-remitters. *p ≤0.05, **p ≤0.01, ***p ≤0.001; p ≤0.05 is considered significant. Abbreviations: BMI, Body Mass Index; HbA1c, glycated hemoglobin; IDAA1c, insulin dose-adjusted HbA1c; non-PR, non-partial remission; PR, partial remission; T1D dx, type 1 diabetes diagnosis.

2. Metabolic and immunological data from patients with T1D at diagnosis could serve as predictive biomarkers for PR

We next tested the PR predictive capacity of all the immune cell subsets, metabolic and clinical parameters analyzed at T1D onset. First, simple logistic regression analyses were used to determine the association between the event of PR and each of the parameters (**Table 14**). Regarding the metabolic and clinical parameters, age (OR = 1.25; 95% CI = 1.09 to 1.49), BMI (OR = 1.36; 95% CI = 1.08 to 1.85) and stimulated C-peptide (OR = 13.27; 95% CI = 1.42 to 287.9) could predict the event of PR, with a 25% increase in the odds of being in PR for each year added, a 36% increase in the odds for each BMI unit increase and 12-fold increased odds for being in PR with each stimulated C-peptide unit increase. As for the immunological parameters, the percentage of B lymphocytes (OR = 0.88, 95% CI = 0.77 to 0.98), Tregs (OR = 0.66, 95% CI = 0.41 to 0.98), $CD27^+$ EM $CD8^+$ T cells (OR = 1.13, 95% CI = 1.03 to 1.25), γδ $CD4^-CD8^-$ T cells (OR = 1.11, 95% CI = 1.02 to 1.23) and activated Tregs (OR = 1.08, 95% CI = 1.00 to 1.19) could also predict the event of remission. In this case, having increasing percentages of $CD27^+$ EM $CD8^+$ T cells, γδ $CD4^-CD8^-$ T cells and activated Tregs would correspond with higher odds of being in remission. Contrarily, having increasing percentages of B lymphocytes and total Tregs would correspond with lower odds of being in remission.

Table 14. ***Simple logistic regressions for determinants of partial remission at T1D diagnosis***

Variable	Coefficient	SE	OR	95% CI for OR	|Z|	P-value
Age (years)	0.23	0.08	1.25	1.09 to 1.49	2.88	**0.004****
BMI (kg/m²)	0.31	0.13	1.36	1.08 to 1.85	2.29	**0.02***
Stimulated C-peptide (ng/mL)	2.59	1.34	13.27	1.42 to 287.9	1.93	**0.05***
B lymphocytes (%)	-0.13	0.06	0.88	0.77 to 0.98	2.12	**0.03***
Tregs (%)	-0.42	0.22	0.66	0.41 to 0.98	1.93	**0.05***
$CD8^+$ EM $CD27^+$ T cells (%)	0.12	0.05	1.13	1.03 to 1.25	2.49	**0.01****
γδ TCR $CD4^-CD8^-$ T cells (%)	0.10	0.05	1.11	1.02 to 1.23	2.19	**0.03***
activated Tregs (%)	0.08	0.04	1.08	1.00 to 1.19	1.89	0.056

*p ≤0.05, **p ≤0.01 after simple logistic regression. P ≤0.05 is considered significant. N=44–56.

In fact, these clinical, metabolic and immunological variables at T1D onset, separated by future remitters and non-remitters, showed how those remitter patients were diagnosed at older ages, with both higher BMI values and stimulated C-peptide concentrations and with lower percentages of B lymphocytes and Tregs and higher percentages of $CD27^+$ EM $CD8^+$ T cells, γδ $CD4^-CD8^-$ T cells and activated Tregs compared to those non-remitter patients (**Figure 15A**). Furthermore, the analysis of the ROC curves of all these variables showed that each of them individually presented a good discriminatory capacity between remitters and non-remitters, especially with regard to age, stimulated C-peptide and the percentage of both $CD27^+$ EM $CD8^+$ and γδ $CD4^-CD8^-$ T cells (**Figure 15B**).

In order to create a full model containing simultaneously the statistically significant variables, we tested if they were monotonically correlated through Pearson's tests. The different clinical and metabolic parameters correlated between them or with immune cell percentages. As expected, positive correlations were found between age and BMI and between stimulated C-peptide with both age and BMI. Also, the percentage of $CD27^+$ EM $CD8^+$ T cells was positively correlated with the BMI. Negative correlations were found between age and the percentage of B lymphocytes, as previously reported [33], and between the percentage of γδ $CD4^-CD8^-$ T cells and stimulated C-peptide (**Figure 16A**). No significant correlations were found between the five immunological variables, which is important to determine that the predictive ability of one variable is not influenced by another. Thus, a model containing only statistically significant independent immune-related variables was created, ruling out the activated Tregs variable.

First, from the ROC curves (**Figure 16B**) we selected the best cut-off values to discriminate between remitters and non-remitters for each of the four significant independent variables, considering both the sensitivity and the specificity. For the percentage of Tregs, the best cut-off value to determine PR was <8.2, for the percentage of $CD27^+$ EM $CD8^+$ T cells, the best cut-off value was >18.95, for the percentage of γδ $CD4^-CD8^-$ T cells, the best cut-off value was >78.35, and for the percentage of B lymphocytes, the best cut-off value was <15.85. Then, since the sample size is limited and to avoid problems of overfitting of the multiple variables, an index including the cut-off's values was created to determine on a 0–4 scale how many conditions or cut-offs the patients meet for entering the PR phase, reducing in that way four variables to one. In that sense, higher values represent more conditions met (0, no condition; 4, all conditions) (**Figure 16B**).

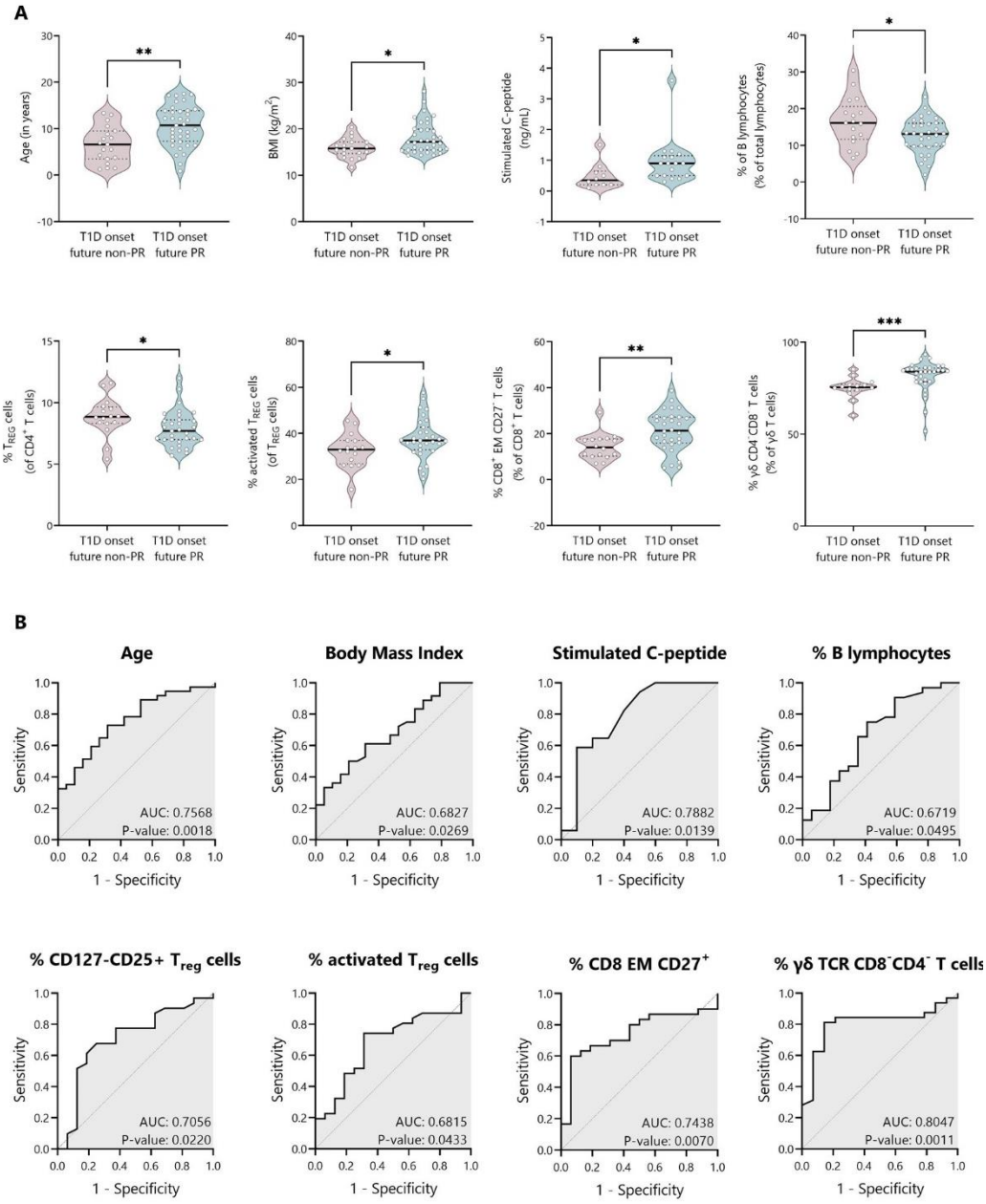

Figure 15. ***Metabolic and immunological variables at T1D onset can discriminate between future remitters and non-remitters.*** *(**A**) Violin plots showing age, body mass index, stimulated C-peptide and the percentage levels of B lymphocytes, Tregs, activated Tregs, CD27⁺ EM CD8⁺ T cells and γδ TCR CD4⁻CD8⁻ T cells at T1D onset separated by future remitters (blue) and non-remitters (pink). Each dot represents an individual patient. Violin plots show the median (thick dashed line) and first and third quartiles (thin dashed lines). *p ≤0.05, **p <0.01 after 2-tailed Mann–Whitney test. P ≤0.05 is considered significant. N=44–56. (**B**) ROC curves plotting sensitivity and 1-specificity for detecting children with PR using age, body mass index, stimulated C-peptide and the percentage*

levels of B lymphocytes, Tregs, activated Tregs, CD27⁺ EM CD8⁺ T cells and γδ TCR CD4⁻CD8⁻ T cells. The AUC is indicated, being a measure of how well a quantitative test can distinguish between patients with and without PR. P-values for AUCs are also reported. P ≤0.05 is considered significant. N=44–56.

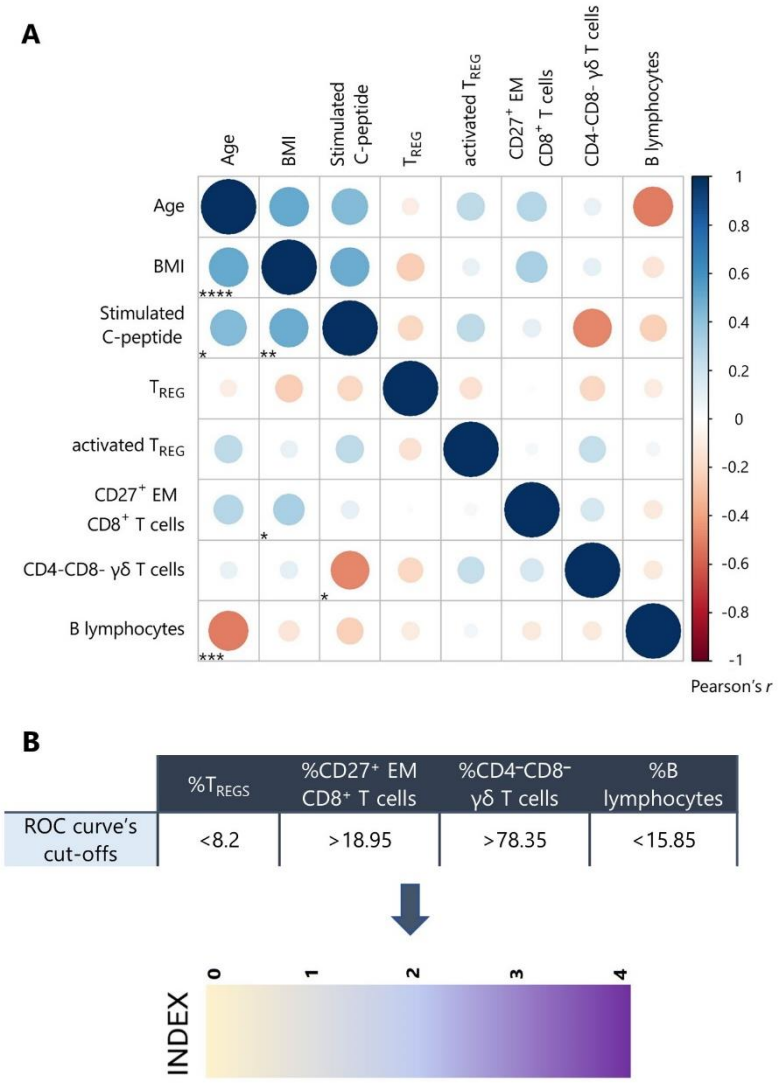

Figure 16. ***Creation of a 0 to 4 scale index with uncorrelated immunological variables. (A)*** *Pearson's correlation coefficient matrix between the statistically significant determinants of PR at diagnosis. The color of the bubbles indicates a positive (blue) or a negative (red) correlation, while the size indicates the statistical significance. Age, BMI and stimulated C-peptide are correlated between them and with some immunological parameters. No correlations were found between the immune cell subsets. *p ≤0.05, **p <0.01, ***p <0.001, ****p ≤0.0001 after Pearson's correlation test. N=44–56.* ***(B)*** *Strategy followed to create an index using independent immunological variables. From ROC curves, the best cut-off values were selected to discriminate between the remitter and the non-remitter groups for the percentage of Tregs (<8.2), CD27⁺ EM CD8⁺ T cells (>18.95), CD4⁻CD8⁻ γδ T*

cells (>78.35), and B lymphocytes (<15.85), considering both the sensitivity and the specificity with 95% CI. An index including the selected cut-off values was created to determine for each patient how many conditions they met for entering PR on a 0–4 scale (0, no condition; 4, all conditions), being the cut-offs the conditions that should be fulfilled.

A machine learning algorithm was used to build the predictive model, dividing the sample into 70% to obtain the estimates ("training" sample) and 30% to validate its predictive ability ("validation" sample). The logistic regression for the index-based model using the "training" sample showed that it was able to predict remission (p-value = 0.003) when adjusted for age and BMI, but those variables were no longer predictive (**Table 15**). In this case, having increasing index values would correspond with higher odds of being in remission.

Table 15. ***Logistic regressions of index as a determinant of partial remission at T1D diagnosis corrected for BMI and age in a machine learning model***

Variable	Coefficient	SE	|Z|	P-value
Index	1.654	0.568	2.91	**0.003****
BMI (kg/m^2)	0.254	0.206	1.23	0.218
Age (years)	0.153	0.150	1.03	0.305

To generate this regression, 70% of the sample ("training" sample) was used (n=40). **p ≤0.01 after logistic regression. P ≤0.05 is considered significant.

Next, a confusion matrix was created using the "validation" sample to determine if the predictions made by the logistic regression model hold true for an independent sample (**Table 16**). The index was able to correctly classify 13 of the 16 patients, 9 as remitters and 4 as non-remitters; presenting 1 false positive and 2 false negatives. The ROC curve analysis derived from the confusion matrix showed that the model was able to discriminate between remitters and non-remitters with good predictive performance (AUC = 0.81). The sensitivity was 66.7% (true positive cases correctly identified) and the specificity was 90% (false cases correctly identified).

Table 16. ***Classification accuracy of the index in a machine learning model***

Observed / Predicted	Negative (non-PR)	Positive (PR)	Sensitivity	Specificity	AUC	P-value
Negative (non-PR)	**4**	1	0.667	0.900	0.81	**0.036***
Positive (PR)	2	**9**				

To generate this confusion matrix, 30% of the sample ("validation" sample) was used (n=16). *p ≤0.05.

Finally, a decision tree was created to classify patients into remitters (first row: 1; second row: right) or non-remitters (first row: 0; second row: left). The supervised algorithm identified both the index and age as important variables that contribute to the final outcome (**Figure 17**). Initially, emphasis is placed on the index value, with individuals exhibiting an index equal to or surpassing 2 being designated as remitters. Nevertheless, when solely focusing on the index, misclassification occurs in 9 out of 55 patients, with one identified as a false positive and eight as false negatives. Subsequently, an additional layer of classification is introduced. For patients whose index value falls below 2, the age becomes a decisive factor. Specifically, if the patient's age is 11 years or older, they are associated with a potential future remission event. In contrast, patients under the age of 11 are classified as non-remitters. Presently, the misclassification rate stands at 6 out of 55 patients, comprising four patients categorized as false positives and two as false negatives. This dual consideration of both index value and age underscores the multifaceted nature of patient classification, incorporating key variables to enhance the precision of prognostic assessments.

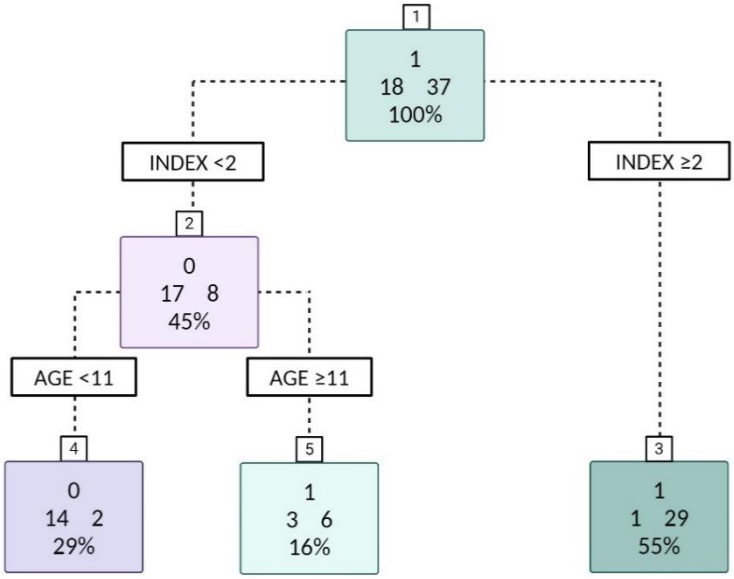

Figure 17. ***Decision tree to classify T1D patients according to the index and age into future remitters and non-remitters.*** *The decision tree considers index and age as key factors in classifying patients. Patients are first classified based on their index value. Age is then taken into account to decrease the number of false positives. The first row within the boxes indicates the state of remission (1) or non-remission (0). The second row within the boxes indicates the number of patients classified as non-PR (left) or PR (right). The percentage indicates the number of patients with respect to the total sample. Patients with an index value ≥2 are more likely to be in remission, whereas if the index is <2 patients are more likely to be classified as non-remitters. However, after adjusting for age, having an index value of 0 or 1 while being 11 years or older is also associated with a future remission event. N=55.*

CHAPTER II. Identification of novel immune and epigenetic biomarkers for partial remission in pediatric type 1 diabetes

The second chapter of this work presents a longitudinal study of 17 pediatric patients newly diagnosed with T1D. The study aims to analyze specific changes during the PR phase by classifying patients as remitters or non-remitters. Divided into two sections, ***section I*** of this chapter identifies immune biomarkers. To this end, up to fifty-five subtypes of peripheral immune cells and the profile of inflammatory and anti-inflammatory cytokines in plasma were analyzed at different time points. Likewise, ***section II*** focuses on analyzing and validating the differential profile of miRNAs in plasma and the molecular pathways they regulate. The aim is to describe the changes that occur during the PR phase, which are well characterized at the metabolic level but not so well characterized at the immunological or epigenetic level, and to identify biological processes involved in establishing this period. The experiments described in this chapter have been published in [361–363].

SECTION I. Immune biomarkers of partial remission

This section aims to characterize immune cell subsets and cytokines during different stages of T1D (diagnosis, remission/non-remission, and 12 months of progression) to identify specific immunological biomarkers for the honeymoon phase.

1. Clinical features and metabolic data of pediatric patients with T1D

Clinical features and metabolic data from control subjects and patients with T1D at each time-point for the longitudinal study are summarized in **Table 17**. HLA typing of DRB1 alleles was determined in patients with T1D to determine genetic predisposition for the disease. As expected, 50% of the patients presented a high-risk HLA-DRB1 genotype and 44% of them were DRB1*03 or *04 positive, having a moderate risk for T1D. Only one patient was negative for DRB1*03 and *04 (**Supplementary Table 2**). No statistically significant differences were found in age and BMI when compared between control subjects and patients at T1D onset; as expected, they were found in terms of plasma C-peptide concentration (1.3 ± 0.4 vs 0.3 ± 0.2; P <0.0001).

The 64.7% of patients with T1D presented PR between 2–6 months after the diagnosis, with an IDAA1c value equal to or less than 9, while the rest did not experience it after 12 months of follow-up. During the PR phase, and in comparison to disease onset, patients

showed increased BMI values, and a non-significant increase in basal C-peptide concentration (0.7 ± 0.5 vs 0.3 ± 0.2; ns), although the levels were still much lower than those of the control group (0.7 ± 0.5 vs 1.3 ± 0.4; P <0.01). After a year of follow-up, 50% of these remitter patients were still in remission. There were no significant differences in terms of age, sex, and BMI between patients with and without PR at 8 months of follow-up. Unlike patients in remission, non-remitter patients (IDAA1c >9) did not present an increase in basal C-peptide concentration after diagnosis (0.3 ± 0.1 vs 0.3 ± 0.2; ns), indicating some β-cell recovery only in remitter patients.

Table 17. ***Clinical features and metabolic data of control subjects and patients with T1D included in the longitudinal study***

	Discovery cohort					
	Ctrl	**T1D dx**	**PR**		**Non-PR**	
	Baseline	Baseline	2–6M	12M	8M	12M
N (no. females)	17 (10)	17 (10)	11 (6)	10 (6)	6 (4)	6 (4)
Age (years)	8.8 ± 3.4	8.7 ± 3.6	9.1 ± 4.3	10.2 ± 4.3	9 ± 2.8	9.2 ± 2.8
BMI (kg/m^2)	18.3 ± 4.3	16.8 ± 2.5	17.7 ± 3	18.6 ± 3.5	17.2 ± 2.1	17 ± 1.9
HbA1c (%)	ND	11.4 ± 2.4	6.9 ± 0.6	7.1 ± 0.8	8.1 ± 0.7	7.9 ± 0.9
Insulin dose (U/kg/day)	ND	0.7 ± 0.2	0.4 ± 0.1	0.5 ± 0.2	0.9 ± 0.1	0.85 ± 0.1
IDAA1c	ND	14.3 ± 3	8.4 ± 0.5	9.2 ± 1.3	11.5 ± 1	11.3 ± 1.2
Basal C-peptide (ng/mL)	1.3 ± 0.4	0.3 ± 0.2	0.7 ± 0.5	0.3 ± 0.3	0.3 ± 0.1	0.15 ± 0.06

Data presented as mean ± SD. In the text, p-value calculated from Mann-Whitney test when comparing control subjects and patients with T1D, and remitter and non-remitter groups. P-value calculated from Wilcoxon test for comparisons of paired data. Abbreviations: BMI, Body Mass Index; Ctrl, controls; HbA1c, glycated hemoglobin; IDAA1c, insulin dose-adjusted HbA1c; ND, not determined; M, months after baseline; non-PR, non-partial remission; PR, partial remission; T1D dx, type 1 diabetes diagnosis.

After 12 months of follow-up, remitter patients showed lower levels of basal C-peptide than levels during remission; however, these doubled those of the non-remitters (0.3 ± 0.3 vs 0.15 ± 0.06; ns). Moreover, remitters still needed a lower daily dose of total insulin than the non-remitters (0.5 ± 0.2 vs 0.85 ± 0.1; P <0.01) and maintained the increased BMI values regarding the disease onset (18.6 ± 3.5 vs 16.8 ± 2.5; P ≤0.05). At 12 months, both remitters and non-remitters maintained practically equal the HbA1c values reached during the PR phase or at 8 months from diagnosis, respectively.

2. Circulating effector memory CD4⁺ and CD8⁺ T lymphocytes are increased during the PR phase

The analysis of the maturation stages of T lymphocytes revealed statistically significant changes in blood from patients during the PR phase. First of all, the percentage of total CD4⁺ T lymphocytes was higher in non-remitter patients at 8 months when compared to patients during the PR phase, to remitter patients at 12 months and controls. As for total CD8⁺ T lymphocytes, a decrease in their percentage was found at disease onset in comparison to the control group. Although no differences between remitters and non-remitters were found regarding CD4⁺ and CD8⁺ absolute numbers, both subpopulations tend to increase with disease progression, especially in remitter patients (**Figure 18**).

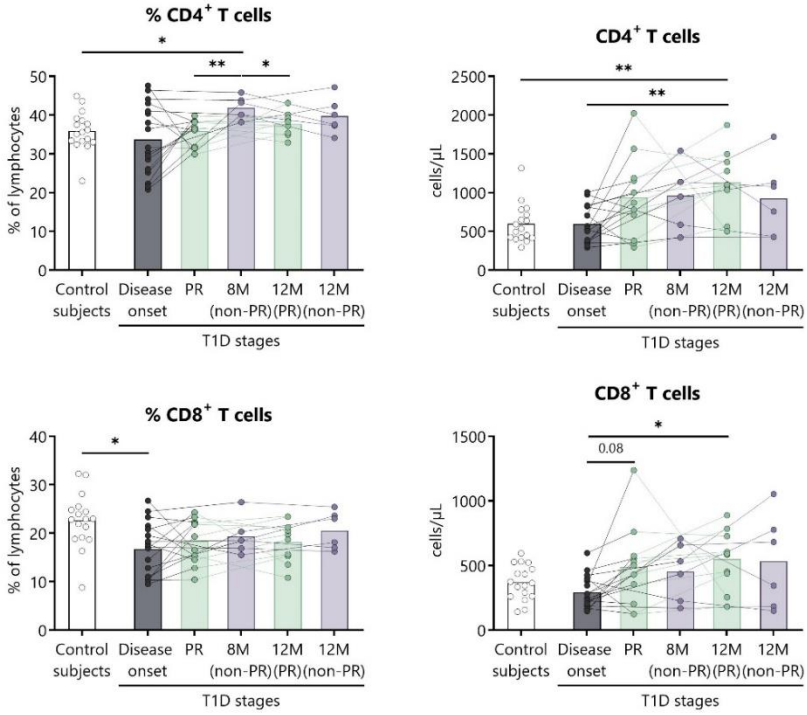

Figure 18. ***Total CD4⁺ and CD8⁺ T lymphocytes are altered at the initial stages of T1D.*** *For CD4⁺ (up) and CD8⁺ (down) T lymphocytes, the percentages (left) and absolute numbers (right) were determined in peripheral blood of control subjects and patients with T1D at different time-points. White bars correspond to control subjects (n=17), grey bars to patients at disease onset (n=17), green bars to patients at partial remission (PR, n=11; at 12M, n=10) and lilac bars to non-remission (non-PR at 8M, n=6; at 12M, n=6). Bar graphs show mean percentage or absolute count values. Each symbol represents an individual patient. Lines link the same patient throughout the time-points. *p ≤0.05, **p <0.01, after mixed effects model with Tukey's post-hoc test for longitudinal data, Kruskal–Wallis with Dunn's post-hoc test for comparisons between control subjects and the different T1D time-points, or 2-tailed Mann–Whitney test for comparisons between two unpaired groups of data. P ≤0.05 is considered significant.*

Regarding CD4⁺ T lymphocytes, non-remitter patients presented higher percentages of naïve CD4⁺ T lymphocytes both at 8 and 12 months in comparison to patients at disease onset (**Figure 19A**). While the percentage of central memory (CM) CD4⁺ T lymphocytes tended to increase with disease progression for the remitter ones —especially at 12 months after T1D onset in comparison to the diagnosis and the control group—, the percentage of this subpopulation tended to decrease at 12 months for non-remitter patients in comparison to the 8 months' time-point, where levels were also higher than those of the control group. However, no significant differences were observed between remitters and non-remitters (**Figure 19B**). The percentage of CD4⁺ terminally differentiated effector memory T cells (T_{EMRA}) cells tended to be higher in remitter patients compared to non-remitters at 8 months (**Figure 19C**) and, in general, increased levels were found in the control group or at diagnosis of T1D than during the progression of the disease. Interestingly, we did find increased percentages of EM and especially early (CD27⁺) EM CD4⁺ T lymphocytes in remitters compared to non-remitters (**Figure 19D, E**). Also, the percentages of both subpopulations were significantly increased during the PR phase in comparison to 12 months for non-remitter patients. The non-remitters at 8 months also showed decreased percentages in comparison to disease onset and control subjects, and at 12 months than patients at diagnosis. Concerning the absolute counts, only CD4⁺ T_{EMRA} lymphocytes significantly increased during the PR phase in comparison to 8 months for non-remitters. No other significant difference was observed between patients with and without PR (**Supplementary Figure 14 A-E**).

Regarding CD8⁺ T lymphocytes, patients at the PR phase presented lower percentages of naïve CD8⁺ T lymphocytes compared to patients without PR at 8 months. Moreover, non-remitter patients showed a higher percentage of this subpopulation than controls (**Figure 20A**). Contrary to what was observed in the CM CD4⁺ T lymphocyte subpopulation, the percentage of CM CD8⁺ T lymphocytes tended to decrease with T1D progression and showed a significant increase at disease onset compared to the control group (**Figure 20B**). The percentage of CD8⁺ T_{EMRA} lymphocytes was lower at 8 months for non-remitter patients in comparison to patients at the PR phase and controls (**Figure 20C**). Lastly, and regarding the percentage of EM and early (CD27⁺) EM CD8⁺ T lymphocytes, no differences were found between groups (**Figure 20D, E**). Concerning the absolute counts of these subsets, no significant differences were found between patients with and without PR (**Supplementary Figure 14 F-J**).

The absolute counts and percentages of both late EM CD4⁺ and CD8⁺ T lymphocytes, RTEs, γδ TCR cells, and Th17 lymphocytes did not differ between patients with and without PR (**Supplementary Figure 15**).

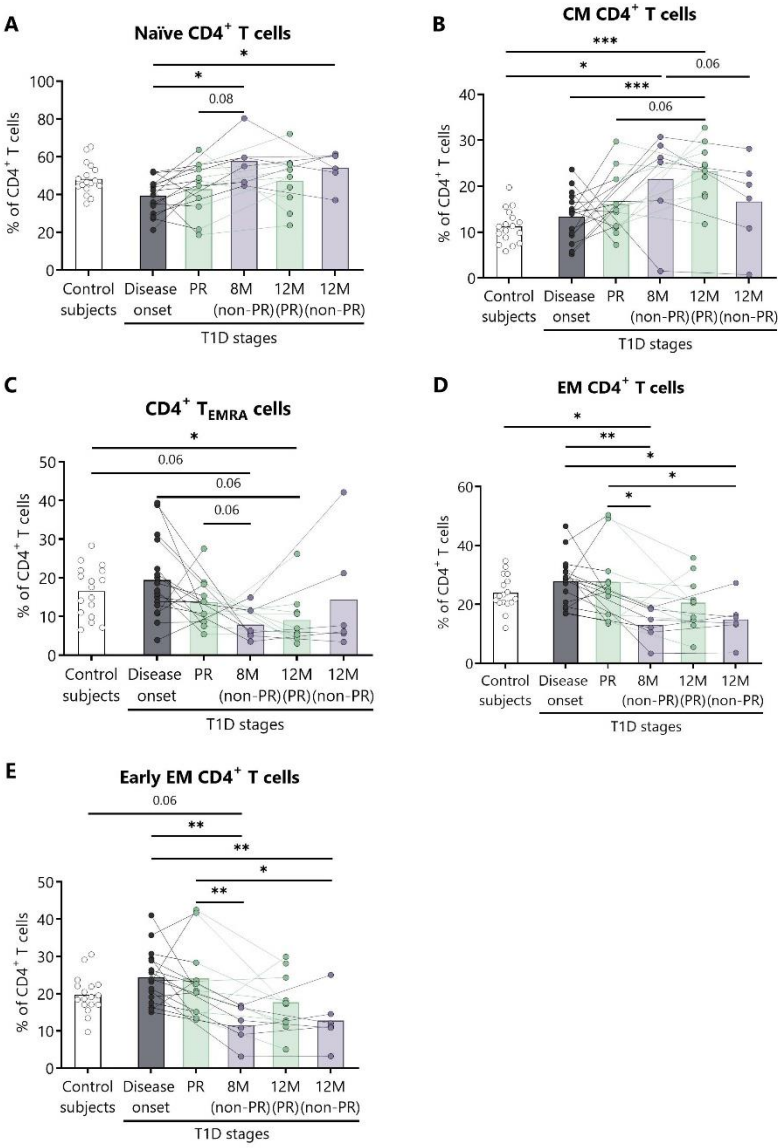

Figure 19. ***Percentages of CD4⁺ T lymphocyte subsets are altered at the initial stages of T1D.*** *For CD4⁺ T lymphocytes, the percentages of* ***(A)*** *naïve T lymphocytes,* ***(B)*** *CM T lymphocytes,* ***(C)*** *T_{EMRA} lymphocytes,* ***(D)*** *EM T lymphocytes, and* ***(E)*** *early EM T lymphocytes were determined in peripheral blood of control subjects and patients with T1D at different time-points. White bars correspond to control subjects (n=17), grey bars to patients at disease onset (n=17), green bars to patients at partial remission (PR, n=11; at 12M, n=10) and lilac bars to non-remission (non-PR at 8M, n=6; at 12M, n=6). Bar graphs show mean percentage values. Each symbol represents an individual patient. Lines link the same patient throughout the time-points. *p ≤0.05, **p <0.01, ***p <0.001 after mixed effects model with Tukey's post-hoc test for longitudinal data, Kruskal–Wallis with Dunn's post-hoc test for comparisons between control subjects and the different T1D time-points, or 2-tailed Mann–Whitney test for comparisons between two unpaired groups of data. P ≤0.05 is considered significant.*

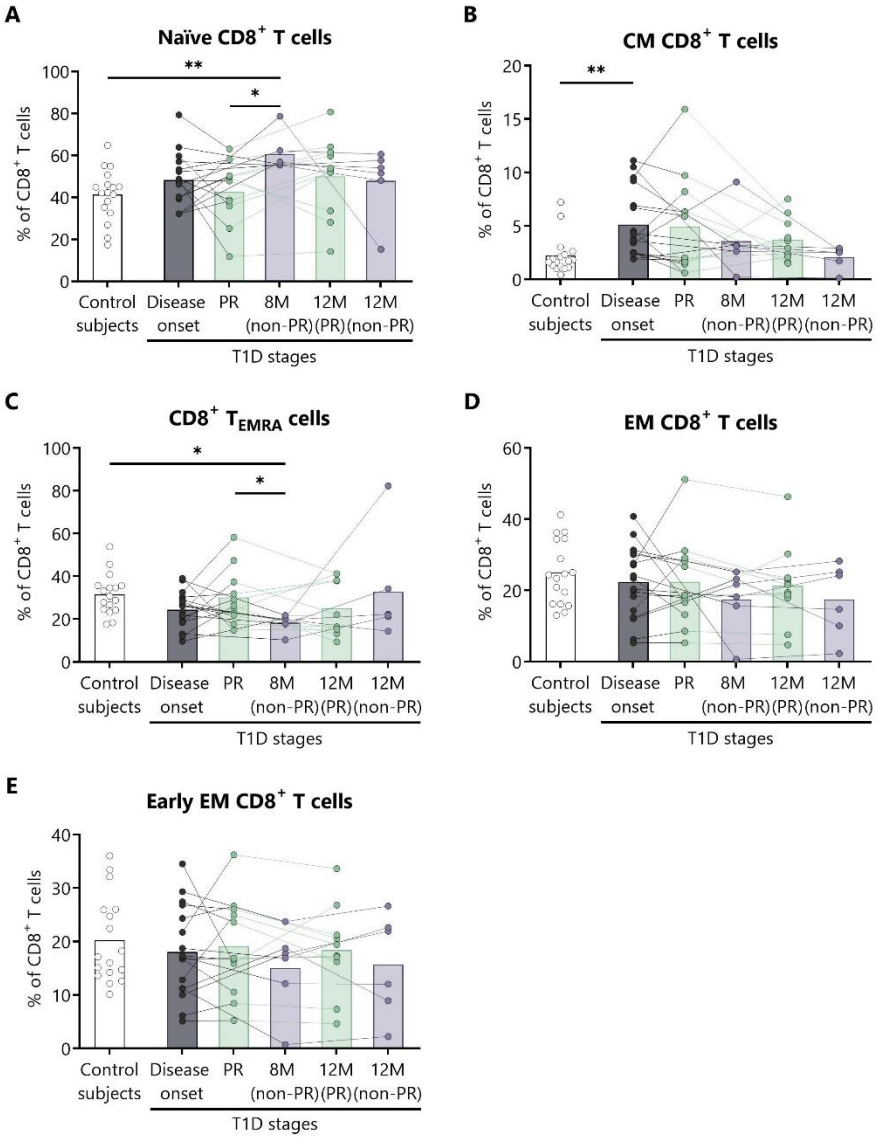

Figure 20. ***Percentages of CD8⁺ T lymphocyte subsets are altered at the initial stages of T1D.*** *For CD8⁺ T lymphocytes, the percentages of* ***(A)*** *naïve T lymphocytes,* ***(B)*** *CM T lymphocytes,* ***(C)*** *T_{EMRA} lymphocytes,* ***(D)*** *EM T lymphocytes, and* ***(E)*** *early EM T lymphocytes were determined in peripheral blood of control subjects and patients with T1D at different time-points. White bars correspond to control subjects (n=17), grey bars to patients at disease onset (n=17), green bars to patients at partial remission (PR, n=11; at 12M, n=10) and lilac bars to non-remission (non-PR at 8M, n=6; at 12M, n=6). Bar graphs show mean percentage values. Each symbol represents an individual patient. Lines link the same patient throughout the time-points. *p ≤0.05 and **p <0.01 after Kruskal–Wallis with Dunn's post-hoc test for comparisons between control subjects and the different T1D time-points, or 2-tailed Mann–Whitney test for comparisons between two unpaired groups of data. P ≤0.05 is considered significant.*

3. Patients in partial remission are characterized by lower levels of total and memory Tregs

Since Tregs are expected to be implicated in the immunoregulatory mechanism behind the PR phase [364], we analyzed peripheral Treg subsets including total, memory, and activated Tregs. Although $CD25^{+}CD127^{lo/-}$ surface staining identifies Tregs in a manner comparable to $CD25^{+}FOXP3^{+}$ staining [365], we confirmed FoxP3 positivity within the Treg population. A representative confirmatory staining for FoxP3 can be found in **Supplementary Figure 5**, where 74.6% of $CD4^{+}CD25^{+}CD127^{lo/-}$ cells do express it.

In T1D subjects, PR was characterized by lower levels of both total Treg and memory Treg compared to non-PR. Non-remitters presented also an increased percentage of total Tregs in comparison to controls and patients at disease onset. After a year of follow-up, remitter patients continued to show a lower percentage of total Tregs compared to the non-remitter ones (**Figure 21A**). Regarding their absolute numbers, total Tregs increased with the disease progression compared to controls and disease onset (**Figure 21B**). The trend was similar to that of total $CD4^{+}$ T lymphocytes.

Concerning memory Tregs, they increased in percentage and number with the disease condition in comparison to the control group. Specifically, non-remitter patients at 8 months and remitter patients at 12 months of progression showed the highest differences (**Figure 21C, D**). Interestingly, patients during the remission phase also presented a lower percentage of memory Tregs compared to non-remitters. As for activated memory Tregs, no differences were found between patients with and without PR (**Supplementary Figure 16**).

A different tendency in the percentage of Treg from disease onset (baseline) to PR was observed for 4 children, who increased this cell subpopulation in contrast to the other remitter patients, just as non-remitter patients did (**Figure 21E**). Since those four children in PR present the same behavior as the non-remitters, differences between the two groups of remitter patients were investigated. Interestingly, these 4 children with increasing percentages of Tregs from baseline were all males and the youngest. Moreover, they presented lower basal C-peptide concentrations and BMI values, required lower doses of insulin, and presented a tendency of a higher percentage of HbA1c in comparison to the other seven remitters with decreasing percentages of Tregs from baseline (**Table 18**). Since pediatric patients diagnosed before age 7 may have a more aggressive form of T1D [23], that could explain the observed changes in Tregs.

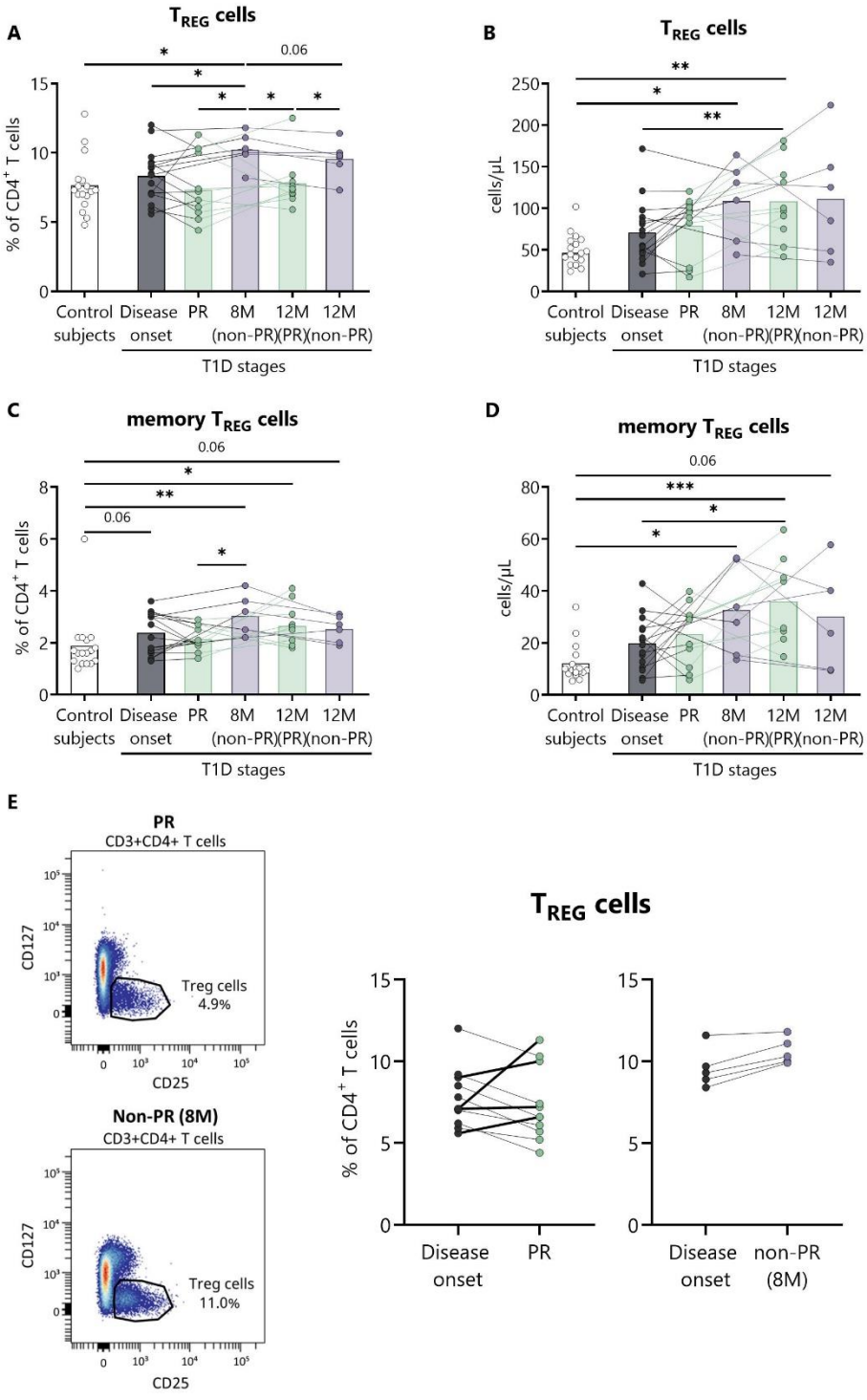

Figure legend on next page

Figure 21. ***Peripheral blood T_{REG} are quantitatively altered at the initial stages of T1D.*** *Percentages (%) and concentrations (cells/μL) of (**A, B**) T_{REG} and of (**C, D**) memory T_{REG} were determined in peripheral blood of controls and patients with T1D at different time-points. (**E**) Representative plots for the difference in the T_{REG} percentage between PR and non-PR (8M), and changes in this cell population from the disease onset to the PR phase or non-PR (8M). White bars correspond to control subjects (n=17), grey bars to patients at disease onset (n=17), green bars to patients at partial remission (PR, n=11; at 12M, n=10) and lilac bars to non-remission (non-PR at 8M, n=6; at 12M, n=6). Bar graphs show mean percentage or absolute count values. Each symbol represents an individual patient. Lines link the same patient throughout the time-points. *p ≤0.05, **p <0.01 and ***p <0.001 after mixed effects model with Tukey's post-hoc test for longitudinal data, Kruskal–Wallis with Dunn's post-hoc test for comparisons between control subjects and the different T1D time-points, or 2-tailed Mann–Whitney test for comparisons between two unpaired groups of data. P ≤0.05 is considered significant.*

Table 18. ***Clinical features and metabolic data of remitter patients classified regarding their decreasing (PR) or increasing (non-PR-like) percentages of Tregs from baseline***

	PR (n=7)	PR (non-PR-like) (n=4)	P-value
Age (years)	11.1 ± 3.98	5.5 ± 1.3	**0.01****
Sex (M/F)	1/6	4/0	**0.006****
BMI (kg/m²)	18.97 ± 3	15.6 ± 1.6	**0.02***
BMI-SDS	-0.1 (-0.6, 1.1)	-0.4 (-1.2, 0.65)	0.53
HbA1c (%)	6.6 ± 0.6	7.3 ± 0.45	0.12
HbA1c (mmol/mol)	49 ± 6.1	55.75 ± 4.8	0.61
Insulin dose (U/Kg/day)	0.44 ± 0.1	0.28 ± 0.01	**0.02***
Basal C-peptide (ng/mL)	1.03 ± 0.5	0.28 ± 0.05	**0.03***

Data presented as mean ± SD, or mean (min, max). P-value calculated from Mann-Whitney test. *p ≤0.05 and **p ≤0.01; p ≤0.05 is considered significant. BMI, Body Mass Index; F, female; HbA1c, glycated hemoglobin; IDAA1c, insulin dose-adjusted HbA1c; M, male; SDS, standard deviation score.

4. Increase in regulatory B lymphocyte subpopulations after one-year follow-up for patients under remission

Because of the described role of B lymphocytes in T1D pathogenesis, we next examined different naïve and memory B lymphocyte subsets. Interestingly, two B lymphocyte subsets with regulatory functions —transitional T1 B lymphocytes and Bregs— were increased at 12 months for remitter patients (**Figure 22**). The percentage of total transitional B lymphocytes was substantially decreased at disease onset when compared to the control group, and their levels tended to recover with time (**Figure 22A**). Within this subpopulation, transitional T1 B lymphocytes increased in percentage at 12 months for patients that experienced the PR phase when compared to the diagnosis, while transitional T2 B lymphocytes decreased (**Figure 22B, C**). Moreover, at this time-point, patients presented a higher T1/T2 ratio than patients at T1D onset (**Figure 22D**). Although no differences were observed in the percentage of Bregs between the different groups (**Figure 22E**), patients in remission at 12 months had a higher concentration of circulating Bregs compared to controls (**Figure 22F**).

Concerning the percentages and absolute counts of total B lymphocytes, naïve B lymphocytes, $CD21^{-/low}$ naïve B lymphocytes, mature naïve B lymphocytes, memory B lymphocytes —including exhausted, unswitched, switched, and IgM memory B lymphocytes— (**Supplementary Figures 17 and 18**) and plasmablasts (**Supplementary Figure 19**), no differences were found between patients with and without PR.

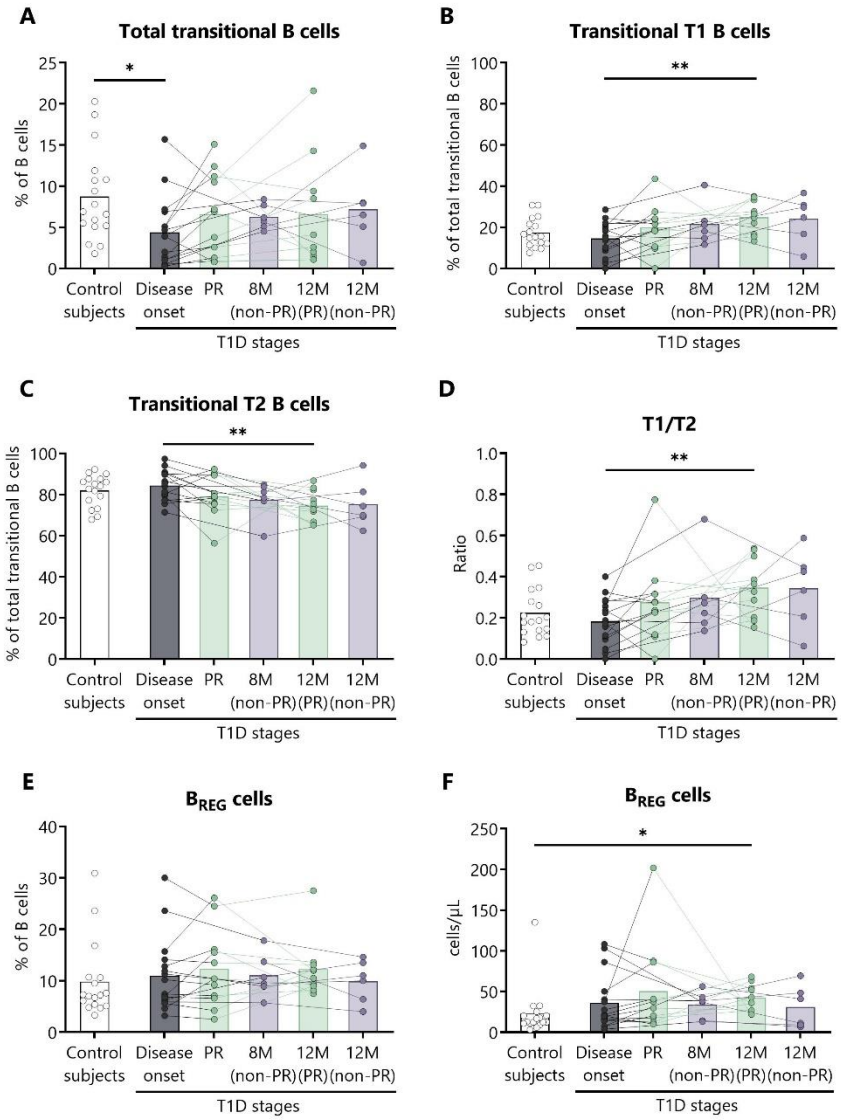

Figure 22. ***Two regulatory subsets of B lymphocytes are quantitatively altered at the initial stages of T1D.*** *Percentages of (**A**) total transitional B lymphocytes and of their subdivision into (**B**) T1, and (**C**) T2, (**D**) the T1/T2 ratio, and (**E, F**) the percentage and concentration (cells/µL) of B_{REG} cells were determined in peripheral blood of controls and patients with T1D at different time-points. White bars correspond to control subjects (n=17), grey bars to patients at disease onset (n=17), green bars to patients at partial remission (PR, n=11; at 12M, n=10) and lilac bars to non-remission (non-PR at 8M, n=6; at 12M, n=6). Bar graphs show mean percentage or absolute count values. Each symbol represents an individual patient. Lines link the same patient throughout the time-points. *p ≤0.05 and **p <0.01 after mixed effects model with Tukey's post-hoc test for longitudinal data, or Kruskal–Wallis with Dunn's post-hoc test for comparisons between control subjects and the different T1D time-points. P ≤0.05 is considered significant.*

5. Increase in regulatory NK cells and decrease in effector NK cells after one-year follow-up for patients under remission

NK cells are cytotoxic innate-like lymphocytes with a reported dual behavior in T1D, one that promotes β-cell destruction and another that protects against the autoimmune attack [366]. This property can be explained by their functional subdivision into NKeffs or regulatory NK cells (NKregs). Therefore, different subsets of NK cells were analyzed. The percentage of total NK cells was decreased in patients at disease onset and during remission, even after 12 months of disease progression, compared to control subjects. Their absolute numbers also followed the same tendency, with lower counts of NK cells at T1D onset compared to control subjects (**Figure 23A**). Regarding their two main cell subsets, a tendency of decreased percentages of NKeffs was found in patients with T1D at all the different time points when compared to control subjects, a difference that was more pronounced in remitters. Moreover, their absolute counts were also reduced at disease onset compared to control subjects (**Figure 23B**). In contrast, the percentage of NKregs tended to increase in patients with T1D compared to controls at all time points, although no statistically significant differences were observed. Compared to diagnosis or non-remission, remitters showed a tendency to increase the percentage of NKregs. Regarding their absolute number, patients tended to have lower levels at disease onset compared to controls, while NKregs recovered with disease progression, especially in remitter patients after 12 months of progression (**Figure 23C**).

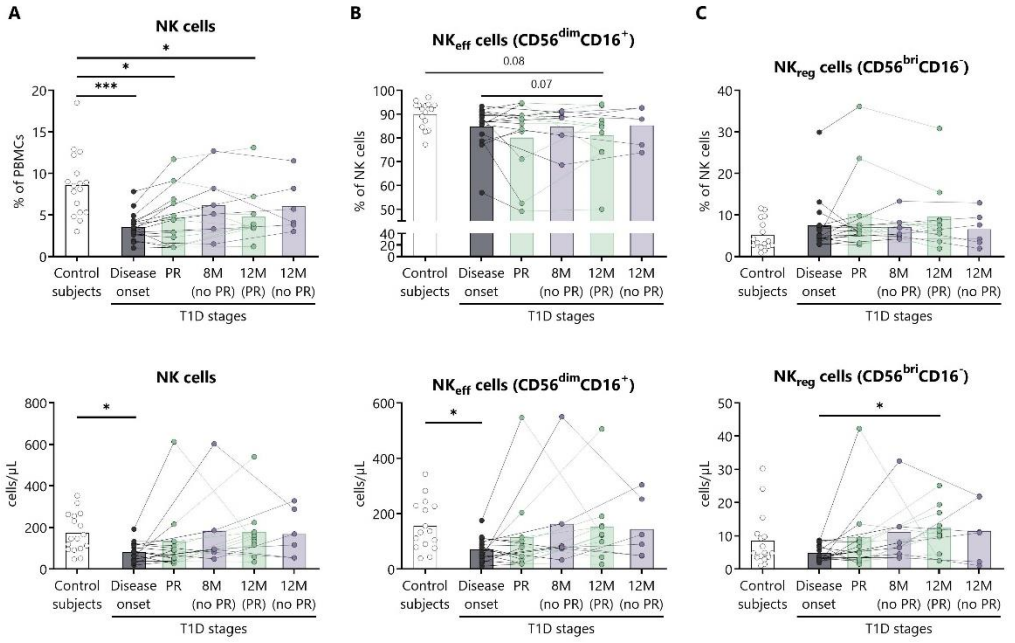

Figure legend on next page

Figure 23. ***Peripheral blood NK subsets are quantitatively altered at the initial stages of T1D.*** *Percentages and concentrations (cells/μL) of (**A**) total NK cells, (**B**) effector NK cells (NK_{eff}) and (**C**) regulatory NK cells (NK_{reg}) were determined in peripheral blood of controls and patients with T1D at different time-points. White bars correspond to control subjects (n=17), grey bars to patients at disease onset (n=17), green bars to patients at partial remission (PR, n=11; at 12M, n=10) and lilac bars to non-remission (non-PR at 8M, n=6; at 12M, n=6). Bar graphs show mean percentage or absolute count values. Each symbol represents an individual patient. Lines link the same patient throughout the time-points. *p ≤0.05, **p <0.01 and ***p <0.001 after mixed effects model with Tukey's post-hoc test for longitudinal data, or Kruskal–Wallis with Dunn's post-hoc test for comparisons between control subjects and the different T1D time-points. P ≤0.05 is considered significant.*

Concerning the percentages and absolute counts of intermediate NK cells ($CD56^{bri}CD16^{+}$) and $CD56^{dim}CD16^{-}$ NK cells, no differences were found between patients with and without PR (**Supplementary Figure 20**).

6. Classical monocytes are increased in remitter patients after diagnosis

Finally, changes in monocytes and DCs were investigated. Although no significant differences were found between groups regarding the percentage of total monocytes (**Figure 24A**), we found an increase in the percentage of classical monocytes during the PR phase in comparison to disease onset, and a subsequent decrease in the percentage of non-classical monocytes (**Figure 24B, C**). The percentage of total dendritic cells, as well as that of their myeloid and plasmacytoid subsets, remained unchanged throughout the different stages of T1D (**Figure 24D–F**). However, at the time of diagnosis, a tendency to a lower percentage of pDC was presented compared to controls.

Concerning the absolute numbers of monocytes and their subsets and myeloid DCs (mDCs) and pDCs, no differences were found between patients with and without PR (**Supplementary Figure 21**). However, one year after onset, non-remitters presented lower counts of total DCs than remitters. When further subdividing the mDC subset according to the expression of Slan and CD16, no differences were found between patients with and without PR (**Supplementary Figure 22**).

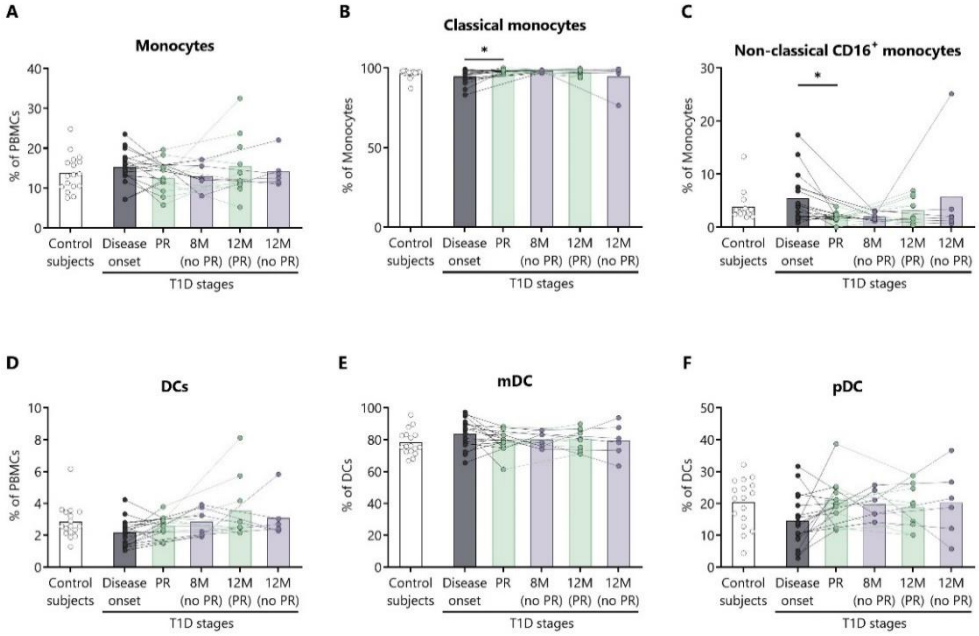

Figure 24. ***Monocytes and DCs are maintained during the different stages of T1D.*** *Percentages of (**A**) Monocytes, (**B**) Classical monocytes, (**C**) Non-classical monocytes, (**D**) DCs, (**E**) mDCs, and (**F**) pDCs were determined in peripheral blood of controls and patients with T1D at different time-points. White bars correspond to control subjects (n=17), grey bars to patients at disease onset (n=17), green bars to patients at partial remission (PR, n=11; at 12M, n=10) and lilac bars to non-remission (non-PR at 8M, n=6; at 12M, n=6). Bar graphs show mean percentage. Each symbol represents an individual patient. Lines link the same patient throughout the time-points. *p ≤0.05 after mixed effects model with Tukey's post-hoc test for longitudinal data. P ≤0.05 is considered significant.*

7. PR shows no variation in plasma cytokine concentration

Different cytokines involved in T1D including IL-2, IL-6, TGF-β1, IL-17A, and IL-10 were prospectively analyzed in the plasma of patients as potential biomarkers of PR. Although no statistically significant differences were found between patients with and without PR, a trend towards higher levels of all cytokines was observed at the onset of T1D compared to controls. No differences in IL-2 levels were observed between the groups (**Figure 25A**). Regarding IL-6, patients at disease onset presented a significant increase compared to non-remitters at 12 months (**Figure 25B**). Furthermore, the higher concentration of TGF-β1 found at diagnosis tended to decrease with disease progression, especially during the PR phase and at 12 months in patients without PR (**Figure 25C**). Regarding IL-17A, a statistically significant increase was found at the onset of T1D compared to controls. Interestingly, remitters tended to maintain lower levels of this cytokine compared to non-remitters, even at 12-month time-point. After one year

of follow-up, non-remitter patients also showed higher IL-17A levels than the control group (**Figure 25D**). Finally, IL-10 remained constant between groups (**Figure 25E**).

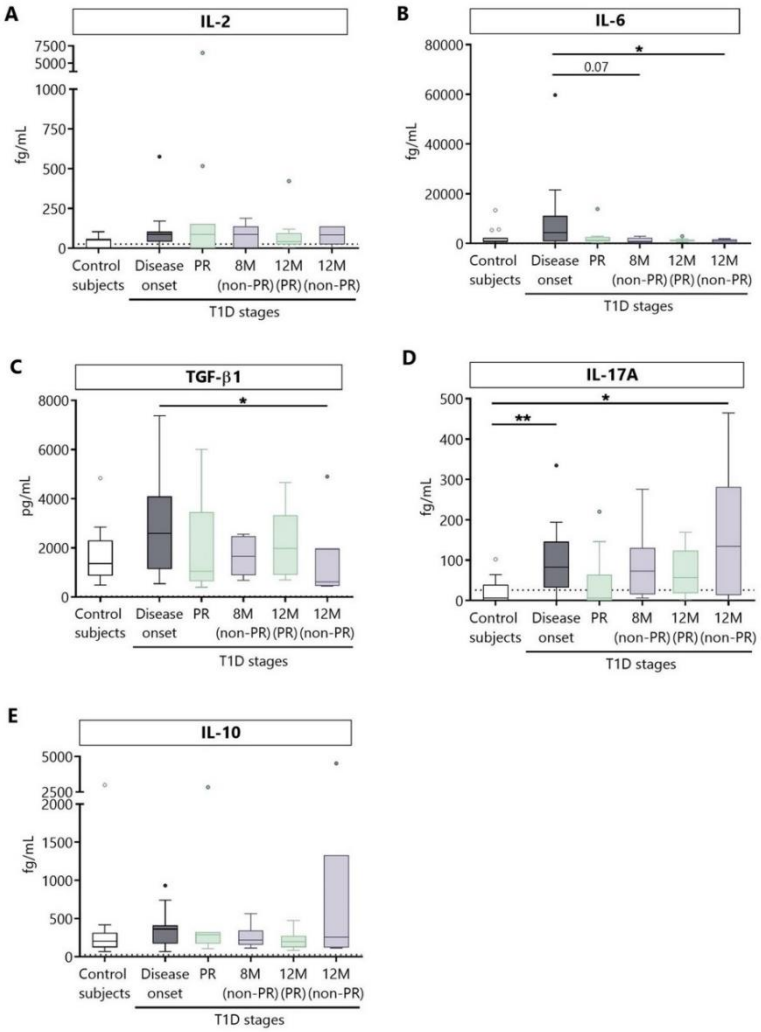

Figure 25. ***Circulating cytokine concentrations at different stages of T1D.*** *Plasma from controls and patients with T1D at different time-points was obtained to quantitatively determine the concentrations of (**A**) IL-2, (**B**) IL-6, (**D**) IL-17A, and (**E**) IL-10 by CBA and of (**C**) TGF-β1 by ELISA. Uncolored boxes represent controls (n=17), and patients are represented by gray boxes at disease onset (n=17), green boxes at PR (n=11) and for remitter patients at 12 months (12M PR) (n=10), and lilac boxes for non-remitter patients at 8 months (8M non-PR) (n=6) and 12 months (12M non-PR) (n=6). Data are presented as box-and-whisker plots. Boxes indicate the first and third quartiles. The horizontal bar in the box indicates the median. Whiskers are drawn using Tukey's criteria of 1.5× the interquartile range. Outliers are shown. *p ≤0.05, **p <0.01 after mixed effects model with Tukey's post-hoc test for longitudinal data, or Kruskal–Wallis with Dunn's post-hoc test for comparisons between controls and T1D time-points. P ≤0.05 is considered significant.*

— SECTION II. Epigenetic biomarkers of partial remission

This section aims to characterize and validate miRNA profiles during different stages of T1D (diagnosis, remission, and non-remission) to identify specific epigenetic markers for the honeymoon phase. Additionally, a bioinformatic study is conducted to analyze the molecular pathways and biological processes targeted by these miRNAs, providing insight into the pathways involved in establishing the phase of PR.

1. Distinct miRNA signature during the PR phase: miR-30d-5p is the most differentially expressed

To identify miRNA expression signatures during PR, small RNA was isolated and sequenced from the plasma of the discovery cohort consisting of 17 newly diagnosed children with T1D (age: 8.7 ± 3.6 years, mean ± SD), of whom 11 were remitters (age: 9.1 ± 4.3 years), and 6 were non-remitters (at eight months after diagnosis; age: 9 ± 2.8) (**Table 19**). The control group consisted of 17 age- and sex-matched non-diabetic children (age: 8.8 ± 3.4) who visited the Germans Trias i Pujol University Hospital.

However, due to the limited amount of small RNAs, only 13 samples out of the 17 at T1D diagnosis time-point could be profiled on the Illumina NextSeq 1000 System. First, we focused on the comparison between remitters and non-remitters to find a specific miRNA signature that defines the PR. The hierarchical clustering heatmap revealed 16 DEMs ($|\log(FC)| > 1$ and p-value ≤ 0.05); 12 of them were upregulated, and 4 were downregulated during the remission phase (**Figure 26A**). To identify the miRNAs with the greatest FC and the lowest p-value, a volcano plot was constructed, where blue dots represent downregulated miRNAs, and red dots represent the upregulated ones. Among the upregulated miRNAs, miR-30d-5p had the greatest FC with the highest statistical significance, followed by miR-106a-5p and miR-20b-5p (**Figure 26B**). Additionally, it is worth mentioning that five miRNAs (miR-106a-5p, miR-106b-5p, miR-18b-5p, miR-17-5p, and miR-20b-5p) belong to the same family of miRNAs, the MIR-17 family. Furthermore, we conducted a principal component analysis based on the miRNA expression of each sample, which effectively differentiated the two clusters of patients: the green cluster represents the remitters (PR), and the lilac cluster represents the non-remitters (non-PR) (**Figure 26C**). Nevertheless, two remitter patients were clustered within the non-remitter group, which coincides with the two of the heatmap that showed a distinct profile in comparison to the other PR patients (marked with an asterisk); one of them also presented celiac disease. The biplot, which displays the principal component scores and miRNAs, helped us identify which miRNA influenced each component. In this

case, the non-PR group was most influenced by miR-25-5p, let-7b-5p, let-7c-5p, and miR-10393-3p (**Supplementary Figure 23**).

Table 19. ***Clinical and metabolic data of patients with T1D from the discovery and validation cohorts***

	Discovery cohort				Validation cohort			
	Ctrl	**T1D dx**	**PR**	**Non-PR**	**Ctrl**	**T1D dx**	**PR**	**Non-PR**
N (no. females)	17 (10)	17 (10)	11 (6)	6 (4)	15 (9)	8 (4)	10 (5)	9 (7)
Age at diagnosis (years)	8.8 ± 3.4	8.7 ± 3.6	9.1 ± 4.3	9 ± 2.8	9.7 ± 3.6	11.6 ± 2.7	11.8 ± 2.9	7.3 ± 3.7
BMI (kg/m^2)	18.3 ± 4.3	16.8 ± 2.5	17.7 ± 3	17.2 ± 2.1	19 ± 4.2	19.4 ± 4.3	20.2 ± 4.6	16.9 ± 1.7
HbA1c (%)	ND	11.4 ± 2.4	6.9 ± 0.6	8.1 ± 0.7	ND	12.6 ± 2.5	6.4 ± 0.6	8.3 ± 0.6
Insulin dose (U/kg/day)	ND	0.7 ± 0.2	0.4 ± 0.1	0.9 ± 0.1	ND	0.77 ± 0.2	0.46 ± 0.2	0.87 ± 0.2
IDAA1c	ND	14.3 ± 3	8.4 ± 0.5	11.5 ± 1	ND	15.7 ± 3.1	8.2 ± 0.79	11.8 ± 1.4
Basal C-peptide (ng/mL)	1.3 ± 0.4	0.3 ± 0.2	0.7 ± 0.5	0.3 ± 0.1	1.97 ± 0.4	0.44 ± 0.3	1 ± 0.57	0.2 ± 0.1

Data presented as mean ± SD. *Abbreviations*: *BMI*, Body Mass Index; *Ctrl*, controls; *HbA1c*, glycated hemoglobin; *IDAA1c*, insulin dose-adjusted HbA1c; *ND*, not determined; *non-PR*, non-partial remission; *PR*, partial remission; *T1D dx*, type 1 diabetes diagnosis.

To identify differences in miRNA expression during PR compared to the other groups (control, diagnosis and non-PR), t-tests were performed using normalized RNA-seq counts. The results confirmed the increased expression of miR-30d-5p during the PR phase compared not only to non-PR but also to the disease diagnosis and control groups. This finding strengthens its potential as a specific biomarker of remission. In contrast, let-7c-5p exhibited a specific increase during the non-PR (**Figure 26D**, **Table 20**).

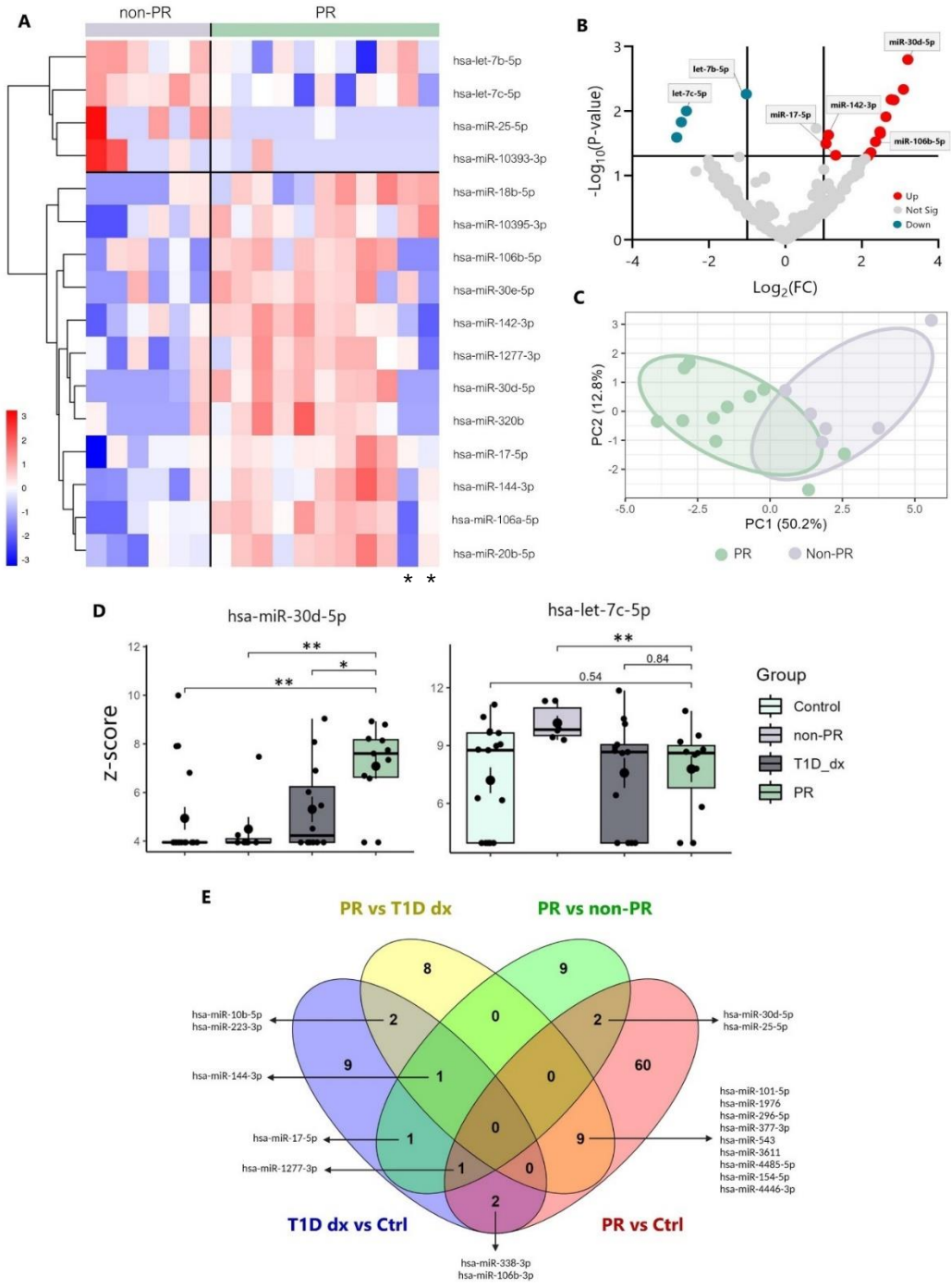

Figure caption on next page

Figure 26. ***Distinct miRNA signature in plasma during the partial remission phase of T1D in pediatric patients.*** *(**A**) Hierarchical clustering heatmap showing the 16 miRNAs with significantly different expression levels (DEMs) in plasma among pediatric patients with T1D in remission (PR, green) and without remission (non-PR, lilac) from the discovery cohort. Each column represents individual samples, and each row represents an individual miRNA. Upregulated miRNAs are shown in red, and downregulated miRNAs are shown in blue. An asterisk below two patients in PR marks their different miRNA expression patterns compared to other remitters. (**B**) Volcano plot showing changes in miRNA levels between pediatric patients with T1D in remission and without remission. Lines indicate log(FC) (x−axis) and p-value (y−axis) cut-offs. Blue and red dots indicate significantly downregulated and upregulated miRNAs during PR, respectively, and grey dots indicate non-significantly different expression levels of miRNAs. (**A, B**) Log(FC) >1 for upregulated DEMs, and log(FC) <1 for downregulated DEMs. P-value ≤0.05 by moderated t-test; n=6–11. (**C**) Principal component analysis plot of the 16 DEMs. Each dot represents a sample. Green: remitter patients (n=11); lilac: non-remitter patients (n=6). (**D**) Boxplot of the normalized expression (z-score) of miR-30d-5p and let-7c-5p from the small RNA-seq data in controls (blue, n=17), T1D diagnosis (dx, grey, n=13), PR (green, n=11) and non-PR (lilac, n=6). Error bars indicate 95% confidence intervals and center line is the median. ns ≥0.05, *p ≤0.05, **p ≤0.01, t-test. (**E**) Venn diagrams showing overlapping DEMs with validated target genes between different comparisons (PR vs. non-PR; PR vs. controls (Ctrl); PR vs. T1D diagnosis (dx), T1D diagnosis vs. controls).*

To examine which of these DEMs during PR were present in other comparisons, we created Venn diagrams. While we observed that miR-30d-5p is quite specific for PR, other miRNAs were more related to the general disease status, such as miR-17-5p or miR-144-3p, which were further differentially expressed between the control group and the diagnosis of T1D in those future remitter patients (**Figure 26E**).

Table 20 shows the DEMs (|log(FC)| >1 and p-value ≤0.05) with validated target genes between PR vs. non-PR (#14) and PR vs. their diagnosis time-point (#20) as well as those that were also differentially expressed between PR vs. controls (#12). The complete list of DEMs between PR vs. controls (#62) and T1D diagnosis vs. controls (#16) is available in **Supplementary Table 3**.

Other miRNAs also demonstrated increased expression during the PR versus non-PR, such as miR-18-5p, miR-20b-5p, miR-30e-5p, miR-106a-5p, and miR-144-3p, and a decreased expression for let-7b-5p (**Figure 27**). However, no significant differences were found when compared to the diagnostic or control group.

Table 20. ***Differentially expressed circulating miRNAs with validated target genes during the partial remission phase***

miRNAs	PR vs Ctrl (FC)	P-value	PR vs T1D dx (FC)	P-value	PR vs non-PR (FC)	P-value
hsa-miR-30d-5p	1.777	0.019	1.780	0.053	3.208	0.001
hsa-let-7b-5p	-	-	-	-	-1.019	0.005
hsa-miR-106a-5p	-	-	-	-	2.771	0.006
hsa-miR-20b-5p	-	-	-	-	2.842	0.006
hsa-let-7c-5p	-	-	-	-	-2.587	0.009
hsa-miR-25-5p	-1.921	0.019	-	-	-2.722	0.014
hsa-miR-320b	-	-	-	-	2.477	0.020
hsa-miR-30e-5p	-	-	-	-	2.485	0.022
hsa-miR-142-3p	-	-	-	-	1.125	0.023
hsa-miR-106b-5p	-	-	-	-	2.361	0.030
hsa-miR-144-3p	-	-	-1.027	0.006	1.064	0.032
hsa-miR-18b-5p	-	-	-	-	2.235	0.043
hsa-miR-17-5p	-	-	-	-	1.319	0.048
hsa-miR-1277-3p	2.126	0.008	-	-	2.162	0.049
hsa-miR-101-5p	-1.935	0.015	-2.910	0.002	-	-
hsa-miR-4485-3p	-	-	-2.890	0.005	-	-
hsa-miR-10b-5p	-	-	2.697	0.005	-	-
hsa-miR-1976	-1.568	0.037	-2.433	0.008	-	-
hsa-miR-296-5p	-1.830	0.018	-2.444	0.009	-	-
hsa-miR-377-3p	-2.028	0.016	-2.558	0.013	-	-
hsa-miR-543	-1.838	0.023	-2.311	0.018	-	-
hsa-miR-24-3p	-	-	2.069	0.019	-	-
hsa-miR-3611	-2.293	0.002	-2.108	0.019	-	-
hsa-miR-4485-5p	-2.883	0.005	-2.846	0.020	-	-
hsa-miR-154-5p	-2.556	0.001	-2.256	0.020	-	-
hsa-miR-223-3p	-	-	1.311	0.021	-	-
hsa-miR-324-3p	-	-	-2.244	0.022	-	-
hsa-miR-1-3p	-	-	-2.263	0.029	-	-
hsa-miR-4449	-	-	-1.951	0.037	-	-
hsa-miR-365a-3p	-	-	2.059	0.039	-	-
hsa-miR-365b-3p	-	-	2.059	0.039	-	-
hsa-miR-4446-3p	-2.194	0.009	-2.025	0.043	-	-
hsa-miR-132-3p	-	-	-1.943	0.045	-	-

Data analyzed by Moderated t-test. Abbreviations: Ctrl, controls; FC; fold change; non-PR, non-partial remission; PR, partial remission; T1D dx, type 1 diabetes diagnosis.

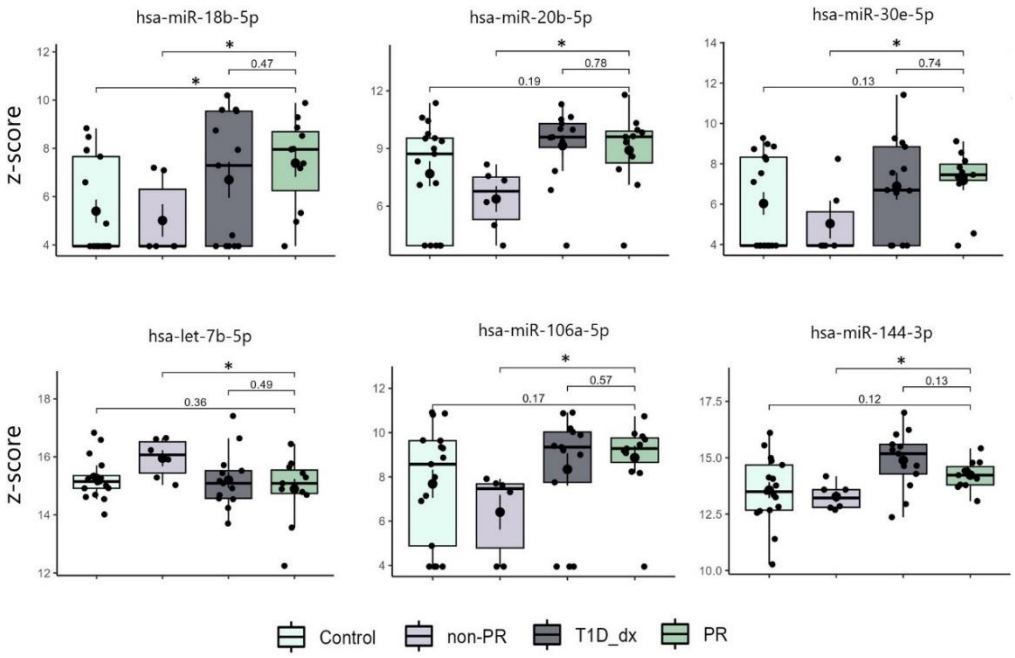

Figure 27. ***Differentially expressed miRNAs during the partial remission phase in comparison to non-remission according to the normalized counts.*** *Boxplots of the normalized expression (z-score) of miR-18b-5p, miR-20b-5p, miR-30e-5p, let-7b-5p, miR-106a-5p and miR-144-3p from the small RNA-seq data in controls (blue, n=17), T1D diagnosis (dx, grey, n=13), PR (green, n=11) and non-PR (lilac, n=6). Error bars indicate 95% confidence intervals and center line is the median. ns ≥0.05, *p ≤0.05, t-test.*

2. Differentially expressed miRNAs during PR target genes related to regeneration, metabolism and immune system

Subsequently, an examination was conducted across various databases to ascertain the target genes associated with each DEM during PR, either predicted or experimentally validated. A considerable number of target genes, exceeding 2,000, were identified for the majority of miRNAs. To manage the substantial volume and intricacy of the data, a selection process was implemented using bioinformatic algorithms. This facilitated the categorization of target genes based on their relevance to processes integral to PR, such as regeneration, metabolism, or the immune system. The outcomes of this classification are presented in **Table 21** for miR-30d-5p and **Supplementary Table 4** for the rest of the DEMs.

Given that miR-30d-5p exhibited the most significant differential expression during PR, an in-depth analysis of its target genes was undertaken. Among the classified target genes, 58% were found to be associated with the immune system, 29% with

regeneration, and 13% with metabolism, as shown in **Table 21**. Notably, miR-30d-5p emerged as one of the miRNAs with the highest count of target genes associated with immune-related processes (**Supplementary Figure 24**). Furthermore, miR-30d-5p is noteworthy for its unique target genes that are directly involved in the activation of T lymphocytes, including *CTLA-4* or *CD226*. Within its target genes linked to the immune system, notable associations include genes involved in leukocyte chemotaxis (*CCL17*, *CCL5*, or *CXCL8*), apoptosis (*DIDO1*, *FAS*), lymphocyte differentiation and activation (*BCL6*, *NFAT5*, *BMP2, CD200*), antigen presentation (*HLA-DRA*), and/or the regulation of cytokine expression (*IL-10*, *IL-21R*, *JAK1*, *SMAD7*, *SOCS1*, or *TGFBR2*). Related to the regeneration, there are genes implicated in cellular death (*BNIP3*, *CASP4*, *DIDO1*, *MCL1*), stem cell function and maintenance (*BCL11A*, *NOTCH*), angiogenesis (*VEGFA*, *VEGFC*, *NRP1*), senescence (*UBN1*), and epithelial growth (*NOTCH*, *ADGRE1*, *GXYLT1*). Other genes were associated to RNA metabolism (*CPEB2*, *DDX6*, *EDC3*, *RIOX2*, *XRN1*), protein metabolism (*HSPA5*) or iron metabolism (*IREB2*).

Table 21. ***Selected target genes for miR-30d-5p related to regeneration, metabolism or the immune system***

miRNA	Genes for regeneration	Genes for metabolism	Genes for immune system
hsa-miR-30d-5p	ADAM9, ADGRE1, APPL1, BCL11A, BNIP3, BNIP3L, CASP4, CASP7, DEGS1, DIDO1, FAT1, GXYLT1, MCL1, NOTCH1, NOTCH2, NRP1, NRXN3, RAB11FIP1, RBBP6, TNC, UBN1, VEGFA, VEGFC, ZFP36L1, ZFP36L2	CPEB2, DDX6, EDC3, HSPA5, IREB2, MYCBP2, OAS1, OAS2, RIOX2, VKORC1L1, XRN1	ATG12, BCL6, BMP2, CCL17, CCL5, CCR1, CD200, CD226, CNOT9, CTLA4, CXCL11, CXCL8, DIDO1, FAF2, FAS, FCRLB, FMOD, GCSAM, GDNF, HLA-DRA, IFITM1, IFITM2, IFITM3, IL10, IL1RAPL1, IL21R, INHBA, ITSN2, JAK1, KLF14, LAMP3, LGR4, MAPK8, MICB, NCR3LG1, NFAT5, NFATC3, NMI, OTUD6B, PRDM1, PTPN13, SKI, SMAD2, SMAD7, SOCS1, STON1, TAF4B, TGFBR2, TGFBR3, TNFSF13B, TNFSF9

3. Enriched biological functions and pathways under the regulation of differentially expressed miRNAs during PR are related to immune system, stress, apoptosis and metabolic processes

To identify potential biological functions and pathways affected by the miRNA signature during PR, we performed in silico miRNA functional analyses based on the inferred miRNA target genes using the DIANA-miRPath v3.0 web server. Only miRNAs with experimentally validated target genes were used in this case, thus excluding miR-10393-3p and miR-10395-3p from the analysis. Biological processes and pathways were investigated using the DIANA-TarBase v7.0 and a Fisher's exact test, and the FDR method (q-values) was used to calculate the enriched targeted ones. The interactive graph of similar non-redundant GO terms was retrieved from the web server REVIGO, and it clearly showed two different clusters of enriched biological processes: one comprising different metabolic processes (e.g., mRNA metabolic process, cellular lipid metabolic process, or cellular protein metabolic process) (upper cluster) and the other including different signaling pathways related to the immune response (e.g., toll-like receptor (TLR)6:TLR2 signaling pathway or Fc-gamma receptor signaling pathway involved in phagocytosis), apoptosis (e.g., intrinsic apoptotic signaling pathway), or stress (e.g., stress-activated MAPK cascade) (lower cluster) (**Figure 28**). These biological functions are relevant to the pathogenesis of T1D.

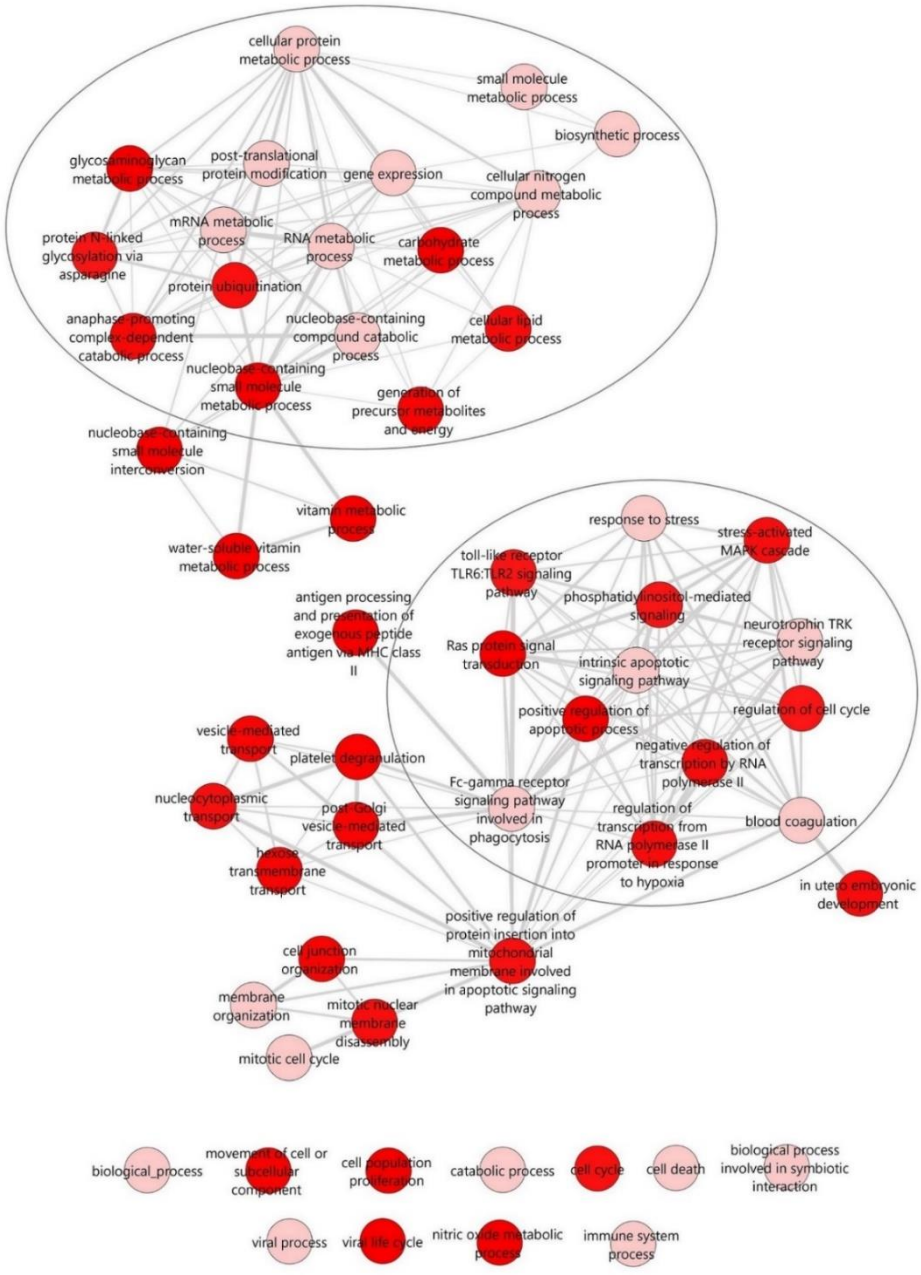

Figure 28. ***Interactive graph of the enriched GO terms for the selected miRNAs.*** *The interactive graph was generated using the web tool REVIGO (http://revigo.irb.hr/, accessed on 21 January 2022), which plots the remaining relevant GO terms (after reducing redundancy) for the 14 DEMs with validated target genes that were retrieved from the DIANA-miRPath v3 (http://www.microrna.gr/miRPathv3, accessed on 21 January 2022) web server using the TarBase v7*

*database. Highly similar GO terms are linked by edges in the graph, where the line width indicates the degree of similarity. The bubble color indicates the provided p-value for the FDR (q-value). Darker red color indicates statistically more significant GO terms. Two main clusters of biological processes were identified: one comprising different signaling pathways related to the immune response, apoptosis, or stress (**upper** circle) and the other comprising metabolic processes (**lower** circle).*

The examination of the biological functions associated with miR-30d-5p was subsequently undertaken. Based on the GO analysis, the miR-30d-5p was enriched in 97 terms in the biological process category and 18 in the molecular function category with a p-value (FDR) ≤0.05. Some of these GO terms were selected and presented in **Figure 29** according to the gene count. Notably, this miRNA exhibited enrichment in various biological processes, including stress response, cellular apoptosis, fatty acid and mRNA metabolism, the insulin receptor signaling pathway, and diverse immune-related processes, encompassing antigen processing and presentation, as well as TLR and TGF-β signaling pathways.

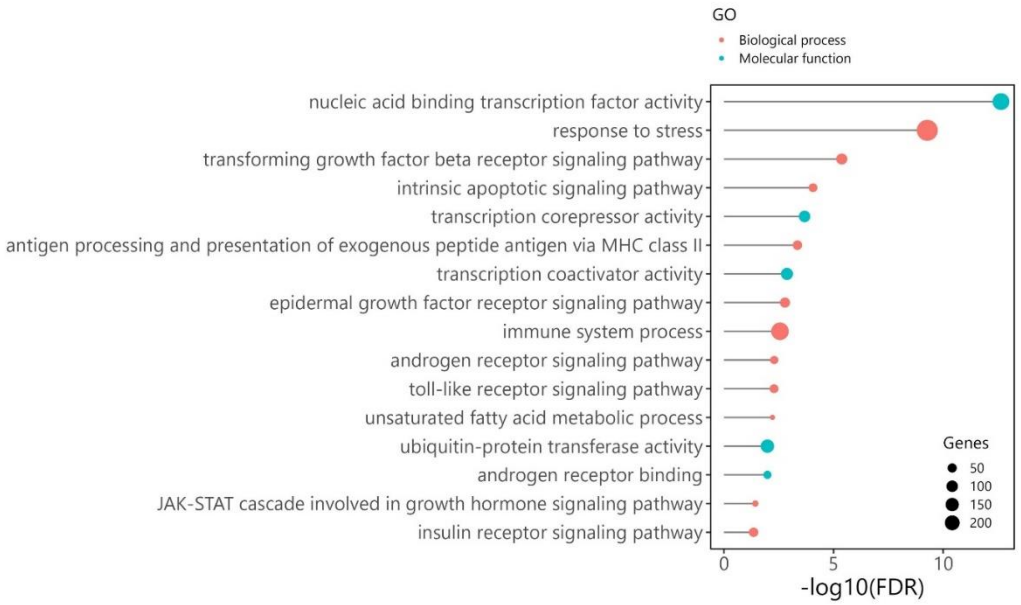

Figure 29. *miR-30d-5p gene ontology analysis.* *Lollipop plot with selected gene ontology (GO) terms associated with miR-30d-5p target genes. Color corresponds to biological process (red) or molecular function (blue). The size of the circle corresponding to the number of genes and -log$_{10}$(FDR) for each specific term is represented.*

The pathway analysis was performed using KEGG annotations. The miRNAs were clustered based on their influence on molecular pathways (see **Figure 30**). The results indicated that miR-17-5p, miR-106b-5p, miR-20b-5p, and miR-106a-5p, all from the

MIR-17 family, targeted similar pathways and had a broad effect among all enriched miRNAs. Some interesting enriched pathways were Wnt (controls cell fate and the proliferation of progenitor cells and regulates T cell development and Treg activation), mTOR (associated with insulin resistance and the regulation of cell proliferation, metabolism, autophagy and apoptosis), FoxO (involved in apoptosis, glucose metabolism, oxidative stress resistance or the formation of Tregs), and MAPK signaling pathways.

The 10 most enriched KEGG pathways are listed in **Table 22**, with fatty acid biosynthesis being the most statistically significant. Interestingly, the TGF-β signaling pathway was among the top 10, which is known for its crucial role in immune homeostasis and tolerance and the induction of pancreatic differentiation and β-cells in early development [367].

Table 22. ***Top ten enriched KEGG pathways of the selected miRNAs***

KEGG pathway	P-value (FDR)	#Genes	#miRNA
Fatty acid biosynthesis	$<1 \times 10^{-325}$	3	2
Prion diseases	$<1 \times 10^{-325}$	6	3
Proteoglycans in cancer	1.110×10^{-16}	99	7
Lysine degradation	1.776×10^{-15}	23	8
Viral carcinogenesis	3.907×10^{-14}	85	7
Pathways in cancer	6.561×10^{-14}	137	6
Hippo signaling pathway	1.068×10^{-13}	72	6
Hepatitis B	4.359×10^{-12}	69	6
Chronic myeloid leukemia	6.311×10^{-11}	42	6
TGF-β signaling pathway	9.317×10^{-11}	39	6

The table shows the top 10 most significant KEGG pathways and the related p-values (FDR), the number of genes involved in the pathways, and the number of miRNAs targeting each one.

Subsequently, an analysis of the molecular pathways enriched for miR-30d-5p was conducted by using the KEGG database. **Figure 31** illustrates the top 30 pathways intricately linked with this specific miRNA. Noteworthy among these pathways are the Wnt signaling pathway, insulin resistance, and pathways pertinent to processes encompassing regeneration, differentiation, and proliferation (e.g., regulation of pluripotency of stem cells, hippo signaling pathways, and cellular senescence). Of particular significance, the cellular senescence pathway emerged as markedly enriched for this miRNA, exerting discernible effects on numerous genes.

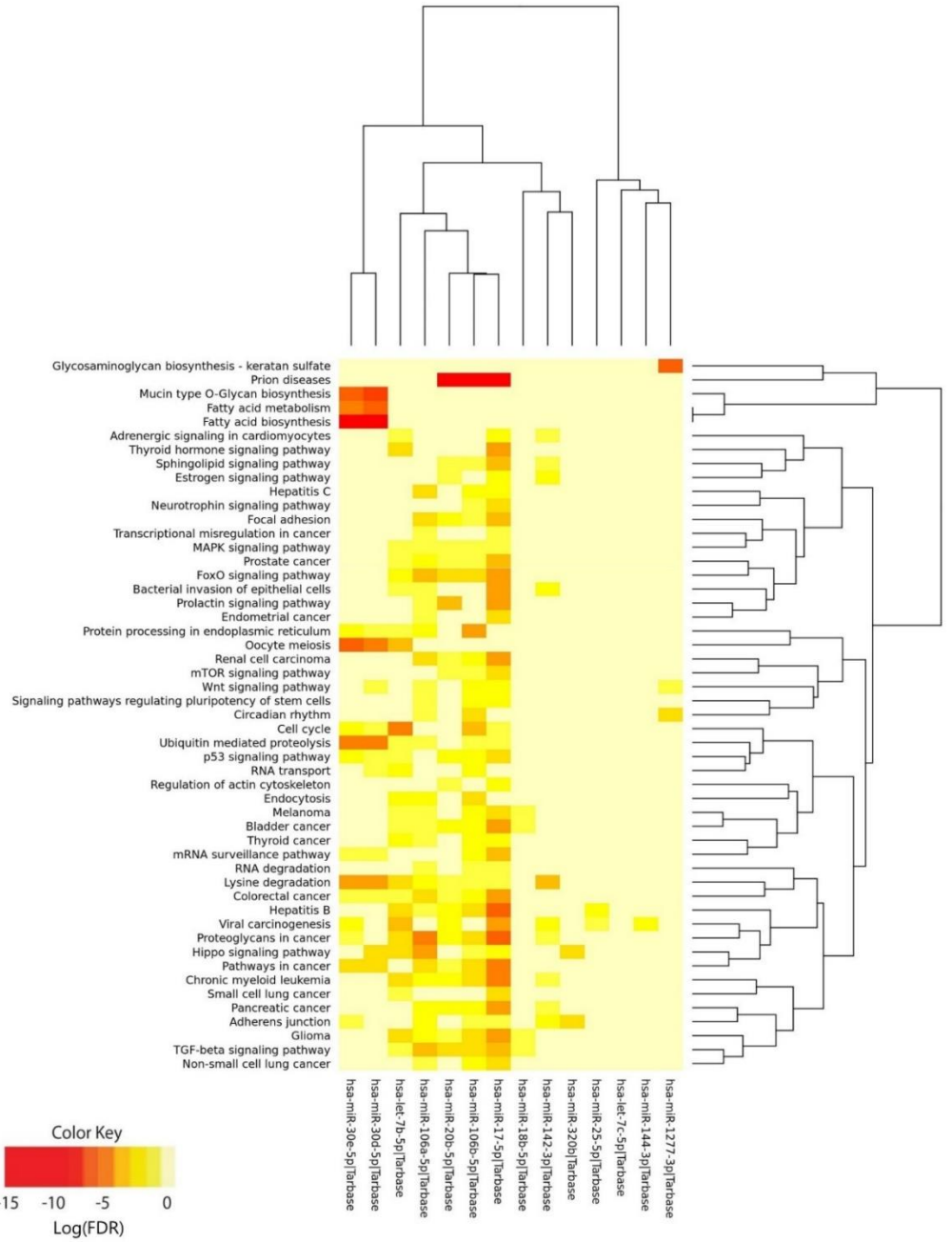

Figure 30. ***KEGG pathway enrichment analysis of the selected miRNAs.*** *The heatmap shows the significantly enriched pathways (q-value ≤0.05) of the selected miRNAs retrieved from the KEGG database in the DIANA-miRPath v3 web server (http://www.microrna.gr/miRPathv3, accessed on 13 September 2022). Hierarchical clustering of miRNAs was performed based on their similar pathway targeting patterns, and pathways were clustered together by related miRNAs. The color code represents the log (p-value (FDR)), with the most significant miRNA-pathway interactions in red.*

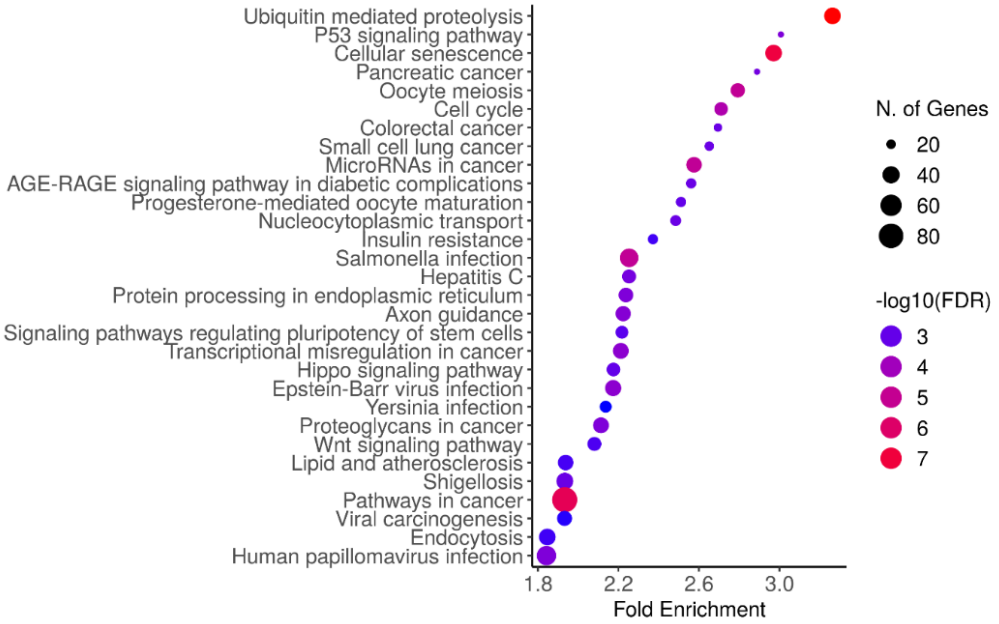

Figure 31. ***miR-30d-5p enriched pathways.*** *Lollipop plot with the top 30 enriched pathways associated with miR-30d-5p. Fold Enrichment indicates the overrepresentation of genes of a certain pathway as it is calculated by dividing the percentage of genes belonging to a pathway by the corresponding percentage in the background. The size of the circle corresponding to the number of genes and -log$_{10}$(FDR) for each specific term is represented.*

4. Validation of differentially expressed miRNAs during the PR phase

To conclude this section, we selected several miRNAs (miR-142-3p, miR-17-5p, miR-106b-5p, miR-20b-5p, let-7b-5p, and let-7c-5p) with the highest number of normalized counts per million that were present in at least 70% of the forty-seven profiled samples from the discovery cohort in order to validate their expression and role as biomarkers by RT-qPCR in another cohort of patients, the validation cohort (**Table 19**). The cohort consisted of 15 age- and sex-matched non-diabetic controls (age: 9.7 ± 3.6), 8 newly diagnosed children with T1D (age: 11.6 ± 2.7), 10 remitter patients (age: 11.8 ± 2.9), and 9 non-remitter patients (age: 7.3 ± 3.7). Five out of six miRNAs were validated as differentially expressed; miR-142-3p was slightly upregulated, and both miR-17-5p and miR-106b-5p were significantly upregulated during PR in comparison to the non-PR group (**Figure 32A–C**). Both let-7b-5p and let-7c-5p were also slightly downregulated at this stage (**Figure 32E, F**). No differences were found regarding the levels of miR-20b-5p between the PR and non-PR groups (**Figure 32D**).

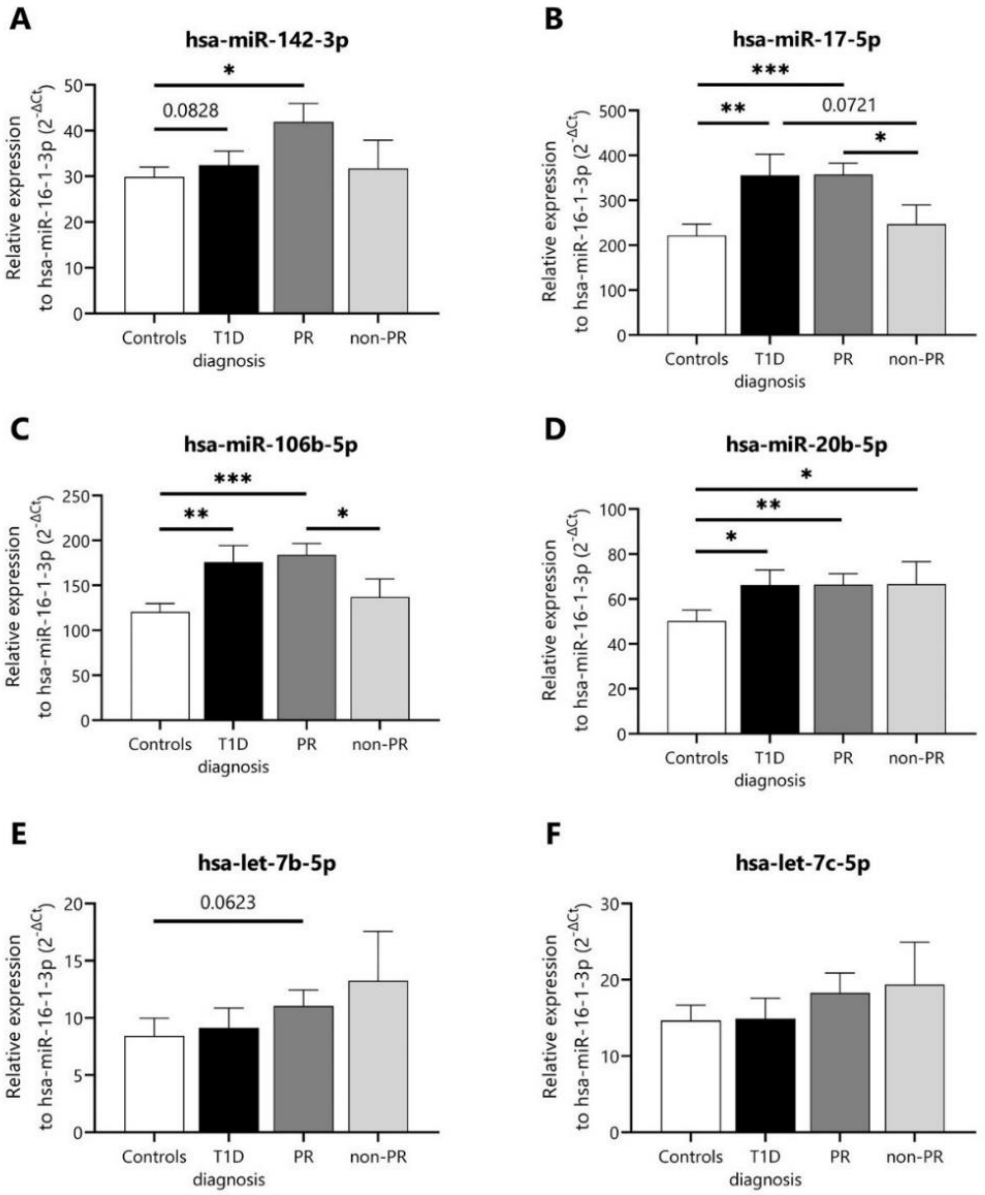

Figure 32. ***Differentially expressed miRNAs in plasma of T1D patients at different stages and non-diabetic control subjects.*** *(**A–F**) Single-assay RT-qPCR validation of some differentially expressed miRNAs in plasma samples of controls (n=15), newly diagnosed patients with T1D (n=8), remitter patients (PR, n=10), and non-remitter patients (non-PR, n=9) from the validation cohort. The miRNA expression signal was normalized to hsa-miR-16-1-3p expression. Values are expressed as $2^{-\Delta Ct}$. Data are presented as mean ± SEM. ns ≥0.05, *p ≤0.05, **p ≤0.01, ***p ≤0.001, Kruskal–Wallis with Dunn's post hoc test.*

CHAPTER III: miR-30d-5p promotes immunoregulatory T-cell pathways and β-cell recovery

The most differentially expressed miRNA during the PR phase was the miR-30d-5p. However, its role in the immune and endocrine systems has been poorly explored. Chapter three of this work is divided into two subsections that focus on the modulation of miR-30d-5p to dig deeper into its ability to induce immunomodulation and promote β-cell recovery and regeneration. Since miR-30d-5p was found to be enriched for biological processes related to the immune system and presented a large number of immune-related target genes (including some that have a direct role in the activation of T lymphocytes, such as *CTLA4* or *CD226*), ***section I*** focuses on determining the immunoregulatory properties of miR-30d-5p. Consequently, a protocol involving electroporation of a miR-30d-5p inhibitor into a primary culture of human T lymphocytes was established to elucidate the phenotype, cytokine secretion, and proliferation changes following the silencing of this miRNA. ***Section II*** explores the ability of miR-30d-5p to induce β-cell recovery and regeneration. To achieve this objective, human pancreatic tissue obtained from non-diabetic deceased donors was sectioned into 120 µM slices, transfected with the miR-30d-5p inhibitor or mimic and maintained *ex vivo* for a duration of 10 days. During this time, we assessed C-peptide secretion in response to glucose, traced β-cell neogenesis, and analyzed the changes in gene expression by RNA-seq. This second section of experiments was conducted at the laboratory for Pancreatic Stem Cell Development at the Diabetes Research Institute in Miami, FL, USA, under the supervision of Dr. Juan Domínguez Bendala and Dr. Ricardo Pastori during a 4-month stay.

— SECTION I. Effect of miR-30d-5p on T-cell immunoregulatory pathways, function and proliferation

This section aims to characterize the functional and phenotypical effects of miR-30d-5p inhibition on human T lymphocytes *in vitro*. For that, we employed a well-known miRCURY LNA-enhanced antisense miRNA inhibitor. Because T lymphocytes are cells that grow in suspension and are difficult to transfect by chemical agents (such as lipid nanoparticles), it was decided to introduce the inhibitory oligonucleotide by electroporation. Then, changes in the expression of inhibitory or activation molecules, secreted cytokines, and proliferation were assessed.

1. miR-30d-5p inhibitor is delivered to T cells and efficiently blocks its target miRNA

First, a protocol for electroporation of human T lymphocytes was developed for efficient delivery of the miR-30d-5p inhibitor. The analysis of inhibitor internalization was conducted through flow cytometry, while the functional effect was tested via RT-qPCR. Various concentrations of the miR-30d-5p inhibitor (from 30 to 1,000 nM) were tested to determine the minimum effective concentration without significantly impacting cell viability. **Figure 33A, B** demonstrate that FAM-positive (transfected) T lymphocytes can be detected 4 hours after electroporation. However, a percentage of transfected cells higher than 20% was only observed from 500 nM. Furthermore, the percentage of transfected T lymphocytes is dependent on the dose, with a greater concentration of miR-30d-5p inhibitor leading to a higher percentage of transfected cells. The signal becomes undetectable by flow cytometry after 24 hours (**Figure 33A**), most likely due to the rapid proliferation of activated T lymphocytes (**Figure 33C**).

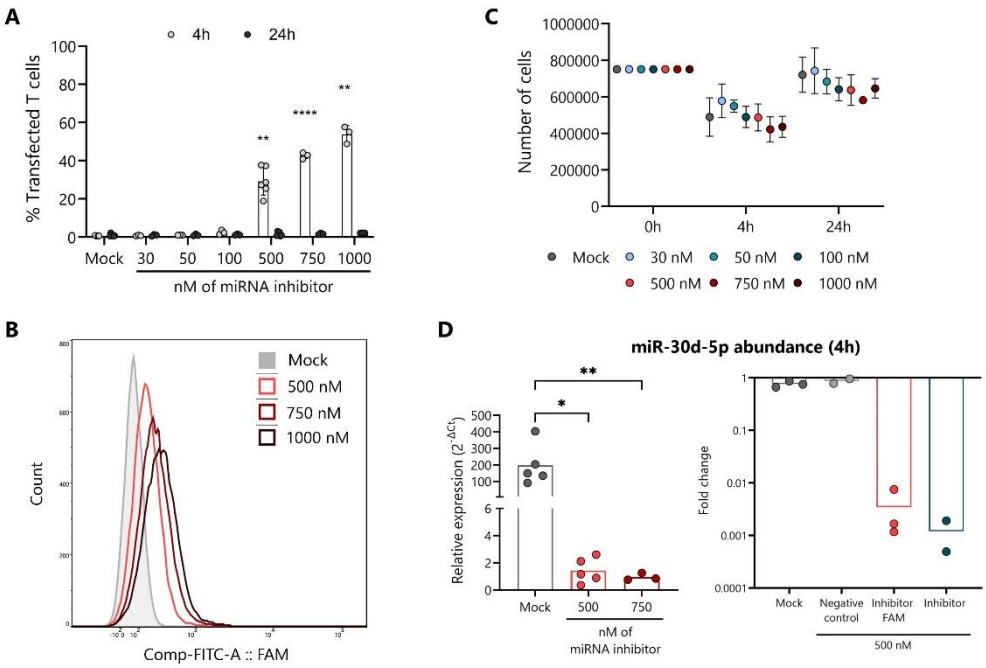

Figure 33. ***miR-30d-5p inhibitor is delivered to T cells and efficiently blocks its target miRNA***. *(**A**) Percentage of transfected T cells 4 and 24 hours after electroporation with different concentrations of miR-30d-5p inhibitor conjugated with FAM. Mixed-effects analysis with Tukey's multiple comparisons test (n=3–6). (**B**) Histogram of a representative miR-30d-5p inhibitor-FAM flow cytometry positivity in T cells 4 hours after electroporation with different concentrations. (**C**) Absolute cell counts 4 and 24 hours after electroporation with different concentrations of miR-30d-5p inhibitor*

*coupled with FAM (n=3–6). (**D, left**) Relative expression of miR-30d-5p analyzed by single-assay RT-qPCR 4 hours after electroporation with 500 or 700 nM of miRNA inhibitor coupled with FAM (n=3–5). The miRNA expression signal was normalized to 5S rRNA expression. Values are expressed as $2^{-\Delta Ct}$. *p ≤0.05, **p ≤0.01, Kruskal–Wallis with Dunn's post hoc test. (**D, right**) Fold change in the miR-30d-5p expression after miR-30d-5p inhibitor (red, conjugated with FAM; blue, uncoupled) or inhibitor control (light grey) using basal transcription (complete medium-cultured T cells) as standard value (n=2–3). The miRNA expression signal was normalized to 5S rRNA expression. Values are expressed as $2^{-\Delta\Delta Ct}$. In all cases, a mock transfection was used as a negative control (cells electroporated without the oligonucleotide).*

The total number of viable T lymphocytes was analyzed 4 and 24 hours after electroporation. As expected, a substantial decrease in the number of viable T lymphocytes was observed after electroporation (4 hours). The cell death was also dependent on the inhibitor concentration, with a greater cell loss observed at higher concentrations. However, the cell death is mainly attributed to the electroporation process itself, as a similar loss was observed in the mock condition (without oligonucleotides). Furthermore, the majority of these T lymphocytes, which were transfected and survived electroporation, demonstrated functionality by exhibiting rapid proliferation within 24 hours and nearly restoring the initial cell count (**Figure 33C**).

Two concentrations of the inhibitor —500 and 750 nM— were selected to analyze its functional effect 4 hours after electroporation. Compared to mock, both concentrations of the inhibitor (conjugated to FAM) led to a drastic reduction of miR-30d-5p expression (**Figure 33D, left**). As the 500 nM concentration of the inhibitor was already sufficient and with results similar to the 750 nM concentration, it was chosen for all subsequent experiments. Next, T lymphocytes were electroporated with 500 nM of either the control inhibitor (negative control), the miR-30d-5p inhibitor conjugated to FAM or the unconjugated inhibitor. As expected, the mock and negative control conditions did not show any change in miR-30d-5p expression compared to the basal level (cultured T cells). However, both the conjugated and unconjugated inhibitors showed up to a 1,000-fold reduction in miR-30d-5p expression with respect to basal (**Figure 33D, right**).

2. miR-30d-5p inhibitor decreases the expression of inhibitory molecules on T lymphocytes

In order to investigate the effects of miR-30d-5p inhibition on T cell phenotype, these were activated, electroporated and phenotyped from 7 newly diagnosed children with T1D (age: 10.6 ± 4.5 years, mean ± SD) and 6 sex and age-matched control children without diabetes (age: 11.5 ± 5.1) who visited the Germans Trias i Pujol University Hospital (**Table 23**). No statistically significant differences were observed in age and BMI

when compared between control subjects and patients at T1D onset. C-peptide levels from T1D subjects were below 0.6 ng/mL, reflecting β-cell loss.

Table 23. ***Clinical and metabolic data of patients with T1D and controls***

	Ctrl	T1D dx
N (no. females)	6 (1)	7 (3)
Age at diagnosis (years)	11.5 ± 5.1	10.6 ± 4.5
BMI (kg/m^2)	20.9 ± 5.3	17.1 ± 4.5
HbA1c (%)	ND	10.9 ± 2.2
Insulin dose (U/kg/day)	ND	0.62 ± 0.23
IDAA1c	ND	13.7 ± 3.2
Basal C-peptide (ng/mL)	ND	0.56 ± 0.42

Data presented as mean ± SD. In the text, p-value calculated from Mann-Whitney test when comparing control subjects and patients with T1D. Abbreviations: BMI, Body Mass Index; Ctrl, controls; HbA1c, glycated hemoglobin; IDAA1c, insulin dose-adjusted HbA1c; ND, not determined; T1D dx, type 1 diabetes diagnosis.

The analysis of different immune checkpoints or co-inhibitory receptors (LAG-3, TIM-3, PD-1, TIGIT, CTLA-4), a co-inhibitory ligand (CD200) and a co-stimulatory receptor (CD226) on T lymphocytes after miR-30d-5p blockade revealed a general decrease in the expression of the inhibitory molecules in the absence of the miRNA, both on CD4$^+$ and CD8$^+$ T cells. **Figures 34, 35** show the mean fluorescence intensity (MFI) for each analyzed molecule.

In both control subjects and individuals with T1D, the expression of CD200, LAG-3, and PD-1 on CD4$^+$ T cells was found to decrease following miR-30d-5p blockade, when compared to the mock or control inhibitor (negative controls) (**Figure 34**). Moreover, a reduction in CTLA-4 expression was evident in the control group in the absence of the miRNA, while a modest decline was observed for TIGIT and TIM-3 in T1D subjects when compared to the control inhibitor. It was unexpected to observe that the expression of CD200 in control subjects was also lower in T cells electroporated with the negative control probe in comparison to the mock condition. This may reflect some kind of unwanted effect of this control oligonucleotide. It is noteworthy that patients with T1D exhibited a lower expression of CD200 than controls when comparing between mock conditions. This observation may reflect a deficiency in the expression of this molecule in patients and a reduced ability to suppress immune responses. With regard to CD8$^+$ T cells, a notable reduction in TIM-3 expression was observed in T1D subjects, while a decline in CTLA-4 levels was evident in controls in the absence of miR-30d-5p.

Furthermore, a slight decrease in LAG-3 and CD226 was also observed in patients with T1D when compared to the control inhibitor (**Figure 35**).

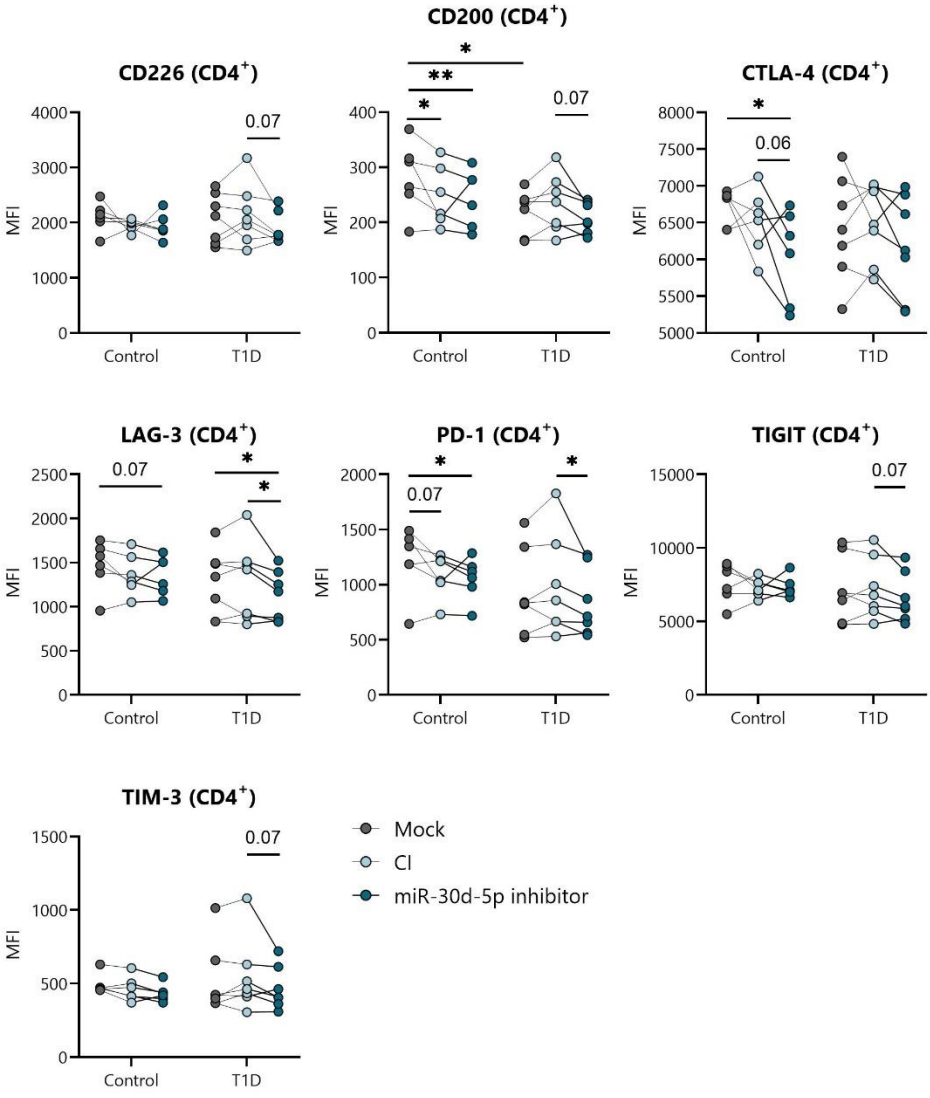

Figure 34. ***miR-30d-5p inhibition decreases the expression of inhibitory molecules on CD4⁺ T lymphocytes.*** *Mean fluorescence intensity (MFI) of CD226, CD200, CTLA-4, LAG-3, PD-1, TIGIT, and TIM-3 expression in CD4⁺ T lymphocytes obtained from T1D (n=7) and control (n=6) subjects. Within each group, grey dots represent T lymphocytes simply electroporated (mock), light blue dots represent T cells electroporated with a control inhibitor (CI) and dark blue dots with a miR-30d-5p inhibitor. ns ≥0.05, *p <0.05, **p <0.01 repeated measures two-way ANOVA with the Geisser-Greenhouse correction and Tukey's multiple comparisons test.*

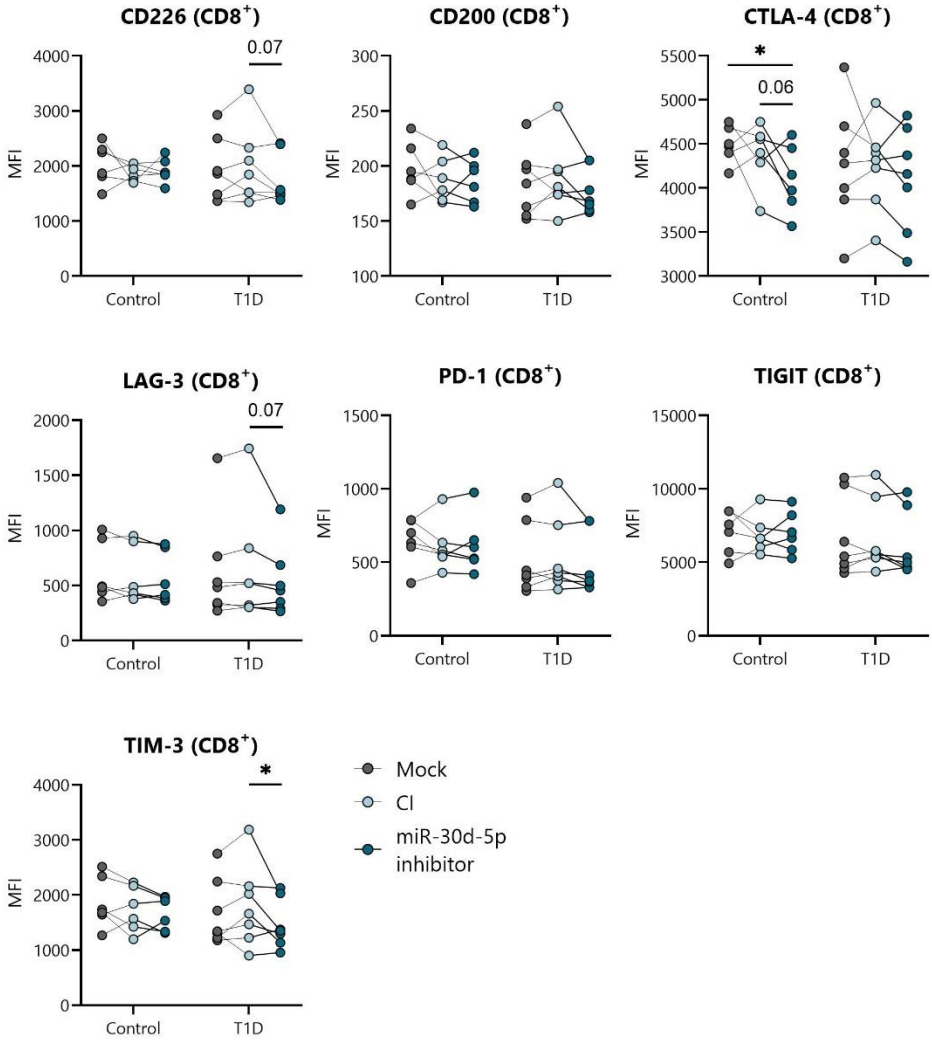

Figure 35. ***miR-30d-5p inhibition decreases the expression of inhibitory molecules on CD8⁺ T lymphocytes.*** *Mean fluorescence intensity (MFI) of CD226, CD200, CTLA-4, LAG-3, PD-1, TIGIT, and TIM-3 expression in CD8⁺ T lymphocytes obtained from T1D (n=7) and control (n=6) subjects. Within each group, grey dots represent T lymphocytes simply electroporated (mock), light blue dots represent T cells electroporated with a control inhibitor (CI) and dark blue dots with a miR-30d-5p inhibitor. ns ≥0.05, *p <0.05 repeated measures two-way ANOVA with the Geisser-Greenhouse correction and Tukey's multiple comparisons test.*

The percentage of CD4⁺ and CD8⁺ T cells expressing these molecules was also analyzed. Once more, a significant decrease was found for CD200, CTLA-4, PD-1 and TIM-3 in CD4⁺ T cells from control subjects after miR-30d-5p inhibition, when compared to the mock control. Moreover, patients with T1D also presented lower percentages of PD-1 and

LAG-3 CD4⁺ T cells after miR-30d-5p silencing (**Figure 36**). As observed for the MFI, patients with T1D exhibited a lower percentage of CD4⁺CD200⁺ T cells than control subjects when comparing between mock conditions. Although not statistically significant, a lower percentage of CD4⁺ T cells from control subjects expressing CD200 and PD-1 was found in the control inhibitor-treated group when compared to the mock condition.

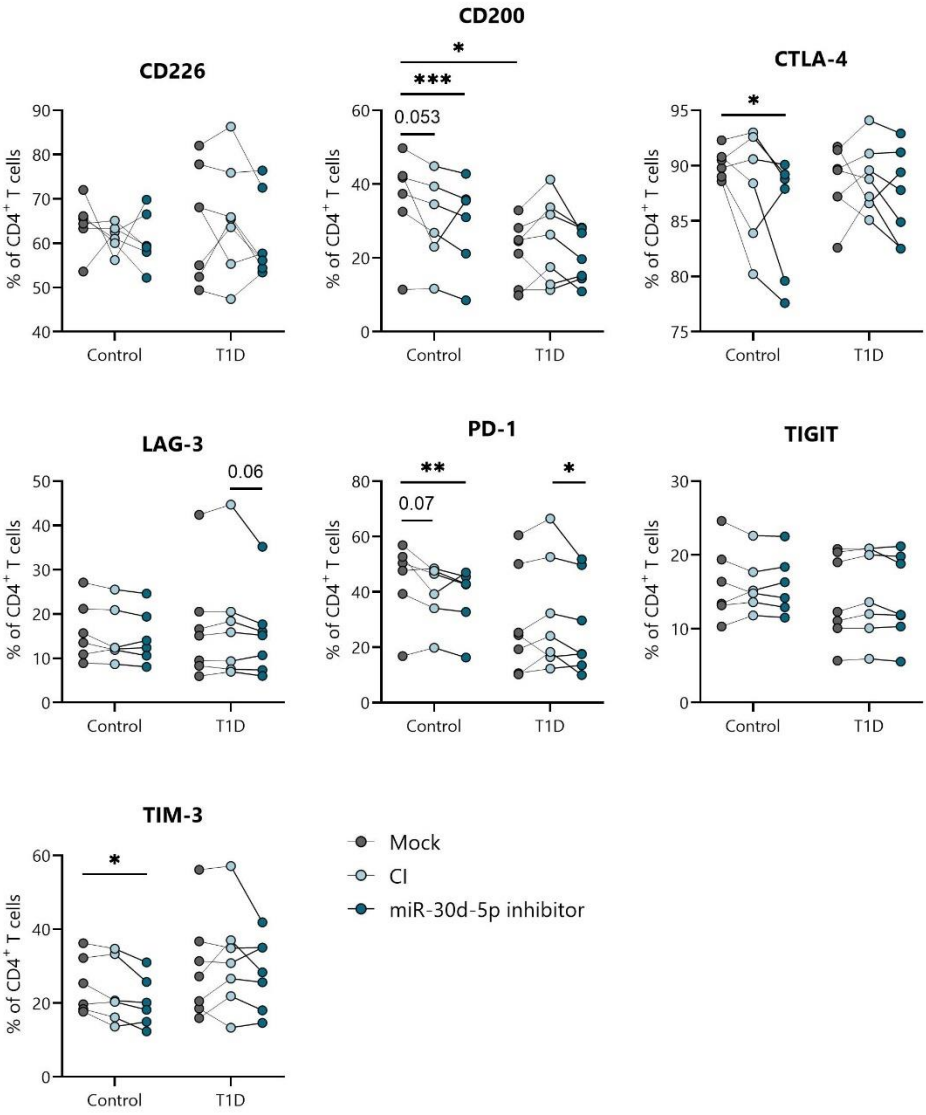

Figure 36. ***miR-30d-5p inhibition decreases the percentage of CD4⁺ T lymphocytes expressing inhibitory molecules.*** *Percentage of CD4⁺ T lymphocytes expressing CD226, CD200, CTLA-4, LAG-3, PD-1, TIGIT, and TIM-3 obtained from T1D (n=7) and control (n=6) subjects. Within each group,*

*grey dots represent T lymphocytes simply electroporated (mock), light blue dots represent T cells electroporated with a control inhibitor (CI) and dark blue dots with a miR-30d-5p inhibitor. ns ≥0.05, *p <0.05, **p <0.01, ***p <0.001 repeated measures two-way ANOVA with the Geisser-Greenhouse correction and Tukey's multiple comparisons test.*

With regard to CD8⁺ T cells, a notable decline in the percentage of cells expressing CD200, CTLA-4, and TIM-3 was observed in control subjects following the blockade of miR-30d-5p, in comparison to the mock control (**Figure 37**).

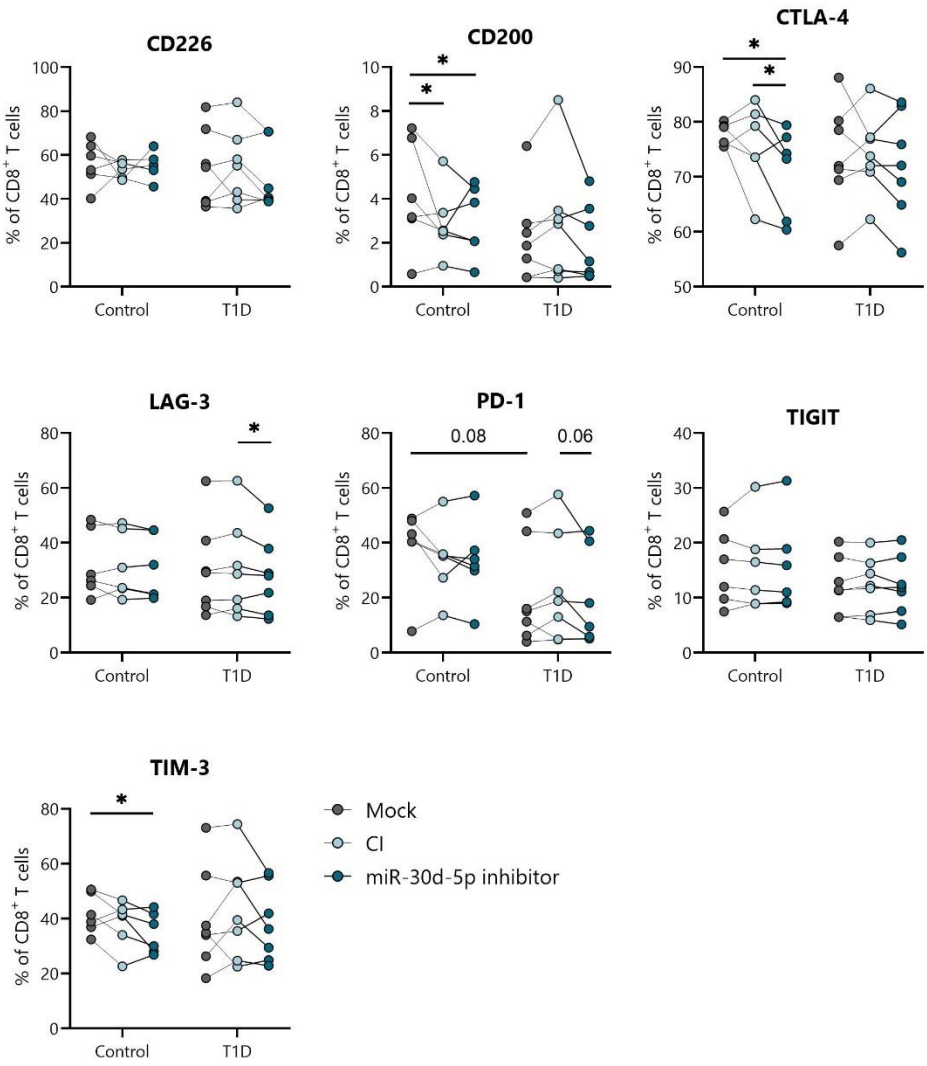

Figure 37. ***miR-30d-5p inhibition decreases the percentage of CD8⁺ T lymphocytes expressing inhibitory molecules.*** *Percentage of CD8⁺ T lymphocytes expressing CD226, CD200, CTLA-4, LAG-3, PD-1, TIGIT, and TIM-3 obtained from T1D (n=7) and control (n=6) subjects. Within each group, grey dots represent T lymphocytes simply electroporated (mock), light blue dots represent T cells*

*electroporated with a control inhibitor (CI) and dark blue dots with a miR-30d-5p inhibitor. ns ≥0.05, *p <0.05 repeated measures two-way ANOVA with the Geisser-Greenhouse correction and Tukey's multiple comparisons test.*

Furthermore, this decline was also evident for CTLA-4 when compared to the control inhibitor. Patients with T1D exhibited a lower percentage of $CD8^+$ T cells expressing LAG-3 in the absence of the miRNA in comparison to the control inhibitor, and a tendency towards a reduced percentage of $CD8^+PD\text{-}1^+$ T cells. In this case, patients with T1D exhibited a tendency towards a diminished percentage of $CD8^+PD\text{-}1^+$ T cells than control subjects when comparing between mock conditions. Again, within the control group, the percentage of $CD8^+$ T cells expressing CD200 was also lower when cells were electroporated with the control inhibitor in contrast to the mock condition (**Figure 37**).

We also investigated whether the absence of miR-30d-5p could influence the maturation, activation, and differentiation of T lymphocytes into Tregs. No significant differences were observed in the percentage of $CD4^+$ or $CD8^+$ T lymphocytes that were positive for CD25 or CD69 (**Supplementary Figure 25**), nor in the expression of FoxP3 (Tregs) or the activation of this regulatory subset (**Supplementary Figure 26**). With regard to CD45RA and CCR7 expression, markers used to identify naïve or memory populations, we observed a modest increase in the proportion of $CD4^+CD45^+CCR7^+$ T cells (naïve) and $CD8^+CD45RA^+CCR7^-$ (EMRA) and a decline in $CD4^+CD45RA^-CCR7^-$ (EM) when miR-30d-5p was suppressed in comparison to the control inhibitor (**Supplementary Figure 27**). Therefore, the absence of miRNA results in an increase in CD45RA-expressing subsets.

3. MiR-30d-5p blockade alters IFN-γ secretion and does not impair T cell proliferation

In instances where a sufficient number of T lymphocytes were present following electroporation, these were re-cultured in complete medium alone or re-stimulated with IL-2 or with anti-CD3/CD2/CD28 plus IL-2 for the purpose of analyzing proliferation and cytokine secretion. With regard to proliferation, no significant differences were observed in the different electroporation groups when re-stimulated with IL-2 or with antibodies plus IL-2 or without re-stimulation (**Supplementary Figure 28**). Overall, no significant differences in IL-4, IL-6, IL-10, IL-17A, TGF-β1 or TNF-α secretion were observed following re-stimulation with antibodies plus IL-2. The sole cytokine to exhibit a change was IFN-γ, which demonstrated a decline following miR-30d-5p inhibition in comparison to the mock condition in both the diabetic and non-diabetic subjects. Additionally, it was

observed that electroporated T cells from patients with T1D exhibited a diminished overall secretion of IFN-γ, IL-21, and CCL5 in comparison to non-diabetic controls (**Figure 38**).

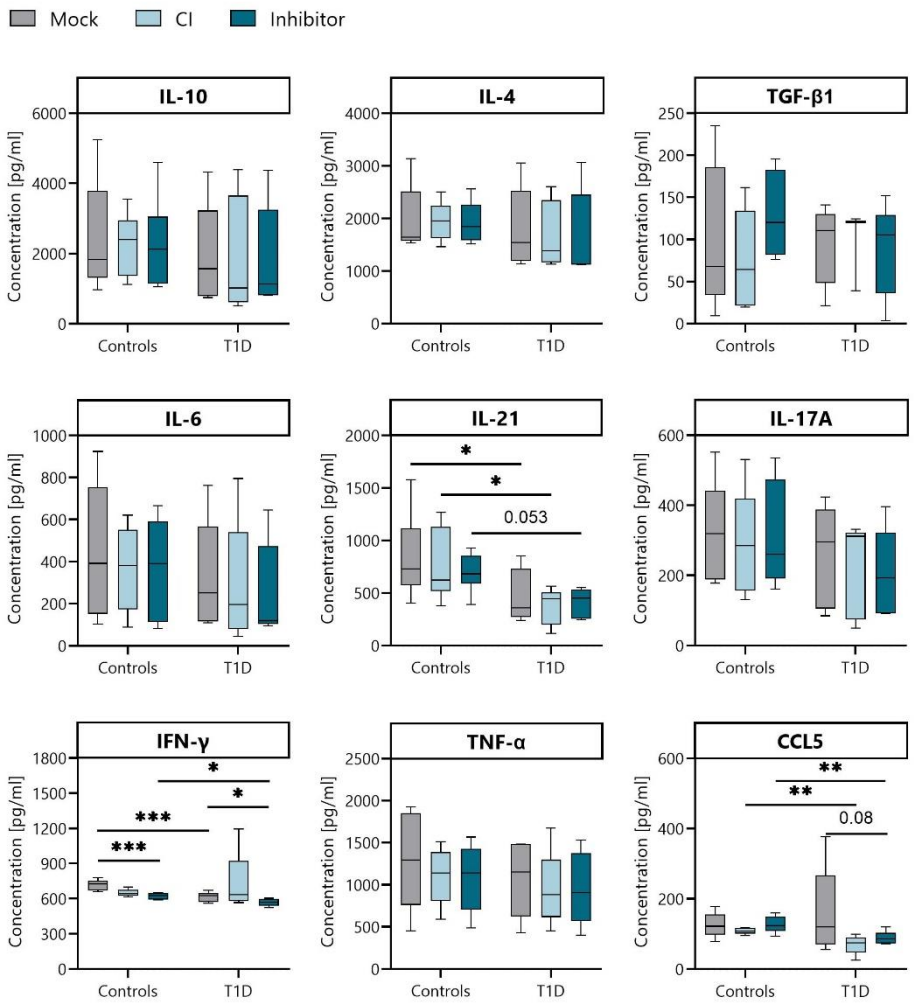

Figure 38. ***Functional effect of miR-30d-5p inhibition on the cytokine profile of T lymphocytes.*** *Concentration of cytokines IL-10, IL-4, TGF-β1, IL-6, IL-21, IL-17A, IFN-γ and TNF-α and chemokine CCL5 in the supernatant of re-stimulated T lymphocytes for 2 days with IL-2 and antibodies anti-CD3/CD28/CD2 obtained from control subjects (n≥5), and patients with T1D (n≥3). Within each group, grey boxes represent T lymphocytes simply electroporated (mock), light blue boxes represent T cells electroporated with a control inhibitor (CI) and dark blue boxes with a miR-30d-5p inhibitor. Data are presented as box-and-whisker plots. Boxes indicate the first and third quartiles. The horizontal bar in the box indicates the median. ns ≥0.05, *p <0.05, **p <0.01, ***p <0.001 repeated measures two-way ANOVA with the Geisser-Greenhouse correction and Tukey's multiple comparisons test.*

— SECTION II. Effect of miR-30d-5p on β-cell function and regeneration

In this section, human pancreatic tissue samples were employed to analyze the contribution of miR-30d-5p to physiological processes such as C-peptide secretion in response to glucose or β-cell neogenesis *ex vivo*. Furthermore, changes in transcriptional levels arising from the overexpression or inhibition of miR-30d-5p were analyzed through bulk RNA-seq, both in endocrine and immune contexts. Demographics of N=6 independent non-diabetic donors can be found in **Table 24**.

Table 24. ***Pancreatic donor demographics***

Case ID	AutoAb (RIA)	Age	Sex	BMI	Cause of death	Experiment
HP2352	NP	21	M	38.1	Head trauma (brain dead)	Inhibitor setup
6613	Negative	13	F	16.8	Cardiac death	Mimic setup
HP2357	NP	55	F	28.6	Stroke (brain dead)	RNA-seq, Perifusion, β-cell neogenesis
6614	NP	20	M	20.7	Cardiac death	RNA-seq
24102-02	NP	34	F	22.86	Cardiac death, Anoxia	RNA-seq, β-cell neogenesis
6615	Negative	14	M	25.96	Cardiac death, Anoxia	Perifusion

NP = not performed

1. miR-30d-5p inhibitor is delivered to human pancreatic slices and efficiently blocks its target miRNA

First, a protocol for transfection of HPSs was developed for efficient delivery of the miR-30d-5p inhibitor by using a lipidic reagent. The analysis of inhibitor internalization was conducted through confocal microscopy, while the functional effect was tested via RT-qPCR. Various concentrations of the miR-30d-5p inhibitor (from 200 to 400 nM) were tested to determine the minimum effective concentration without significantly impacting cell viability. Twenty-four hours after transfection with different concentrations of inhibitor bound to FAM (200, 300, and 400 nM), the presence of this molecule in human pancreatic tissue and specifically in β-cells was analyzed by immunostaining (**Figure 39A**). As anticipated, the elevated inhibitor concentration resulted in a heightened green signal, both in terms of the total number of cells (as observed through nuclear staining with DAPI, indicated in blue) and the number of β-cells (as evidenced by insulin staining,

indicated in white). Our negative control was untransfected slices (basal), from which we could not observe a green signal. Furthermore, confocal microscopy images demonstrate the colocalization of insulin and miR-30d-5p inhibitor within the same β-cell, indicating that the inhibitor is being transfected into the cells of interest. In addition, a fluorescence-based assay was performed to detect mitochondria in live cells to determine tissue viability 24 and 168 hours after transfection. Staining showed good tissue viability after transfection (**Supplementary Figure 29**).

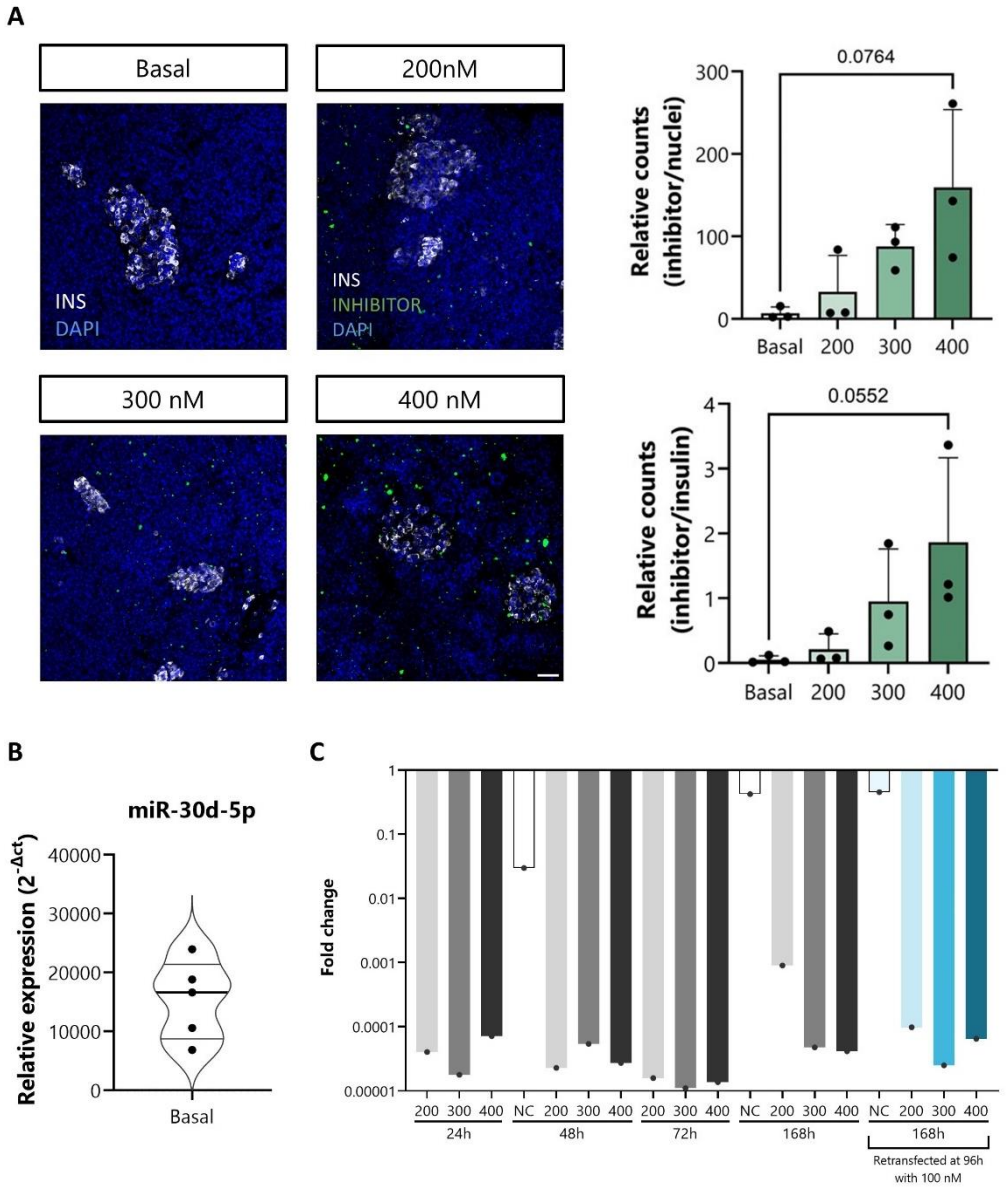

Figure legend on next page

Figure 39. ***miR-30d-5p inhibitor is delivered to human pancreatic slices and efficiently blocks its target miRNA***. *(**A**) Representative confocal microscopy immunostaining of HPSs after 24 hours of miR-30d-5p inhibitor transfection (coupled with FAM) at different concentrations (200, 300 and 400 nM). MiR-30d-5p inhibitor in green, insulin in white and DAPI in blue. Scale: 50 µm. Green bars on the right represent the counts of miR-30d-5p inhibitor with respect to the total number or cells (up) or β-cells (down) in the different concentrations used (n=3 different images for each condition) Statistical significance by Kruskal–Wallis with Dunn's post-hoc test. (**B**) Relative expression levels of miR-30d-5p in HPSs just right after slicing and without treatment. MiR-30d-5p expression was normalized to U6 expression. Values are expressed as $2^{-\Delta Ct}$. Violin plot shows the median (thick line) and first and third quartiles (thin lines). N=5 different pancreases. (**C**) Time-course fold change in the miR-30d-5p expression using basal transcription (complete medium-cultured HPSs) as the standard value. Expression of miR-30d-5p was analyzed by single-assay RT-qPCR 24, 48, 72 and 168 hours after transfection with 200, 300 or 400 nM of miRNA inhibitor or 100 nM of the control inhibitor (negative control, NC). Blue bars represent slices retransfected at 96 hours with another 100 nM of miRNA inhibitor or NC before analyzing miR-30d-5p expression at 168 hours. The miRNA expression signal was normalized to U6 expression. Values are expressed as $2^{-\Delta\Delta Ct}$. N=1 pancreas, hence no error bars.*

Then, following the confirmation of miR-30d-5p expression in HPSs (**Figure 39B**), a time-course experiment was conducted in one pancreas to determine the concentration at which optimal inhibition of miR-30d-5p was achieved and to assess the necessity of retransfection to maintain inhibition over time, given that the slices would be maintained for up to 10 days in culture. First of all, we observed that a single transfection with all tested concentrations was sufficient to maintain an inhibition of miR-30d-5p of up to almost 10,000-fold up to 7 days later (from 24 to 168h). Therefore, re-transfection at day 4 with an extra 100 nM of inhibitor is not necessary in any case (blue bars) (**Figure 39C**). We also observed a small reduction in miRNA expression after transfection with the inhibitor control (negative control (NC)), but negligible compared to that observed with the inhibitor, which may be due to the transfection process itself. As recovery of miR-30d-5p expression was observed at day 7 with a concentration of 200 nM, it was decided to perform the next experiments with 300 nM.

A time-course experiment was also performed with the miR-30d-5p mimic using three different concentrations (0.05, 5 and 50 nM). However, we were not able to detect an increase in the miRNA with any of the concentrations after 72 and 168 hours of transfection. Therefore, as 200 nM was the minimum concentration at which a functional effect was observed in the case of the inhibitor, we decided to use this concentration in the following experiments with miR-30d-5p mimic (**Supplementary Figure 30**).

2. miR-30d-5p overexpression elicits β-cell neogenesis

Qadir et al. established proof of principle that extended culture of HPSs could be used to study regeneration, and that treatment with BMP receptor agonists such as BMP-7 results in detectable β-cell neogenesis in pancreatic slices [354]. Based on this study, slices were generated from deceased non-diabetic donors and co-transduced with adenoviruses carrying the reporter construct CMV-*loxP*-dsRED-*loxP*-BFP-2A-GCaMP6 and a HIP-driven Cre recombinase. By using this model, we predicted that doubly transduced non-β-cells would be tagged red and pre-existing β-cells would be tagged blue. Moreover, there is a window during which the dsRED protein has not been degraded yet but BFP is already expressed. Hence, the transient violet (red + blue) color of these cells can be used to identify β-cell neogenesis (insulin$^+$ cells arising from non-β-cells). Then, slices were transfected with miR-30d-5p inhibitor/mimic or their respective controls to analyze the effect of miRNA modulation on β-cell regeneration. As a positive control of regeneration, slices were treated with 100 pg/mL BMP-7 for 5 days, followed by removal for 5 days.

Figure 40A is a representative image of the red (dsRED), blue (BFP), and violet (merge) signal on day 6 from the same pancreas treated with BMP-7 or transfected with the miR-30d-5p inhibitor (300 nM) or mimic (200 nM). As expected, after 5 days of treatment with BMP-7, the BFP signal (β-cells) was higher than the one found in the untreated slices (negative control). It is noteworthy that the BFP signal was considerably higher in the slices treated with the miR-30d-5p mimic than in the remaining conditions, including the positive control. In addition, the violet signal (representing newly formed β-cells) was also observed to be elevated in the presence of the mimic.

The quantification of the fluorescent signals on specific regions of interest over the days (from day 6 to day 10, n=2 slices per each condition) on the two pancreases confirmed a higher percentage of the slice expressing the blue signal in those treated with BMP-7 or miR-30d-5p mimic in comparison to the untreated slices (**Figure 40B**). Furthermore, a clear significant increase in the slice expressing the violet signal (red+blue) was found only in those treated with the miR-30d-5p mimic in comparison to the untreated slices, revealing that the upregulation of this miRNA promotes the formation of new insulin-producing cells from non-β-cells present in the pancreas. No differences were found between the other treatment groups or regarding the percentage of the slice expressing the red signal (non-β-cells).

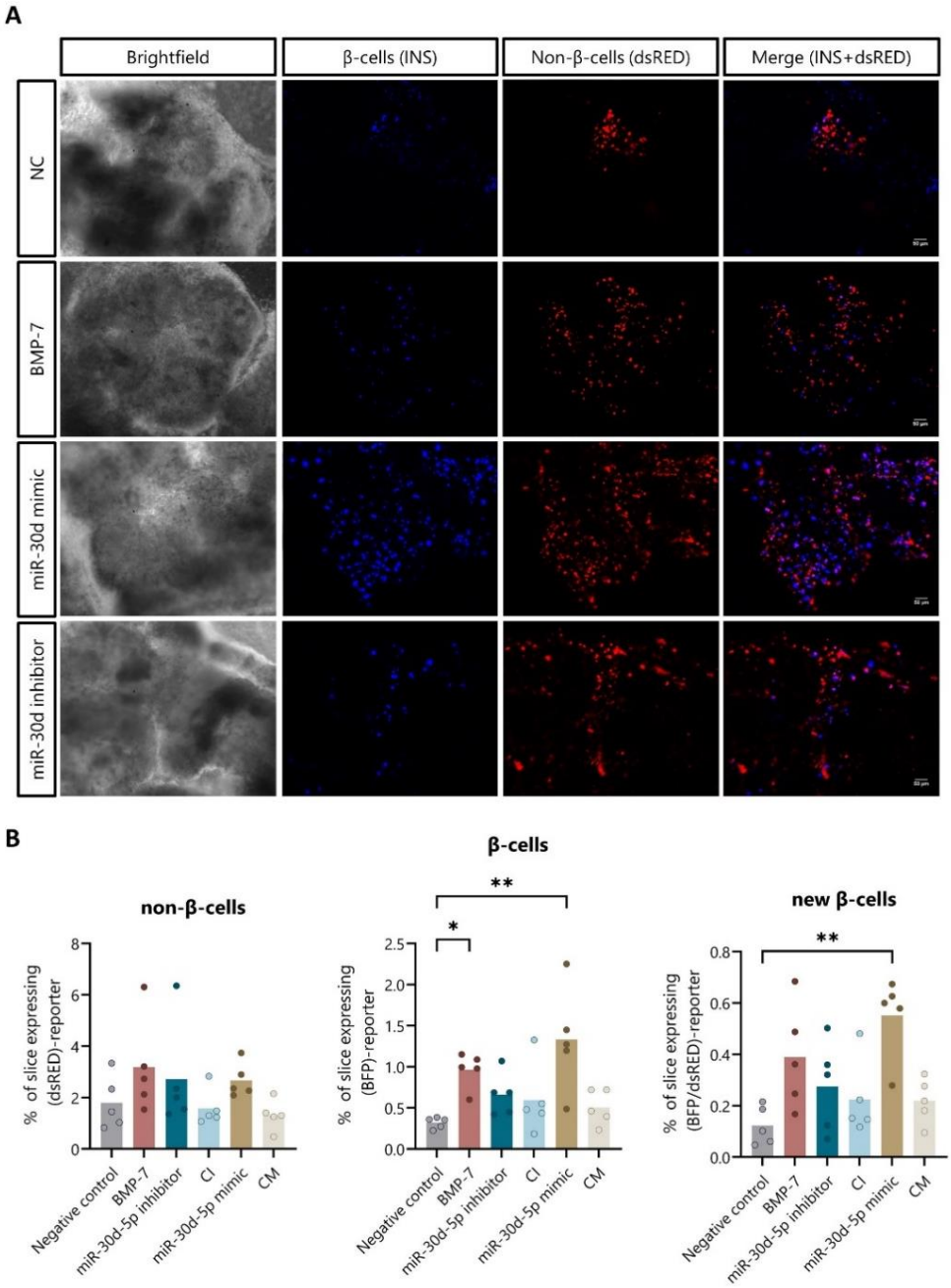

Figure 40. ***miR-30d-5p overexpression elicits β-cell regeneration through neogenesis.*** *(**A**) Representative immunofluorescence imaging of HPSs of one pancreas at day 6 co-transduced with adenoviral HIP-Cre tracer and lox/dsRED/lox-BFP-2A-GCaMP6 reporter and transfected with miR-30d-5p inhibitor or mimic. In the case of the negative control (NC), slices were only transduced. In the case of the positive control, BMP-7 was added for 5 days after transduction and then withdrawn. Merge images show the appearance of insulin-expressing cells (β-cells in blue) from insulin⁻ cells (non-β-cells in red) through an intermediate violet (red + blue; merge) stage. Scale*

*50 µm. (**B**) Quantification of dsRED (non-β-cells), BFP (β-cells) and dsRED+BFP (new β-cells) expression across the different treatment groups. Between 1 and 3 regions of interest were analyzed for each condition of a pancreas (n=2 slices per condition) and the mean was generated. Each dot represents the mean of the pancreases analyzed on one day from D6 to D10 (n=2 pancreases). Data are presented as mean ± SD. ns ≥0.05, *p <0.05, and **p <0.01 by Kruskal–Wallis with Dunn's post-hoc test. CI = control inhibitor; CM = control mimic.*

3. MiR-30d-5p inhibition induces β-cell dysfunction

We assessed β-cell function in HPSs using a perifusion system to more accurately replicate the physiological secretion of C-peptide [368]. HPSs were maintained in complete medium (non-treated) or were transfected with 300 nM of miR-30d-5p inhibitor 10 days prior to perifusion. The inhibition of miR-30d-5p in two different pancreases led to β-cell dysfunction (**Figure 41A**), resulting in a significant decrease in first-phase C-peptide secretion by 16.6% and 27.8% (**Figure 41B**, above and below), respectively, compared to the control (non-treated). Moreover, the viability of the slices was good after 10 days of culture (**Supplementary Figure 31**).

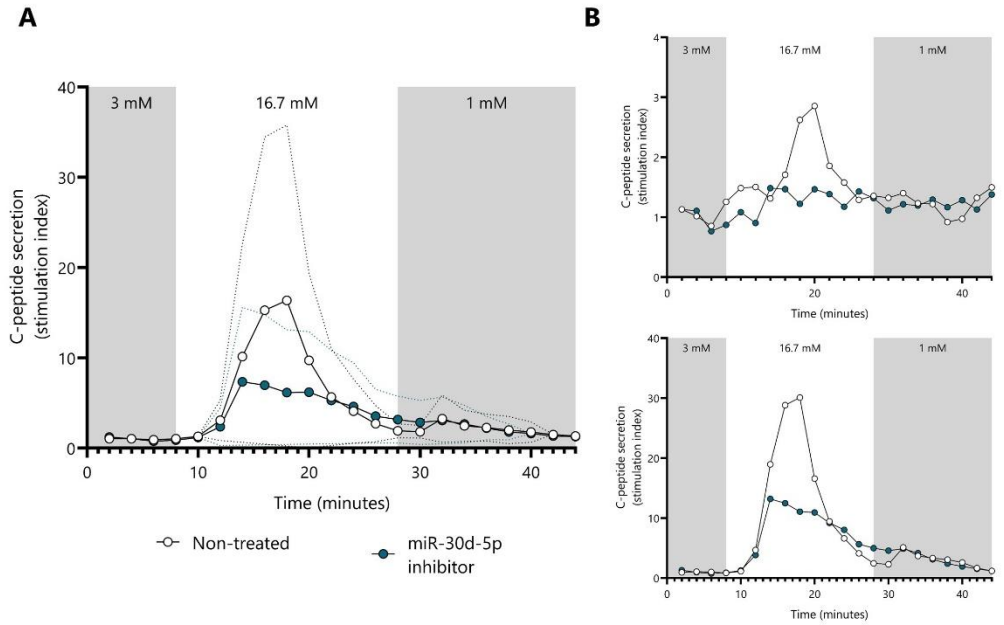

Figure 41. *miR-30d-5p inhibition impairs β-cell function*. *(**A**) Dynamic C-peptide secretion in response to glucose after 10 days of miR-30d-5p inhibition (blue dots) or without treatment (white dots) in two different non-diabetic control pancreases. Perifusion was made by using high glucose (16.7 mM) and low glucose (3 or 1 mM) stimulation. X-axis: time/[Glucose]; Y-axis: stimulation index. Data are mean ± SD (dotted lines) and normalized to 3 mM of glucose values. N=6 slices in the perifusion chamber for each treatment condition. (**B**) Individual perifusion experiments.*

4. MiR-30d-5p modulation induces expression changes related to β-cell function, survival and regeneration

To directly detect alterations in pancreatic gene expression resulting from the inhibition or upregulation of miR-30d-5p levels, we obtained bulk RNA-seq data from two HPSs per condition (non-treated —basal—, inhibitor, control inhibitor, mimic, or control mimic) from three different pancreases. Seventy-two hours following the transfection of the corresponding molecules, we confirmed the successful inhibition of miR-30d-5p in comparison to the basal condition, achieving a reduction of up to 10,000-fold (**Figure 42A**). Again, no significant increase in miR-30d-5p levels was observed following the application of the mimic. As anticipated, transfection with the inhibitor and mimic controls did not result in notable alterations in miRNA expression.

The unsupervised PCA plots of gene expression profiles revealed that the four samples (control mimic, control inhibitor, inhibitor, and mimic) per donor clustered together along the first principal component axis. This indicates that inter-donor variation was more pronounced than the differences between experimental treatment groups (**Supplementary Figure 32**). After accounting for donor variation by performing a ComBat correction with the donor as a covariate, the differences between experimental groups became more apparent (**Figure 42B**). In order to facilitate comparisons between experimental treatments, the mimic and inhibitor controls were treated as a single group. A total of 273 DEGs were identified when the inhibitor was compared with the controls, 66 of them up- and 207 downregulated (**Figure 42C**). Similarly, 518 DEGs were identified when the mimic was compared with the controls, 231 of them up- and 287 downregulated (**Figure 42D**), and 480 DEGs when comparing the inhibitor with the mimic, 209 of them up- and 271 downregulated (**Figure 43E**). The top upregulated DEGs (based on the FC) after miR-30d-5p silencing included GLUT6 —a glucose transporter that modulates glycolysis— (*SLC2A3P1*), genes associated with enhanced immune responses (*PRG2*, *EYA4*), DNA repair (*HROB*, *EYA4*), cell proliferation and differentiation (*TGFB3*) or cholesterol and steroids synthesis (*CYP4F8*). In contrast, the top downregulated DEGs included those involved in cell cycle regulation (*UTP14C*), catabolic processes (*GUSBP3*, *KDM6A*), mitochondrial protein synthesis (*MRPL15*, *MRPL39*), cell differentiation (*RNF112*) or cell growth (*DLK1*) (**Figure 42C**). After miR-30d-5p upregulation, the top upregulated DEGs included genes related to endocytosis (*HOOK1*), inhibition of proteases (*A2ML1*), cell-cell adhesion (*CDH8*), iron metabolism (*HEPH*), steroid metabolism (*UGT2B28*), or potassium channel activity (*KCNH2*). Conversely, the top downregulated genes included genes related to the negative regulation of the cell cycle (RB1), cell growth (*PRDM10*), regulation of gene activity (*MED12*), or the signal transduction of cytokines (*STAT5B*) (**Figure 42D**).

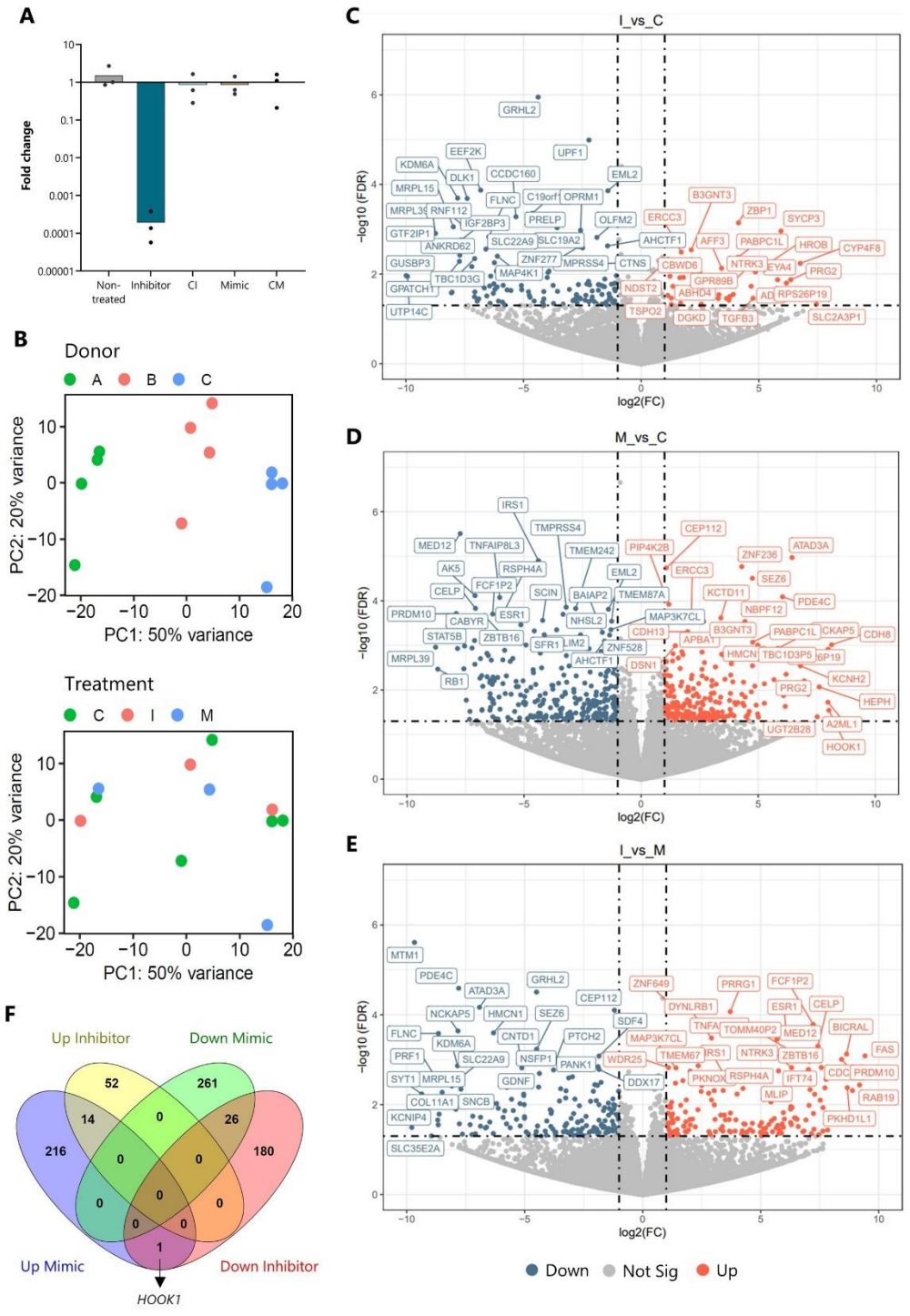

Figure legend on next page

Figure 42. *Transcriptomic changes after miR-30d-5p modulation.* *(**A**) Fold change in the miR-30d-5p expression using basal transcription (complete medium-cultured HPSs) as the standard value. Expression of miR-30d-5p was analyzed by single-assay RT-qPCR 72 hours after non-treatment or after transfection with 300 nM of miRNA inhibitor and control inhibitor (CI) or 200 nM of the miRNA mimic and control mimic (CM). The miRNA expression signal was normalized to U6 expression. Values are expressed as $2^{-\Delta\Delta Ct}$. N=3 pancreases. (**B**) Principal component analysis (PCA) of the differentially expressed genes (DEGs) after correcting for the batch effect. The first PCA shows the variance explained by the donor variable (donor A, donor B and donor C) and the second by the treatment variable (I for inhibitor, M for mimic, and C for control mimic and control inhibitor). (**C-E**) Volcano plots of gene expression in the I vs C, M vs C and I vs M comparisons. The control group comprises both CI and CM-treated slices. Lines indicate log(FC) (x−axis) and -log_{10}(FDR) (y−axis) cut-offs. Blue and red dots indicate significantly downregulated and upregulated genes, respectively, and grey dots indicate non-significantly different expression levels. Log(FC) >0.5 for upregulated DEGs, and log(FC) <0.5 for downregulated DEGs. FDR adjusted p-value ≤0.05. (**F**) Venn diagrams showing overlapping up- or downregulated DEGs between different comparisons (mimic vs control; inhibitor vs control).*

After inhibiting miR-30d-5p and compared to the mimic group, the top upregulated DEGs included genes associated with cell apoptosis (*FAS*), cell growth (*PRDM10*), autophagy (*RAB19*) or cell proliferation (*CDCA4*) (**Figure 43E**). Only one gene, *HOOK1*, was found to be upregulated after miR-30d-5p mimic transfection and downregulated after miR-30d-5p inhibition in comparison to the controls (**Figure 43F**).

Given our interest in observing alterations at the level of regeneration and functionality in the β-cell, as well as changes in immune responses, we selected some genes of interest from those that were differentially expressed for comparison of their expression patterns among the three treatment groups (**Figures 44A and B**). In the heatmap, we observed three clusters of DEGs. The first one shows downregulated genes after transfection with the miR-30d-5p mimic, such as *FAS*, *ERFE*, *STAT5B*, *IRS1*, *IGF1*, or *MAP4K1* (**Figure 44A**). In this case, both insulin-like growth factor 1 (IGF-1) and insulin receptor substrate 1 (IRS-1) are part of the insulin signaling pathway [369], which appears to be downregulated by the miRNA. Nevertheless, although not statistically significant, miR-30d-5p mimic has been observed to enhance the expression of the insulin gene, *INS*, in comparison to controls or miRNA inhibitor (**Figure 44B**). Therefore, these changes may reflect the autocrine negative feedback effect of insulin on pancreatic β-cells [370,371]. The second cluster shows genes generally upregulated after transfection with both miR-30d-5p mimic and inhibitor, such as *IL21R*, *NR1H2*, *SLC12A8*, or *SLC12A5* (**Figure 44A**). Among these, we also observe clear differences between inhibitor and mimic. For example, inhibition of miR-30d-5p leads to a significant increase in the expression of *ZBP1* —a potent innate immune sensor [372], *IL21R* —which helps to maintain an inflammatory environment [373], or *NR1H2* —which encodes for liver X receptor beta (LXR-β), whose

activation can impair insulin secretion [374] (**Figure 44B**). On the other hand, the mimic upregulates genes such as *IL22RA1*, *TTR*, *ISL1*, or *CACNB3* compared to the inhibitor. In particular, islet-1 (ISL-1) is related to the proper function and survival of β-cells [375,376], while transthyretin (TTR) promotes insulin stimulus secretion [377]. Contrarily, voltage-gated Ca^{2+} (Cav)β3 (*CACNB3*) decreases the frequency of Ca^{2+} oscillations, modulating further insulin secretion [378] (**Figure 44B**). Finally, the third cluster shows genes whose expression decreases after miR-30d-5p inhibition compared to the control and mimic groups (**Figure 44A**). Among these genes, we find *MAPK12*, which is associated with cellular responses evoked by stress, *BMPR1B* and *KLF2*, which are linked to the BMP signaling pathway and play a role in the differentiation of pancreatic endocrine progenitors [379], *INS*, or *CELA3A*, a pancreatic elastase.

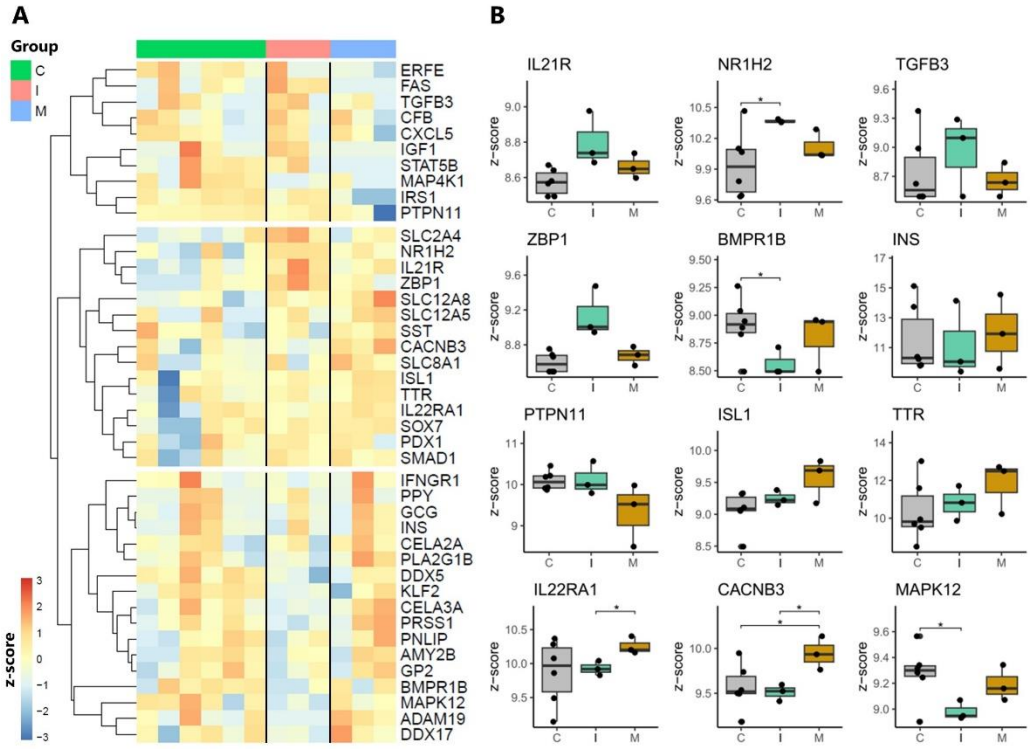

Figure 43. ***Selected gene expression pattern after miR-30d-5p modulation.*** *(**A**) Hierarchical clustering heatmap showing selected genes with significantly different expression levels (DEGs) between the control group (green, comprising both control mimic and control inhibitor), the inhibitor (red) and the mimic (blue). Each column represents individual samples (treated slices from 3 pancreases), and each row represents an individual gene. Log(FC) >0.5 for upregulated DEGs (red), and log(FC) <0.5 for downregulated DEGs (blue); FDR adjusted p-value ≤0.05. (**B**) Boxplots of the normalized expression (z-score) of some genes from the bulk RNA-seq data in controls (grey), miR-30d-5p inhibitor (blue), and miR-30d-5p mimic (orange). Error bars indicate 95% confidence intervals and the center line is the median. N=3 pancreases (ns ≥0.05, *p <0.05, by t-test).*

The GO analysis showed no overlap between the enriched biological processes associated with the up- or downregulated genes following modulation of miR-30d-5p expression (**Figure 44A**). After miRNA silencing, functional categories such as quality control of misfolded or incompletely synthesized proteins and intracellular transport of sterols and cholesterol were enriched among the set of upregulated genes. In contrast, functional categories such as regulation of muscle cell differentiation, the androgen receptor pathway, and miRNA metabolic process were enriched among the set of deregulated genes. Therefore, the absence of miR-30d-5p could be related to cellular stress caused by misfolded proteins and a lack of cell differentiation and signaling processes through the androgen receptor, which can activate various signaling pathways that have an impact on β-cell survival, proliferation, and insulin secretion, including PI3K/AKT [380].

After increasing the functional effect of miR-30d-5p with the mimic, we observed enriched functional categories such as chloride ion and monoatomic anion homeostasis as well as inorganic cation import across plasma membrane and mesenchyme morphogenesis in the upregulated cluster genes. These GO categories may indicate the initiation of electrical activity essential for insulin secretion [381] as well as the differentiation of cells. Conversely, functional categories such as positive regulation of cellular response to insulin stimulus or glucose import were enriched among the downregulated gene set (**Figure 44A**), once more reflecting the negative feedback signal of insulin within the islet.

Subsequently, we investigated TFs that may be involved in the transcriptomic alterations observed following modulation of miR-30d-5p levels. Despite the inability to identify any enriched TF following miR-30d-5p silencing in comparison to the control group, the upregulated genes following miR-30d-5p mimic treatment exhibited associations with FOXO3, NOTCH3, JUND, and NR1H2, which have been linked to β-cell proliferation, survival, and function (**Figure 44B**). The most enriched transcription factor was ZNF592, which is not directly associated with β-cell mechanisms. A comparison of the regulon of the inhibitor versus the mimic revealed that JUND and FOXO3 were associated with downregulated genes (**Figure 44B**).

To sum up, the modulation of miR-30d-5p expression appears to be associated with the regulation of genes involved in insulin synthesis, β-cell survival and proliferation, and immune system activation, among others. Nevertheless, a validation of these genes would enhance the robustness of the findings.

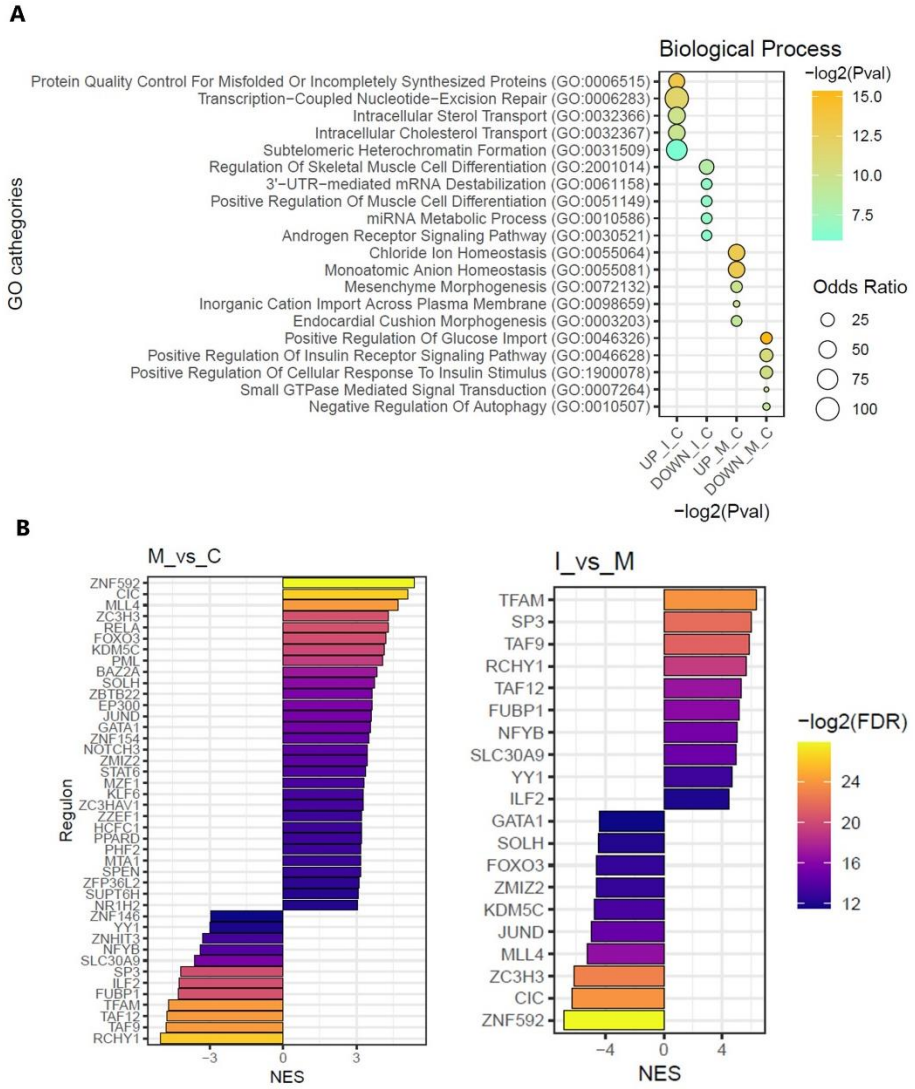

Figure 44. ***Biological processes and transcription factors enriched after miR-30d-5p modulation.*** *(**A**) Gene ontology (GO) overrepresentation of GO Biological Process categories comprising the upregulated and downregulated DEGs in comparison to the control group after miR-30d-5p functional silencing or upregulation. The odds ratios for each group and the – log2(p-value) are shown. Selected significant categories (p-value ≤0.05) are shown. (**B**) Discriminant Regulon Expression Analysis (DoRothEA) of miR-30d-5p mimic vs. control (left) and miR-30d-5p inhibitor vs. mimic (right). Normalized enrichment score (NES) and -log2(FDR adjusted p-value) of transcription factor expression are depicted.*

CHAPTER IV: miR-30d-5p modulates the ongoing autoimmune process in NOD mice

Chapter four of this work focuses on the modulation of miR-30d-5p *in vivo* to determine its pathological implications in the context of islet autoimmunity. To achieve this, prediabetic NOD mice with ongoing autoimmunity were treated briefly with an LNA-miR-30d-5p inhibitor. Immunophenotyping was conducted on both the spleen and PLN. Additionally, the expression of miR-30d-5p target genes was analyzed, and the insulitis score in the pancreatic tissue was determined. The experiments described in this chapter were previously published in [361].

1. *In vivo* inhibition of miR-30d-5p is safe and does not advance the onset of diabetes

To address the immunological relevance of miR-30d-5p *in vivo*, we analyzed the effect of miR-30d-5p inhibition in nine-week-old prediabetic NOD mice. We employed a well-known LNA-miRNA-inhibitor that, when administered systematically, has been shown to accumulate in different tissues, including lymphoid tissues and the pancreas, thus promoting *in vivo* miRNA silencing [124]. The miR-30d-5p inhibitor or control inhibitor (negative control A probe; miRNA control group) was applied four times by intraperitoneal (i.p.) injection at 9 mg/kg every three days, whereas in the sham group, mice were treated with 200 µL PBS following the same pattern. Along with the treatment with the miRNA inhibitor, mice exhibited normal glycosuria and glycemia at the end of the study and maintained weight within a normal range, which led us to think that the inhibition of this miRNA did not have a toxic effect on mice, nor did it significantly advance the onset of diabetes (**Figures 45A–C**). Moreover, the viability of splenocytes and PLN cells was optimal in the three groups (always higher than 80%), despite small significant differences (**Figure 45D**).

2. *In vivo* inhibition of miR-30d-5p potentiates Treg expansion by increasing CD200 levels

First, PLN cells and splenocytes were collected and immunophenotyped. To begin with, we investigated the effect of blocking miR-30d-5p on Tregs in the NOD mice. This was based on the observation that remitter patients with T1D have higher levels of miR-30d-5p and lower percentages of Tregs compared to non-remitters. **Figure 46A** shows representative fluorescence-activated cell sorting (FACS) plots indicating the percentage of $CD4^+CD25^+FoxP3^+$ Tregs in PLN of the sham (left, grey), control inhibitor (middle,

blue), and miRNA inhibitor (right, red) treatment groups. At the end of the study, the blockade of miR-30d-5p resulted in an increased percentage of Treg cells in the PLN in comparison to both the sham group and the miRNA control group (**Figure 46B**). In order to understand the reason for this increase, we investigated which target genes of miR-30d-5p could be overexpressed after its inhibition. Among the genes classified under the "immune system" category (**Table 21**), *CD200* emerged, which is associated with Treg expansion [382].

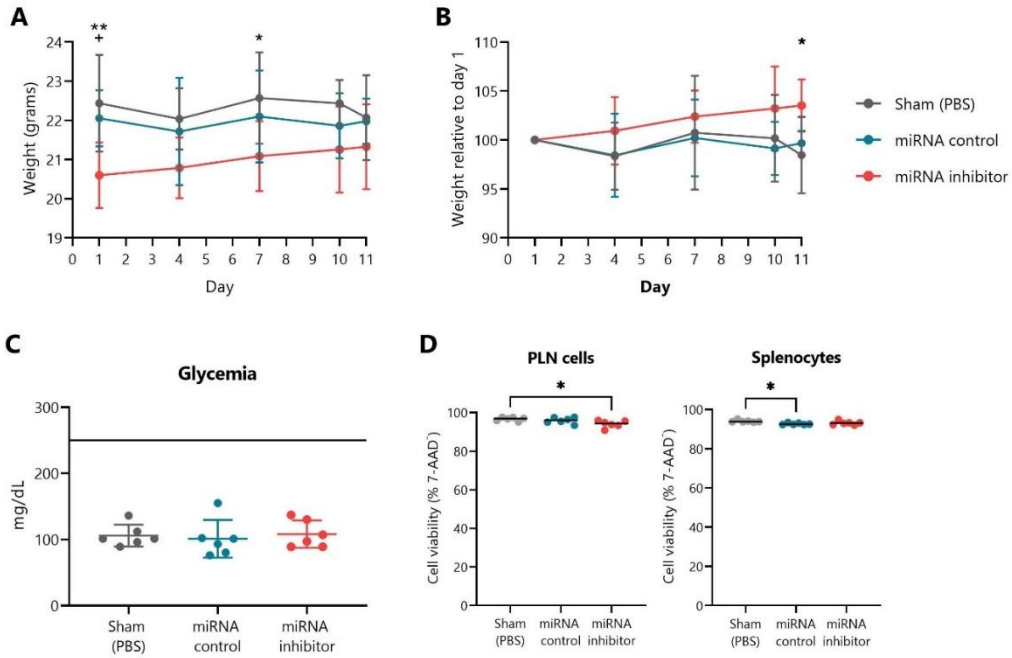

Figure 45. ***Normal weight and glycemia values, and optimal cell viability after the treatment with miR-30d-5p inhibitor***. *(**A**) Weight was measured through the treatment period at days 1 (pre-treatment), 4, 7, 10 and 11 (24h after the last injection). (**B**) Weight relative to day 1 (pretreatment) measured at days 4, 7, 10 and 11 (24h after the last injection). Grey lines and dots correspond to the sham group, blue lines and dots to the control inhibitor group, and red lines and dots to the miR-30d-5p inhibitor group. ns ≥0.05, *p ≤0.05 **p ≤0.01 (inhibitor vs sham), ⁺p ≤0.05 (inhibitor vs control), two-way ANOVA. (**C**) Blood glucose levels (mg/dL) after the short treatment, measured at day 11 (24h after the last injection) in sham mice, mice treated with a control inhibitor, or mice treated with the miR-30d-5p inhibitor. Data are presented as mean ± SD. The black line indicates the level from which hyperglycemia is considered in mice. Significant differences were not found between groups. (**D**) Viability of PLN cells and splenocytes from sham mice, mice treated with a control inhibitor, or mice treated with the miR-30d-5p inhibitor assessed by 7-AAD staining. Black lines indicate the median percentage of cell viability. ns ≥0.05, *p ≤0.05, Kruskal-Wallis with Dunn's post-hoc test. N=6 per group.*

To demonstrate the efficacy of the delivered miR-30d-5p inhibitor in the pancreatic tissue and local immune cells, we analyzed the expression of *CD200* in the remaining immune cells from PLN. We observed higher levels of CD200 mRNA in the absence of miR-30d-5p in comparison to the miRNA control group, validating the *in vivo* effect of miR-30d-5p inhibition (**Figure 46C**). Interestingly, a significant positive correlation was found between *CD200* expression levels and the percentage of Treg cells, further confirming the role of this CD200 inhibitory molecule in immune tolerance and Treg generation (**Figure 46D**). Therefore, it can be concluded that the miR-30d-5p inhibitor was successfully delivered to immune tissues such as PLN, resulting in an increase in the percentage of Tregs by ceasing to block CD200, a molecule associated with their expansion.

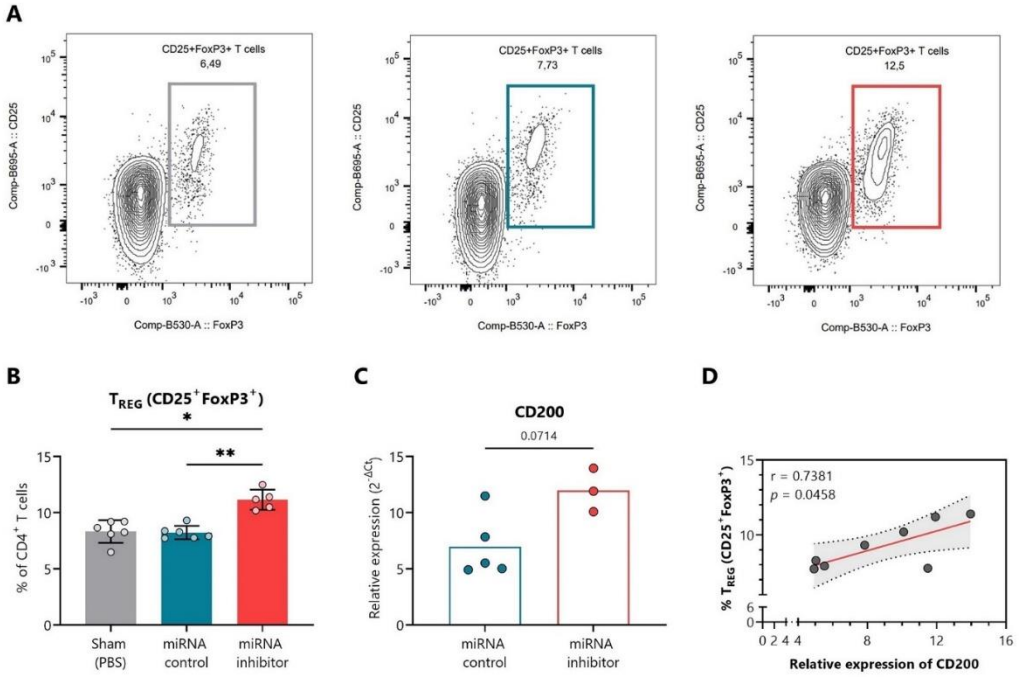

Figure 46. ***In vivo miR-30d-5p inhibition promotes Treg expansion by upregulating CD200 in pancreatic lymph nodes.*** *(**A**) Representative FACS plots indicating the percentage of CD4⁺CD25⁺FoxP3⁺ Tregs in the PLN of the sham (left, grey), control inhibitor (middle, blue), and miRNA inhibitor (right, red) treatment groups. (**B**) Percentage of total CD4⁺CD25⁺FoxP3⁺ Tregs in the PLN of sham mice (n=6, left, grey), mice treated with a control inhibitor (n=6, middle, blue), or mice treated with the miR-30d-5p inhibitor (n=5, right, red). Data are presented as mean ± SD. ns ≥0.05, *p ≤0.05, **p ≤0.01, Kruskal–Wallis with Dunn's post hoc test. (**C**) Levels of CD200 mRNA (a validated target of miR-30d-5p) on the remaining PLN cells of mice treated with a control inhibitor (n=5, left, blue) or the miR-30d-5p inhibitor (n=3, right, red). Gene expression signal was normalized to GAPDH expression. Values are expressed as $2^{-\Delta Ct}$. Data are presented as mean ± SD. P-value was derived by the Mann–Whitney test. (**D**) Correlation between levels of CD200 mRNA and the*

percentage of total Tregs ($CD4^+CD25^+FoxP3^+$). A significant positive correlation was found between both parameters (Spearman's r = 0.7381, p = 0.0458, Spearman's correlation analysis).

3. *In vivo* inhibition of miR-30d-5p reduces PD-1 expression on splenocytes

PD-1 expression was then analyzed to determine the exhaustion status of T cells. **Figures 47A, C** show representative FACS plots indicating the percentage of $CD4^+PD\text{-}1^+$ T cells and $PD\text{-}1^+$ Tregs, respectively, in the spleen of the sham (left, gray), control inhibitor (middle, blue), and miRNA inhibitor (right, red) treatment groups. At the end of the study, the inhibition of miR-30d-5p resulted in a significant decrease in both the percentage and total number of $CD4^+$ T cells that tested positive for PD-1 when compared to both the sham group and the miRNA control group (**Figure 47B**). In addition, this decrease in PD-1 expression was very noticeable in Treg cells, both in terms of percentage and total number of cells (**Figure 47D**). *PDCD1* (PD-1 gene) is not a direct target gene of miR-30d-5p, but we found *PRDM1*, a repressor of PD-1 encoding for BLIMP1 transcription factor, which is [383] (**Table 21**).

Thus, to establish a link between the low expression of PD-1 and the upregulation of one of its repressors in the absence of miR-30d-5p, we analyzed the expression levels of *PRDM1* and *PDCD1* in splenocytes. We found no differences in the expression of *PRDM1* between the miRNA inhibitor and control groups (**Figure 47E**). However, we observed decreased *PDCD1* mRNA levels in the miRNA inhibitor group, resulting in lower expression of PD-1 at both the gene and protein levels (**Figure 47F**). Further investigation is warranted to determine if the miR-30d-5p affects PD-1 through an alternative pathway. Gene expression levels of *TGFBR2* and *PRDM1* in the remaining PLN and of *TGFBR2* and *CD200* in the splenocytes were also checked, but no differences were found between the miRNA control and miRNA inhibitor groups (**Supplementary Figure 33**).

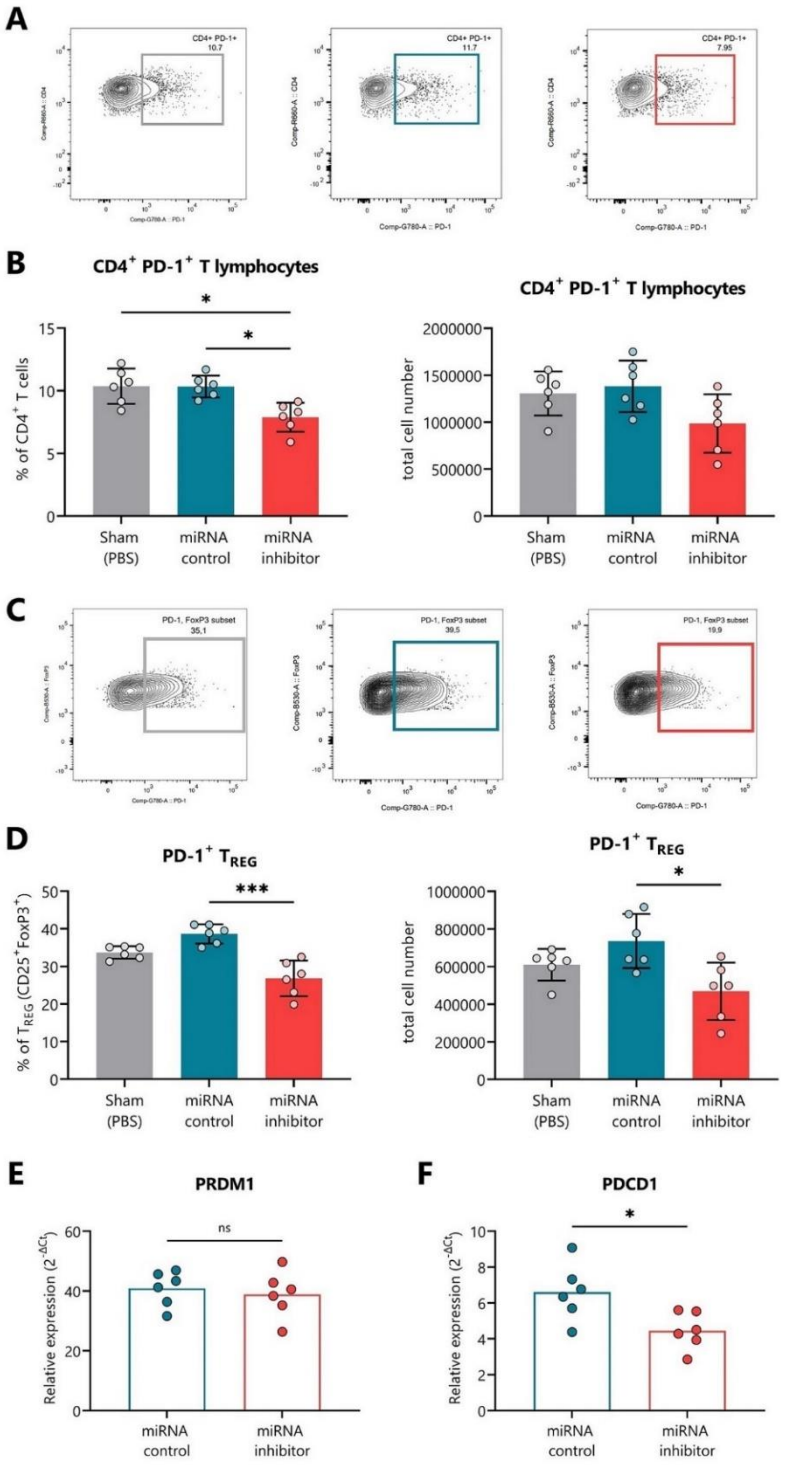

Figure caption on next page

Figure 47. ***In vivo* miR-30d-5p inhibition is related to decreased levels of PD-1 in the spleen.** (***A, C***) *Representative FACS plots indicating the percentage of (**A**) CD4⁺PD-1⁺ T lymphocytes or (**C**) PD-1⁺ Tregs in the spleen of the sham (left, grey), control inhibitor (middle, blue), and miRNA inhibitor (right, red) treatment groups. (**B, D**) Percentage (left) and total cell numbers (right) of (**B**) CD4⁺PD-1⁺ T lymphocytes or (**D**) PD-1⁺ Tregs in the spleen of sham mice (n=6, left, grey), mice treated with a control inhibitor (n=6, middle, blue), or mice treated with the miR-30d-5p inhibitor (n=6, right, red). Data are presented as mean ± SD. ns ≥0.05, *p ≤0.05, ***p ≤0.001 Kruskal–Wallis with Dunn's post-hoc test. (**E, F**) Levels of (**E**) PRDM1 (a validated target of miR-30d-5p and a repressor of PDCD1) and (**F**) PDCD1 mRNAs in the splenocytes of mice treated with a control inhibitor (n=6, left, blue) or the miR-30d-5p inhibitor (n=6, right, red). Gene expression signal was normalized to GAPDH expression. Values are expressed as $2^{-\Delta Ct}$. Data are presented as mean ± SD. ns ≥0.05, *p ≤0.05, Mann–Whitney test.*

4. *In vivo* inhibition of miR-30d-5p displays changes in additional T cell differentiation subsets

To examine the effect of the miR-30d-5p blockade on the maturation of the immune system and different immune cell populations, we analyzed CD4⁺ and CD8⁺ T lymphocytes (differentiating between naïve, CM, EM, and pre-effector-like T cells), B lymphocytes, and cDCs. First, no differences in the percentages of total CD4⁺ and CD8⁺ T cells, DCs, or B lymphocytes were found between the three treatment groups in either PLN (**Figures 48A–D**) or the spleen (**Figures 48F–I**). Representative FACS plots for the analysis of B lymphocytes and DCs in PLN and the spleen are respectively shown in **Figures 48E, J**.

Figures 49A, C display FACS plots representing the percentage of naïve, CM, EM, and pre-effector-like CD4⁺ and CD8⁺ T cells, respectively, in the PLN of miRNA control and miRNA inhibitor groups. The miR-30d-5p blockade did not result in any significant changes, but we observed a slight increase in the percentage of CD4⁺ EM T lymphocytes (**Figure 49B**) and a decrease in the percentage of CD8⁺ pre-effector-like T lymphocytes (**Figure 49D**), along with an increase in the CD8⁺ CM ones (**Figure 49E**).

Figure 50A shows representative FACS plots indicating the percentage of naïve, CM, EM, and pre-effector-like CD4⁺ T lymphocytes in the spleen. The miR-30d-5p blockade tended to decrease the percentages and total cell numbers of CD4⁺ pre-effector-like T cells (**Figure 50B**) and significantly reduced the percentages of CD4⁺ CM T cells, which could also be observed regarding their numbers (**Figure 50C**). No differences were found within splenic CD8⁺ T cell subsets.

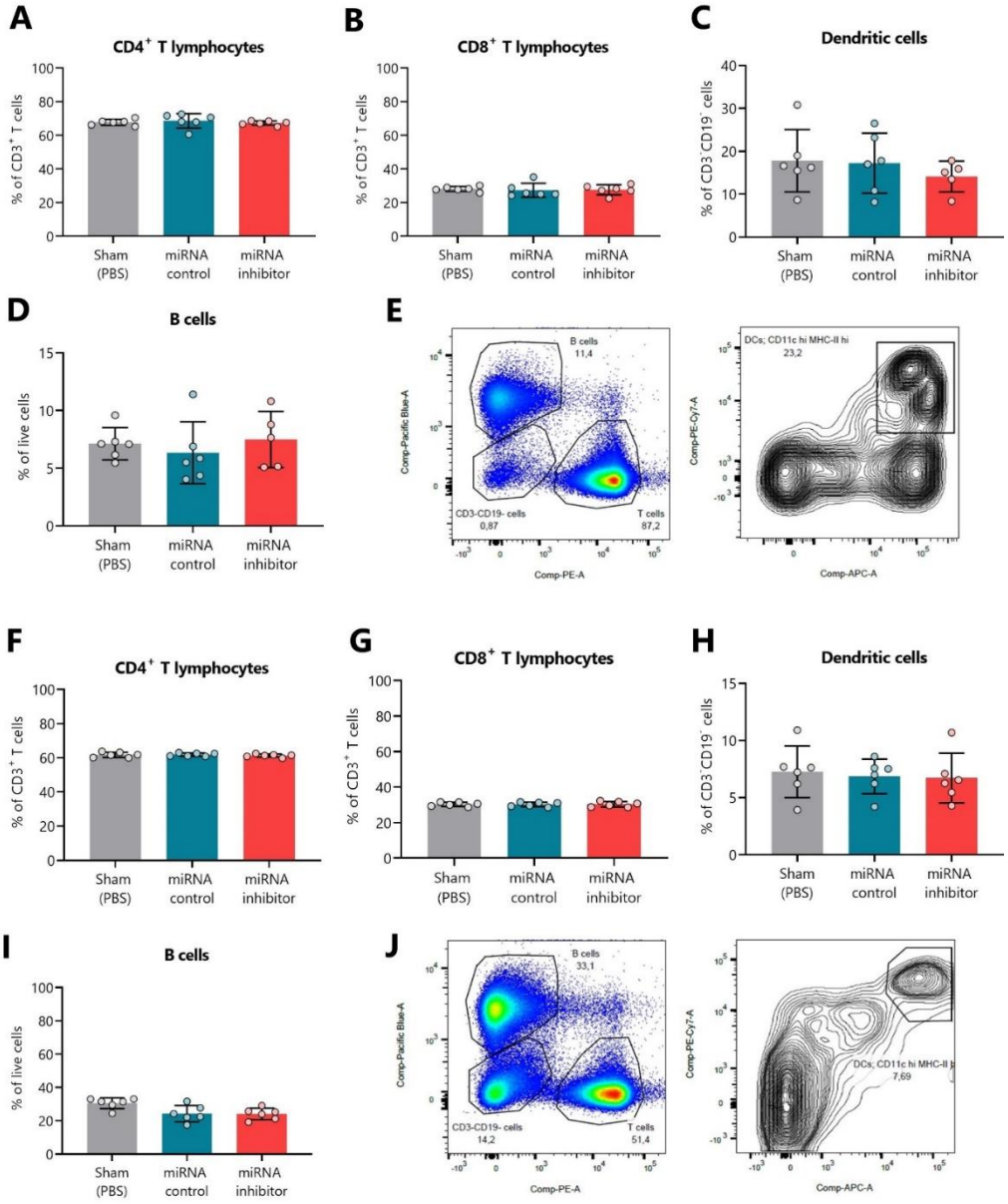

Figure 48. ***miR-30d-5p inhibition does not affect the percentages of total CD4⁺ and CD8⁺ T cells, B cells, or dendritic cells.*** *(**A-D** and **F-I**) Percentages of CD4⁺ T cells, CD8⁺ T cells, dendritic cells, and B cells in (**A-D**) PLN or (**F-I**) the spleen of sham mice (n=6, left, grey), mice treated with a control inhibitor (n=6, middle, blue) or mice treated with the miR-30d-5p inhibitor (n=5–6, right, red). Data are presented as mean ± SD. Significant differences were not found between groups. (**E** and **J**) Representative gating strategy for B cells, T cells, and DCs (from CD3⁻CD19⁻ cells) in (**E**) PLN and (**J**) the spleen.*

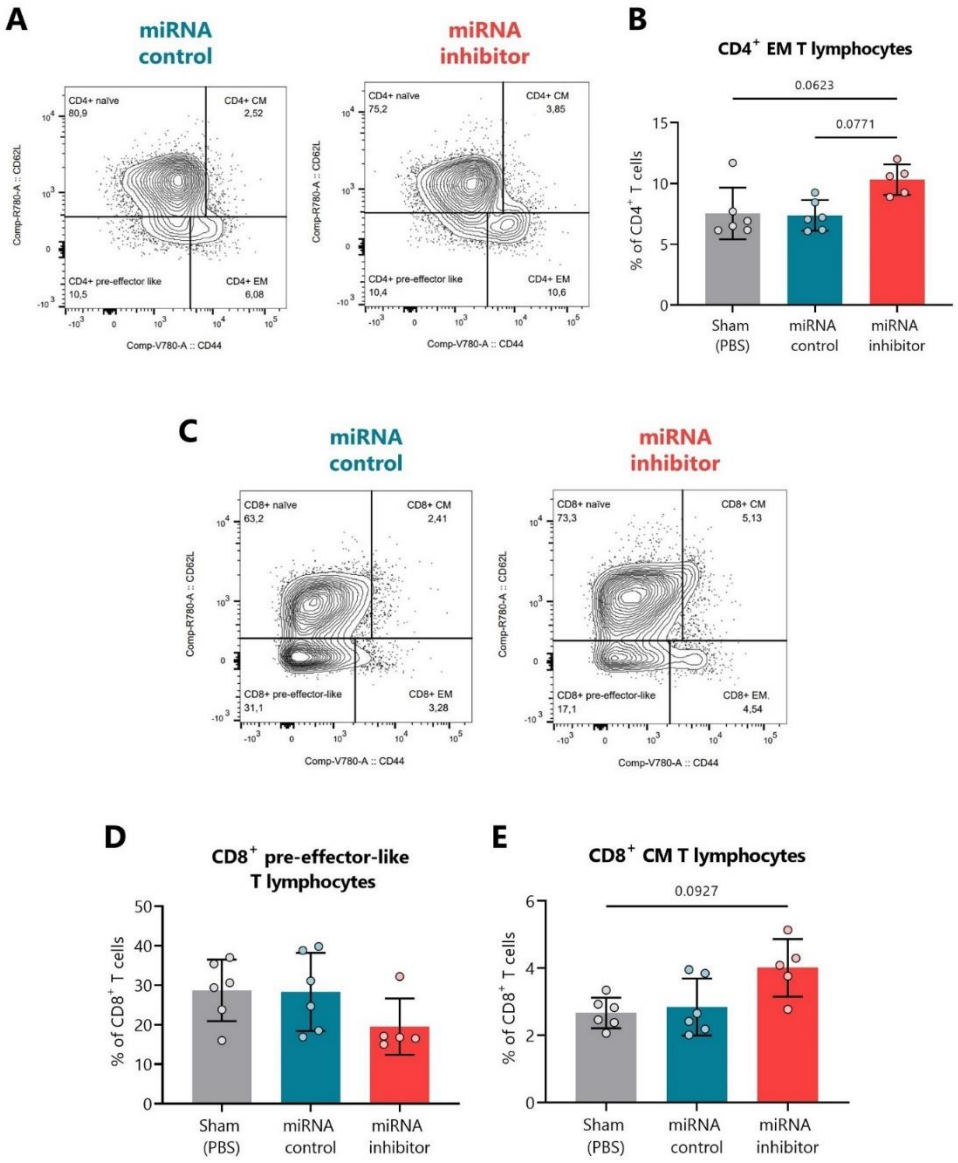

Figure 49. ***In vivo miR-30d-5p inhibition resulted in T cell subset changes in the pancreatic lymph nodes.*** *(**A**) Representative FACS plots indicating the percentage of CD4⁺ naïve, EM, CM, and pre-effector-like T cells in PLN of the control inhibitor (left, blue) and miRNA inhibitor (right, red) treatment groups. (**B**) Percentage of CD4⁺ EM T cells in PLN of sham mice (n=6, left, grey), mice treated with a control inhibitor (n=6, middle, blue), or mice treated with the miR-30d-5p inhibitor (n=5, right, red). (**C**) Representative FACS plots indicating the percentage of CD8⁺ naïve, EM, CM, and pre-effector-like T cells in PLN of the control inhibitor (left, blue) and miRNA inhibitor (right, red) treatment groups. (**D, E**) Percentages of (**D**) CD8⁺ pre-effector-like T cells or (**E**) CD8⁺ CM T cells in PLN of sham mice (n=6, left, grey), mice treated with a control inhibitor (n=6, middle, blue) or mice treated with the miR-30d-5p inhibitor (n=5, right, red). Data are presented as mean ± SD. P-values were determined by Kruskal–Wallis with Dunn's post hoc test.*

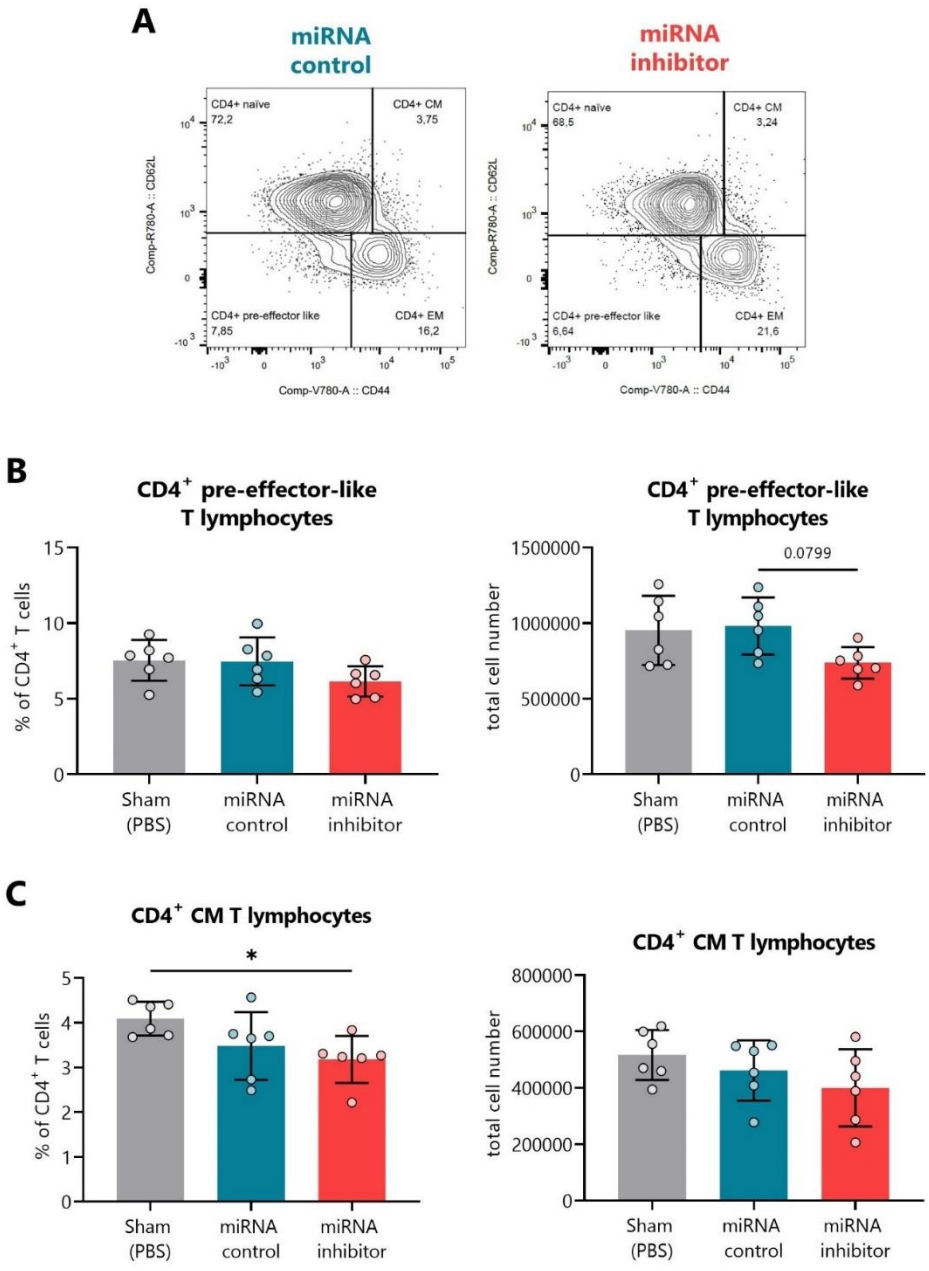

Figure 50. ***In vivo miR-30d-5p inhibition decreases both CD4⁺ pre-effector-like and CM T cells in the spleen***. (***A***) *Representative FACS plots indicating the percentage of CD4⁺ naïve, EM, CM, and pre-effector-like T cells in the spleen of the control inhibitor (left, blue) and miRNA inhibitor (right, red) treatment groups. (**B, C**) Percentage (left) and total cell numbers (right) of (**B**) CD4⁺ pre-effector-like T cells and (**C**) CD4⁺ CM T cells in the spleen of sham mice (n=6, left, grey), mice treated with a control inhibitor (n=6, middle, blue), or mice treated with the miR-30d-5p inhibitor (n=6, right, red). Data are presented as mean ± SD. ns ≥0.05, *p ≤0.05, Kruskal–Wallis with Dunn's post hoc test.*

5. *In vivo* inhibition of miR-30d-5p tends to increase leukocyte islet infiltration

Finally, the insulitis score was determined at the end of the short treatment. As expected, the mice in the sham group showed a similar degree of insulitis (0.96 ± 0.39, mean ± SD) to that of the miRNA control group (1.182 ± 0.25) (**Figure 51A**). The mice that were treated with the miR-30d-5p inhibitor showed a biological trend towards an increased insulitis score (1.33 ± 0.51) compared to both control groups. Additionally, 37.3% of their islets were infiltrated or destroyed (scores 2–4), whereas only 27.3% and 33.5% of the islets were destroyed in the sham and the miRNA control groups, respectively (**Figure 51B**).

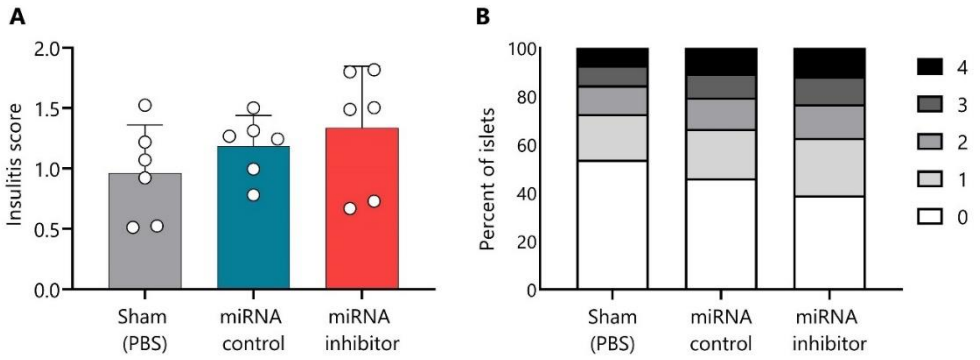

Figure 51. ***Slight increase in insulitis after a short treatment with miR-30d-5p inhibitor.*** *(**A**) Insulitis score from prediabetic NOD mice at the end of the short treatment (10 weeks and 3 days) with PBS (sham, n=6, left, grey), control inhibitor (n=6, middle, blue), or the miR-30d-5p inhibitor (n=6, right, red). Data are presented as mean ± SD. (**B**) Percentage of islets in each of the infiltration categories: white = 0, no insulitis; light grey = 1, peri-insular; medium grey = 2, mild insulitis (<25% of the infiltrated islet); dark grey = 3, 25–75% of the islet infiltrated; black = 4, >75% islet infiltration. Significant differences were not found between groups.*

5

DISCUSSION

The PR phase of T1D is an underexplored period characterized by endogenous insulin production and downregulation of the immune response. Understanding remission in the natural history of T1D is crucial for advancing treatment approaches and improving patient quality of life. Despite its significance, there is a notable lack of comprehensive knowledge in this area. Biomarkers are invaluable tools in the management of T1D, facilitating early diagnosis, disease monitoring, treatment personalization, the development of novel therapies, and the prediction of complications or disease progression. Additionally, they may reflect biological processes occurring during specific phases or stages of the disease and assist in identifying potential pathways for immunoregulation and β-cell recovery. In the present doctoral thesis, we have focused on post-diagnostic heterogeneity to characterize, at the immunological and epigenetic level, one of the most interesting and little-studied phases of T1D: the PR phase. This characterization has led us to study miR-30d-5p-related pathways involved in the restoration of immune tolerance and β-cell functional recovery and regeneration, which could present future therapeutic targets.

Predicting partial remission using biomarkers

The prediction of T1D is of significant importance, as early intervention can facilitate the treatment of autoimmunity prior to the onset of hyperglycemia, thereby avoiding the necessity for replacement therapies or reducing the likelihood of diabetic ketoacidosis [384]. For instance, prognostic biomarkers have been developed for disease staging and the identification of high-risk individuals, who can be treated to delay the onset of the disease, as has been demonstrated with *Teplizumab* [385]. However, it is expensive and time-consuming to detect all patients who eventually develop T1D because a comprehensive screening of the entire population would be needed [386]. In fact, the study with *Teplizumab*, a humanized anti-CD3 monoclonal antibody, was conducted with relatives of patients with T1D who were at high risk of developing clinical diabetes. This group accounts for less than 10% of T1D cases in the general population. It is currently unclear whether these findings will apply to individuals without a family history of diabetes and who appear to be at risk for the disease. It is therefore essential to use biomarkers to stratify subjects at various T1D stages, including post-diagnosis. In this regard, once diagnosed, the PR stage offers another opportunity for interventions aimed at preserving the remaining β-cell mass or modulating the immune system. Therefore, constant monitoring of patients is important, as well as being able to predict and detect this stage correctly.

As previously stated, some studies have been conducted with the aim of predicting the occurrence of PR at the time of diagnosis. However, the majority of these studies primarily focus on anthropometric, clinical, or metabolic factors and recruit a relatively small number of participants. A unifying aspect of these studies is that age at diagnosis is a pivotal factor that significantly influences the likelihood of remission. Indeed, age exerts a discernible impact on the velocity with which the disease progresses from the initial detection of autoantibodies to the clinical diagnosis of T1D. Younger patients tend to exhibit a more rapid and aggressive progression. Furthermore, the prevalence of risk factors has been shown to fluctuate with age [387,388]. In particular, autoantibodies have demonstrated age-specific incidence patterns that have been linked with particular rates of disease progression [389]. Recently, age has also been associated with immunological factors at the time of diagnosis. T1D diagnosed in early childhood is characterized by extensive and early β-cell destruction, aggressive insulitis with abundant $CD8^+$ T and $CD20^+$ B cells, aberrant proinsulin processing, and an elevated circulating proinsulin to C-peptide ratio [29].

Keeping this in mind, in **chapter 1** we extensively immunophenotyped 56 newly diagnosed pediatric patients with T1D and evaluated the predictive value of remission for each variable analyzed. As expected, our findings confirmed that age is the most significant clinical variable in predicting remission, with younger pediatric patients being less likely to experience remission compared to older patients. Consistent with previous research, we also found that patients with higher BMI and stimulated C-peptide levels at diagnosis are more prone to experience remission. In terms of immunological variables, we identified that the percentages of B lymphocytes, Tregs, EM $CD8^+$ T cells and double negative (DN; $CD4^-CD8^-$) γδ T cells are independent predictors of the PR phase. Notably, patients with lower percentages of B lymphocytes and Tregs at diagnosis are more likely to enter remission. In fact, newly diagnosed T1D children and autoantibody-positive children have a higher frequency of Treg cells in comparison to autoantibody-negative children, but less PD-1 expression [281]. In this context, our analysis of activated Tregs ($HLA\text{-}DR^+$) suggests that patients with fewer but more activated Tregs —potentially more functional and suppressive— are more likely to experience the PR phase. However, functional assays are required to confirm this hypothesis. Furthermore, long-standing diabetic patients also have a deficiency in Treg activation due to reduced expression of PD-1 on their surface [390]. On the other hand, B cells have a clear pathogenic role in the pathogenesis of T1D through a variety of mechanisms, including autoantibody production, antigen presentation, and cytokine secretion. This is further supported by the evidence that B-cell-depleting agents can prevent and even reverse T1D in the NOD

mouse model [391]. Consequently, a lower proportion of these cells at the time of disease diagnosis may be associated with an increased likelihood of future remission.

Furthermore, our findings indicate that patients are more likely to achieve remission in the future when the percentage of DN γδ T cells and EM $CD8^+$ T cells in the periphery is higher at diagnosis. γδ T cells represent a discrete subset of lymphoid cells that exhibit features of both innate and adaptive immunity. Most of them remain DN and develop into mature γδ T cells before exiting the thymus [392]. DN T cells were initially associated with the induction of peripheral immunological tolerance and immunomodulatory activities aimed at disease prevention. Nevertheless, the precise function of γδ T cells in the context of diabetes remains to be elucidated, as some studies indicate a potentially protective role, while others suggest a more deleterious one [393]. It is important to note, however, that newly diagnosed patients exhibit a lower percentage than non-diabetic controls, with a further depletion of γδ T cells after one year of insulin treatment [394]. Consequently, patients with a higher percentage of γδ T cells at diagnosis may be more likely to experience remission. In contrast, EM $CD8^+$ T cells constitute the predominant component of insulitis in recent-onset T1D [395,396]. The increased percentage found in the periphery at the time of diagnosis could be related to future PR, as it can reflect their lower migration to the pancreas.

Considering these immunological variables with predictive capacity, we generated through machine learning a single predictive index using 70% of the cohort, which demonstrated an enhanced ability to distinguish remitters from non-remitters. Even after adjusting for potential confounders such as age and BMI, the index remained a significant predictor of PR. The advantage of creating a predictive index that incorporates multiple individually predictive variables lies in its improved accuracy and reliability. By combining multiple variables, the index can capture a greater complexity and diversity of factors influencing the outcome, which increases accuracy and robustness, reduces variance, and increases sensitivity and specificity [397]. Furthermore, we validated the predictive accuracy of this index using the remaining 30% of the cohort. Finally, in order to facilitate the use of this index in clinical practice, a decision tree was constructed to classify patients at diagnosis based on their probability of experiencing remission. The supervised algorithm identified age and the generated index as significant variables. According to the decision tree, patients with an index value of 2 or higher and an age of 11 or older are more likely to experience remission.

In summary, chapter 1 proposes a novel immune-based predictive model of remission, which would allow for a more personalized therapeutic management to ensure the prevention of early hyperglycemia and to reduce the risk of secondary complications in those children who are less likely to experience remission. Importantly, the fact of classifying patients with better or worse prognoses can facilitate the selection process for clinical trials, leading to greater effect sizes. Although the number of patients included in the predictive model is limited (reflecting the patient volume of a secondary hospital with approximately 15 diagnoses in the pediatric population per year), this work represents a crucial first step toward building a robust model for predicting PR. A significant strength of this analysis is the use of flow cytometry panels based on international consensus. Additionally, flow cytometry, the primary method for monitoring immune responses during disease progression, facilitates biomarker discovery, validation, and informed clinical decision-making.

Monitoring partial remission using biomarkers

Given the great inter-subject variability in T1D, the search for new biomarkers has become essential to understand the different courses of the disease and stratify patients. In this regard, although up to almost 80% of pediatric patients experience the PR phase after the initiation of insulin therapy, it is still an under-explored period, although it is of great interest both metabolically and immunologically. Moreover, it is crucial to understand the mechanisms behind this phase since it is associated with better glycemic control and the consequent reduction in secondary complications [261]. Therefore, in **chapter 2** we aimed to investigate novel immunological and epigenetic biomarkers specific of PR.

Immunological biomarkers

First, an analysis of up to 55 peripheral immune cell subpopulations and different cytokines in plasma was carried out during one year from T1D diagnosis. Specific alterations during the PR phase have been discovered in terms of total $CD4^+$ T cells, EM T lymphocytes, T_{ERMA} lymphocytes, Tregs, Bregs, transitional T1 B lymphocytes, NKregs and classical and non-classical monocytes. Despite needing independent validation, these candidate immunological biomarkers to monitor PR corroborate that this stage is governed by both metabolic and immunological factors. Although some studies investigating the PR phase have been reported, only a few have performed a longitudinal follow-up together with comparisons between remitter and non-remitter patients at an immunological level [263,296,297,322,398,399]. To the best of our knowledge, and based on the IDAA1c index to define remission, this is the first study that prospectively monitors

immune cell subsets and cytokines in children and adolescents with T1D from disease onset to the first year after diagnosis, focusing on the PR phase and comparing between remitters and non-remitters to find reliable specific biomarkers.

As mentioned before, $CD8^+$ T cells are one of the predominant components of insulitis in recent-onset T1D. The here reported increase in the percentages of peripheral blood $CD4^+$ and $CD8^+$ T_{ERMA} lymphocytes and EM $CD4^+$ T lymphocytes at PR could reflect their lower migration to the pancreas, resulting in reduced percentages of peripheral naïve T lymphocytes. In addition, we have already seen that higher percentages of EM $CD8^+$ T cells in the periphery at diagnosis are also associated with a higher likelihood of remission (**chapter 1**), so both observations may be related to the ability of these cells to migrate to the target tissue. According to these findings, increased percentages of circulating cytotoxic T lymphocytes positive for IFN-γ, T_H1 lymphocytes, and T_H17 lymphocytes have been found during the PR phase in comparison to the disease onset [300], and also after the first year from diagnosis for $CD4^+$ and $CD8^+$ T_{ERMA} lymphocytes, EM $CD4^+$ T lymphocytes, and T_H17 lymphocytes [312]. Of note, islets from patients with T1D express CXCL10, a chemokine involved in autoreactive T lymphocyte recruitment, while in controls, neither $CXCL10^+$ endocrine cells nor $CXCR3^+$ lymphocytes were detected [400]. That could partially explain the lower percentages of EM $CD8^+$ T cells observed at T1D onset in the periphery [401]. Also, β-cells from patients with T1D hyperexpress HLA class I, thus increasing autoantigen presentation to autoreactive $CD8^+$ T cells [170], which were found within the islets showing an antigen-experienced phenotype ($CD45RA^-$) [402,403]. Since the main mediators of β-cell destruction in T1D are autoreactive effector $CD4^+$ and $CD8^+$ T cells, and supposing that EM T lymphocytes are acting less *in situ*, their increase in the periphery during PR could reflect an attempt at immunoregulation and β-cell recovery.

On the other hand, homeostasis between Tregs and effector T lymphocytes is crucial for the induction and maintenance of peripheral tolerance. Evidence supports that having higher frequencies of insulin-specific Tregs in the prediabetic period is associated with a slow progression to clinically symptomatic T1D [404]. However, at this time-point, Tregs are dysfunctional, thus contributing directly to disease development (reviewed in [311]) and the need to constantly generate new cells to cope with the autoimmune attack. Until recently, it was generally accepted that the overall frequency of peripheral blood $CD4^+FoxP3^+$ Tregs is unaltered in patients with T1D [192,405,406]. Nonetheless, contradictory data on Tregs have been reported, probably because of the different ways that these cells can be identified. Here, we found that $CD4^+CD25^+CD127^{-/low}$ (total Tregs) and memory Tregs ($CCR4^+CD45RO^+$) are decreased in percentage at PR in comparison

to patients without PR. One possible explanation is that these cells could recover their impaired function with the rapid rectification of hyperglycemia after T1D onset, being more active in secondary lymphoid organs and the target tissue. This recovery would not happen in non-remitter patients, who would require continuous generation of additional Tregs. In line with this finding, our predictive analysis pointed out that fewer Tregs but with a more activated phenotype at onset are associated with increased odds of presenting future remission (**chapter 1**). Using the same markers, Fitas et al. found a decrease in total Tregs after a year from T1D onset [300], while we previously found an increase in activated Tregs at this time point, which could be related to PR [312]. Other studies investigating the association of T lymphocytes and PR found that its length positively correlates with the higher frequency of activated Tregs [301] and $CD4^+CD25^+CD127^{hi}$ T cells (which display a Th2 bias but are neither Treg nor type 1 regulatory cells) at disease onset [299]. Furthermore, IL-10-dependent regulatory $CD4^+$ T lymphocyte pathways are involved in long-term remission of T1D [264], and islet-specific $IL\text{-}10^+$ immune responses but not $CD4^+CD25^+FoxP3^+$ cells at diagnosis predict glycemic control. It was also found that patients with higher levels of both Tregs and Th17 showed higher remission rates [282], and conversely, presenting diminished peripheral antigen-specific Tregs was also a feature of remission compared with the diagnosis time-point [298]. Furthermore, we found a diminished percentage of total Tregs in most of our remitter patients except four. Those patients presented a similar behavior to non-remitters, and exhibited increased percentages of Tregs cells from disease onset. Interestingly, they are the youngest within the PR group. Since pediatric patients diagnosed before age 7 may have a more aggressive form of T1D, that could be related to the observed changes in Tregs cells [23]. In conclusion, further characterization of Tregs subsets in terms of phenotype and function needs to be addressed to dissect their role during PR.

In addition, after 12 months of follow-up, only patients who experienced PR showed increased levels of Bregs, transitional T1 B lymphocytes, and NKregs. According to our results, studies in new-onset T1D have not found alterations in other B cell subsets [401,407], while transitional B cells and Bregs increase in pediatric patients one year after diagnosis, which could be related to PR [312]. Both Bregs and transitional B lymphocytes (especially the T1 subset) have immunoregulatory properties and can inhibit effector T cell proliferation [408,409]. Some results indicate that B cell subsets may be involved in the pathogenesis of T1D. For instance, both the percentage of $IL\text{-}10^+$ Bregs and $IL\text{-}10^+$ immature transitional B cells are significantly lower in patients with T1D at diagnosis or with worse glycemic control than in controls [410,411]. In accordance with the findings of previous studies, our results showed a decrease in the number and percentage of total

NK cells and NKeffs at disease onset when compared to control subjects [300,312,401]. The presence of NK cells in healthy human pancreatic islets evidences the innate capacity of these cells to migrate to the pancreas [197] as well as in response to inflammatory mediators [78]. Because NK cells are among the first ones to migrate to the pancreas upon cytokine activation [217], we propose that the reduction in NKeffs we observed in the periphery at onset could be explained by an active migration of these cells into the pancreas and draining nodes. Alternatively, given that chronic exposure to ligands recognizing their activating receptors can result in NK cell hyporesponsiveness [412–414], we suggest that the observed NK cell reduction after 1 year of follow-up could be explained by their loss of functionality rather than an active migration. Indeed, another study demonstrated that the reduction in NK cell activation in patients with T1D occurs approximately 1 year after the onset of the disease and that the lower expression of the activating natural killer group 2 member D (NKG2D) receptor in these cells was not a genetic defect, suggesting an indirect modulatory effect [415]. Furthermore, only patients undergoing remission 12 months after the diagnosis showed an increased number of NKregs. These cells can regulate adaptive immunity by suppressing autoreactive T cell responses and proliferation and by killing over-stimulated lymphocytes, macrophages, or dendritic cells [416,417]. Altogether, the here reported higher ratio of T1/T2 cells and the increased counts of Bregs and NKregs after a year of follow-up for remitter patients could reflect an immunoregulatory attempt.

Innate immune cells are also crucial players in the development and progression of T1D and a crosstalk occurs between them and lymphocytes. Here, we detected an increase in classical monocytes ($CD14^{+}CD16^{-}$) and a decrease in non-classical monocytes ($CD14^{dim}CD16^{+}$) only in remitter patients when compared to the disease onset. While non-classical monocytes are typically inflammatory, classical monocytes do not usually present inflammatory features [418]. Thus, the increased percentage of the classical ones could help mitigating the inflammation during the PR phase. This aligns with data indicating that the $CD16^{+}$ subset of monocytes is increased in certain autoimmune diseases and may play a role in initiating the inflammatory immune response [419–421].

Cytokines orchestrate multiple interactions between β-cells and immune cells, and their anti-inflammatory or proinflammatory functions are context-dependent [422]. Cytokines produced by immune and pancreatic cells influence T1D development and progression by inducing regulatory or proinflammatory phenotypes. For instance, a type I IFN-inducible transcriptional signature is increased in the peripheral blood before the development of islet autoimmunity [423]. Typically, regulatory cytokines like IL-10, IL-4, IL-5, IL-35 and TGF-β, promote anti-inflammatory responses, while proinflammatory

cytokines, such as TNF-α, IL-6 and IL-17, enhance inflammation via proliferation and activation of diabetogenic immune cells [424]. Other cytokines like IFN-γ appear to have dual effects on T1D development. The protective role of IFN-γ is associated with the suppression of diabetogenic $CD8^+$ T-cell responses by inhibiting STAT1 expression and reducing Th1 cell-related cytokines [425,426]; while the destructive role of this cytokine is associated with the aberrant expression of MHC-I and MHC-II in β-cells, which represents a mechanism for cytotoxic reactions against them [427,428]. Additionally, β-cells' high cytokine receptor expression heightens their sensitivity to apoptosis or regeneration [164]. Here, none of the analyzed cytokines showed significant differences between remitters and non-remitters, which would limit their use as biomarkers of remission or T1D progression. While published data are sometimes contradictory, PR tends to be associated with decreased levels of proinflammatory cytokines [300]. We found increased levels of IL-17A, a relevant cytokine in T1D [191], at disease onset, and a trend to reduce this cytokine in remitter patients. In T1D, IL-17A expression is upregulated in the pancreas of both humans and animal models [192,429], and its primary source of production in the human pancreatic tissue is β- and α-cells [430]. Among other effects, it exacerbates chemokine expression by human islets, thereby aggravating insulitis [431]. Indeed, the blockade of the IL-17 pathway together with anti-TCR therapy has been shown to be an effective approach in restoring normoglycemia in rodent models of T1D [432]. Because IL-23 and/or TGF-β plus IL-6 drive the production of IL-17 by T cells, the here reported IL-17A increase together with the higher levels of TGF-β and IL-6 could reflect the inflammatory state at diagnosis, which is less evident at PR. In a previous non-longitudinal study, low TGF-β levels were a feature of PR [312], which can be observed in this study as an inconclusive trend. Other results also suggest that low levels of circulating IFN-γ are a distinct feature of PR [43,60]. However, a clear correlation between decreased cytokine/chemokine levels and PR does not appear to be evident, and further investigation is needed to elucidate their function as biomarkers.

Epigenetic biomarkers

Epigenetic biomarkers have greatly enhanced our understanding of disease origins and progression. The epigenetic modifications are reversible, different among cell types, and can potentially lead to disease susceptibility by producing long-term changes in gene transcription [433,434]. Among them, circulating miRNAs have huge potential as a novel class of non-invasive biomarkers that reflect disease activity and attempts at β-cell regeneration or immune regulation [120,435]. Indeed, they are an excellent choice as a biomarker because, in addition to being involved in many biological processes, their expression normally changes with pathological stress. Moreover, miRNAs present a high

biochemical stability and can be detected by a variety of reproducible techniques, including qPCR, next generation sequencing, microarrays, and *in situ* hybridization. These molecules are also found in abundance in body fluids such as blood or urine, making them accessible through minimally invasive procedures. Finally, they exhibit high specificity and sensitivity, which enables the prediction, diagnosis, and detection of changes during the development of a disease and the monitoring of treatment responses [436].

The onset of islet autoimmunity has been associated with several dysregulated miRNAs both in circulation [137,139,290,437–439] and in peripheral blood mononuclear cells or T lymphocytes [124,138,440,441]; however, only a few studies have addressed changes in miRNA levels over time upon diagnosis [140,141]. Specifically in children, one of the first studies found that miR-25 levels in sera are associated with improved glycemic control and stimulated C-peptide three months after diagnosis [136]. Similarly, levels of the miR-23~24~27 cluster in newly diagnosed children predict C-peptide loss over time and are upmodulated upon disease progression [135]. A study conducted on the Danish Remission Phase Cohort found that the miR-197-3p at three months —when PR usually occurs— is the strongest predictor of residual β-cell function one year after diagnosis in children with T1D [442]. Nevertheless, none of them evaluated specific changes in miRNA levels during the PR phase in a longitudinal pediatric cohort of patients.

On the one hand, we identified 12 upregulated miRNAs in pediatric remitter patients versus non-remitters. Of those, five belong to the MIR-17 family (miR-20b-5p, miR-17-5p, miR-106a-5p, miR-106b, and miR-18b-5p). Some of these miRNAs have been previously associated with β-cell apoptosis/regeneration processes and immunomodulation. For instance, the inflammatory microenvironment causes β-cells to downregulate the expression of miR-17, a miRNA that negatively affects ERAP1 mRNA, increasing the processing of preproinsulin signal peptide antigen and promoting its recognition by autoreactive $CD8^+$ T cells [128]. Thus, the upregulation of miR-17 during the PR phase could be related to the decreased inflammatory environment and might be involved in decreasing β-cell visibility to the immune system. Moreover, whereas miR-17-92 and miR-106b-25 clusters positively regulate β-cell proliferation and insulin secretion in mice and are important for normal endocrine function [443,444], miR-20b can inhibit T cell proliferation and activation by targeting NFAT [445]. Hence, both facts would contribute to the hypothesis that behind PR, there are processes of immunoregulation and β-cell regeneration that are controlled by epigenetics. On the other hand, we identified four downregulated miRNAs during PR in comparison to non-PR, including let-7b-5p and let-7c-5p. Recently, it was reported that let-7b-5p

overexpression impairs insulin production and secretion and inhibits β-cell proliferation in mice [446,447], which could be related to the diminished residual β-function in patients without remission. Notably, of the 16 DEMs, miR-10395-3p, miR-10393-3p, and miR-1277-3p are described for the first time in relation to T1D. Furthermore, the GO analysis revealed several enriched metabolic, immunological, apoptosis, and stress processes, which are pathways closely related to T1D immunopathogenesis. The functional annotation of genes regulated by these miRNAs also implies that TGF-β and FoxO signaling pathways (among others) may be involved in the occurrence of PR, which can control the development and function of FoxP3$^+$ Tregs [448] or β-cell proliferation and function [449].

In summary, chapter 2 of the doctoral thesis has contributed to a more complete picture of specific circulating biomarkers of PR (**Figure 52**), expanding our knowledge of immune cell and cytokine changes and providing new biomarkers such as miRNAs. These biomarkers can reflect the mechanisms occurring behind this intriguing period and help identifying the different factors that affect the progression of T1D and its immunopathology, especially those pathways leading to β-cell protection and immune modulation.

However, this study has limitations that must be taken into account when interpreting the results. First of all, the sample size is relatively small, which lowers the statistical power. However, such data are very hard to obtain. While the immunological biomarkers should be validated in larger cohorts of individuals (and desirably in different centers), we were able to validate some of the miRNAs by RT-qPCR in another cohort of patients, a highly recommended step [450]. Moreover, even though we verified the absence of batch effects and the suitability of the normalized data for the differential expression analysis, another limitation in the RNA-seq experiment was the absence of technical replicates between runs. Another weak point of our cohort is the wide range of ages (from 1 to 18) and the variability that this entails regarding the physiological changes that the subjects undergo (e.g., puberty). Whereas variations in the levels of immune cell subpopulations over one year in healthy pediatric or adult subjects are subtle or inexistent [33,451], changes are observed within longer tracking periods [452]. In that sense, we performed correlations between age and the percentage or absolute counts of the different analyzed immune cell subsets both in controls and patients at T1D onset and found that the changes were likely to be a consequence of T1D progression rather than age-linked. Furthermore, the differential expression of miRNAs was not either related to age (data now shown).

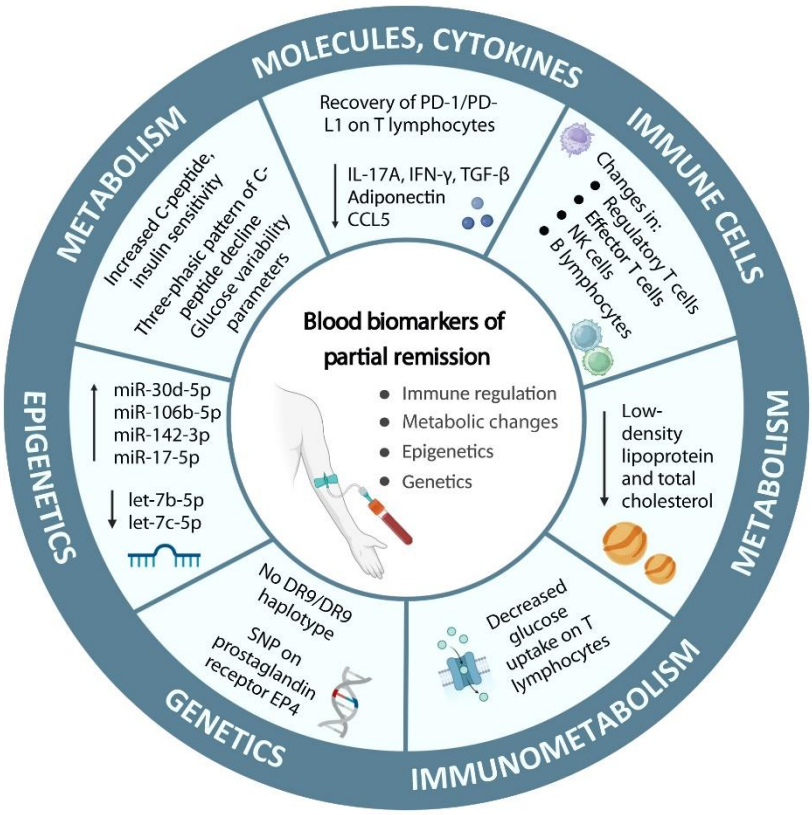

Figure 52. ***Circulating biomarkers of partial remission in type 1 diabetes.*** *Summary of biomarkers that reflect immunoregulatory processes and/or functional β-cell improvement during the partial remission phase. Decreased levels of certain cytokines, such as IL-17A, IFN-γ, TGF-β, CCL5, or adiponectin, as well as recovery of programmed death (PD)-1/PD ligand 1 (PD-L1) expression in T lymphocytes have been observed during this period. Changes in the percentages of immune system cells, such as effector or regulatory T lymphocytes, NK cells, or B lymphocytes, have also been found. In addition, T lymphocytes also show a characteristic metabolism in this phase by taking up less glucose. Regarding changes in metabolic biomarkers, a reduction in total cholesterol and low-density lipoproteins has been observed, as well as a less acute loss of C-peptide and an improvement in both glucose variability parameters and insulin sensitivity. A unique profile of miRNAs during partial remission and an increased risk of non-remission in patients presenting the DR9/DR9 haplotype has also been described. In terms of genetics, a single nucleotide polymorphism (SNP) on prostaglandin receptor EP4 was found to be associated with remission occurrence and extension.*

Although the usage of peripheral blood as a source of biomarkers is a non-invasive technique, immune cells are tightly regulated by their generation in primary lymphoid organs and their migration to tissues, thus making their changes in the periphery difficult to interpret. The analysis of the target organ and further studies on the functionality of immune cells (e.g., cytokine production) —including antigen-specific T cells— are

needed to correlate changes in the periphery with the events occurring in the pancreas. Since a limited amount of blood was obtained from pediatric patients, IAA have not been explored. However, due to its β-cell specificity, the baseline titer of IAA could be of interest for the study of the PR phase. Still focusing on this stage, we are not evaluating its length, which could be related to the persistence and activity of certain immune cells. The strengths of the biomarker discovery study include the longitudinal picture of T1D early stages, the characterization of the PR phase versus non-remission by a wide range of immune subpopulations, cytokines, and miRNAs and the use of IDAA1c of ≤9 to define PR, an index that includes glycemic control and insulin doses, that correlates with C-peptide levels, and that has been validated in a large cohort of young patients with T1D [248].

The discovery of these novel biomarkers holds great potential for physicians, because they enable the prediction and detection of subsequent remission stages that might otherwise go unnoticed. Prolonging the honeymoon phase as much as possible, or even inducing it, becomes highly pertinent for patients, given the association between residual β-cell function and reduced long-term complications [272,273]. Preserving the function of remaining β-cells beyond the honeymoon stage, while halting the autoimmune attack, is also a promising strategy. Since PR is a stage of partial recovery of β-cell function, it offers a unique therapeutic window to rebalance the immune system through immunotherapies. The concept of immunointervention during this stage has strongly evolved over the past few years, with the success of clinical trials being influenced not only by the efficacy of the therapy, but also by the appropriate timing of intervention. By targeting these interventions during periods of reduced inflammation or heightened immunoregulatory activity, the outcomes of clinical trials may be favorably influenced. Currently, no reported clinical trials are being conducted during the PR phase. Nonetheless, the potential for monitoring the outcomes of interventional studies in stages 2 and 3 of T1D appears promising through the utilization of distinct biomarkers associated with this stage. Moreover, identifying suitable individuals for enrollment in clinical trials poses challenges. Patient stratification based on the presence or absence of remission can not only enhance their selection for clinical trials, but also enable a more precise therapeutic approach.

In returning to the subject of miRNAs, miR-30d-5p was the most upregulated one during PR, where insulin synthesis and secretion are improved. This is a glucose-regulated miRNA that has been associated with both the induction of insulin production by activating MafA in pancreatic β-cells and the protection of β-cell function from impairment caused by proinflammatory cytokines [453,454]. Even though we are

uncertain about which cells are producing this miRNA and thus contributing to its circulating pool, it is known to be highly expressed by pancreatic β-cells, suggesting that they are likely one of its primary sources [454]. In tumor cells, miR-30d-5p induces IL-10 expression (an immunosuppressive cytokine), at least in part by repressing the *GALNT7* gene, resulting in pro-metastatic effects *in vivo* [455]. Regarding autoimmunity, miR-30d-5p is capable of regulating the intestinal microbiome in the experimental autoimmune encephalomyelitis model, which in turn results in enhanced immunosuppression and the amelioration of the multiple-sclerosis-like symptoms [456]. In the context of T1D, miR-30d is found both up- [457] and downregulated [139] in the plasma of people with T1D versus control subjects and is also increased in exosomes from lactating mothers with T1D [458]. Nevertheless, little is known about its immunological functions. In this work, multiple lines of evidence point to a link between miR-30d-5p and immunoregulatory processes. By analyzing its potential targets, we found that miR-30d-5p is enriched for different biological processes like responses to stress, insulin signaling, cell death or fatty acid biosynthesis, which have key roles in T cell development and immune responses [459]. Moreover, it was enriched for diverse immune-related processes like antigen processing and presentation, as well as TLR and TGF-β signaling pathways. Also, we managed to classify some of its predicted and validated targets and discovered that this miRNA could affect genes such as *CD200*, *CCL5*, *CTLA4*, *NFAT5*, *PRDM1*, and *TGFBR2*. Of note, the pathway enrichment also encompassed processes relevant to regeneration, differentiation, and proliferation. Examples of these pathways include the regulation of pluripotency of stem cells, hippo signaling pathways, and cellular senescence.

Thus, it is evident that this miRNA plays a pivotal role in regulating crucial pathways that contribute to the pathogenesis of T1D. However, miR-30d-5p did not fulfill the criteria for validation in another cohort, primarily due to its low plasma concentration. Consequently, we were unable to validate its high and specific upregulation during the PR phase in another cohort and using another technique (data not shown). To detect these subtle differences, more sensitive techniques, such as small RNA-seq, may be necessary. Nevertheless, as it was the sole miRNA exhibiting specific upregulation during PR and that can regulate insulin secretion, we were interested in determining whether it also regulates immune responses and β-cell regeneration and functional recovery.

MiR-30d-5p-mediated immunoregulatory pathways

Firstly, we sought to examine the impact of miR-30d-5p inhibition on the main cells responsible for β-cell destruction, the T lymphocytes, mainly with regard to immune checkpoint receptors and cytokine secretion (**chapter 3**). To this end, we designed a novel protocol for the electroporation of primary human T lymphocytes, with the objective of facilitating the targeted delivery of miR-30d-5p inhibitor. This approach was deemed necessary due to the inherent characteristics of these cells, since they are resistant to common chemical transfection reagents [460]. Retroviral/lentiviral delivery is also widely used in T cell therapies [461,462]; however, viral vectors are expensive to manufacture, integrate genes in semirandom patterns and their transduction efficiency varies between patients [463]. Therefore, the most effective non-viral-based delivery method to primary T lymphocytes is electroporation [464].

Electroporation is a frequently used physical transfection method that uses electrical voltage to transiently increase the cell membrane permeability, thereby facilitating the entry of foreign nucleic acid [465]. This method is commonly employed to transfect difficult-to-transfect cells such as primary cells [349]. Nevertheless, the main drawback is the excessive cell death and permanent damage that it may cause. Moreover, the transfection efficiency of T lymphocytes highly depends on their cellular state. When cells are activated, the mean diameter is increased, resulting in enhanced transfection efficiency and a greater likelihood of material delivery into the nucleus [466]. Several mRNA electroporation protocols into primary T lymphocytes have been developed for genetically modified T cells in preclinical studies [467–469]. In the present work, we used an LNA miRNA inhibitor to be delivered into T lymphocytes, a type of modified oligonucleotide that possesses an extra methylene bridge in at least one of its nucleotides to enhance the stability of its ribose ring structure. This modification showed higher efficiency, stability, and binding affinity than traditional oligonucleotides, which results in long-lasting antisense activity [470]. The inhibitor binds to the complementary miR-30d-5p to antagonize its activity, thereby increasing the targeted gene expression.

In general, the inhibition of miR-30d-5p on pre-activated T lymphocytes from both control subjects and patients with T1D resulted in a reduction in the expression of certain immune checkpoint molecules or inhibitory receptors, including CD200, CTLA-4, PD-1, LAG-3, and TIM-3. Accordingly, the elevated expression of this miRNA during the PR phase may be associated with the enhanced expression of these inhibitory molecules and the downregulation of T-cell responses, indicating an immunoregulatory function of miR-30d-5p.

In this study, CD200 and CTLA-4 have been identified as potential target genes for this miRNA. However, only one database evaluating a single experiment has demonstrated that CD200 is an experimentally validated target (TarBase v9.0). In human T lymphocytes, it appears that neither CD200 nor CTLA-4 are target genes, as their expression should increase in the absence of the miRNA, yet they behave in a manner opposite to what would be expected. It is noteworthy that electroporation with the control inhibitor also results in a reduction in CD200 expression levels compared to the mock condition. This suggests that this molecule may be particularly susceptible to the effects of electroporation and extracellular material uptake.

Among immune checkpoint receptors or inhibitory receptors, CTLA-4 and PD-1 are the most well-studied and are known to downregulate T-cell activation to maintain peripheral tolerance [471]. When PD-1 or CTLA-4 are expressed on activated T lymphocytes and bind, respectively, to their ligands PD-L1 or CD80/86, they prevent these lymphocytes from attacking the body's own cells. Many studies have recognized the association of PD-1/PD-L1 with the pathogenesis of T1D [194,472–474]. As early as 2003, it was shown that inhibition of PD-1 and PD-L1 in the animal model of T1D, the NOD mouse, could induce the disease, while overexpression of these molecules could inhibit the response of autoreactive T lymphocytes and reverse diabetes [317]. In addition, other immunosuppressive axes have also been implicated. For example, the binding of Galectin-9 and TIM-3 negatively regulates the Th1 response, and it was observed that overexpression of these molecules could prevent the development of diabetes in the NOD mouse [475,476]. LAG-3 is an immune checkpoint receptor that exerts a negative regulatory effect on T cell activation, proliferation, and homeostasis by binding to the MHC class II. LAG-$3^{-/-}$ NOD mice develop diabetes at a substantially accelerated rate, with 100% incidence. This is primarily due to the fact that LAG-3 limits the pathogenic potential of $CD4^{+}$ T cells [477]. Polymorphisms in the CTLA-4 gene have also been found to be associated with an increased susceptibility to developing T1D [478], especially in the pediatric population.

Newly diagnosed patients with T1D are characterized by increased levels of plasma-soluble checkpoint inhibitor molecules (e.g., PD-1, PD-L1, CTLA-4, LAG-3, TIM-3, etc.), which are associated with the risk of developing other autoimmune diseases [479]. Moreover, patients at disease onset have reduced expression of PD-1 and LAG-3 in T lymphocytes compared to controls [480–482]. In addition, functional pancreatic β-cells (those that still synthesize and secrete insulin) from patients with T1D express PD-L1, compared to insulin-deficient β-cells from the same patients or β-cells from non-diabetic subjects [483]. Thus, it is possible that these insulin-positive β-cells remaining after

diagnosis of T1D express PD-L1 as a defensive mechanism against the autoimmune attack [484,485]. Given that remitter patients have a greater reserve of functional pancreatic β-cells than non-remitters, it is reasonable to hypothesize that PD-L1 expression in their islets will be higher and that they will present enhanced immunoregulation. Interestingly, at the level of T lymphocytes in the periphery, remitter patients show a higher percentage of these cells positive for both PD-1 and PD-L1, thus recovering the low levels reached during the diagnosis of the disease and promoting tolerance [263]. These changes, however, were not observed in non-remitter patients. These findings align with those observed in our treated T lymphocytes, as a reduced expression of miR-30d-5p (which occurs during non-remission (**chapter 2**)) is associated with a diminished expression of PD-1.

Exhausted T cells display sustained upregulation of inhibitory receptors including PD-1, CTLA-4, LAG-3, TIM-3 and TIGIT in the absence of co-stimulatory receptors [486]. The triggering of these inhibitory receptors results in a progressive loss of effector functions, desensitization of TCR, and failure to acquire a memory phenotype [487]. In fact, in the absence of the miR-30d-5p, there is an increase in the $CD45RA^+$ subsets, typically associated with a more naïve phenotype, but also with T_{EMRA}. Thus, the higher levels of miR-30d-5p during PR may be related to a lower acquisition of a T_{EMRA} phenotype on $CD8^+$ T cells —possibly related to the expression of the inhibitory receptors—, which not only possess cytotoxic functions but also display a proinflammatory phenotype and secrete multiple inflammatory factors [488]. Also, the possible association of miR-30d-5p with an exhausted T-cell phenotype (because the expression of inhibitory receptors depends on it) may elucidate a protective mechanism that occurs during this phase. In line with these results, it was recently shown a negative relationship between PD-1 and glucose uptake in $CD8^+$ T lymphocytes during the PR phase in children [322]. This observation holds significant importance since the presence of pathways that counteract co-stimulation negatively impacts glucose metabolism, especially glycolysis, the main metabolic pathway for T cell activation and proliferation [323].

Regarding T lymphocyte functionality, miR-30d-5p inhibition affected IFN-γ levels, decreasing them. IFN-γ is an anti-viral cytokine known for its central role in the regulation of immune cascades, such as antigen presentation or cell proliferation. Although it has typically been associated with acute inflammatory responses, recent studies have indicated that it may also have protumourigenic effects, as it induces PD-L1 expression [489,490]. Indeed, in response to IFN-γ production, β-cells upregulate PD-L1 expression, thereby limiting the activity of self-reactive T cells [484]. In addition, genetic knockout of IFN-γ in CAR T cells has been shown to reduce the expression of immune checkpoint

molecules such as CTLA-4, PD-1, LAG-3 and TIM-3 [491,492]. Given that IFN-γ acts through autocrine signaling too, it can be postulated that decreased IFN-γ secretion and signaling on T lymphocytes may be related to the decreased expression of immune checkpoint molecules observed in the absence of miR-30d-5p.

Collectively, it can be reasonably concluded that miR-30d-5p promotes the expression of inhibitory receptors or immune checkpoint molecules on T lymphocytes and that the upregulation of this miRNA —and probably others [493]— during the honeymoon could be behind the immunoregulatory processes taking place during this period.

In light of the *in vitro* results, in **chapter 4** we sought to investigate the role of miR-30d-5p in the ongoing autoimmune attack *in vivo*. The direct inhibition of miR-30d-5p in the prediabetic NOD mice led to changes in different immune cell subsets in secondary lymphoid organs and immune cell infiltration in the pancreatic islets. Upon miR-30d-5p inhibition, the levels of Tregs were significantly increased in PLN. In this model, we found that the expansion of these regulatory cells could be explained by the increase in the expression levels of *CD200* in PLN cells, acting in this case as a target gene for miR-30d-5p. In other words, what we expected to occur also in T lymphocytes *in vitro* has only occurred *in vivo*: the lower expression of miRNA leads to a higher expression of its target gene. In fact, CD200-CD200R-mediated immunosuppression can occur through the induction of FoxP3$^+$ Tregs [494,495]. Since miR-30d-5p is upregulated in PR vs. non-PR, we should expect lower levels of Tregs along this phase; and that is precisely what we observed in our longitudinal study (**chapter 2**). These results are accordant with other studies in humans showing diminished Treg levels during the honeymoon phase or after one year [298,300]. Furthermore, although we could not confirm a miR-30d-5p/Blimp-1(*PRDM1*)/PD-1(*PDCD1*) axis acting on splenocytes of NOD mice, miR-30d-5p is influencing again PD-1 expression through other mechanisms that need further research. What is clear from what we have observed both *in vivo* (**chapter 4**) and *in vitro* (**chapter 3**) is that miR-30d-5p expression is associated with increased PD-1 expression in T lymphocytes, which may be an important mechanism behind the induction of the PR phase. In fact, insulin-coupled APCs can induce remission in diabetic NOD mice, which is maintained through the PD-1/PD-L1 pathway [496].

Moreover, the increased levels of EM and CM T lymphocytes upon miR-30d-5p inhibition could reflect the wave of differentiation into the effector and memory phenotypes, which have a key role in amplifying inflammation. In fact, the expansion of CM T cells might boost the pathogenic potential of the peripheral T cell pool and favor autoimmunity. Finally, the slight increase in the immune cell infiltration into the pancreatic islets could

be related to the enhanced effector function of these T lymphocytes and the reduced expression of PD-1. It has been suggested that elevated PD-1 expression on islet-reactive $CD4^+$ T cells intrinsically regulates them by suppressing their proliferation and inhibiting pancreatic tissue infiltration [472]. Therefore, the upregulation of miR-30d-5p during the PR might be related to a decreased immune cell infiltration in the islets of Langerhans and the amelioration of the inflammatory microenvironment, with the consequent prevention of β-cell apoptosis. Nevertheless, it would be interesting to identify the nature of the infiltrating T lymphocytes. We must take into consideration that the observed insulitis after miRNA blockade might be enriched on Tregs since there is an increase in these regulatory cells in the draining lymph nodes.

Although the NOD model spontaneously recapitulates autoimmunity in pancreatic islets, there are key differences in disease development between NOD mice and humans, like islet cell composition, the severity of the autoimmune reaction in terms of β-cell destruction or the fact that mice do not undergo spontaneous remission [497]. Another important point to consider is that despite having been able to indirectly test the effect of the miR-30d-5p inhibitor by analyzing the up- or downregulation of some miRNA target genes, it could be interesting to test its specific delivery to T lymphocytes *in vivo*. In this sense, numerous studies have used inhibitory/mimic miRNAs coupled to fluorescent molecules to see their accumulation in different tissues, including lymph nodes [123,498–500].

Taking all these data together, we hypothesize that in the absence of miR-30d-5p (non-remission scenario), T lymphocytes do not receive the inhibitory signal through PD-1 because of its low expression levels, which could potentiate their effector functions and their contribution to the inflammatory immune cell infiltrate into the pancreatic islets. At the same time, increased levels of Tregs are generated —in part due to the *CD200* upregulation— to try to tackle this enhanced immune response.

MiR-30d-5p impacts β-cell function and regeneration

Lastly, in **chapter 3** we also sought to ascertain whether, in addition to its immunomodulatory functions, miR-30d-5p plays a role in β-cell recovery and regeneration. In order to gain insight into the impact of this miRNA in human β-cells, rather than relying on cell lines, isolated human islets or animal models, we employed the long-term culture of HPSs. Qadir et al. described a novel method that uses oxygen-enhancing culture techniques of HPSs that results in the functional preservation of endocrine and exocrine cells for at least 10 days without significant deterioration [354].

Previously, no other report on organotypic human pancreatic tissues was able to culture them for longer than 5 days [501,502]. Moreover, in contrast to previous reports using pancreatic tissue cultures or human islets, the HPSs largely preserve the anatomical integrity of the native organ without experimenting β-cell dedifferentiation processes [503]. Thus, this approach allows for the examination of the impact of miRNAs on β-cells in a manner that closely resembles the actual human context.

The combination of long-term slice culture and virally-mediated lineage tracing (red-blue reporter and an insulin lineage tracer) also allows for the detection and quantification of β-cell regeneration events [354]. Regeneration can occur through multiple mechanisms like β-cell replication [504], α-to-β-cell transdifferentiation [505,506], or ductal progenitor cell differentiation [507]. In our model, we were able to quantify neogenesis by the differentiation of any non-β-cell to a new insulin-producing cell. As a positive control for β-cell regeneration, we used BMP-7, an FDA–approved homodimeric protein from the TGF-β superfamily with dual TGF-β inhibition and BMP activation abilities [508], both necessary to activate pancreatic progenitors. Previously, it was found that BMP-7 was able to convert primary human pancreatic exocrine tissue into functional islet endocrine cells through a ducto-acinar-endocrine differentiation axis [269], with neogenic β-cells exhibiting glucose responsiveness [509]. In order to observe differences in the neogenesis of β-cells, we decided to use for these experiments a miR-30d-5p mimic, as we believed that it would exert comparable effects to BMP-7. After the co-transduction and treatment with BMP-7, slices displayed an upward trend in BFP signal (β-cells) in comparison to non-treated slices, and also a trend to a higher red-blue (violet) signal co-localization, suggesting the additional formation of β-cells from non-β-cells after the initial labeling of the resident ones. Interestingly, a significant upregulation in both the blue and violet signal was observed after transfection with miR-30d-5p mimic in comparison to the non-treated slices, even at higher levels than BMP-7. No such effect was observed for the control inhibitor and control mimic used, suggesting a specific effect of miR-30d-5p upregulation. As expected, no differences were noticed after the inhibition of the miRNA in comparison to the non-treated slices. This is because the absence of the miRNA precludes regeneration; and at the same time, regeneration cannot occur in the absence of stimulation. To our knowledge, this is the first time that a role for β-cell neogenesis is described for miR-30d-5p. However, we must be cautious in interpreting the results because in transgenic mouse lines specifically overexpressing miR-30d in β-cells and fed a high-fat diet, it was found that appropriate levels of miR-30d are essential to maintain normal β-cell identity and that too high levels of this miRNA can have the opposite effect and lead to its loss [510]. We did not observe higher miR-30d-5p levels than the basal ones after applying the mimic, and the

phenotypical changes observed can be ascribed to it since we made sure that the transfection method worked with the FAM-labeled inhibitor. Apart from miR-30d-5p, other miRNAs have been described to have a role in β-cell regeneration. For instance, miR-132 and miR-375 promote the proliferation of these cells [511,512], the inhibition of miR-23a promotes α-to-β-cell transdifferentiation [513], and the inhibition of miR-7 activates mTOR signaling and β-cell replication [514].

As previously stated, it has been demonstrated that miR-30d activates MafA and insulin production by targeting TNF-α-activated MAP4K4 in MIN6 cells (mouse pancreatic β-cell line) and isolated islets [453,454,515]. In this study, we employed a perifusion system to evaluate the functionality of islets in HPSs. The tissue was maintained at 37°C, which provided a consistent temperature environment that resembled the *in vivo* situation. The collected fraction was cooled to 4°C to protect the integrity of the eluted C-peptide [358]. C-peptide is a reliable indicator of insulin secretion, as both insulin and C-peptide are stored in secretory vesicles and released in equimolar concentrations upon stimulation of β-cells by glucose. The inhibition of miR-30d-5p after seven days of culture resulted in a reduction in C-peptide secretion in response to high glucose concentration when compared to non-treated slices, confirming what was observed in the literature. In this case, as the number of perifusion chambers limited the control groups, it remains uncertain whether the observed outcome can be attributed to the transfection process itself or miRNA inhibition. It should also be noted that the stimulation index is very different between the two pancreases used, even though the experimental conditions were the same and the values represented are normalized to the low glucose concentration (3 mM). However, this normalization does not directly address the variability in β-cell number, which may also influence the total amount of C-peptide secreted. Using additional normalization methods, such as normalization to total protein or DNA, may be useful to control for variability in cell number [516]. Other factors that could influence the response to stimulation may be age (high stimulating index: pancreas from a 14-year-old donor; low stimulation index: pancreas from a 55-year-old donor) [517] or cell damage/stress. Nevertheless, viability staining following transfection and at days 6 and 10 of culture indicated no evidence of excessive cell death in comparison to untreated slices, thereby suggesting that β-cell functionality should be preserved. In conclusion, the metabolic improvement observed during the PR phase could be due to both the metabolic recovery of the remaining β-cells and the formation of new ones after increasing miR-30d-5p levels.

Lastly, the RNA-seq data demonstrated that the upregulation of miR-30d-5p function subsequent to mimic treatment was correlated with an altered gene expression that includes upregulation of insulin secretion-related genes. While no statistically significant differences were observed in the expression of the insulin gene (*INS*) between the control and experimental groups, there was a tendency for increased expression after 72 hours of transfection with the mimic. Indeed, *TTR*, which encodes transthyretin —a transport protein for thyroxine that promotes a glucose-induced increase in cytoplasmic free Ca^{2+} concentration and insulin release [377]—, also tends to be upregulated. Moreover, the mimic has been observed to slightly elevate the expression of genes such as *ISL1*. ISL-1 is a critical TF for the development of pancreatic β-cells, playing an indispensable role in their differentiation and maturation during pancreatic development [518]. Additionally, ISL-1 may facilitate the maintenance of β-cell identity and function in the adult pancreas by regulating the expression of key genes involved in insulin secretion. On the other hand, an immediate effect of insulin secretion can initiate a negative feedback loop that regulates and prevents the overproduction of insulin. In this regard, we found that the expression of *KCNH2*, which encodes Kv11.1, a potassium channel that regulates insulin secretion and limits intracellular Ca^{2+} influx [519], is also higher in the presence of miR-30d-5p. Indeed, it has been demonstrated that insulin-induced β-cell hyperpolarization is sufficient to abolish intracellular Ca^{2+} concentration oscillations measured in pancreatic islets. Following the treatment of miR-30d-5p, the gene encoding Cavβ3, a subunit of the voltage-dependent calcium channel, was also observed to be upregulated. This subunit functions as a brake on Ca^{2+} release, reducing the frequency of Ca^{2+} oscillations in a cell-autonomous manner [378]. On the other hand, the inhibition of this specific miRNA has been linked to elevated expression of LXR-β (*NR1H2*). LXR activation has been observed to rapidly suppress insulin secretion by the inhibition of mitochondrial metabolism and the reduction in the cytosolic ATP concentration [374,520]. However, this stands in contrast to the findings that LXR-β knockout mice display impaired glucose tolerance and reduced glucose-induced insulin secretion [521]. To sum up, the findings indicate that miR-30d-5p modulates the expression of multiple genes associated with insulin synthesis and secretion, such as *TTR*, *ISL1*, *KCNH2*, and *CACNB3*, which influence calcium dynamics and β-cell function. This suggests that miR-30d-5p plays a critical role in regulating pancreatic β-cell activity by balancing insulin release and maintaining cellular homeostasis.

In the context of regeneration, we observed that the expression of BMP pathway genes, such as *BMPR1B* and *KLF2*, was downregulated following the silencing of miR-30d-5p, whereas the expression of TGF-β pathway genes, such as *TGFB3*, tended to be upregulated. As we mentioned earlier in the discussion, BMP signaling is required for the

expression of β-cell genes such as *PDX1* or *NKX6.1* in pancreatic progenitors [508] and even to induce transdifferentiation of human pancreatic non-endocrine tissue (e.g., ductal-mediated β-cell regeneration) to glucose-responsive β-like cells [269,352]. Although BMP is included in the prototypical TGF-β superfamily signaling, increasing evidence suggests that the TGF-β and BMP pathways play an opposing role [522]. Indeed, TGF-β signaling decreases β-cell lineage in development [449]. Therefore, miR-30d-5p favors the repression of the TGF-β signaling pathway and activates the BMP one. Moreover, in the GO analysis, downregulated genes related to the silencing miR-30d-5p are associated with cell differentiation processes. Interestingly, the MiR-17~92 cluster that includes miRNAs that we found increased during the honeymoon phase (e.g., miR-17) can also enhance BMP signaling and downregulate TGF-β pathway components [523]. Among the TFs enriched after the application of the miR-30d-5p mimic, we found NOTCH3, a key regulator of cell self-renewal that contributes to both multipotent progenitor cell amplification during pancreatic development [524] and regeneration after pancreatitis [525]. Then, the activation of progenitor cells by BMP and the process of transdifferentiation of terminally differentiated cells could be associated with the Notch pathway. Indeed, *DDX5* and *DDX17* were among the downregulated genes after silencing miR-30d-5p, which participate in the Notch signaling pathway [526]. Summarizing, these results suggest that miR-30d-5p promotes β-cell regeneration and the activation of progenitor cells by acting on the Notch, TGF-β and BMP signaling pathways.

Another gene that is upregulated after miR-30d-5p mimic is *IL22RA1*. IL-22 has been shown to reduce ER and oxidative stress in human pancreatic islets and promote the secretion of insulin from β-cells. Furthermore, IL-22 receptor alpha 1 (IL-22RA1) plays a crucial role in β-cell regeneration and the reduction of inflammation [527]. Additionally, genes involved in the inflammatory response, such as *IL21R* and *ZBP1*, tend to be upregulated in the absence of miR-30d-5p. Conversely, the TF STAT5B is downregulated in its presence, which is stimulated in response to a variety of cytokines, including IL-21, IL-7, and IL-15 [528]. Consequently, elevated levels of this miRNA are associated with a diminished inflammatory environment. Also, it can be related to enhanced responses to external stimuli like stress by the increased expression of *MAPK12* [529]. Indeed, FOXO3 was one of the TFs enriched after the application of the miR-30d-5p mimic. Studies have shown that FOXO3 activity protects β-cells against oxidative stress by regulating antioxidant enzymes [530,531]. However, JUND was also an enriched TF whose depletion protects β cells from oxidative stress and apoptosis [532]. Altogether, these data underscore the role of miR-30d-5p in modulating inflammation and stress responses in pancreatic cells.

Nevertheless, it is imperative to exercise caution when interpreting these results, as the high inter-donor variability may potentially influence the observations, and the relatively limited sample size may introduce a degree of uncertainty. However, the analysis was performed by including the donor as a covariate. Although these experiments represent a proof of concept and a preliminary study, it would be necessary to validate the differential expression of these genes in additional pancreatic samples and by another reproducible technique, taking into account that these samples are very difficult to obtain. A strength of this study is that a protocol for transfection of miRNAs in HPSs has been generated for the first time which may lead to future functional studies of other miRNAs in β-cell function and regeneration in a living tissue. In future experiments, it would be convenient to use other technologies like single-cell RNA-seq that allow the study of the transcriptome of the different cells within the pancreatic tissue instead of having bulk samples of many cells. Furthermore, although not ethically justifiable today, obtaining pancreatic biopsies from patients with T1D, particularly during the PR phase, would allow the long-term culture of HPSs with miRNAs, potentially providing new insights into the pathology and treatment of the disease.

In summary, chapters 3 and 4 of the doctoral thesis demonstrate that miR-30d-5p —the most upregulated miRNA during PR— not only promotes pivotal immunoregulatory processes that inhibit autoreactive responses like the upregulation of the PD-1/PD-L1 axis but also enhances pancreatic β-cell function. These findings may establish a link between the elevated plasma miR-30d-5p concentration during the honeymoon phase and the observed increased endogenous insulin secretion together with the activation of β-cell neogenesis (**Figure 53**).

Future perspectives

Although much progress has been made in understanding the mechanisms that ultimately lead to the development of T1D, less attention has been given to the progression of the disease once diagnosed. In this sense, constant monitoring of patients is important, as well as being able to predict and detect the PR phase stage correctly. First, an accurate and universal definition of this phase should be applied in clinical practice, such as IDAA1c ≤9, thus reducing one of the main variables in detecting remitting patients. In addition, recent studies have focused on finding biomarkers that reflect immunoregulatory processes, downmodulation of inflammation, and β-cell recovery during PR. However, these studies typically involve small patient cohorts. Future research should include larger, more representative samples and focus on longitudinal analyses of PR and possible waves of immune regulation. Furthermore, the

implementation of both radiological (e.g., positron emission tomography) and non-radiological methodologies (e.g., magnetic resonance imaging) throughout the different disease stages and the PR phase could provide insights into the changes in the degree of leukocyte infiltration into the islets, its composition, the fluctuations in β-cell mass and its metabolic activity [533]. Finally, studies of this phase using -omics technologies to gain a better understanding of the disease are lacking. These would give us deeper insights into the functionality of cell populations in the blood, their gene expression, and metabolomic, proteomics, and epigenetics patterns. Integrating all this information would yield new and reliable biomarkers of remission.

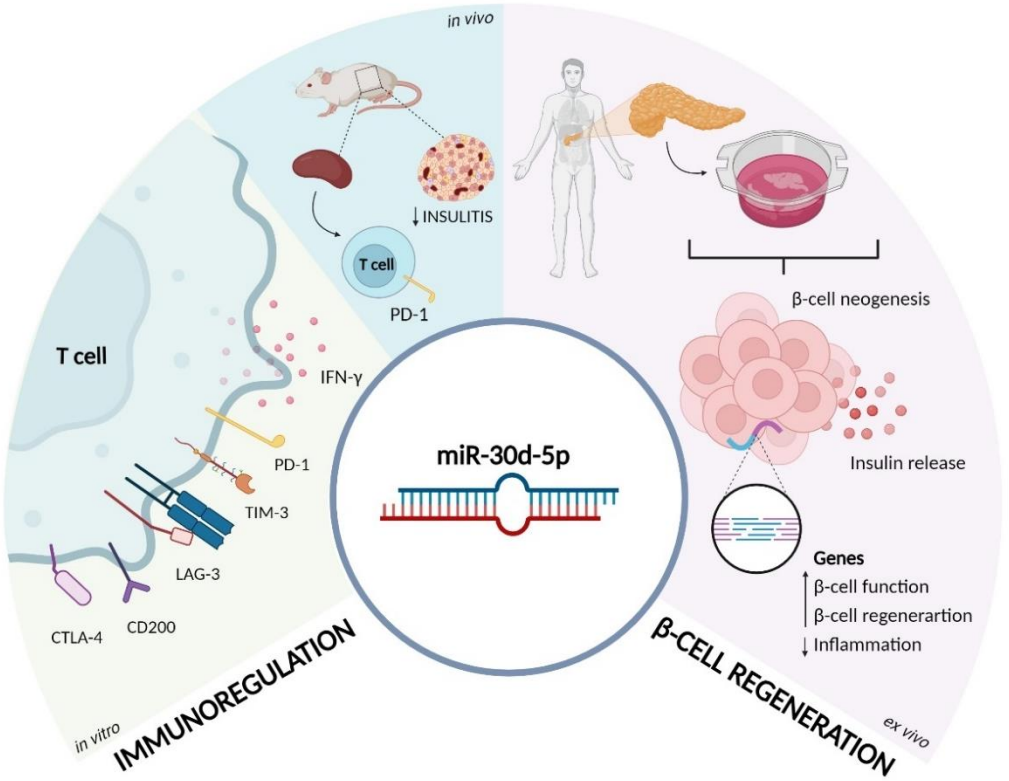

Figure 53. ***Effects of miR-30d-5p on immunoregulation and β-cell regeneration and function.*** *MiR-30d-5p is linked to elevated expression of inhibitory receptors, including CTLA-4, CD200, LAG-3, TIM-3, and PD-1, as well as increased secretion of IFN-γ in human T cells in vitro. Furthermore, in cultured human pancreatic slices, it promotes β-cell neogenesis and insulin release by influencing the expression of genes involved in these processes. In NOD mice, the miRNA reduces leukocyte infiltration into the islets of Langerhans (insulitis) and enhances the expression of PD-1 on splenic T cells. Figure created using BioRender.*

Furthermore, grasping the natural mechanisms that lead to β-cell protection by the immune system will give us clues as to how we can tackle the autoimmune attack or at least minimize it. To date, different studies on PR have demonstrated immunoregulatory attempts that can be explored as direct targets to extend or induce this favorable phase. For example, the modulation of immune metabolism [322], the activation of IL-10-related pathways [264] and, as we propose, the overexpression of PD-1, may be possible mechanisms specific for remission. Overall, this emerging field of research will contribute to understanding the different T1D progression patterns and to improving clinical management and interventions.

6

CONCLUSIONS

1. An index-based model was developed for the prediction of PR in pediatric patients at the diagnosis of T1D. The index, which is composed of four immunological variables, together with age constitute key factors in determining the probability of experiencing remission in the future. The proposed decision model can serve for early monitoring of patients and can help stratify between those who will have a better or worse prognosis, facilitating more personalized therapeutic management.

2. The longitudinal study of newly diagnosed pediatric patients with T1D shows changes during the PR phase in peripheral leukocyte subpopulations —particularly effector and regulatory T lymphocytes, regulatory and transitional B lymphocytes, regulatory NK cells and monocytes—, reflecting immunoregulatory processes specific to this phase. These biomarkers are useful to characterize remission and detect possible waves of immunoregulation during the progression of the disease, thus helping to identify optimal phases of immune intervention.

3. The concentration of various inflammatory and anti-inflammatory cytokines in plasma remains unvaried between remitter and non-remitter patients, limiting their use as candidate biomarkers of remission. However, the PR phase may be associated with reduced levels of IL-17A, potentially indicating reduced inflammation and autoimmunity.

4. A unique plasma miRNA signature during the PR phase that is involved in pathways related to the pathogenesis of T1D was identified and validated. These new miRNA candidate biomarkers for the monitoring of this period in pediatric patients with T1D may be used for patient stratification and applied in future clinical research.

5. MiR-30d-5p is the most differentially expressed miRNA during the PR phase. This miRNA is necessary for the expression of different inhibitory molecules on T lymphocytes, such as PD-1, CTLA-4, CD200, TIM-3 and LAG-3, as well as for the secretion of IFN-γ, demonstrating its immunoregulatory potential in halting autoimmune responses and shedding light on the mechanisms underlying this phase.

6. MiR-30d-5p stimulates the formation of new insulin-expressing cells and activates the synthesis and secretion of C-peptide in human pancreatic tissues. This is achieved by regulating gene expression, thereby demonstrating that it can modulate both the function and regeneration of human β-cells. This finding fits well with the enhanced endogenous insulin production that characterizes the PR phase.

7. MiR-30d-5p modifies the ongoing autoimmune attack in the prediabetic NOD mouse. Its inhibition aggravates the autoimmune attack by increasing the degree of insulitis and promoting an effector phenotype in T lymphocytes. Moreover, its silencing decreases PD-1 expression and promotes Treg expansion, highlighting the importance of miRNA-mediated immunoregulation that may contribute to the PR phase.

SUPPLEMENTARY DATA

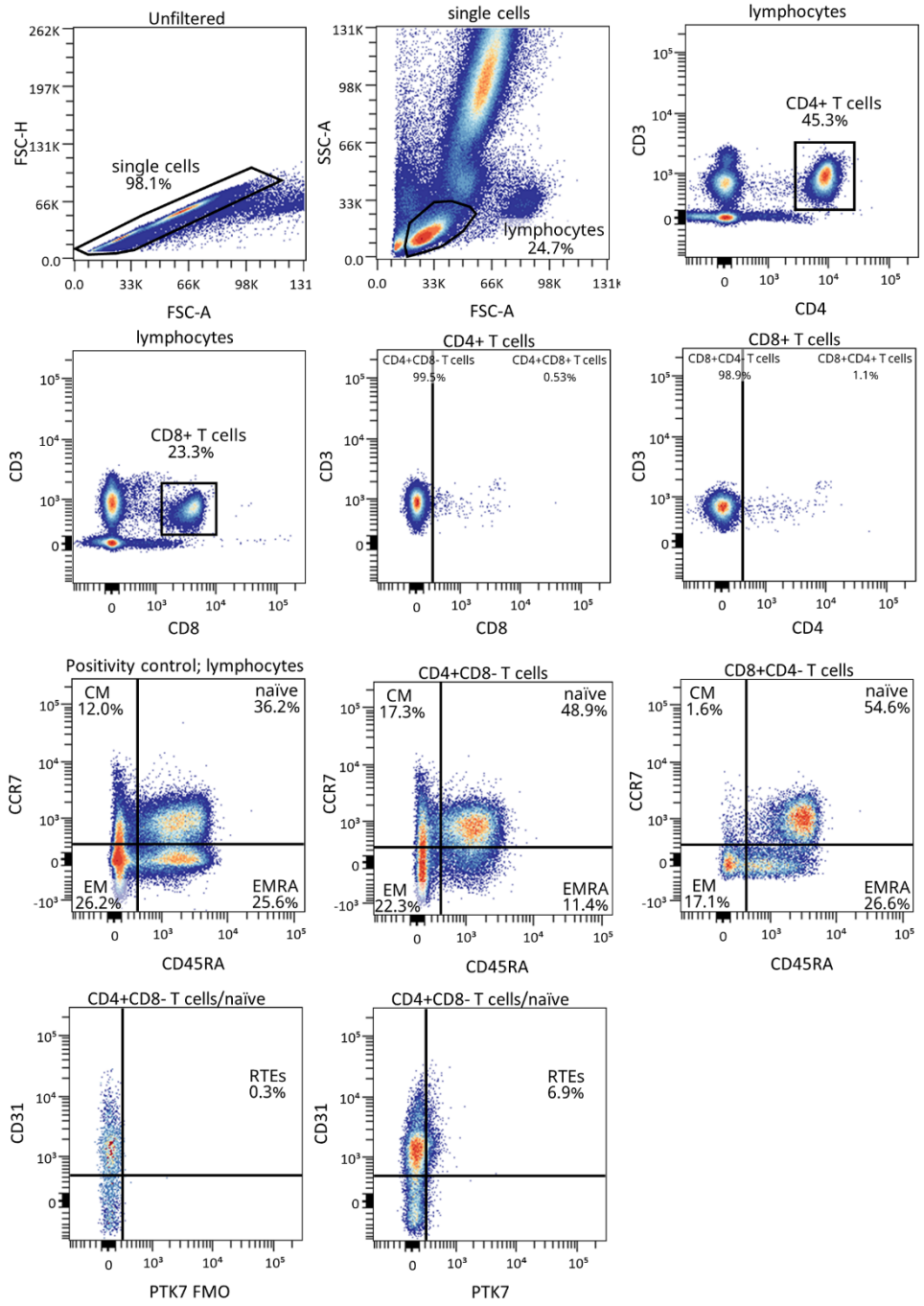

Figure legend on next page

Supplementary Figure 1. ***Representative gating strategy for the T lymphocyte maturation stages (panel 1).*** *Gating strategy used to analyze the percentages of the different CD4⁺ and CD8⁺ T cell subsets based on the expression of the markers CD3, CD4, CD8, CD45RA and CCR7: naïve (CD45RA⁺CCR7⁺), central memory (CD45RA⁻CCR7⁺), effector memory (CD45RA⁻CCR7⁻) and T_{EMRA} (CD45RA⁺CCR7⁻). CD31 and PTK7 were used to characterize recent thymic emigrants (RTEs). Positivity controls for CCR7 vs CD45RA using lymphocytes and FMO control for PTK7 were used.*

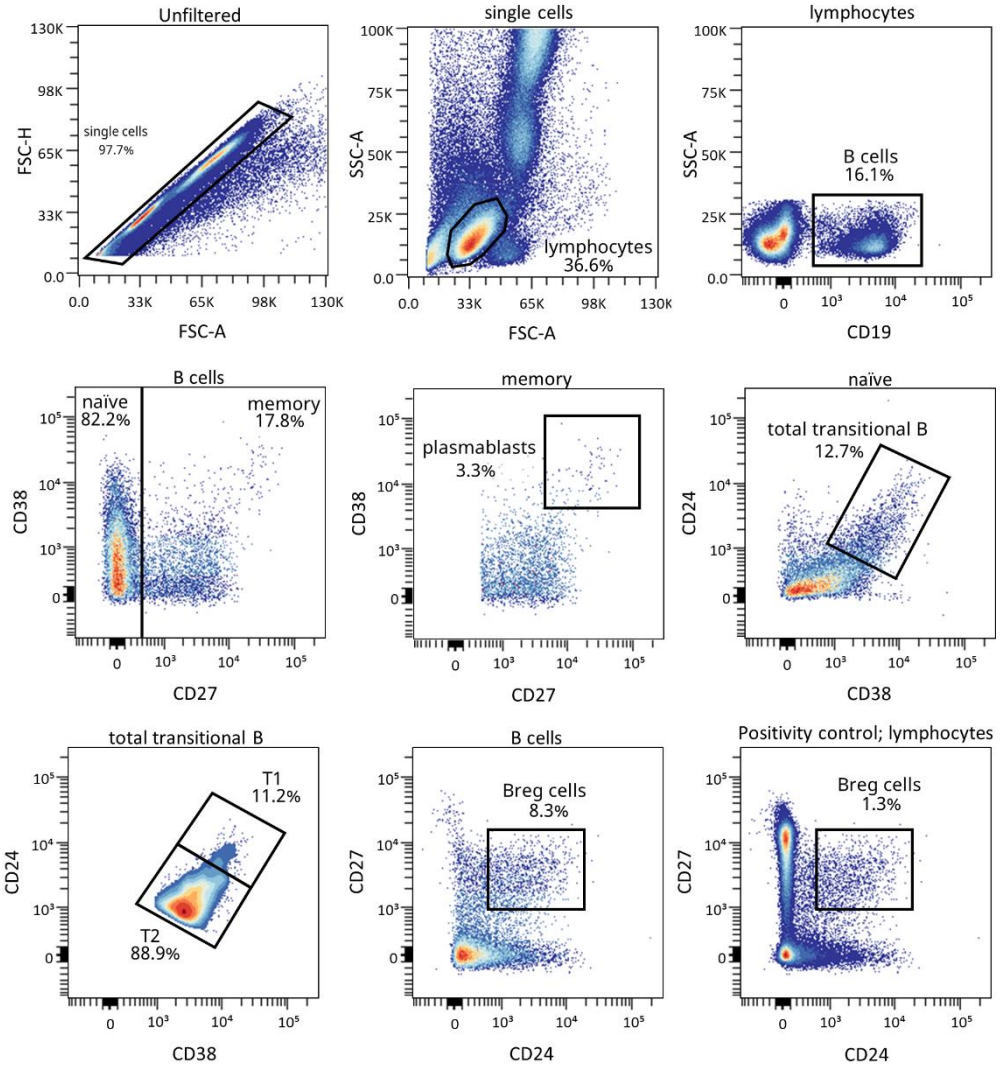

Supplementary Figure 2. ***Representative gating strategy for B cell subpopulations (panel 2).*** *Gating strategy used to analyze the percentages of transitional B cells (total, T1, and T2), Bregs and plasmablasts based on the expression of the markers CD19, CD27, CD38, and CD24. Positivity control for CD27 vs CD24 using lymphocytes as an internal reference population was used.*

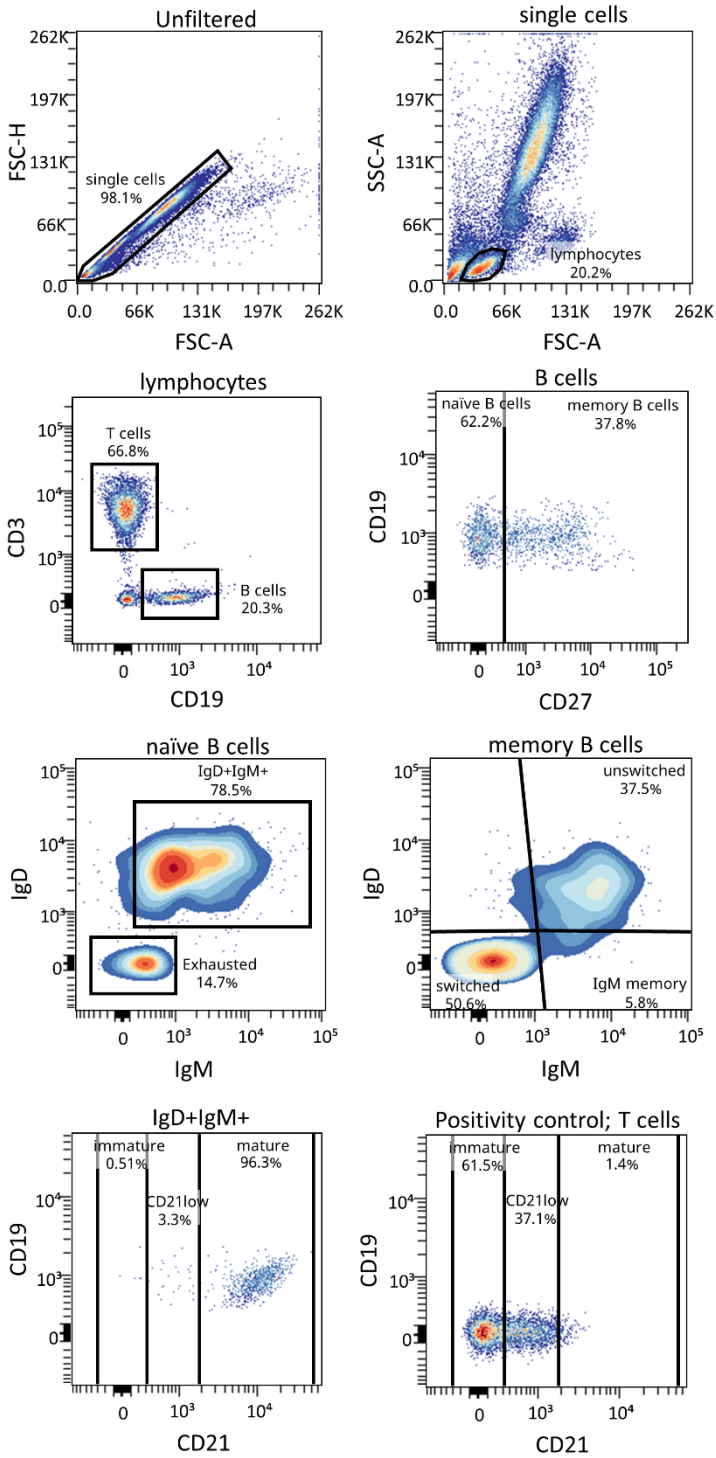

Figure legend on next page

Supplementary Figure 3. ***Representative gating strategy for the B lymphocyte maturation stages (panel 3).*** *Gating strategy used to analyze the percentages of the different naïve and memory B cell subsets based on the expression of the markers CD19, CD27, IgM, IgD, and CD21. Positivity control for CD19 vs CD21 using CD3⁺ T lymphocytes as an internal reference population was used.*

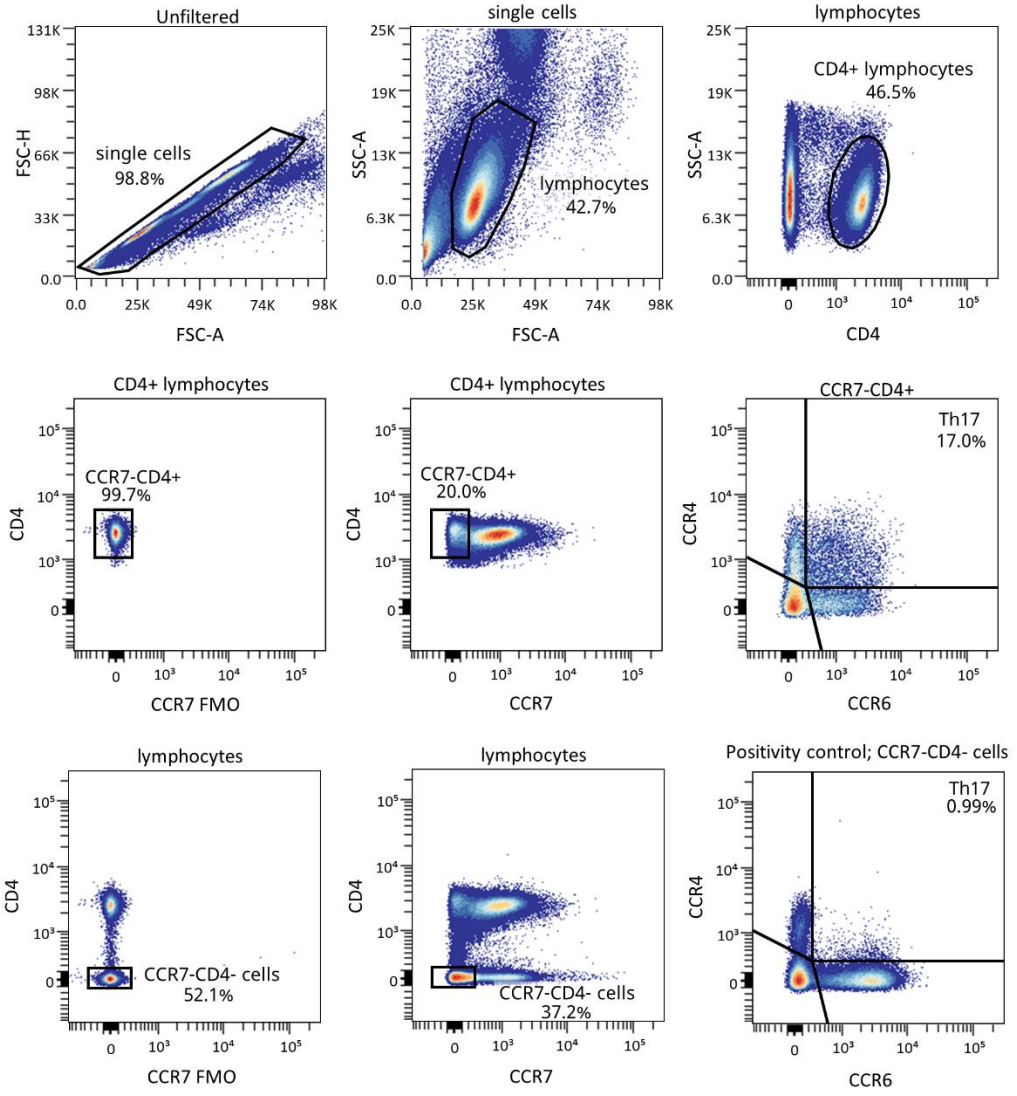

Supplementary Figure 4. ***Representative gating strategy for Th17 cells (panel 4).*** *Gating strategy used to analyze the percentage of Th17 cells ($CD4^+CCR7^-CCR4^+CCR6^+$) based on the expression of the markers CD4, CCR7, CCR4 and CCR6. FMO control for CCR7 and positivity control for CCR4 vs CCR6 using $CCR7^-CD4^-$ lymphocytes as an internal reference population were used.*

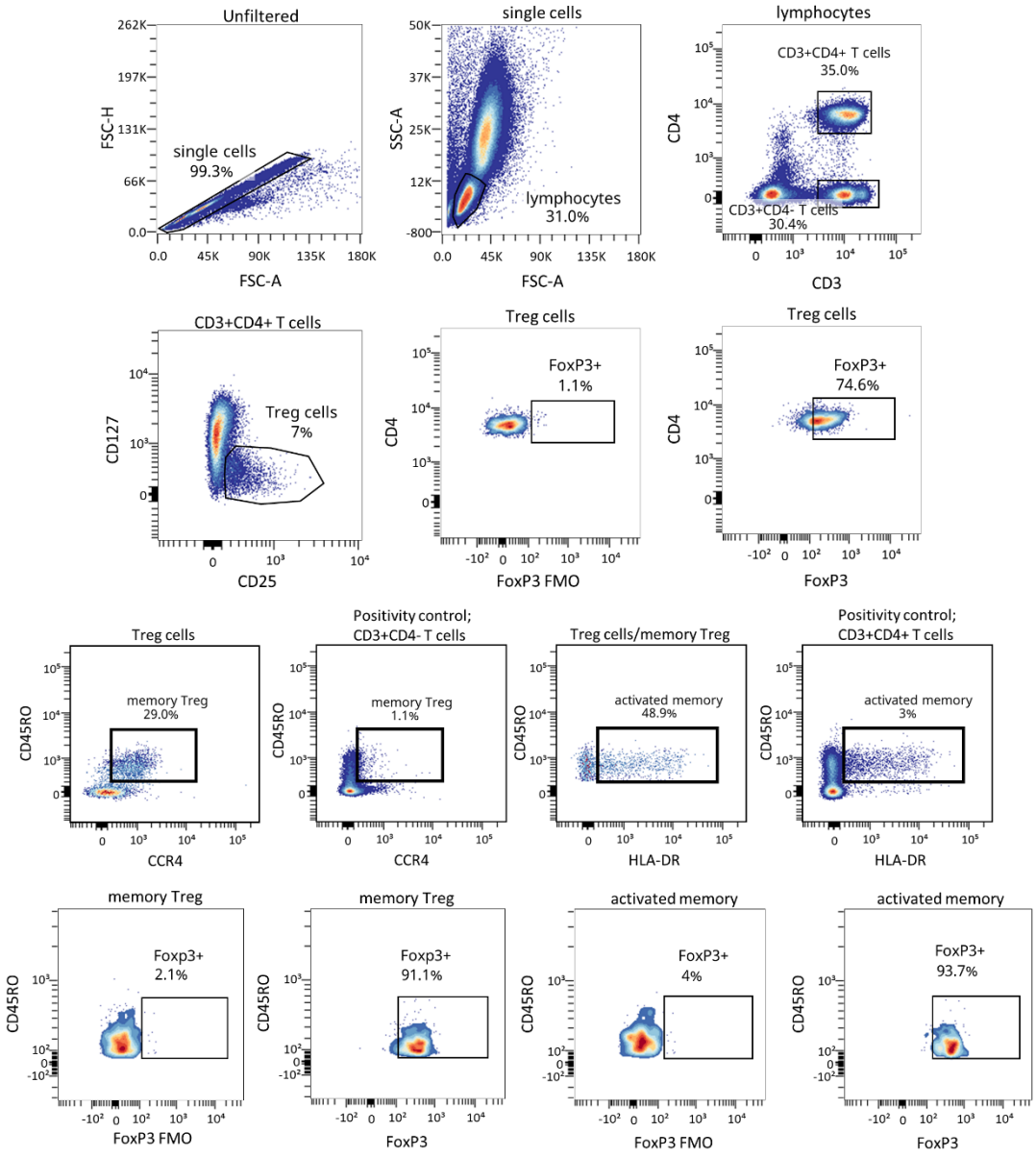

Supplementary Figure 5. ***Representative gating strategy for Tregs (panel 5) and FoxP3 staining.*** *Gating strategy used to analyze the percentages of Treg subsets based on the expression of the markers CD3, CD4, CD127, CD25, CD45RO, CCR4 and HLA-DR. Expression of FoxP3 was determined on total ($CD3^+CD4^+CD25^+CD127^{-/low}$), memory ($CD45RO^+CCR4^+$) and activated ($HLA\text{-}DR^+$) Tregs. Positivity controls for CD45RO vs CCR4 using $CD4^-$ T cells and for CD45RO vs HLA-DR using $CD4^+$ T cells as internal reference populations were used. FMO for FoxP3 was used.*

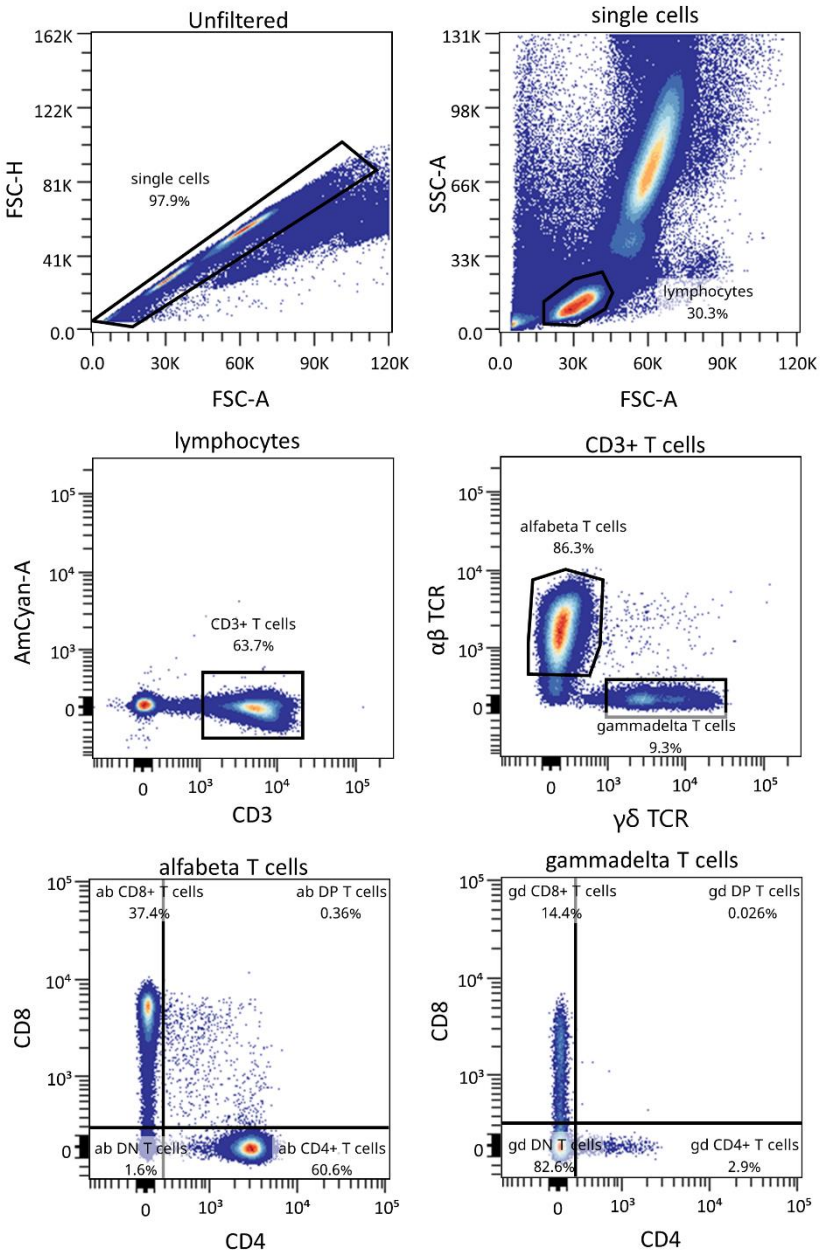

Supplementary Figure 6. ***Representative gating strategy for αβ and γδ TCR T cells (panel 6).*** *Gating strategy used to analyze the percentages of the αβ and γδ TCR of CD4⁺, CD8⁺, CD4⁺CD8⁺ (DP), and CD4⁻CD8⁻ (DN) T cells.*

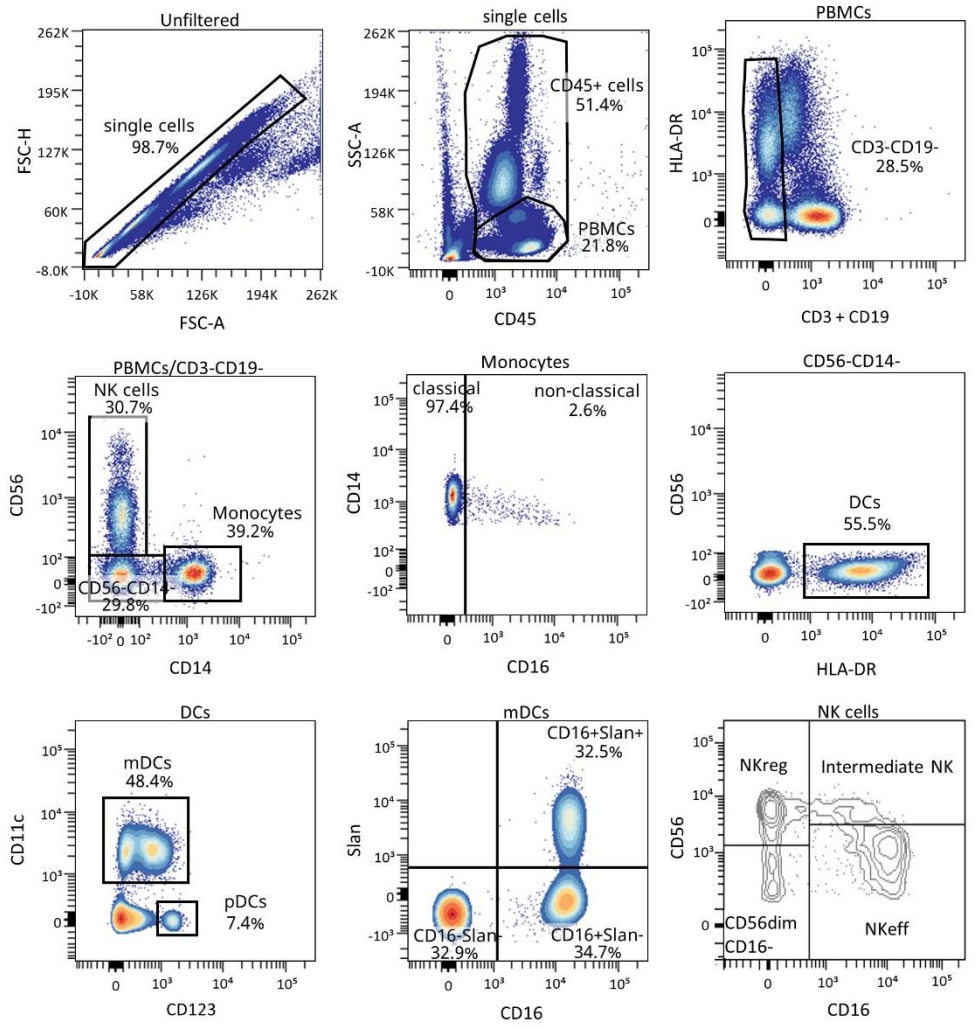

Supplementary Figure 7. ***Representative gating strategy for innate immune cells (panel 7).*** *Gating strategy used to analyze the percentages of DCs and monocytes. Cells were first gated for singlets, PBMCs, and CD3$^-$CD19$^-$ cells. With the use of CD56 and CD14, cells were divided into NK cells and monocytes —which were both further divided into their subsets with the use of CD16—, and DCs (lineage negative and HLA-DR$^+$). Different subsets of DCs (mDC and pDC) were analyzed using CD123 and CD11c, and mDCs were further divided into their subsets with the use of CD16 and Slan.*

Supplementary Table 1. ***List of keywords to classify gene targets of miRNAs into regeneration, metabolism or immune system groups***

Regeneration
Beta cells, Alfa cells, Islet of Langerhans, Neogenesis, Transdifferentiation, Apoptosis, Stem cells, Dedifferentiation, Differentiation, Multipotency, Pluripotency, Progenitor cell, Survival, Cell division, Ductal cells, PCSK1, PCSK2, PAX6, EGF, Neurogenin 3, GLP-1, GLP-1R, REG3A, REG3G, PDX1, Glis3, Manf, MAFA, Cell cycle, Cellular senescence, Fibrinogen, Caspase, LRH-1, NR5A2, BCL2AI, Bcl
Metabolism
Metabolic reprogramming, Insulin, Insulin production, Insulin secretion, Insulin granules, Insulin sensitivity, Glucagon, Glucose, Glycemia, Insulin signaling pathway, Endocrine cells, Type 1 diabetes, Pancreas, UTR, C-peptide, Proinsulin, Trypsinogen, Growth factors, mTOR signaling pathway, Lipid metabolism, FoxO signaling pathway, Ras signaling pathway, Cell stress, Oxidative stress, Glucotoxicity, Glycolysis, Glutaminolysis, Oxidative phosphorylation, Tricarboxylic acid cycle, Fatty acid oxidation, Pentose phosphate pathway, Gluconeogenesis, INSR, IGF1R, IRS-2, c-Myc, Anabolism, Catabolism, Glucocorticoids, NR3C1, Somatostatin, Glucocorticoid receptor, RNA degradation, IAPP, PPY, LYZ, FGC, CPE
Immune System
T cell activation, Regulatory T cells, Effector T Lymphocytes, Memory T Lymphocytes, T cells, TCR, B cells, BCR, Antigen processing and presentation, Antigen presenting cell, Antibody production, Antibody, Autoantibody, Cell migration, Cell adhesion molecules, Regulatory T cell induction, Cytokines, Interferon, Interleukin, Chemokine, Inflammation, Islet autoimmunity, Exhausted T cells, Tolerance, Autoreactive T cells, Cytotoxicity, Cytotoxic T Lymphocyte, Adaptive immunity, Innate immunity, Development, Lymphocyte, Dendritic cell, Neutrophil, Monocyte, Macrophage, M1 macrophage, M2 macrophage, Natural killer cell, Gammadelta T cell, NKT cell, Eosinophil, Basophil, Leukocytes, Plasma cell, Granulocyte, T helper cell, T cell anergia, T cell suppression, T cell proliferation, Insulitis, Apoptosis, Necrosis, Immunosuppression, Efferocytosis, Phagocytosis, Major Histocompatibility Genes (HLA), HLA-DR, HLA-DQ, HLA-DP, HLA-A, HLA-B, HLA-C, Toll-like receptors, Fc receptors, Opsonins, Complement, Autoantigens, Glutamic Acid Decarboxylase, Cortisol, PI3K-AKT signaling pathway, Wnt signaling pathway, Calcium signaling

pathway, AMPK signaling pathway, TLR signaling pathway, JAK-STAT signaling pathway, NF-kB signaling pathway, TCR signaling pathway, BCR signaling pathway, TGF-β signaling pathway, Leukocyte transendothelial migration, Th1 and Th2 differentiation, Th17 differentiation, NK cell mediated cytotoxicity, Eomes, Tigit, Perforin, Granzyme, Endocytosis, Exocytosis, Exosome, Autophagy, Ki-67, AIRE, Fas ligand, Fas receptor, Prostaglandin receptor EP4, RORC, TBX21, GATA3, FOXP3, VEGFA, VCAM, CRP, IL8BP, TGFbeta2, KLRK1, MERTK, CR, CASP3, SOCS2, LAG3, C5AR1, IL-17, IL-17R, IL-10, IL-10R, IL-21, IL-21R, IL-1beta, IL-1R, IL-6, IL-6R, IL-23, IL-23R, IL-12RB1, IL-22, IL-22R, IL-10Rbeta, IL-2, IL-8, IL-8R, TNF-alfa, IFN-beta, IFN-alfa, IFN-gamma, TGF-beta, CXCL10, CCL2, CXCL5, CXCL1, CCR5, CXCL6, CXCR4, CCR2, CXCL12, CCR7, CD80, CD86, CD28, CD25, CD40, CD69, CD57, CD59, CD300A, CD36, CD54, CD163, CD68, CD52, CD14, CD20, CD1D

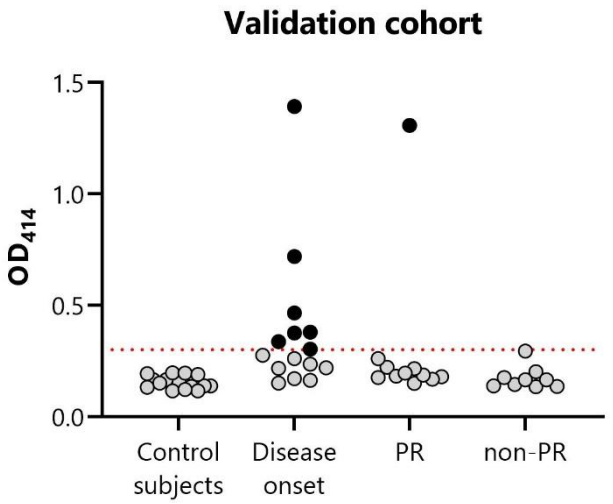

Supplementary Figure 8. ***Analysis of the hemolysis in plasma samples.*** *The degree of hemolysis was checked in control subjects (n=15), patients at disease onset (n=15), at PR (n=11), or non-PR (n=9) by measuring the optical density at 414 nm (absorbance peak of free hemoglobin) by spectrophotometry. The severely hemolyzed samples (OD_{414} >0.3) were discarded. Black dots represent discarded samples and grey dots the samples used in further experiments. The red discontinuous line indicates the OD_{414} = 0.3.*

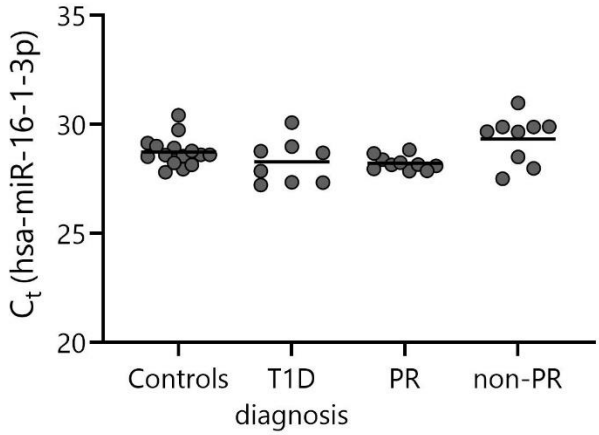

Supplementary Figure 9. ***Raw cycle threshold (Ct) values of miR-16-1-3p.*** *The raw C_t values of miR-16-1-3p were obtained by RT-qPCR in plasma samples of controls (n=15), patients at T1D diagnosis (n=8), at PR (n=10), and non-PR (n=9). No differences were found between the different groups (by Kruskal-Wallis with Dunn's post-hoc test).*

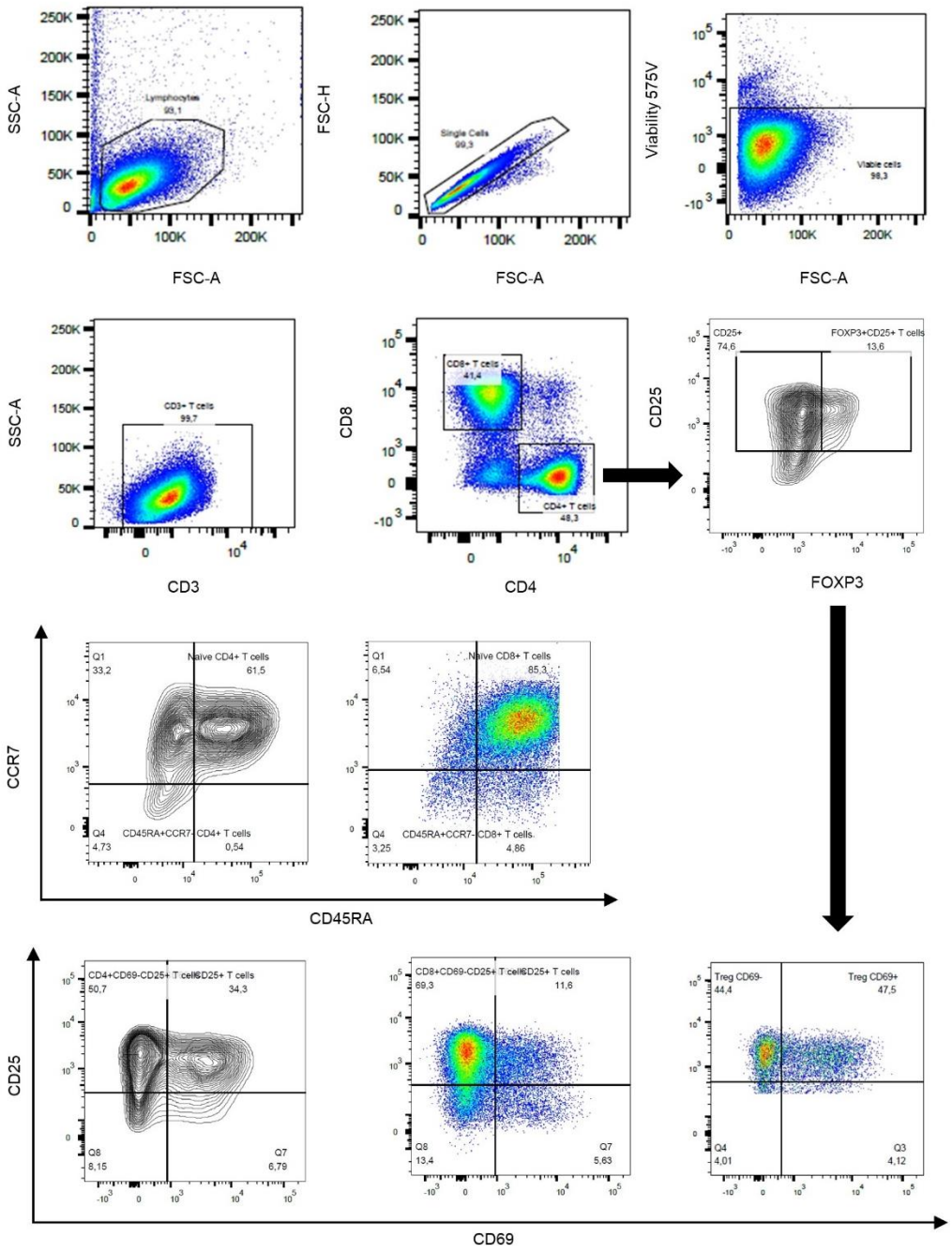

Supplementary Figure 10. ***Representative gating strategy for the activation and maturation status of T cells.*** *Gating strategy used to analyze the percentages of the different maturation CD4⁺ and CD8⁺ T cell subsets based on the expression of the markers CD45RA and CCR7. FoxP3⁺CD25⁺CD4⁺ cells are Tregs. Activation of Tregs and CD4⁺ and CD8⁺ T cells were analyzed based on the expression of the markers CD25 and CD69. FMO controls for CD25, CD69 and Foxp3 were used to set the appropriate gates (not shown).*

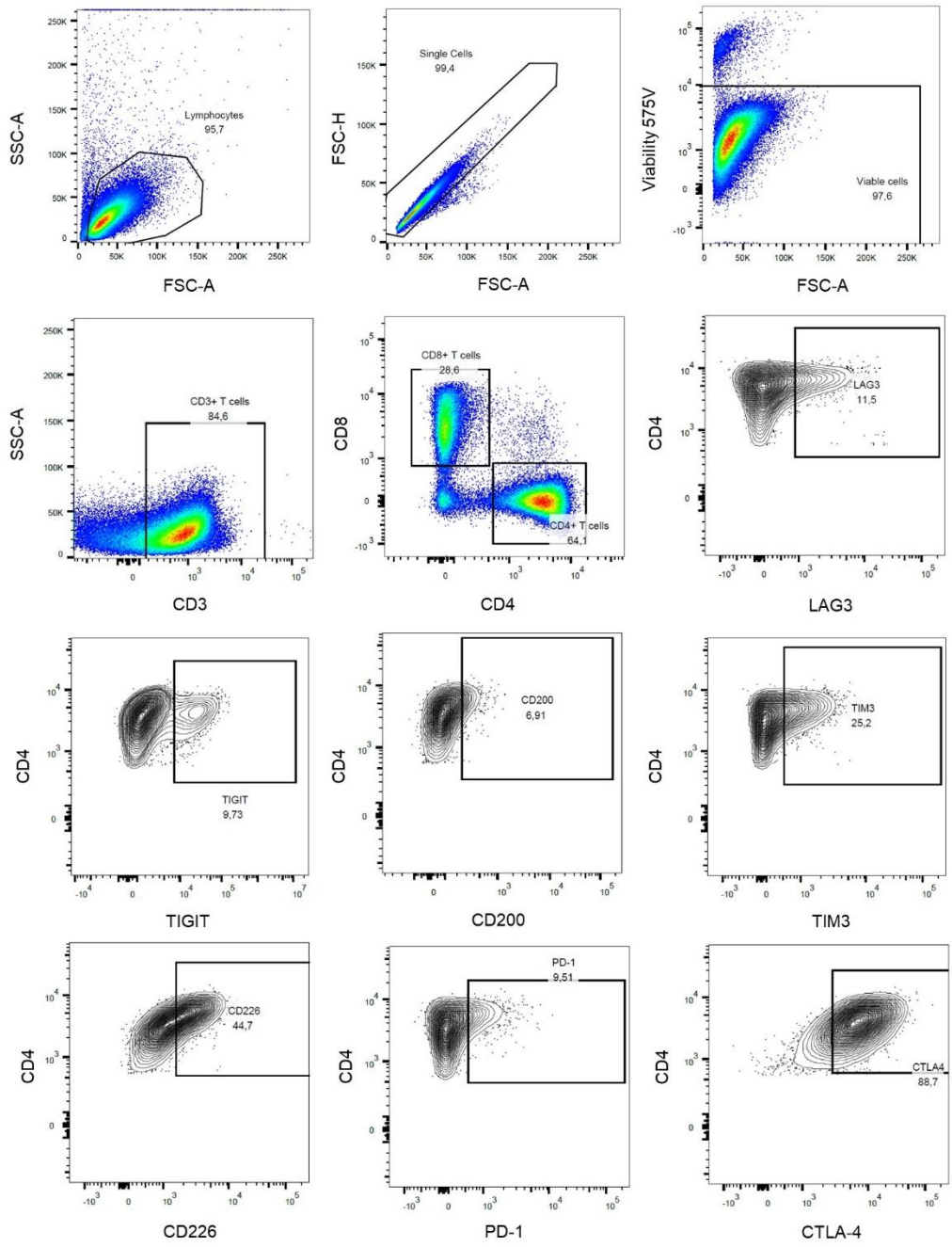

Supplementary Figure 11. ***Representative gating strategy for inhibitory and activation molecules on T cells.*** *Gating strategy used to analyze the percentages of T cells positive for different inhibitory and activation molecules on both $CD4^+$ (shown) and $CD8^+$ T cells (not shown). FMO controls for CD200, TIGIT, TIM-3, LAG-3, CTLA-4, PD-1, and CD226 were used to set the appropriate gates (not shown).*

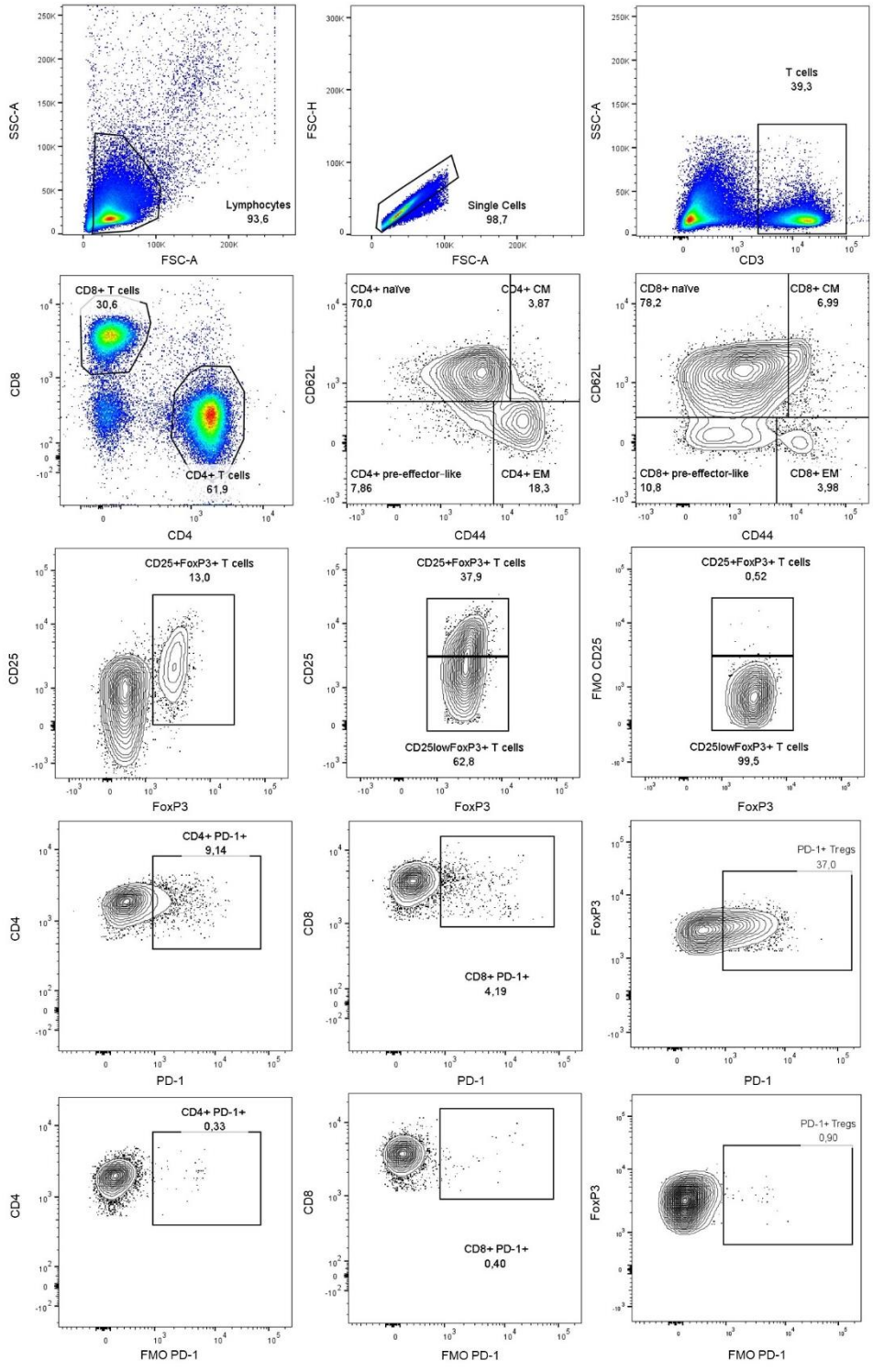

Figure legend on next page

Supplementary Figure 12. ***Representative gating strategy for splenocytes and pancreatic lymph node cells (panel 1).*** *Gating strategy used to analyze the different CD4⁺ and CD8⁺ T cell subsets based on the expression of the markers CD3, CD4, CD8, CD44 and CD62L: naïve (CD62L^{hi} CD44^{low}), central memory (CD62L⁺CD44⁺), effector memory (CD62L⁻CD44⁺) and pre-effector-like T cells (CD62L⁻CD44⁻). Tregs were analyzed based on the expression of Foxp3 and CD25. PD-1 expression was evaluated on CD4⁺, CD8⁺ and Tregs. FMO for FoxP3 (not shown), CD25 and PD-1 were used. Plots show splenocytes from a prediabetic NOD mouse.*

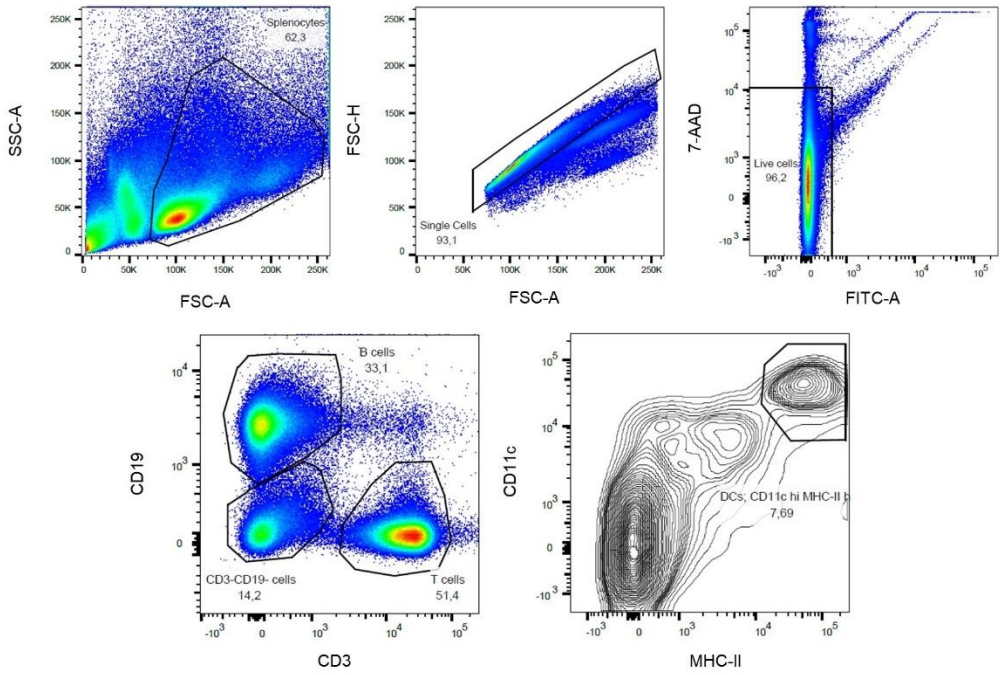

Supplementary Figure 13. ***Representative gating strategy for splenocytes and pancreatic lymph node cells (panel 2).*** *Gating strategy used to analyze T cells (CD3⁺), B cells (CD19⁺) and dendritic cells (CD11C^{hi} MHC-II^{hi}). Plots show splenocytes from a prediabetic NOD mouse.*

Supplementary Table 2. ***HLA typing of DRB1 alleles in patients with T1D of the discovery cohort***

PATIENTS	ALLELE 1	ALLELE 2	RISK
ONSET 1	DRB1*03	DRB1*04	High
ONSET 2	DRB1*04	DRB1*09	Moderate
ONSET 3	DRB1*03	DRB1*-	-
ONSET 4	DRB1*07	DRB1*08	Neutral
ONSET 5	DRB1*03	DRB1*04	High
ONSET 6	DRB1*01	DRB1*04	Moderate
ONSET 7	DRB1*03	DRB1*07	Moderate
ONSET 8	DRB1*03	DRB1*04	High
ONSET 9	DRB1*04	DRB1*04	High
ONSET 10	DRB1*03	DRB1*04	High
ONSET 11	DRB1*03	DRB1*04	High
ONSET 12	DRB1*01	DRB1*04	Moderate
ONSET 13	DRB1*03	DRB1*07	Moderate
ONSET 14	DRB1*04	DRB1*13	Moderate
ONSET 15	DRB1*03	DRB1*04	High
ONSET 16	DRB1*04	DRB1*07	Moderate
ONSET 17	DRB1*03	DRB1*04	High

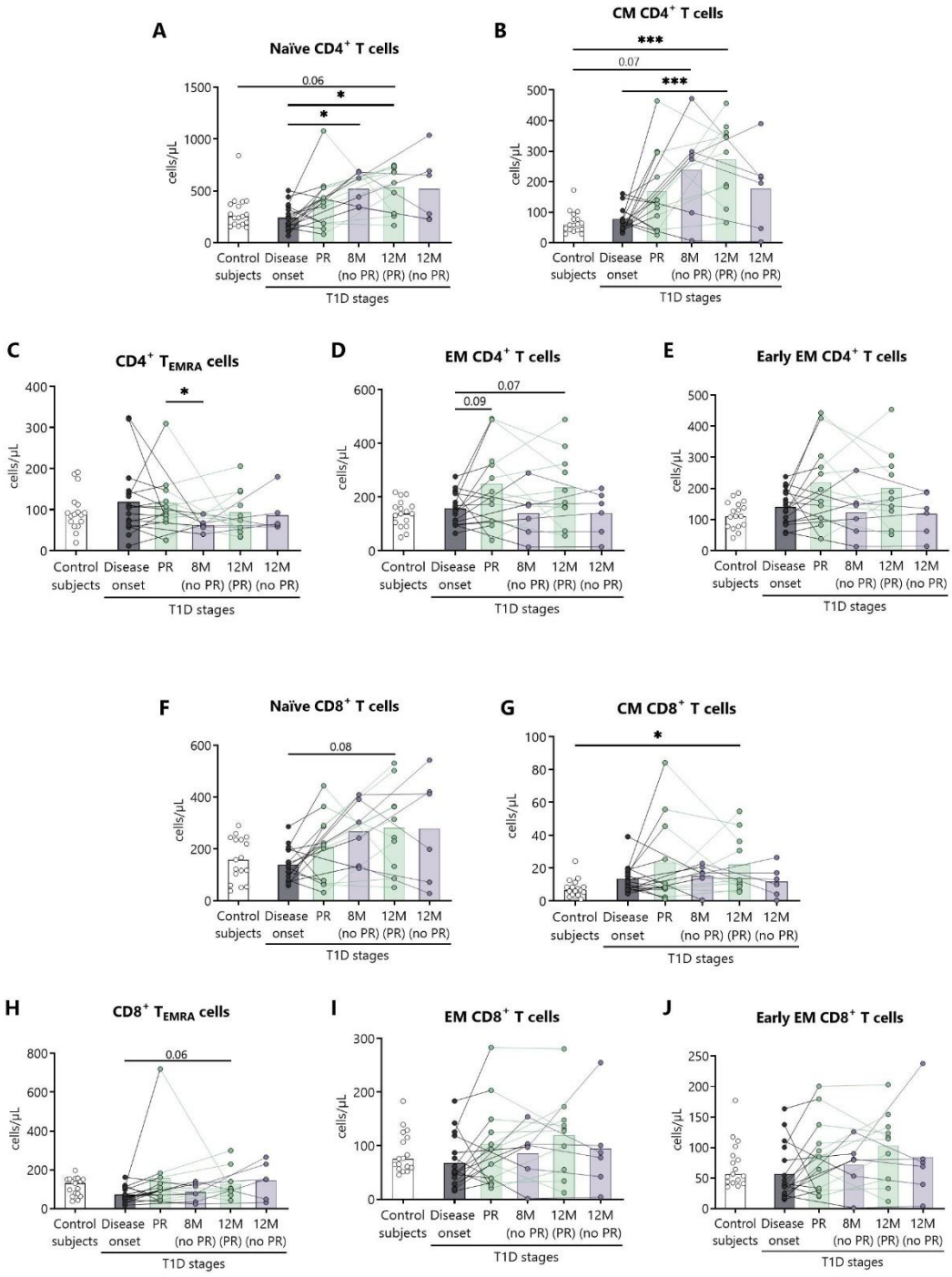

Figure legend on next page

Supplementary Figure 14. ***Absolute counts of CD4⁺ and CD8⁺ T lymphocyte subsets are altered at the initial stages of T1D.*** *For CD4⁺ and CD8⁺ T lymphocytes, respectively, the absolute counts (cells/μL) of (**A and F**) naïve T lymphocytes, (**B and G**) central memory (CM) T lymphocytes, (**C and H**) terminally differentiated effector memory (EMRA) T lymphocytes, (**D and I**) effector memory (EM) T lymphocytes, and (**E and J**) early EM T lymphocytes were determined in peripheral blood of control subjects and patients with T1D at different time-points. White bars correspond to control subjects (n=17), grey bars to patients at disease onset (n=17), green bars to patients at partial remission (PR, n=11; at 12M, n=10) and lilac bars to non-remission (non-PR at 8M, n=6; at 12M, n=6). Bar graphs show mean percentage or absolute count values. Each symbol represents an individual patient. Lines link the same patient throughout the time-points. *p ≤0.05 and ***p <0.001 after mixed effects model with Tukey's post-hoc test for longitudinal data, Kruskal–Wallis with Dunn's post-hoc test for comparisons between control subjects and the different T1D time-points, or 2-tailed Mann–Whitney test for comparisons between two unpaired groups of data. P ≤0.05 is considered significant.*

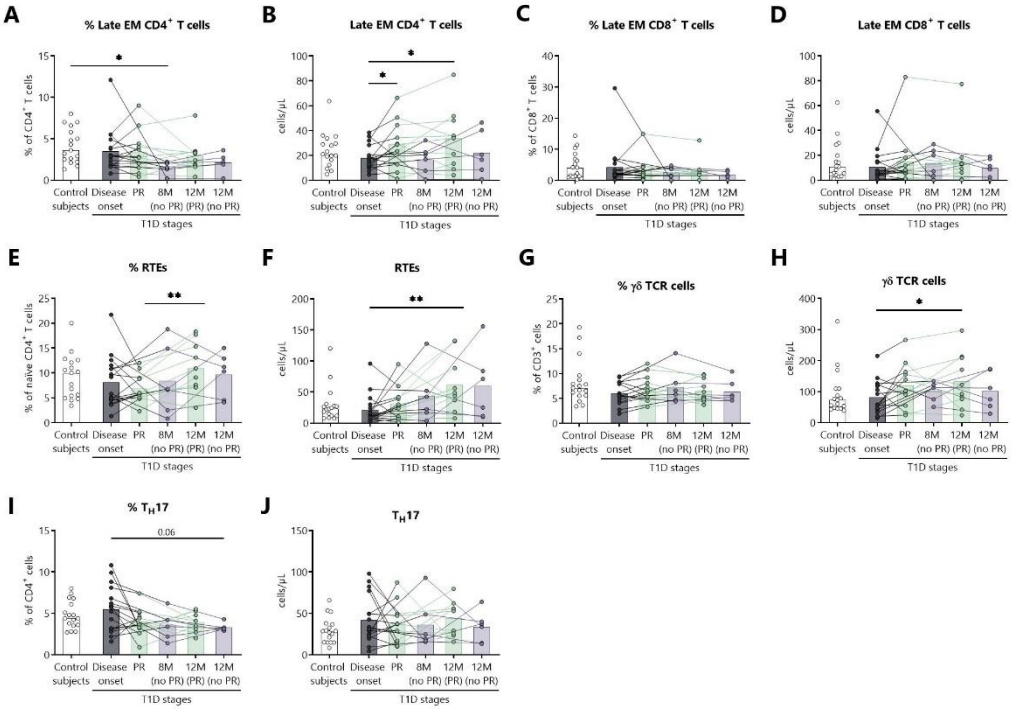

Supplementary Figure 15. ***Absolute counts and percentages of T lymphocyte subsets do not differ between remitters and non-remitters.*** *Percentages (%) and absolute counts (cells/μL) of (**A and B**) late effector memory (EM) CD4⁺ T lymphocytes, (**C and D**) late EM CD8⁺ T lymphocytes, (**E and F**) recent thymic emigrants (RTEs), (**G and H**) γδ TCR T lymphocytes, and (**I and J**) Th17 lymphocytes were determined in peripheral blood of control subjects and patients with T1D at different time-points. White bars correspond to control subjects (n=17), grey bars to patients at disease onset (n=17), green bars to patients at partial remission (PR, n=11; at 12M, n=10) and lilac bars to non-remission (non-PR at 8M, n=6; at 12M, n=6). Bar graphs show mean percentage or*

*absolute count values. Each symbol represents an individual patient. Lines link the same patient throughout the time-points. *p ≤0.05 and **p <0.01 after mixed effects model with Tukey's post-hoc test for longitudinal data, Kruskal–Wallis with Dunn's post-hoc test for comparisons between control subjects and the different T1D time-points, or 2-tailed Mann–Whitney test for comparisons between two unpaired groups of data. P ≤0.05 is considered significant.*

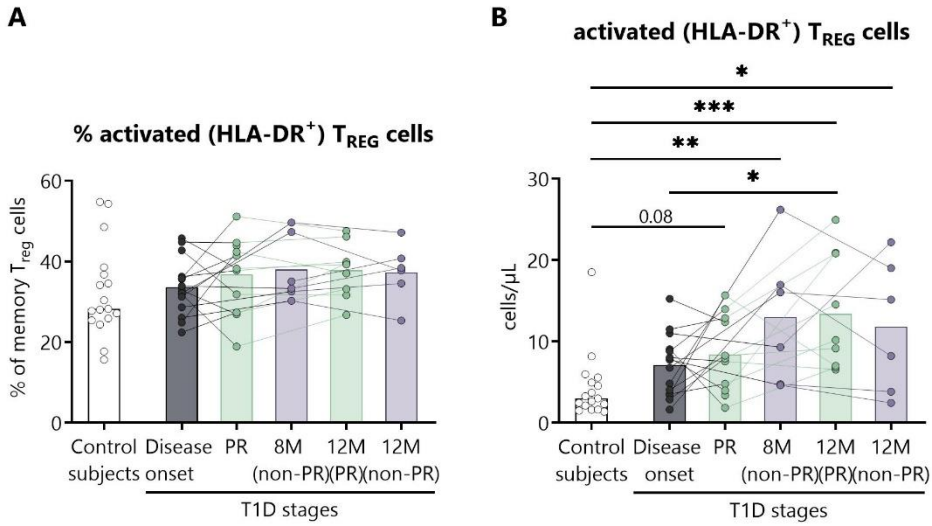

Supplementary Figure 16. ***Absolute counts of activated regulatory T lymphocytes, but not the percentage, are altered at the initial stages of T1D.*** *(**A**) Percentages (%) and (**B**) concentrations (cells/µL) of activated regulatory T cells (aTreg) were determined in peripheral blood of control subjects and patients with T1D at different time-points. White bars correspond to control subjects (n=17), grey bars to patients at disease onset (n=17), green bars to patients at partial remission (PR, n=11; at 12M, n=10) and lilac bars to non-remission (non-PR at 8M, n=6; at 12M, n=6). Bar graphs show mean percentage or absolute count values. Each symbol represents an individual patient. Lines link the same patient throughout the time-points. *p ≤0.05, **p <0.01 and ***p <0.001 after mixed effects model with Tukey's post-hoc test for longitudinal data, Kruskal–Wallis with Dunn's post-hoc test for comparisons between control subjects and the different T1D time-points, or 2-tailed Mann–Whitney test for comparisons between two unpaired groups of data. P ≤0.05 is considered significant.*

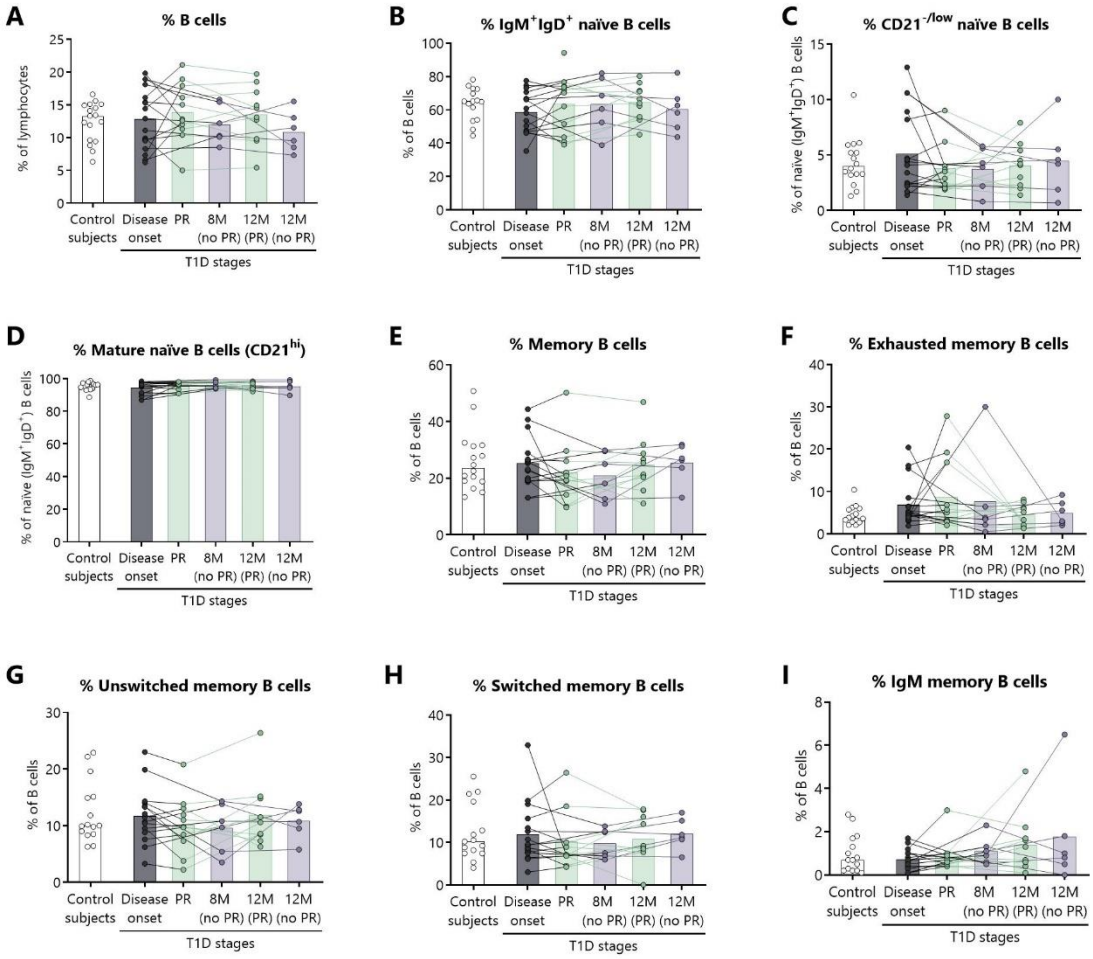

Supplementary Figure 17. ***The percentage of different maturation stages of B lymphocytes is not altered at the initial stages of T1D.*** *Percentages (%) of (**A**) B lymphocytes, (**B**) IgM^{+}IgD^{+} naïve B lymphocytes, (**C**) CD21$^{-/low}$ naïve B lymphocytes, (**D**) mature naïve B lymphocytes, (**E**) memory B lymphocytes, (**F**) exhausted memory B lymphocytes, (**G**) unswitched memory B lymphocytes, (**H**) switched memory B lymphocytes, and (**I**) IgM memory B lymphocytes were determined in peripheral blood of control subjects and patients with T1D at different time-points. White bars correspond to control subjects (n=17), grey bars to patients at disease onset (n=17), green bars to patients at partial remission (PR, n=11; at 12M, n=10) and lilac bars to non-remission (non-PR at 8M, n=6; at 12M, n=6). Bar graphs show mean percentage or absolute count values. Each symbol represents an individual patient. Lines link the same patient throughout the time-points. Data analyzed by mixed effects model with Tukey's post-hoc test for longitudinal data, Kruskal–Wallis with Dunn's post-hoc test for comparisons between control subjects and the different T1D time-points, or 2-tailed Mann–Whitney test for comparisons between two unpaired groups of data. P ≤0.05 is considered significant.*

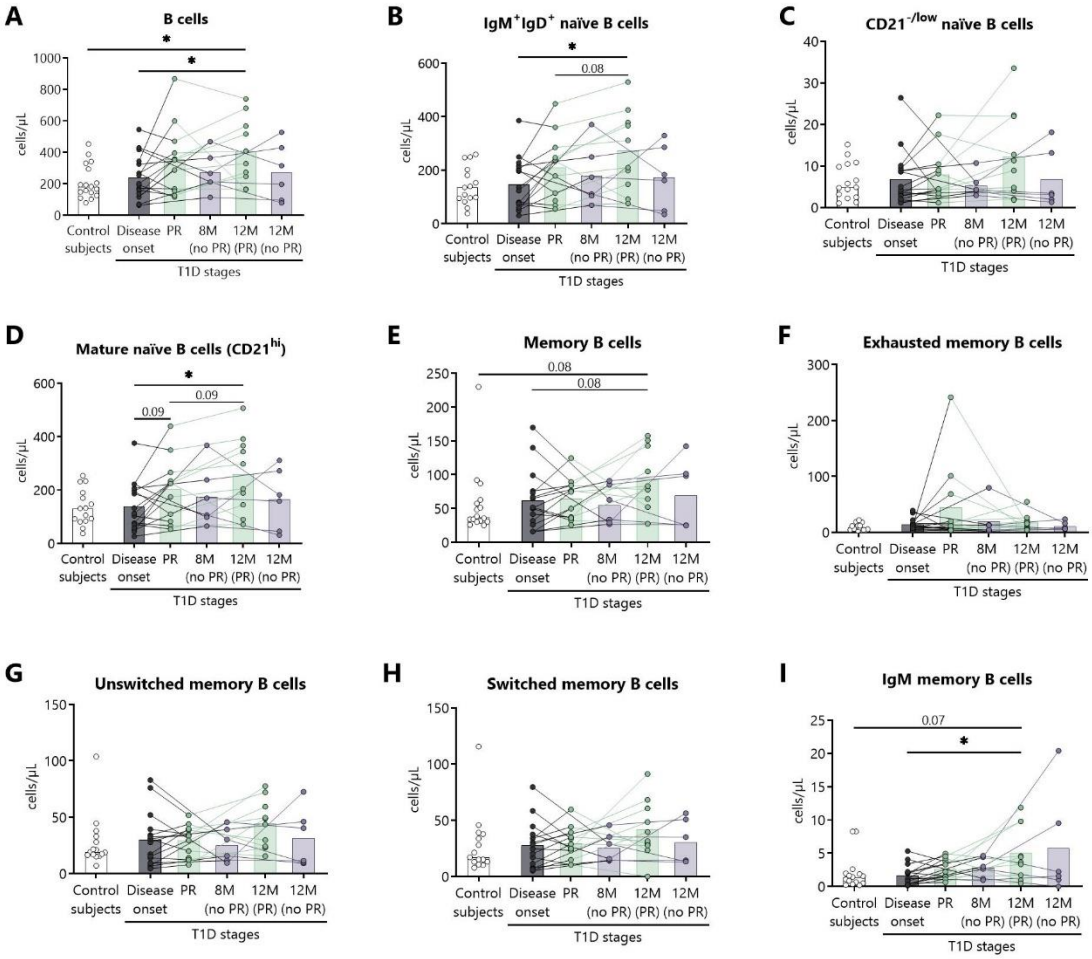

Supplementary Figure 18. ***Absolute counts of B lymphocytes at different maturation stages barely differ between the initial stages of T1D.*** *Absolute counts (cells/µL) of (**A**) B lymphocytes, (**B**) IgM⁺IgD⁺ naïve B lymphocytes, (**C**) CD21$^{-/low}$ naïve B lymphocytes, (**D**) mature naïve B lymphocytes, (**E**) memory B lymphocytes, (**F**) exhausted memory B lymphocytes, (**G**) unswitched memory B lymphocytes, (**H**) switched memory B lymphocytes, and (**I**) IgM memory B lymphocytes were determined in peripheral blood of control subjects and patients with T1D at different time-points. White bars correspond to control subjects (n=17), grey bars to patients at disease onset (n=17), green bars to patients at partial remission (PR, n=11; at 12M, n=10) and lilac bars to non-remission (non-PR at 8M, n=6; at 12M, n=6). Bar graphs show mean percentage or absolute count values. Each symbol represents an individual patient. Lines link the same patient throughout the time-points. *p ≤0.05 after mixed effects model with Tukey's post-hoc test for longitudinal data, Kruskal–Wallis with Dunn's post-hoc test for comparisons between control subjects and the different T1D time-points, or 2-tailed Mann–Whitney test for comparisons between two unpaired groups of data. P ≤0.05 is considered significant.*

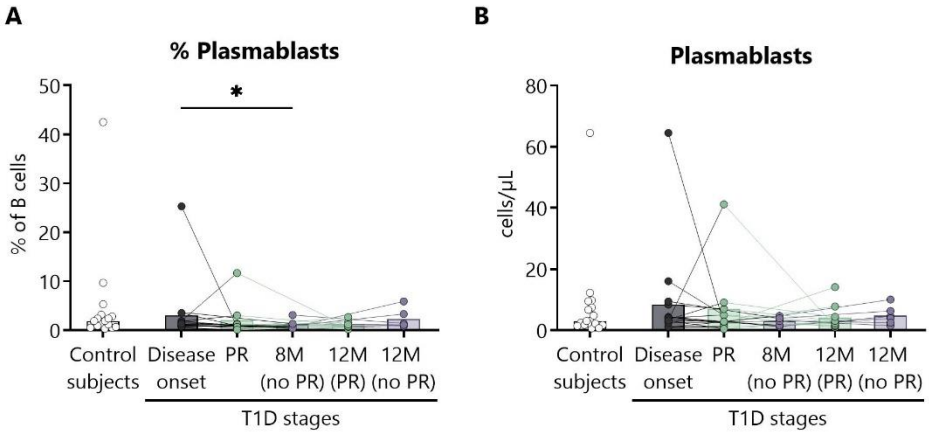

Supplementary Figure 19. ***The amount of plasmablasts do not differ between remitter and non-remitter patients with T1D.*** *(**A**) Percentage (%) and (**B**) concentration (cells/µL) of plasmablasts were determined in peripheral blood of control subjects and patients with type 1 diabetes (T1D) at different time-points. White bars correspond to control subjects (n=17), grey bars to patients at disease onset (n=17), green bars to patients at partial remission (PR, n=11; at 12M, n=10) and lilac bars to non-remission (non-PR at 8M, n=6; at 12M, n=6). Bar graphs show mean percentage or absolute count values. Each symbol represents an individual patient. Lines link the same patient throughout the time-points. *p ≤0.05 after mixed effects model with Tukey's post-hoc test for longitudinal data, Kruskal–Wallis with Dunn's post-hoc test for comparisons between control subjects and the different T1D time-points, or 2-tailed Mann–Whitney test for comparisons between two unpaired groups of data. P ≤0.05 is considered significant.*

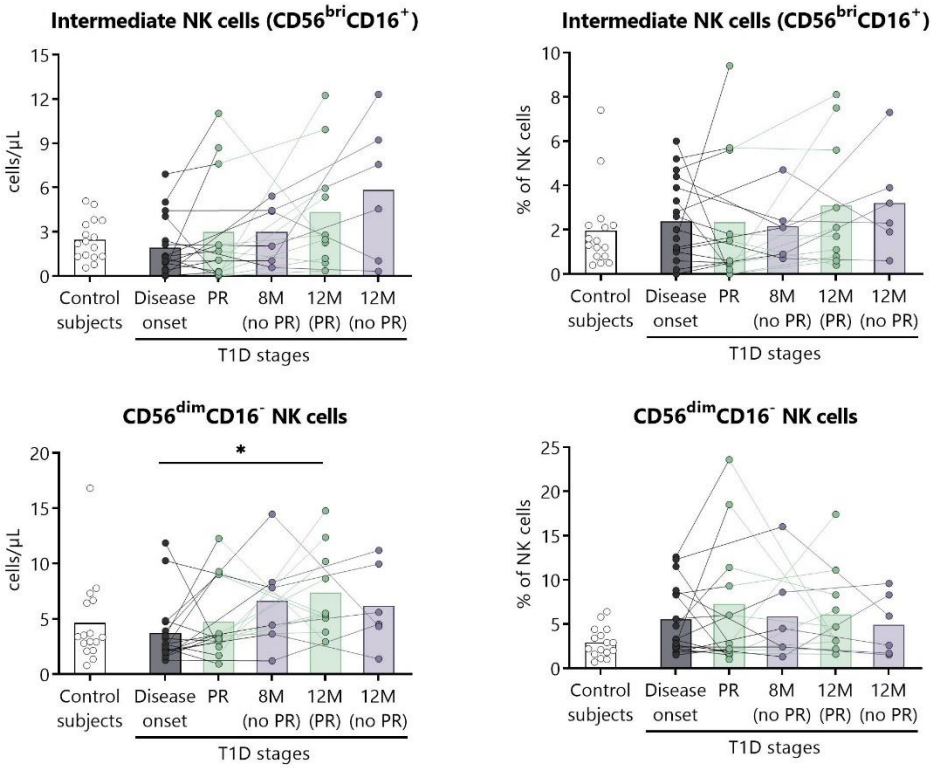

Supplementary Figure 20. ***The amount of intermediate NK cells and CD56^{dim}CD16^{-} NK cells do not differ between remitter and non-remitter patients with T1D.*** *Concentration (left) and percentage (right) of total intermediate NK cells and CD56^{dim}CD16^{-} NK cells. White bars correspond to control subjects (n=17), grey bars to patients at disease onset (n=17), green bars to patients at partial remission (PR, n=11; at 12M, n=10) and lilac bars to non-remission (non-PR at 8M, n=6; at 12M, n=6). Bar graphs show mean percentage or absolute count values. Each symbol represents an individual patient. Lines link the same patient throughout the time-points. *p ≤0.05 after mixed effects model with Tukey's post-hoc test for longitudinal data, Kruskal–Wallis with Dunn's post-hoc test for comparisons between control subjects and the different T1D time-points, or 2-tailed Mann–Whitney test for comparisons between two unpaired groups of data. P ≤0.05 is considered significant.*

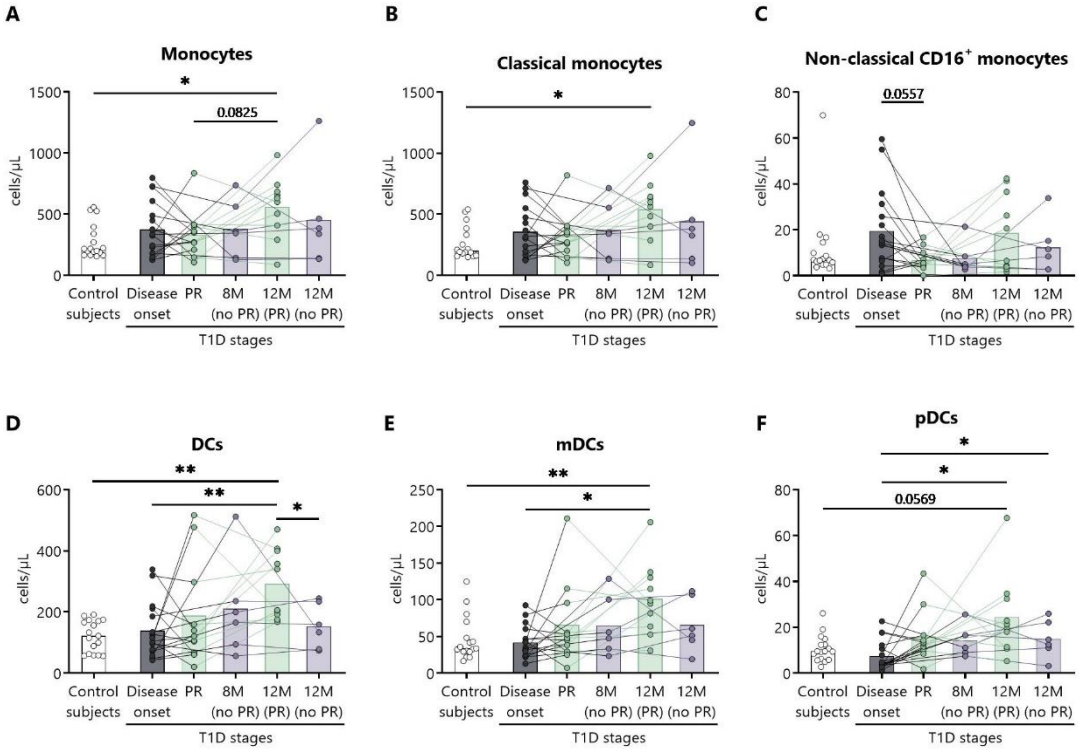

Supplementary Figure 21. ***Absolute counts of monocytes and dendritic cells are altered at the initial stages of T1D.*** *Absolute counts (cells/µL) of (**A**) monocytes and their subsets (**B**) classical and (**C**) non-classical, and of (**D**) dendritic cells (DCs) and their subsets (**E**) myeloid (mDCs) and (**F**) plasmacytoid (pDCs) were determined in peripheral blood of control subjects and patients with T1D at different time-points. White bars correspond to control subjects (n=17), grey bars to patients at disease onset (n=17), green bars to patients at partial remission (PR, n=11; at 12M, n=10) and lilac bars to non-remission (non-PR at 8M, n=6; at 12M, n=6). Bar graphs show mean percentage or absolute count values. Each symbol represents an individual patient. Lines link the same patient throughout the time-points. *p ≤0.05 and **p <0.01 after mixed effects model with Tukey's post-hoc test for longitudinal data, Kruskal–Wallis with Dunn's post-hoc test for comparisons between control subjects and the different T1D time-points, or 2-tailed Mann–Whitney test for comparisons between two unpaired groups of data. P ≤0.05 is considered significant.*

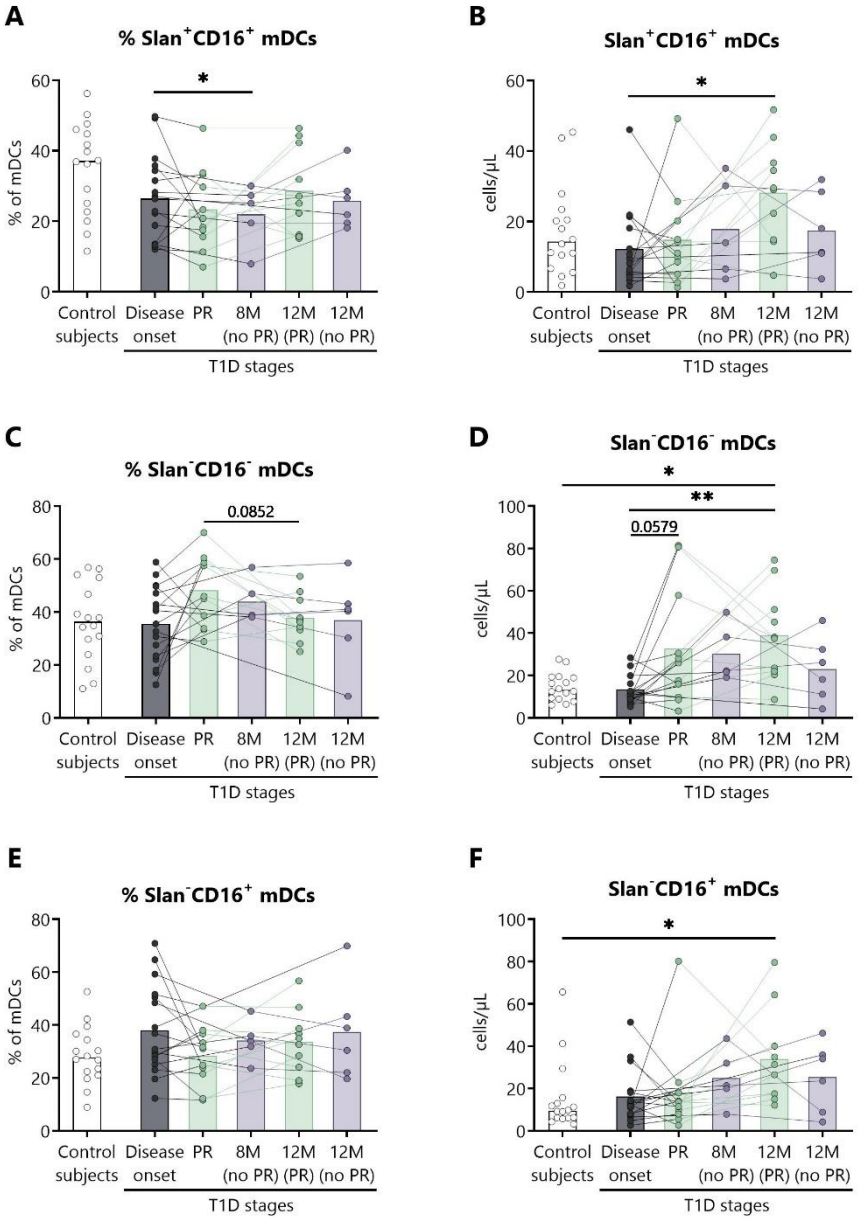

Supplementary Figure 22. ***Subsets of myeloid dendritic cells defined by the expression of Slan and CD16 are altered at initial stages of T1D.*** *(**A, C, E**) Percentages (%) and (**B, D, F**) concentrations (cells/µL) of (**A and B**) Slan⁺CD16⁺ myeloid dendritic cells (mDCs), (**C and D**) Slan⁻CD16⁻ mDCs, and (**E and F**) Slan⁻CD16⁺ mDCs were determined in peripheral blood of control subjects and patients with T1D at different time-points. White bars correspond to control subjects (n=17), grey bars to patients at disease onset (n=17), green bars to patients at partial remission (PR, n=11; at 12M, n=10) and lilac bars to non-remission (non-PR at 8M, n=6; at 12M, n=6). Bar graphs show mean percentage or absolute count values. Each symbol represents an individual patient. Lines*

*link the same patient throughout the time-points. *p ≤0.05 and **p <0.01 after mixed effects model with Tukey's post-hoc test for longitudinal data, Kruskal–Wallis with Dunn's post-hoc test for comparisons between control subjects and the different T1D time-points, or 2-tailed Mann–Whitney test for comparisons between two unpaired groups of data. P ≤0.05 is considered significant.*

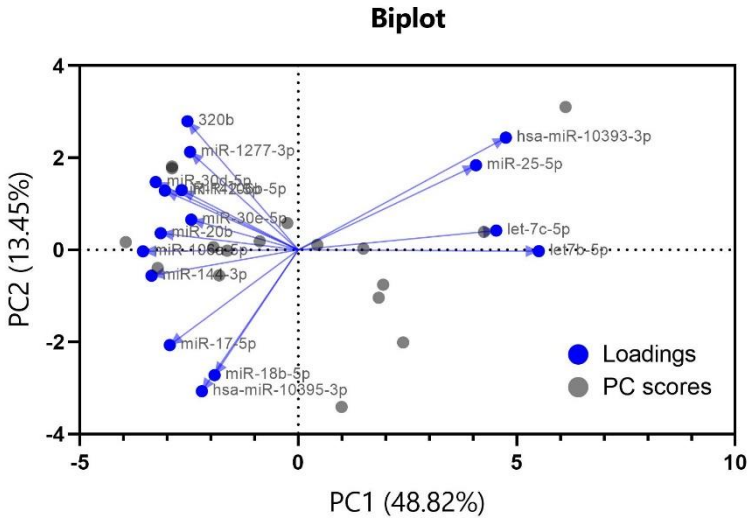

Supplementary Figure 23. ***Biplot of the principal component analysis for differentially expressed miRNAs during the partial remission phase.*** *The two principal components (PC1 and PC2) explained 62.27% of the total variation in miRNA data and showed clear partitioning of PR and non-PR samples along the PC1. Let-7b-5p and let-7c-5p were the miRNAs influencing the most the non-PR group. Blue arrows represent the differentially expressed miRNAs, and circles in grey represent sampling points (PR and non-PR).*

Supplementary Table 3. ***Differentially expressed circulating miRNAs with validated target genes during the partial remission phase or at T1D diagnosis versus non-diabetic controls***

miRNAs	**PR vs Ctrl (FC)**	P-value	**T1D dx vs Crtl (FC)**	P-value
hsa-miR-3173-5p	-2.491	0.001	-	-
hsa-miR-21-3p	-2.415	0.001	-	-
hsa-miR-940	-2.463	0.001	-	-
hsa-miR-769-5p	-2.322	0.002	-	-
hsa-miR-205-5p	-2.197	0.003	-	-
hsa-miR-30e-3p	2.316	0.003	-	-
hsa-miR-4433b-5p	-2.241	0.004	-	-
hsa-miR-424-5p	1.852	0.004	-	-
hsa-miR-3138	-2.293	0.004	-	-
hsa-miR-133a-3p	-2.059	0.005	-	-
hsa-miR-362-5p	-2.098	0.005	-	-
hsa-miR-410-3p	-2.178	0.005	-	-
hsa-miR-3200-5p	-2.546	0.005	-	-
hsa-miR-424-3p	-2.178	0.006	-	-
hsa-miR-3202	-2.154	0.006	-	-
hsa-miR-203a-3p	-2.013	0.007	-	-
hsa-miR-194-5p	2.015	0.008	-	-
hsa-miR-190a-5p	2.044	0.009	-	-
hsa-miR-26a-2-3p	-2.080	0.009	-	-
hsa-miR-23a-5p	-1.968	0.010	-	-
hsa-miR-338-3p	1.942	0.010	2.299	0.007
hsa-miR-92b-5p	-1.851	0.014	-	-
hsa-miR-33b-5p	-1.922	0.015	-	-
hsa-miR-432-5p	-1.800	0.015	-	-
hsa-miR-655-3p	-1.801	0.015	-	-
hsa-miR-877-5p	-2.106	0.016	-	-
hsa-miR-580-3p	-1.823	0.017	-	-
hsa-miR-429	-1.819	0.018	-	-
hsa-miR-1307-3p	-1.836	0.018	-	-
hsa-miR-455-5p	-1.798	0.019	-	-
hsa-miR-106b-3p	1.600	0.020	-	-
hsa-miR-130b-5p	-1.709	0.020	-	-
hsa-miR-6891-3p	-1.718	0.021	-	-
hsa-miR-181a-3p	-1.764	0.022	-	-
hsa-miR-6503-5p	-1.697	0.022	-	-
hsa-miR-3613-5p	1.647	0.022	-	-
hsa-miR-152-3p	-1.904	0.023	-	-
hsa-miR-103a-3p	1.729	0.023	-	-
hsa-miR-495-5p	-1.786	0.024	-	-

hsa-miR-6734-5p	-1.761	0.024	-	-
hsa-miR-556-3p	-1.783	0.026	-	-
hsa-miR-331-3p	-1.767	0.027	-	-
hsa-miR-26a-1-3p	-1.671	0.027	-	-
hsa-miR-3200-3p	-1.666	0.027	-	-
hsa-let-7g-3p	-1.645	0.027	-	-
hsa-miR-376a-3p	-1.695	0.028	-	-
hsa-miR-495-3p	-1.686	0.028	-	-
hsa-miR-1908-5p	-1.639	0.029	-	-
hsa-miR-454-3p	1.292	0.032	-	-
hsa-miR-186-5p	1.422	0.032	-	-
hsa-miR-218-5p	-1.643	0.032	-	-
hsa-miR-4484	-1.711	0.033	-	-
hsa-miR-144-5p	1.059	0.035	-	-
hsa-miR-1301-3p	-1.579	0.036	-	-
hsa-miR-3179	-1.590	0.039	-	-
hsa-miR-16-2-3p	1.372	0.040	-	-
hsa-miR-570-3p	-1.531	0.041	-	-
hsa-miR-501-3p	-1.526	0.043	-	-
hsa-miR-374a-5p	1.265	0.044	-	-
hsa-miR-378a-3p	-1.676	0.045	-	-
hsa-miR-411-3p	-1.553	0.048	-	-
hsa-miR-107	1.522	0.049	-	-
hsa-miR-144-3p	-	-	1.425	0.0004
hsa-miR-130a-3p	-	-	1.456	0.011
hsa-miR-17-5p	-	-	1.272	0.015
hsa-miR-106b-3p	-	-	1.813	0.020
hsa-miR-10b-5p	-	-	-2.170	0.022
hsa-miR-140-5p	-	-	-2.164	0.024
hsa-miR-20a-5p	-	-	1.045	0.032
hsa-miR-3648	-	-	-1.732	0.033
hsa-miR-1277-3p	-	-	1.957	0.035
hsa-miR-223-3p	-	-	-1.189	0.036
hsa-miR-183-5p	-	-	1.712	0.041
hsa-miR-197-3p	-	-	-1.876	0.043
hsa-miR-582-5p	-	-	-1.675	0.045
hsa-miR-22-3p	-	-	1.740	0.047
hsa-miR-191-5p	-	-	1.123	0.049

Data analyzed by Moderated *t*-test. *Abbreviations*: *Ctrl*, controls; *FC*; fold change; *PR*, partial remission; *T1D dx*, type 1 diabetes diagnosis.

Supplementary Table 4. ***Selected target genes for the other DEMs during the partial remission phase related to regeneration, metabolism or the immune system***

miRNA	Genes for Regeneration	Genes for Metabolism	Genes for Immune System
hsa-miR-106a-5p	ADAM17, ADAM9, APPL1, ARHGAP1, ASPH, BCL2L11, CASP7, CCDC50, DEGS1, EPS15, EREG, FLT1, MCL1, NOTCH2, PDGFB, RAB11FIP1, RBBP6, SH3GLB1, STAT3, VEGFA	CNOT6, CPEB2, DMTF1, DNPH1, MTPAP, OAS2, SNIP1, VKORC1L1	ACVR1B, APC, BAMBI, BMP2, BMP8B, BMPR2, CCL5, CD274, CDKN1A, CNOT4, CNOT6, CXCL8, DGCR2, FAF2, FAS, FASTK, GDF11, GDF15, IL10, IL17RD, IL6, IRAK4, JAK1, KIF14, LEF1, LRBA, MAPK8, MICA, MICB, NFAT5, PABPC4, SKI, SNIP1, SOCS1, TGFB1, TGFBR2, TGFBR3, TCF7L1, TCF7L2, TLR7, ZBTB33
hsa-miR-20b-5p	ADAM9, ARHGAP1, BCL2L11, BNIP3L, CASP2, CELSR2, DEGS1, EREG, MCL1, PDGFB, RAB11FIP1, SH3GLB1, STAT3, VEGFA, ZFP36L1	CNOT6, DMTF1, DNPH1, ERBIN, MTPAP	ACVR1B, BAMBI, BMP2, BMP8B, BMPR2, CCL1, CCL5, CDKN1A, CNOT4, CNOT6, CXCL8, DKK3, FAF2, FASTK, GDF11, GDF15, IL17RD, IRAK4, JAK1, KIF14, LGR4, LTBP1, MAPK8, MAP3K8, MICA, MICB, NFAT5, NFKBIZ, PRKAR2B, PTPRK, SKI, SMAD2, SMAD6, SOCS1, TCF7L1, TCF7L2, TGFBR2, TGFBR3, TLR7, ZBTB33
hsa-miR-142-3p	CASP8, FAT1, FLT1, RAB11FIP1, SPART, ZFP36L1, ZFP36L2	CPEB2, DMTF1, HERPUD1, VKORC1L1	APC, BMP8A, BMPR2, CCR6, DCP1A, CNOT4, CSRP2, IL6, LGR5, MAML2, SH2D1A, SMAD7, TGFBR1, TIRAP
hsa-miR-106b-5p	ACIN1, ADAM9, AKT1, APPL1, ARHGAP1, ASPH, BCL2L11, CASP2, CASP7, CASP8, CCDC50, DEGS1, DFFB, DIDO1, EOGT, EP300, EPS8, EREG, GXYLT1, KDR, MCL1, NOTCH2, PDGFB, RAB11FIP1, RBBP6, SH3GLB1, SPART, STAT3, VEGFA	CDCA7, CNOT6, DDX6, DMTF1, DNPH1, EXOSC6, MTPAP, OAS2, VKORC1L1	ACIN1, ACVR1B, APC, B3GAT1, BAMBI, BLNK, BMP2, BMP8B, BMPR2, CCL1, CCL5, CD109, CD274, CDKN1A, CNOT4, CNOT6, CXCL8, DAP3, DFFB, DIDO1, EOMES, FAF2, FAS, FASTK, GDF11, GDF15, HVCN1, IFITM2, IFITM3, IL17RD, IRAK4, JAK1, KIF14, LAMP3, LGR4, LTBP1, MAP3K8, MAPK8, MICA, MICB, NFAT5, NMI, PABPC4, PRKAR2B, RNF128, RORC, SKI, SMAD6, SMAD7, SMAD9, SOCS1, STON1, TCF7L1, TCF7L2, TGFBR1, TGFBR2, TLR7, TNFSF11, ZBTB33
hsa-miR-17-5p	ADAM15, ADAM17, ADAM9, AKT1, APPL1, ARHGAP1, BCL11A, BCL2L11, BNIP3L, CASP1, CASP10, CASP2, CASP8, CCDC50,	CDCA7, CNOT6, DDX6, DMTF1, DNPH1, ERBIN, EXOSC6,	ACVR1B, BAMBI, BCL2A1, BMP2, BMP8B, BMPR2, CCL1, CCL5, CD274, CDKN1A, CHRNA5, CNOT4, CNOT6, CXCL8, CYTH1, DCP1A, DKK3, FAF1, FAF2, FAS, FASTK, FKBP1A, GDF11, GDF15, GSKIP, IGBP1, IL17RD, IRAK4, JAK1, KIF14, LGR4, LTBP1, MAP3K8, MAPK8, MICA, MICB, NFAT5,

	CELSR2, DEGS1, EP300, EREG, MCL1, MOAP1, NOTCH2, NRP1, NRP2, PDGFB, RAB11FIP1, RBBP6, SELE, SH3GLB1, SPART, STAT3, TNC, VEGFA, ZFP36L1, ZFP36L2	IREB2, MTPAP, MYCBP2, VKORC1L1	NFATC3, NMI, PABPC4, PRKAR2B, PTPRK, RNF128, RORC, RYK, SKI, SMAD2, SMAD6, SOCS1, TCF7L1, TCF7L2, TGFB1, TGFB2, TGFBR2, TGFBR3TLR7, TNFSF14, ZBTB33
hsa-let-7b-5p	ACIN1, ADAM15, ADAM9, AKT1, APPL1, ARHGAP1, ASPH, BCL2L11, BNIP3L, CCDC50, DFFA, DIDO1, EGFR, EP300, EPS8, EREG, FAT1, FBLN5, GAREM1, GXYLT1, MCL1, NOTCH2, NRDC, NRP1, PDGFB, RBBP6, SH3GLB1, STAB2, TEK, UBASH3B, VEGFB, ZFP36L1, ZFP36L2, ZNF124	ATF6B, CDCA7, CNOT6, CPEB2, DDX6, ERBIN, HERPUD1, HSPA5, IREB2, JAK2, MYCBP2, OAS1, RASAL3, XRN1, ZC3HAV1	ABL1, ACIN1, ACTRT2, ACVR1, ACVR1B, ACVR2B, APC, ASPSCR1, ATG12, ATG4B, BMP15, BMP2, BMP4, BMP5, BMP7, BMPR2, C3, CASP8AP2, CCL2, CCL22, CCR5, CD109, CD274, CD59, CD70, CD80, CDKN1A, CFH, CNOT2, CNOT4, CNOT6, CRKL, CSRP2, CXCL8, CYTH1, DAP3, DFFA, DIDO1, DKK3, DKKL1, DSE, FAS, FCMR, FKBP1A, GDF11, HSH2D, IFITM2, IFITM3, IGFL1, IL17RC, IL17RD, IL18R1, IL2RA, IL32, IL6, IL6R, INHBE, ITSN2, JAK1, JAK2, KLHL12, LAMP3, LEFTY1, LGR4, LGR5, LRBA, LTBP2, MAPK8, MICB, NCR3LG1, NFAT5, NFATC1, NFATC3, NOG, NXN, OTUD6B, PAG1, PELI3, PRKAR2B, PTK7, PTPN13, QSOX2, RNF111, SART3, SCYL2, SKI, SMAD7, SMAD9, SOCS1, SPN, TCF7L2, TDP2, TGFB2, TGFBR1, TGFBR2, TGFBR3, TICAM1, TNFRSF11A, TNFRSF25, TNFRSF8, TNFSF9, TNIK, VTCN1
hsa-let-7c-5p	ADAM9, ASPH, BCL2L11, CASP6, CCDC50, DIDO1, FAT1, GXYLT1, NOTCH2, NRP1, PDGFB, RBBP6, SH3D19, SH3GLB1, STAT3, UBASH3B, ZFP36L1	ATF6B, CNOT6, CPEB2, DDX6, HERPUD1, MYCBP2, XRN1, ZC3HAV1	ACVR1B, ACVR2B, APC, ATG12, CASP8AP2, CD59, CD80, CDKN1A, CNOT4, CNOT6, CRKL, CXCL8, DIDO1, FAS, FKBP1A, GDF11, IL10, IL6, IL6R, ITSN2, JAK1, LEFTY1, LGR4, LRBA, MAPK8, MICB, NCR3LG1, NFAT5, PAG1, QSOX2, RNF111, SKI, SMAD6, SMAD7, SOCS1, TCF7L2, TICAM1, TGFBR1, TGFBR2, TGFBR3, TNFRSF11A, TNFSF9,
hsa-miR-320b	ADAM17, APPL1, BCL2L11, BCL2L12, CASP2, FGB, FGL1, GXYLT1, MCL1, RBBP6, STAT1, UBASH3B, ZFP36L1	CNOT6, HSPA5, IREB2, JAK2	ACVR2A, ACVR2B, C3, CD274, CNOT4, CNOT6, DCP1A, FKBP1A, GNL1, HLA-DPA1, JAK2, KIF14, LEF1, NOCT, PAG1, SKI, SMAD7, TNFSF14, ZBTB33
hsa-miR-30e-5p	ADAM9, APPL1, BCL11A, BNIP3L, CASP4, DEGS1, DIDO1, FAT1,	CPEB2, DDX6, EDC3, HSPA5, IREB2, MYCBP2,	ATG12, BCL6, BMP2, CD226, CNOT9, CXCL11, DIDO1, FAF2, FAS, FMOD, GCSAM, GDNF, HLA-DRA, IL21R, INHBA, ITSN2, JAK1, LGR4, MAPK8, MICB,

	GXYLT1, MCL1, NOTCH1, NOTCH2, NRP1, NRXN3, RAB11FIP1, RBBP6, UBN1, VEGFA, VEGFC, ZFP36L1, ZFP36L2	RIOX2, VKORC1L1, XRN1	NCR3LG1, NFAT5, NFATC3, OTUD6B, PTPN13, SKI, SMAD2, SMAD7, SOCS1, TAF4B, TGFBR2, TNFSF9, ZBTB33
hsa-miR-144-3p	BCL2L11, CASP14, DIDO1, EP300, FGB, MCL1, NOTCH1, ZFP36L2	HERPUD1, IREB2	DIDO1, ITSN2, LEFTY1, LGR4, MAP3K8, RNF111, TCF7L2, TGFB1, TGFBR3
hsa-miR-18b-5p	ADAM9, CELSR2, DFFA, MCL1, NOTCH2, STAT3, ZFP36L1	DDX6, EXOSC6, MTPAP	ACVR2A, ACVR2B, ASPSCR1, CDKN1A, CNOT4, DFFA, GDF11, GNL1, HLA-DQA1, KIF14, LGR4, OTUD6B, PTPN13, QSOX2, SMAD2
hsa-miR-1277-3p	NOTCH1	ERN1	IL6R
hsa-miR-25-5p	ARHGAP1	IREB2, MTPAP	C3, CCR4, CD180, CDKN1A, ITGAX, SKI

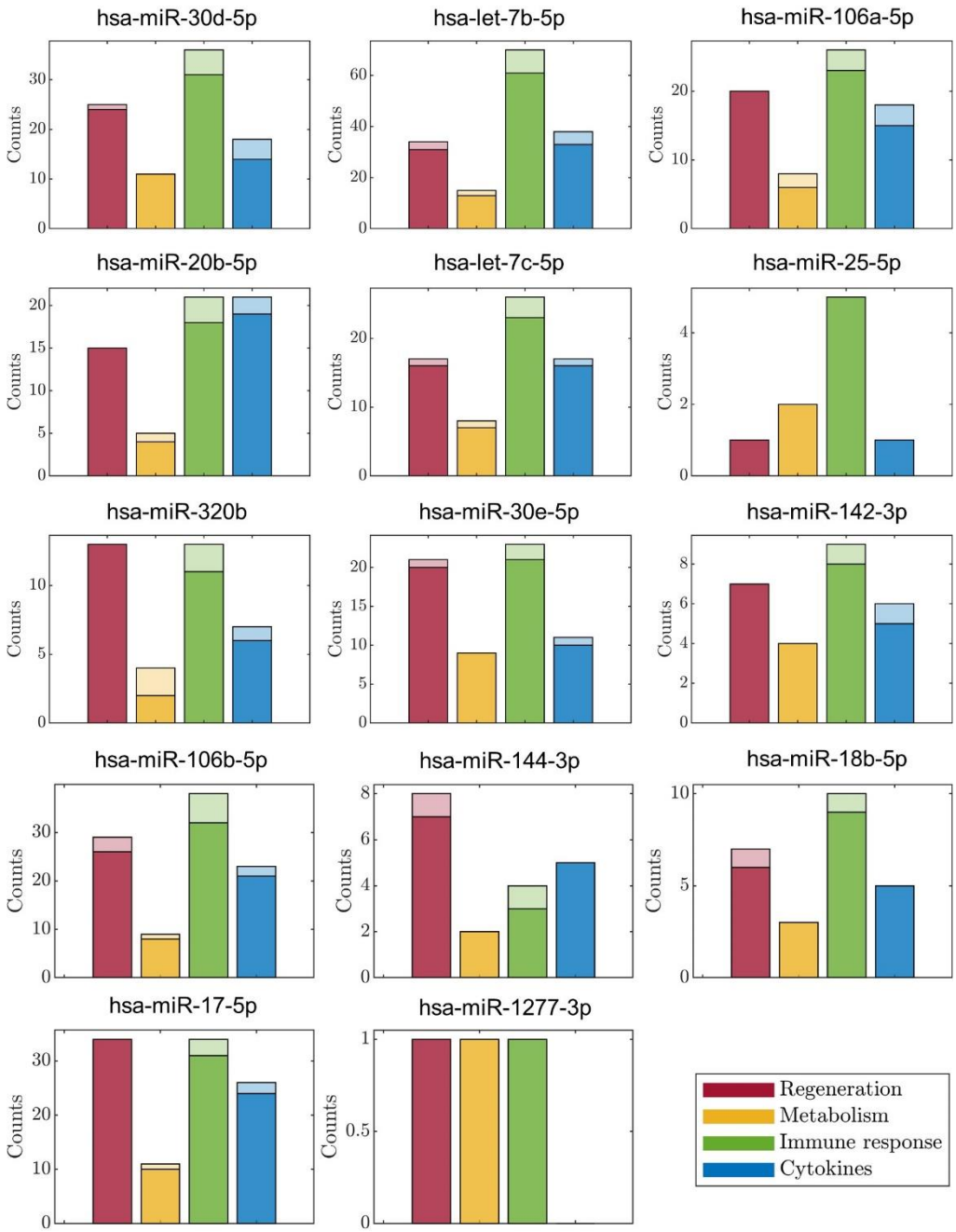

Supplementary Figure 24. ***Gene counts belonging to each group.*** *According to the keywords found in the Entrez summary of each gene, they have been classified into the groups regeneration (red), metabolism (yellow) or immune system (green and blue) for each microRNA differentially expressed during partial remission. The light color is the sum of all genes appearing in each group. The darker color is the sum of all genes appearing only in that group.*

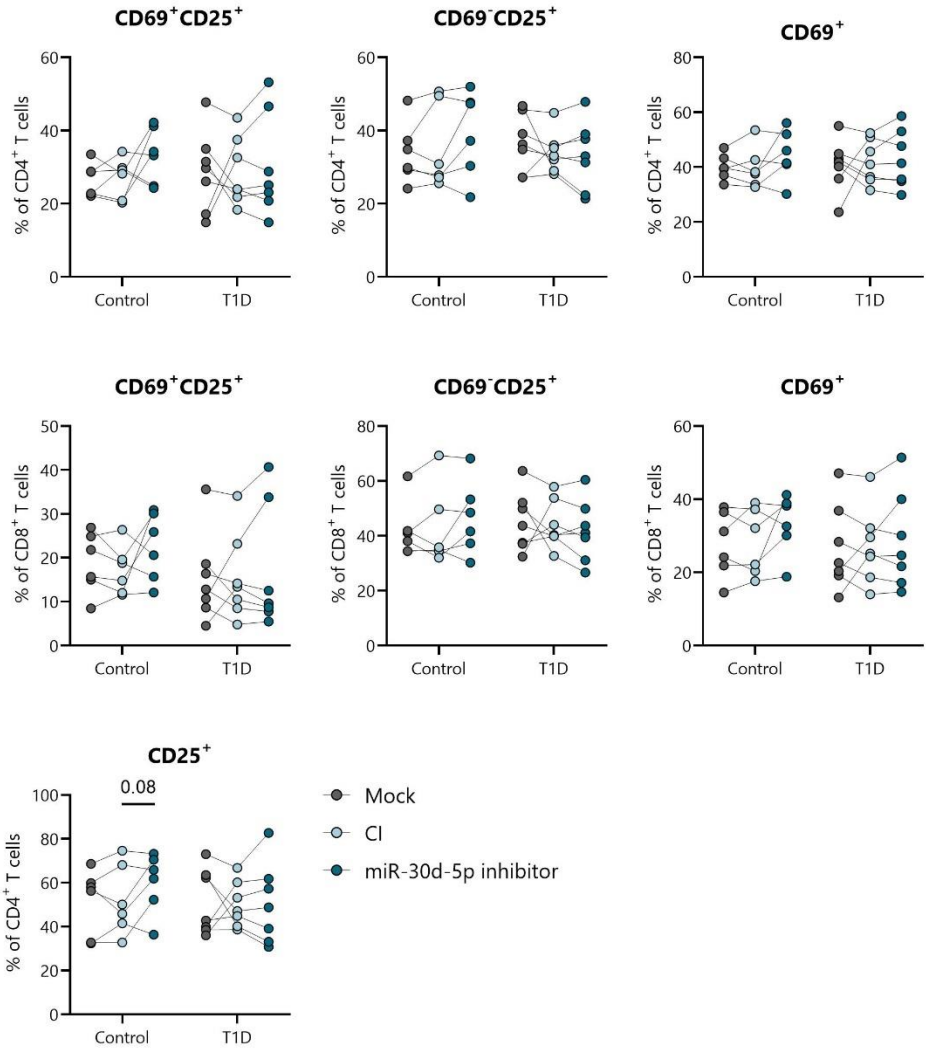

Supplementary Figure 25. ***miR-30d-5p inhibition does not alter the percentage of activated T cells.*** *Percentage of CD4⁺ and CD8⁺ T lymphocytes expressing the activating markers CD69 and CD25 obtained from T1D (n=7) and control (n=6) subjects. Within each group, grey dots represent T lymphocytes simply electroporated (mock), light blue dots represent T cells electroporated with a control inhibitor (CI) and dark blue dots with a miR-30d-5p inhibitor. ns ≥0.05, repeated measures two-way ANOVA with the Geisser-Greenhouse correction and Tukey's multiple comparisons test.*

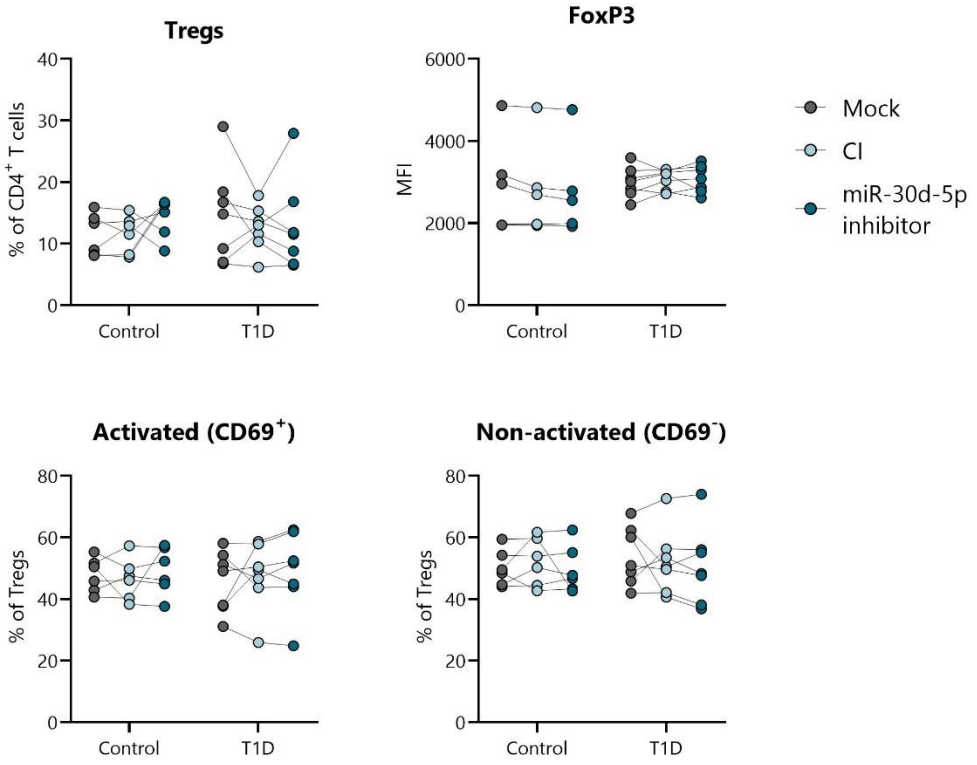

Supplementary Figure 26. ***miR-30d-5p inhibition does not alter the percentage of Tregs or the expression of FoxP3.*** *Percentage of total ($CD4^+CD25^+FoxP3^+$), activated (CD69+) and non-activated Tregs ($CD69^-$) and MFI of FoxP3 expression obtained from T1D (n=7) and control (n=6) subjects. Within each group, grey dots represent T lymphocytes simply electroporated (mock), light blue dots represent T cells electroporated with a control inhibitor (CI) and dark blue dots with a miR-30d-5p inhibitor. ns ≥0.05, repeated measures two-way ANOVA with the Geisser-Greenhouse correction and Tukey's multiple comparisons test.*

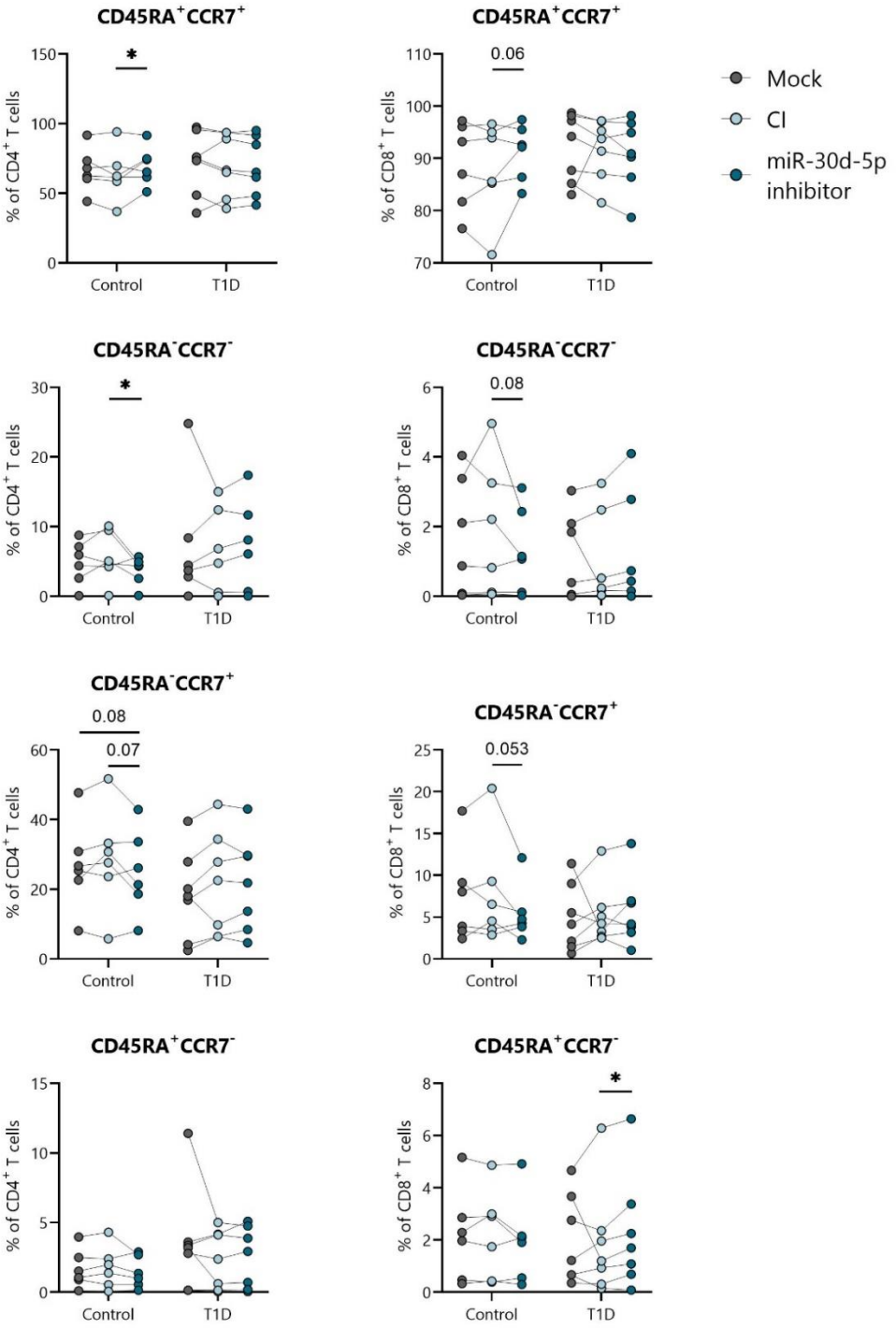

Figure legend on next page

Supplementary Figure 27. ***miR-30d-5p inhibition promotes the increase in CD45RA⁻ expressing subsets.*** *Percentage of CD4⁺ (left) and CD8⁺ (right) T lymphocytes expressing the markers CD45RA and CCR7 obtained from T1D (n=7) and control (n=6) subjects. Within each group, grey dots represent T lymphocytes simply electroporated (mock), light blue dots represent T cells electroporated with a control inhibitor (CI) and dark blue dots with a miR-30d-5p inhibitor. ns ≥0.05, and *p <0.05 repeated measures two-way ANOVA with the Geisser-Greenhouse correction and Tukey's multiple comparisons test.*

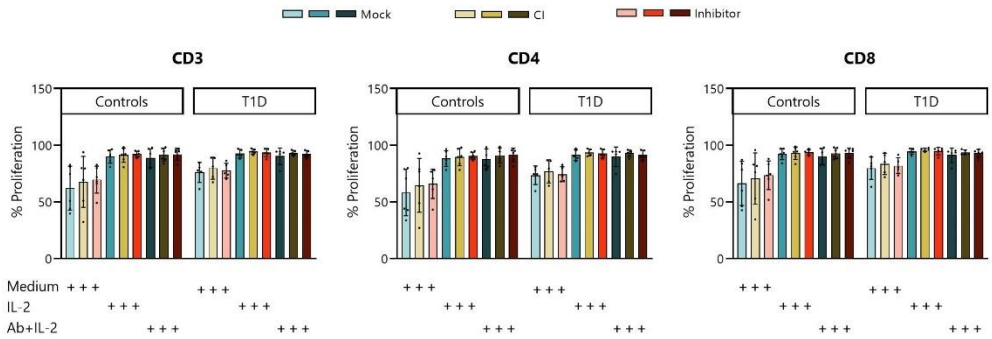

Supplementary Figure 28. ***miR-30d-5p inhibition does not affect the proliferation of re-stimulated T cells.*** *Percentage of CD3⁺, CD4⁺ and CD8⁺ T lymphocyte proliferation. T lymphocytes from controls (n=6) or T1D patients (n=5) previously activated and electroporated with no oligonucleotides (mock, blue bars), control inhibitor (CI, yellow bars) or miR-30d-5p inhibitor (orange bars) were stained with CellTrace Violet (CTV) and only re-cultured (light colors) or re-stimulated with either IL-2 (medium colors) or antibodies against CD3/CD28/CD2 plus IL-2 (dark colors) for 2 days. CD3⁺CD4⁺ and CD3⁺CD8⁺ T cell proliferation was measured as the percentage of CTV^{low} cells. ns ≥0.05, repeated measures two-way ANOVA with the Geisser-Greenhouse correction and Tukey's multiple comparisons test.*

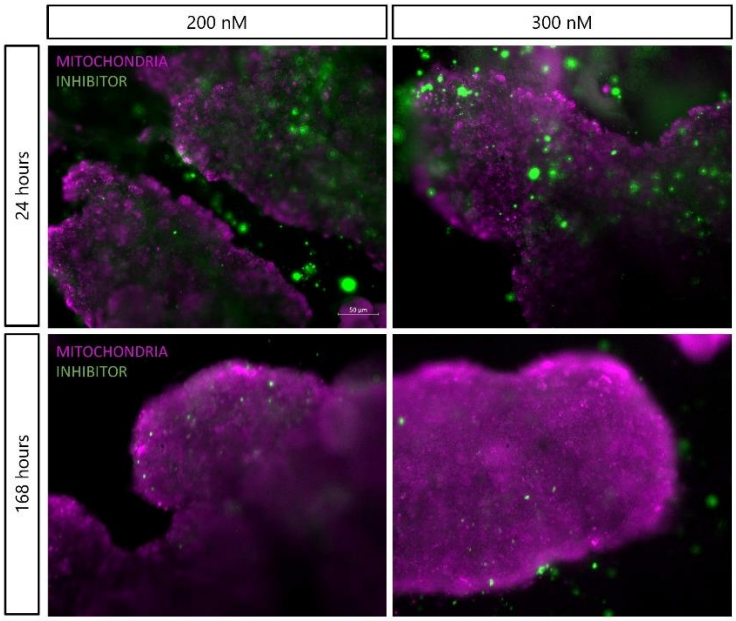

Supplementary Figure 29. ***Human pancreatic slices viability after transfection.*** *Representative staining showing tissue viability 24 and 168 hours after transfection with 200 or 300 nM of miR-30d-5p inhibitor. Images showing mitochondrial staining (purple) and miRNA inhibitor coupled with FAM (green). Scale: 50 µm for all panels.*

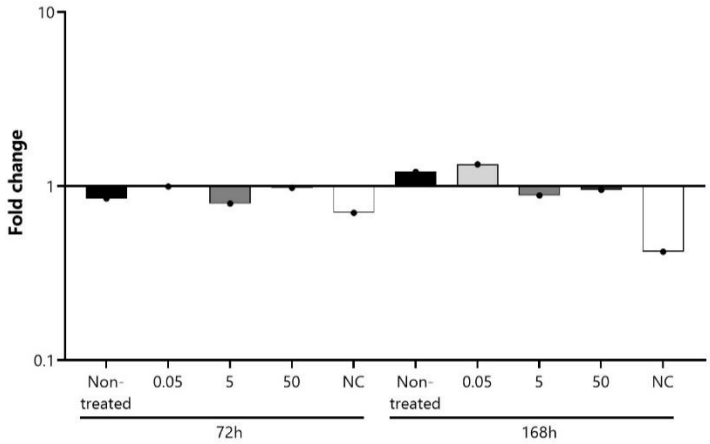

Supplementary Figure 30. ***Time-course fold change in the miR-30d-5p expression after mimic transfection.*** *Expression of miR-30d-5p was analyzed by single-assay RT-qPCR 72 and 168 hours after transfection with 0.05, 5 or 50 nM of miRNA mimic or 5 nM of the control mimic (negative control, NC). Basal transcription (complete medium-cultured HPSs) was used as the standard value. The miRNA expression signal was normalized to U6 expression. Values are expressed as* $2^{-\Delta\Delta Ct}$*. N=1 pancreas, hence no error bars.*

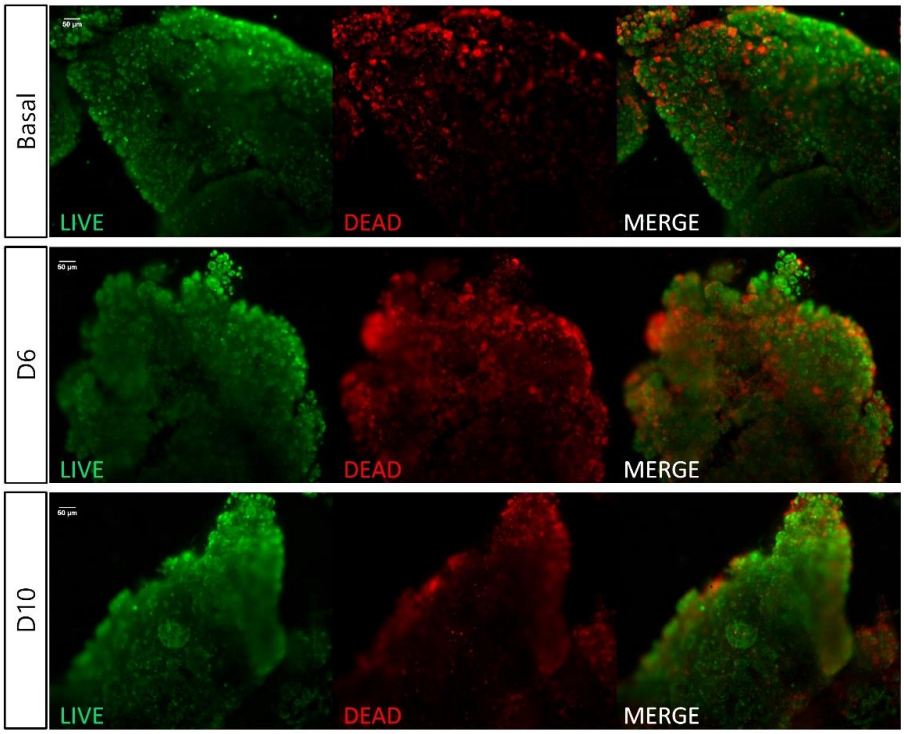

Supplementary Figure 31. ***Human pancreatic slices viability over time.*** *Representative immunostaining showing tissue viability at the time of tissue slicing (basal), and at days 6 and 10 of culture. Images showing live (green) and dead (red) regions. Scale: 50 µm for all panels.*

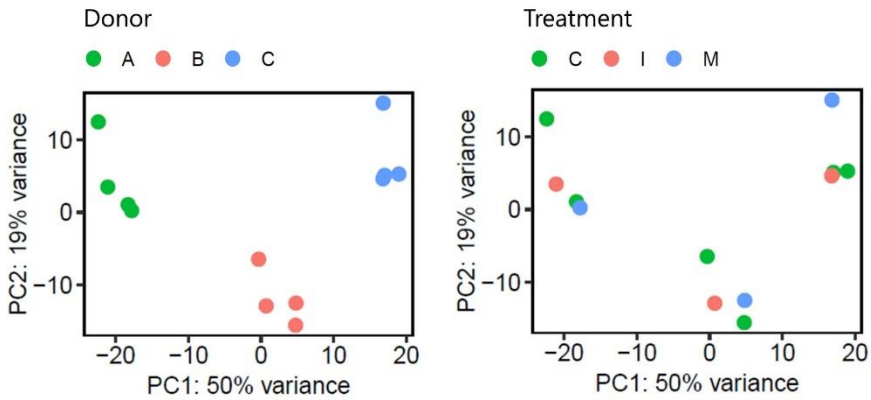

Supplementary Figure 32. ***Principal component analysis before correcting for the batch effect.*** *The first PCA (left) shows the variance explained by the donor variable (donor A, donor B and donor C) and the second (right) by the treatment variable (I for inhibitor, M for mimic, and C for control mimic and control inhibitor).*

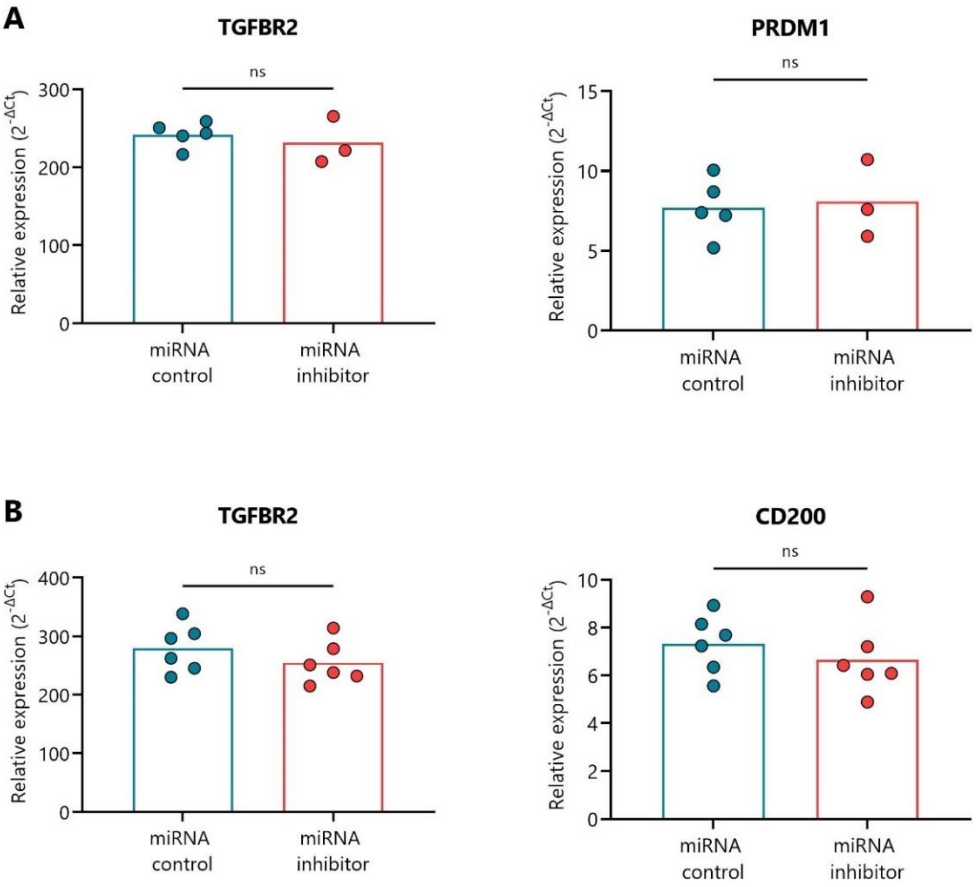

Supplementary Figure 33. ***Gene expression levels of TGFBR2, PRDM1, and CD200. (A)*** *Levels of TGFBR2 and PRDM1 mRNAs on the remaining PLN cells of mice treated with a control inhibitor (n=5, left, blue) or the miR-30d-5p inhibitor (n=3, right, red).* ***(B)*** *Levels of TGFBR2 and CD200 mRNAs on the remaining splenocytes of mice treated with a control inhibitor (n=6, left, blue) or the miR-30d-5p inhibitor (n=6, right, red). Gene expression signal was normalized to GAPDH expression. Values are expressed as* $2^{-\Delta Ct}$*. Data are presented as mean ± SD. Significant differences were not found between groups.*

REFERENCES

1. Katsarou, A. *et al.* (2017) Type 1 diabetes mellitus. *Nat Rev Dis Primers* 3, 17016

2. Da Silva Xavier, G. (2018) The Cells of the Islets of Langerhans. *J Clin Med* 7

3. Mobasseri, M. *et al.* (2020) Prevalence and incidence of type 1 diabetes in the world: a systematic review and meta-analysis. *Health Promot Perspect* 10, 98–115

4. Gregory, G.A. *et al.* (2022) Global incidence, prevalence, and mortality of type 1 diabetes in 2021 with projection to 2040: a modelling study. *Lancet Diabetes Endocrinol* 10, 741–760

5. Patterson, C.C. *et al.* (2019) Worldwide estimates of incidence, prevalence and mortality of type 1 diabetes in children and adolescents: Results from the International Diabetes Federation Diabetes Atlas, 9th edition. *Diabetes Res Clin Pract* 157, 107842

6. Ward, Z.J. *et al.* (2022) Estimating the total incidence of type 1 diabetes in children and adolescents aged 0–19 years from 1990 to 2050: a global simulation-based analysis. *Lancet Diabetes Endocrinol* 10, 848–858

7. Saeedi, P. *et al.* (2019) Global and regional diabetes prevalence estimates for 2019 and projections for 2030 and 2045: Results from the International Diabetes Federation Diabetes Atlas, 9th edition. *Diabetes Res Clin Pract* 157, 107843

8. Chobot, A. *et al.* (2017) Updated 24-year trend of Type 1 diabetes incidence in children in Poland reveals a sinusoidal pattern and sustained increase. *Diabetic Medicine* 34, 1252–1258

9. Diaz-Valencia, P.A. *et al.* (2015) Global epidemiology of type 1 diabetes in young adults and adults: a systematic review. *BMC Public Health* 15, 255

10. Rogers, M.A.M. *et al.* (2017) Fluctuations in the incidence of type 1 diabetes in the United States from 2001 to 2015: a longitudinal study. *BMC Med* 15, 199

11. Sun, H. *et al.* (2022) IDF Diabetes Atlas: Global, regional and country-level diabetes prevalence estimates for 2021 and projections for 2045. *Diabetes Res Clin Pract* 183, 109119

12. Ortiz-Marrón, H. *et al.* (2021) Evolution of the incidence of type 1 diabetes mellitus in the Community of Madrid, 1997–2016. *Anales de Pediatría (English Edition)* 95, 253–259

13. Flier, J.S. *et al.* (1986) Type I Diabetes Mellitus. *New England Journal of Medicine* 314, 1360–1368

14. Couper, J.J. *et al.* (2018) ISPAD Clinical Practice Consensus Guidelines 2018: Stages of type 1 diabetes in children and adolescents. *Pediatr Diabetes* 19, 20–27

15. Insel, R.A. *et al.* (2015) Staging Presymptomatic Type 1 Diabetes: A Scientific Statement of JDRF, the Endocrine Society, and the American Diabetes Association. *Diabetes Care* 38, 1964–1974

16. 2. Classification and Diagnosis of Diabetes: Standards of Medical Care in Diabetes—2022. *Diabetes Care* 45, S17–S38

17. Ziegler, A.G. *et al.* (2013) Seroconversion to Multiple Islet Autoantibodies and Risk of Progression to Diabetes in Children. *JAMA* 309, 2473

18. Bloem, S.J. and Roep, B.O. (2017) The elusive role of B lymphocytes and islet autoantibodies in (human) type 1 diabetes. *Diabetologia* 60, 1185–1189

19. Warncke, K. *et al.* (2022) Elevations in blood glucose before and after the appearance of islet autoantibodies in children. *Journal of Clinical Investigation* 132

20. Roep, B.O. *et al.* (2021) Type 1 diabetes mellitus as a disease of the β-cell (do not blame the immune system?). *Nat Rev Endocrinol* 17, 150–161

21. Newby, B.N. and Mathews, C.E. (2017) Type I Interferon Is a Catastrophic Feature of the Diabetic Islet Microenvironment. *Front Endocrinol (Lausanne)* 8

22. Atkinson, M.A. *et al.* (2011) How Does Type 1 Diabetes Develop? *Diabetes* 60, 1370–1379

23. Leete, P. *et al.* (2016) Differential Insulitic Profiles Determine the Extent of β-Cell Destruction and the Age at Onset of Type 1 Diabetes. *Diabetes* 65, 1362–1369

24. Jensen, E.T. *et al.* (2021) Increase in Prevalence of Diabetic Ketoacidosis at Diagnosis Among Youth With Type 1 Diabetes: The SEARCH for Diabetes in Youth Study. *Diabetes Care* 44, 1573–1578

25. Gomez-Muñoz, L. *et al.* (2024) Immunometabolic biomarkers for partial remission in type 1 diabetes mellitus. *Trends in Endocrinology & Metabolism* 35, 151–163

26. Jones, A.G. and Hattersley, A.T. (2013) The clinical utility of C-peptide measurement in the care of patients with diabetes. *Diabetic Medicine* 30, 803–817

27. Ilonen, J. *et al.* (2013) Patterns of β-Cell Autoantibody Appearance and Genetic Associations During the First Years of Life. *Diabetes* 62, 3636–3640

28. Battaglia, M. *et al.* (2020) Introducing the Endotype Concept to Address the Challenge of Disease Heterogeneity in Type 1 Diabetes. *Diabetes Care* 43, 5–12

29. Redondo, M.J. and Morgan, N.G. (2023) Heterogeneity and endotypes in type 1 diabetes mellitus. *Nat Rev Endocrinol* 19, 542–554

30. Campbell-Thompson, M.L. *et al.* (2013) The diagnosis of insulitis in human type 1 diabetes. *Diabetologia* 56, 2541–2543

31. Leete, P. *et al.* (2020) Studies of insulin and proinsulin in pancreas and serum support the existence of aetiopathological endotypes of type 1 diabetes associated with age at diagnosis. *Diabetologia* 63, 1258–1267

32. Arif, S. *et al.* (2014) Blood and Islet Phenotypes Indicate Immunological Heterogeneity in Type 1 Diabetes. *Diabetes* 63, 3835–3845

33. Garcia-Prat, M. *et al.* (2019) Extended immunophenotyping reference values in a healthy pediatric population. *Cytometry B Clin Cytom* 96, 223–233

34. Donath, M.Y. (2022) Type 1 diabetes: what is the role of autoimmunity in β cell death? *Journal of Clinical Investigation* 132

35. Nederstigt, C. *et al.* (2019) Associated auto-immune disease in type 1 diabetes patients: a systematic review and meta-analysis. *Eur J Endocrinol* 180, 135–144

36. Biondi, B. *et al.* (2019) Thyroid Dysfunction and Diabetes Mellitus: Two Closely Associated Disorders. *Endocr Rev* 40, 789–824

37. Keenan, H.A. *et al.* (2010) Residual Insulin Production and Pancreatic β-Cell Turnover After 50 Years of Diabetes: Joslin Medalist Study. *Diabetes* 59, 2846–2853

38. Hao, W. *et al.* (2016) Fall in C-Peptide During First 4 Years From Diagnosis of Type 1 Diabetes: Variable Relation to Age, HbA1c, and Insulin Dose. *Diabetes Care* 39, 1664–1670

39. Barker, A. *et al.* (2014) Age-dependent decline of β-cell function in type 1 diabetes after diagnosis: a multi-centre longitudinal study. *Diabetes Obes Metab* 16, 262–267

40. Campbell-Thompson, M.L. *et al.* (2016) The influence of type 1 diabetes on pancreatic weight. *Diabetologia* 59, 217–221

41. Wright, J.J. *et al.* (2020) Decreased pancreatic acinar cell number in type 1 diabetes. *Diabetologia* 63, 1418–1423

42. Lam, A. *et al.* (2021) A little help from residual β cells has long-lasting clinical benefits. *Journal of Clinical Investigation* 131

43. Gibb, F.W. *et al.* (2020) Preserved C-peptide secretion is associated with fewer low-glucose events and lower glucose variability on flash glucose monitoring in adults with type 1 diabetes. *Diabetologia* 63, 906–914

44. Willcox, A. *et al.* (2010) Evidence of increased islet cell proliferation in patients with recent-onset type 1 diabetes. *Diabetologia* 53, 2020–2028

45. von Herrath, M. *et al.* (2007) Type 1 diabetes as a relapsing–remitting disease? *Nat Rev Immunol* 7, 988–994

46. Leete, P. *et al.* (2018) The Effect of Age on the Progression and Severity of Type 1 Diabetes: Potential Effects on Disease Mechanisms. *Curr Diab Rep* 18, 115

47. Redondo, M.J. *et al.* (2008) Concordance for Islet Autoimmunity among Monozygotic Twins. *New England Journal of Medicine* 359, 2849–2850

48. Redondo, M.J. *et al.* (2001) Heterogeneity of Type I diabetes: analysis of monozygotic twins in Great Britain and the United States. *Diabetologia* 44, 354–362

49. Bonifacio, E. and Ziegler, A.G. (2010) Advances in the Prediction and Natural History of Type 1 Diabetes. *Endocrinol Metab Clin North Am* 39, 513–525

50. Steck, A.K. and Rewers, M.J. (2011) Genetics of type 1 diabetes. *Clin Chem* 57, 176–85

51. Noble, J.A. and Valdes, A.M. (2011) Genetics of the HLA Region in the Prediction of Type 1 Diabetes. *Curr Diab Rep* 11, 533–542

52. Noble, J.A. (2015) Immunogenetics of type 1 diabetes: A comprehensive review. *J Autoimmun* 64, 101–112

53. Pugliese, A. *et al.* (2016) HLA-DRB1*15:01-DQA1*01:02-DQB1*06:02 Haplotype Protects Autoantibody-Positive Relatives From Type 1 Diabetes Throughout the Stages of Disease Progression. *Diabetes* 65, 1109–19

54. Vafiadis, P. *et al.* (1997) Insulin expression in human thymus is modulated by INS VNTR alleles at the IDDM2 locus. *Nat Genet* 15, 289–292

55. Pugliese, A. *et al.* (1997) The insulin gene is transcribed in the human thymus and transcription levels correlate with allelic variation at the INS VNTR-IDDM2 susceptibility locus for type 1 diabetes. *Nat Genet* 15, 293–297

56. Chu, X. *et al.* (2022) A genome-wide functional genomics approach uncovers genetic determinants of immune phenotypes in type 1 diabetes. *Elife* 11

57. Michalek, D.A. *et al.* (2024) A multi-ancestry genome-wide association study in type 1 diabetes. *Hum Mol Genet* 33, 958–968

58. Nyaga, D.M. *et al.* (2018) The genetic architecture of type 1 diabetes mellitus. *Mol Cell Endocrinol* 477, 70–80

59. Barrett, J.C. *et al.* (2009) Genome-wide association study and meta-analysis find that over 40 loci affect risk of type 1 diabetes. *Nat Genet* 41, 703–707

60. Grant, S.F.A. *et al.* (2009) Follow-Up Analysis of Genome-Wide Association Data Identifies Novel Loci for Type 1 Diabetes. *Diabetes* 58, 290–295

61. Rowshanravan, B. *et al.* (2018) CTLA-4: a moving target in immunotherapy. *Blood* 131, 58–67

62. Chiou, J. *et al.* (2021) Interpreting type 1 diabetes risk with genetics and single-cell epigenomics. *Nature* 594, 398–402

63. Herold, K.C. *et al.* (2024) The immunology of type 1 diabetes. *Nat Rev Immunol* 24, 435–451

64. Triolo, T.M. *et al.* (2019) Identical and Nonidentical Twins: Risk and Factors Involved in Development of Islet Autoimmunity and Type 1 Diabetes. *Diabetes Care* 42, 192–199

65. Xia, Y. *et al.* (2019) Incidence and trend of type 1 diabetes and the underlying environmental determinants. *Diabetes Metab Res Rev* 35

66. Tuomilehto, J. *et al.* (2020) Update on Worldwide Trends in Occurrence of Childhood Type 1 Diabetes in 2020. *Pediatr Endocrinol Rev* 17, 198–209

67. Berhan, Y. *et al.* (2011) Thirty Years of Prospective Nationwide Incidence of Childhood Type 1 Diabetes. *Diabetes* 60, 577–581

68. Oilinki, T. *et al.* (2012) Prevalence and characteristics of diabetes among Somali children and adolescents living in Helsinki, Finland. *Pediatr Diabetes* 13, 176–180

69. Söderström, U. *et al.* (2012) Being born in Sweden increases the risk for type 1 diabetes – a study of migration of children to Sweden as a natural experiment. *Acta Paediatr* 101, 73–77

70. Fourlanos, S. *et al.* (2008) The Rising Incidence of Type 1 Diabetes Is Accounted for by Cases With Lower-Risk Human Leukocyte Antigen Genotypes. *Diabetes Care* 31, 1546–1549

71. Redondo, M.J. *et al.* (2018) Genetics of type 1 diabetes. *Pediatr Diabetes* 19, 346–353

72. Op de Beeck, A. and Eizirik, D.L. (2016) Viral infections in type 1 diabetes mellitus — why the β cells? *Nat Rev Endocrinol* 12, 263–273

73. Dahlquist, G. (2006) Can we slow the rising incidence of childhood-onset autoimmune diabetes? The overload hypothesis. *Diabetologia* 49, 20–24

74. Rodriguez-Calvo, T. (2018) Enterovirus infection and type 1 diabetes: unraveling the crime scene. *Clin Exp Immunol* 195, 15–24

75. Green, J. *et al.* (2004) Coxsackie B virus serology and Type 1 diabetes mellitus: a systematic review of published case-control studies. *Diabetic Medicine* 21, 507–514

76. Oikarinen, S. *et al.* (2021) Characterisation of enterovirus RNA detected in the pancreas and other specimens of live patients with newly diagnosed type 1 diabetes in the DiViD study. *Diabetologia* 64, 2491–2501

77. Nekoua, M.P. *et al.* (2022) Persistent coxsackievirus B infection and pathogenesis of type 1 diabetes mellitus. *Nat Rev Endocrinol* 18, 503–516

78. Dotta, F. *et al.* (2007) Coxsackie B4 virus infection of β cells and natural killer cell insulitis in recent-onset type 1 diabetic patients. *Proceedings of the National Academy of Sciences* 104, 5115–5120

79. Richardson, S.J. *et al.* (2009) The prevalence of enteroviral capsid protein vp1 immunostaining in pancreatic islets in human type 1 diabetes. *Diabetologia* 52, 1143–1151

80. Honkanen, H. *et al.* (2017) Detection of enteroviruses in stools precedes islet autoimmunity by several months: possible evidence for slowly operating mechanisms in virus-induced autoimmunity. *Diabetologia* 60, 424–431

81. Honeyman, M.C. *et al.* (2010) Evidence for Molecular Mimicry between Human T Cell Epitopes in Rotavirus and Pancreatic Islet Autoantigens. *The Journal of Immunology* 184, 2204–2210

82. Stene, L.C. *et al.* (2010) Enterovirus Infection and Progression From Islet Autoimmunity to Type 1 Diabetes. *Diabetes* 59, 3174–3180

83. Vehik, K. *et al.* (2019) Prospective virome analyses in young children at increased genetic risk for type 1 diabetes. *Nat Med* 25, 1865–1872

84. Kondrashova, A. *et al.* (2013) The 'Hygiene hypothesis' and the sharp gradient in the incidence of autoimmune and allergic diseases between Russian Karelia and Finland. *APMIS* 121, 478–493

85. Zheng, D. *et al.* (2020) Interaction between microbiota and immunity in health and disease. *Cell Res* 30, 492–506

86. Rosell-Mases, E. *et al.* (2023) Mutual modulation of gut microbiota and the immune system in type 1 diabetes models. *Nat Commun* 14, 7770

87. Vatanen, T. *et al.* (2018) The human gut microbiome in early-onset type 1 diabetes from the TEDDY study. *Nature* 562, 589–594

88. Bélteky, M. *et al.* (2023) Infant gut microbiome composition correlated with type 1 diabetes acquisition in the general population: the ABIS study. *Diabetologia* 66, 1116–1128

89. Dedrick, S. *et al.* (2020) The Role of Gut Microbiota and Environmental Factors in Type 1 Diabetes Pathogenesis. *Front Endocrinol (Lausanne)* 11

90. Takahashi, D. *et al.* (2020) Microbiota-derived butyrate limits the autoimmune response by promoting the differentiation of follicular regulatory T cells. *EBioMedicine* 58, 102913

91. Furusawa, Y. *et al.* (2013) Commensal microbe-derived butyrate induces the differentiation of colonic regulatory T cells. *Nature* 504, 446–450

92. Rouxel, O. *et al.* (2017) Cytotoxic and regulatory roles of mucosal-associated invariant T cells in type 1 diabetes. *Nat Immunol* 18, 1321–1331

93. de Groot, P. *et al.* (2021) Faecal microbiota transplantation halts progression of human new-onset type 1 diabetes in a randomised controlled trial. *Gut* 70, 92–105

94. Russell, J.T. *et al.* (2019) Genetic risk for autoimmunity is associated with distinct changes in the human gut microbiome. *Nat Commun* 10, 3621

95. Paun, A. *et al.* (2019) Association of HLA-dependent islet autoimmunity with systemic antibody responses to intestinal commensal bacteria in children. *Sci Immunol* 4

96. Butalia, S. *et al.* (2016) Environmental Risk Factors and Type 1 Diabetes: Past, Present, and Future. *Can J Diabetes* 40, 586–593

97. Esposito, S. *et al.* (2019) Environmental Factors Associated With Type 1 Diabetes. *Front Endocrinol (Lausanne)* 10

98. Wang, Z. *et al.* (2017) Epigenetic Alterations in Cellular Immunity: New Insights into Autoimmune Diseases. *Cellular Physiology and Biochemistry* 41, 645–660

99. Chang, P. V *et al.* (2014) The microbial metabolite butyrate regulates intestinal macrophage function via histone deacetylase inhibition. *Proc Natl Acad Sci U S A* 111, 2247–52

100. Schübeler, D. (2015) Function and information content of DNA methylation. *Nature* 517, 321–326

101. Stefan, M. *et al.* (2014) DNA methylation profiles in type 1 diabetes twins point to strong epigenetic effects on etiology. *J Autoimmun* 50, 33–37

102. Paul, D.S. *et al.* (2016) Increased DNA methylation variability in type 1 diabetes across three immune effector cell types. *Nat Commun* 7, 13555

103. Belot, M.-P. *et al.* (2013) CpG Methylation Changes within the IL2RA Promoter in Type 1 Diabetes of Childhood Onset. *PLoS One* 8, e68093

104. Starskaia, I. *et al.* (2022) Early DNA methylation changes in children developing beta cell autoimmunity at a young age. *Diabetologia* 65, 844–860

105. Rakyan, V.K. *et al.* (2011) Identification of Type 1 Diabetes–Associated DNA Methylation Variable Positions That Precede Disease Diagnosis. *PLoS Genet* 7, e1002300

106. Johnson, R.K. *et al.* (2020) Longitudinal DNA methylation differences precede type 1 diabetes. *Sci Rep* 10, 3721

107. Rui, J. *et al.* (2016) Methylation of insulin DNA in response to proinflammatory cytokines during the progression of autoimmune diabetes in NOD mice. *Diabetologia* 59, 1021–1029

108. Miao, F. *et al.* (2008) Lymphocytes From Patients With Type 1 Diabetes Display a Distinct Profile of Chromatin Histone H3 Lysine 9 Dimethylation. *Diabetes* 57, 3189–3198

109. Ha, M. and Kim, V.N. (2014) Regulation of microRNA biogenesis. *Nat Rev Mol Cell Biol* 15, 509–524

110. Kozomara, A. *et al.* (2019) miRBase: from microRNA sequences to function. *Nucleic Acids Res* 47, D155–D162

111. Stavast, C. and Erkeland, S. (2019) The Non-Canonical Aspects of MicroRNAs: Many Roads to Gene Regulation. *Cells* 8, 1465

112. O'Brien, J. *et al.* (2018) Overview of MicroRNA Biogenesis, Mechanisms of Actions, and Circulation. *Front Endocrinol (Lausanne)* 9

113. Eulalio, A. *et al.* (2009) Deadenylation is a widespread effect of miRNA regulation. *RNA* 15, 21–32

114. Wang, X. (2014) Composition of seed sequence is a major determinant of microRNA targeting patterns. *Bioinformatics* 30, 1377–1383

115. Friedman, R.C. *et al.* (2009) Most mammalian mRNAs are conserved targets of microRNAs. *Genome Res* 19, 92–105

116. Brennecke, J. *et al.* (2005) Principles of MicroRNA–Target Recognition. *PLoS Biol* 3, e85

117. Guo, L. *et al.* (2014) Integrated evolutionary analysis of human miRNA gene clusters and families implicates evolutionary relationships. *Gene* 534, 24–32

118. Dwivedi, S. *et al.* (2019) MicroRNAs and Diseases: Promising Biomarkers for Diagnosis and Therapeutics. *Indian Journal of Clinical Biochemistry* 34, 243–245

119. Margaritis, K. *et al.* (2021) Micro-RNA Implications in Type-1 Diabetes Mellitus: A Review of Literature. *Int J Mol Sci* 22, 12165

120. Scherm, M.G. and Daniel, C. (2020) miRNA-Mediated Immune Regulation in Islet Autoimmunity and Type 1 Diabetes. *Front Endocrinol (Lausanne)* 11

121. Osmai, M. *et al.* (2016) MicroRNAs as regulators of beta-cell function and dysfunction. *Diabetes Metab Res Rev* 32, 334–349

122. Serr, I. *et al.* (2016) miRNA92a targets KLF2 and the phosphatase PTEN signaling to promote human T follicular helper precursors in T1D islet autoimmunity. *Proceedings of the National Academy of Sciences* 113

123. Serr, I. *et al.* (2018) A miRNA181a/NFAT5 axis links impaired T cell tolerance induction with autoimmune type 1 diabetes. *Sci Transl Med* 10

124. Scherm, M.G. *et al.* (2019) miRNA142-3p targets Tet2 and impairs Treg differentiation and stability in models of type 1 diabetes. *Nat Commun* 10, 5697

125. Zhang, Y. *et al.* (2016) MicroRNAs in CD4 + T cell subsets are markers of disease risk and T cell dysfunction in individuals at risk for type 1 diabetes. *J Autoimmun* 68, 52–61

126. Abuhatzira, L. *et al.* (2015) Multiple microRNAs within the 14q32 cluster target the mRNAs of major type 1 diabetes autoantigens IA-2, IA-2β, and GAD65. *FASEB J* 29, 4374–83

127. Li, Z. and Rana, T.M. (2014) Therapeutic targeting of microRNAs: current status and future challenges. *Nat Rev Drug Discov* 13, 622–638

128. Thomaidou, S. *et al.* (2020) β-Cell Stress Shapes CTL Immune Recognition of Preproinsulin Signal Peptide by Posttranscriptional Regulation of Endoplasmic Reticulum Aminopeptidase 1. *Diabetes* 69, 670–680

129. Sims, E.K. *et al.* (2017) MicroRNA 21 targets BCL2 mRNA to increase apoptosis in rat and human beta cells. *Diabetologia* 60, 1057–1065

130. Roggli, E. *et al.* (2012) Changes in MicroRNA Expression Contribute to Pancreatic β-Cell Dysfunction in Prediabetic NOD Mice. *Diabetes* 61, 1742–1751

131. Krishnan, P. *et al.* (2024) miR-146a-5p mediates inflammation-induced β cell mitochondrial dysfunction and apoptosis. *bioRxiv* 2024.03.18.585543

132. Syed, F. *et al.* (2023) β Cell microRNAs Function as Molecular Hubs of Type 1 Diabetes Pathogenesis and as Biomarkers of Diabetes Risk. *bioRxiv* 2023.06.15.545170

133. Zheng, Y. *et al.* (2015) miR-101a and miR-30b contribute to inflammatory cytokine-mediated β-cell dysfunction. *Laboratory Investigation* 95, 1387–1397

134. Erener, S. *et al.* (2013) Circulating miR-375 as a Biomarker of β-Cell Death and Diabetes in Mice. *Endocrinology* 154, 603–608

135. Garavelli, S. *et al.* (2020) Plasma circulating miR-23~27~24 clusters correlate with the immunometabolic derangement and predict C-peptide loss in children with type 1 diabetes. *Diabetologia* 63, 2699–2712

136. Nielsen, L.B. *et al.* (2012) Circulating Levels of MicroRNA from Children with Newly Diagnosed Type 1 Diabetes and Healthy Controls: Evidence That miR-25 Associates to Residual Beta-Cell Function and Glycaemic Control during Disease Progression. *Exp Diabetes Res* 2012, 1–7

137. Assmann, T.S. *et al.* (2018) MicroRNA expression profile in plasma from type 1 diabetic patients: Case-control study and bioinformatic analysis. *Diabetes Res Clin Pract* 141, 35–46

138. Salas-Pérez, F. *et al.* (2013) MicroRNAs miR-21a and miR-93 are down regulated in peripheral blood mononuclear cells (PBMCs) from patients with type 1 diabetes. *Immunobiology* 218, 733–7

139. Garavelli, S. *et al.* (2020) Blood Co-Circulating Extracellular microRNAs and Immune Cell Subsets Associate with Type 1 Diabetes Severity. *Int J Mol Sci* 21

140. Erener, S. *et al.* (2017) Profiling of circulating microRNAs in children with recent onset of type 1 diabetes. *JCI Insight* 2, e89656

141. Samandari, N. *et al.* (2018) Influence of Disease Duration on Circulating Levels of miRNAs in Children and Adolescents with New Onset Type 1 Diabetes. *Noncoding RNA* 4, 35

142. Culina, S. *et al.* (2018) Islet-reactive CD8+ T cell frequencies in the pancreas, but not in blood, distinguish type 1 diabetic patients from healthy donors. *Sci Immunol* 3

143. Bettini, M. and Bettini, M.L. (2021) Function, Failure, and the Future Potential of Tregs in Type 1 Diabetes. *Diabetes* 70, 1211–1219

144. Zamani, M.R. *et al.* (2016) PD-1/PD-L and autoimmunity: A growing relationship. *Cell Immunol* 310, 27–41

145. McClymont, S.A. *et al.* (2011) Plasticity of Human Regulatory T Cells in Healthy Subjects and Patients with Type 1 Diabetes. *The Journal of Immunology* 186, 3918–3926

146. Lindley, S. *et al.* (2005) Defective suppressor function in CD4(+)CD25(+) T-cells from patients with type 1 diabetes. *Diabetes* 54, 92–9

147. Long, S.A. *et al.* (2010) Defects in IL-2R signaling contribute to diminished maintenance of FOXP3 expression in CD4(+)CD25(+) regulatory T-cells of type 1 diabetic subjects. *Diabetes* 59, 407–15

148. Butte, M.J. *et al.* (2007) Programmed Death-1 Ligand 1 Interacts Specifically with the B7-1 Costimulatory Molecule to Inhibit T Cell Responses. *Immunity* 27, 111–122

149. Jiang, T.T. *et al.* (2016) Programmed Death-1 Culls Peripheral Accumulation of High-Affinity Autoreactive CD4 T Cells to Protect against Autoimmunity. *Cell Rep* 17, 1783–1794

150. Yu, W. *et al.* (2020) PD-L1 promotes tumor growth and progression by activating WIP and β-catenin signaling pathways and predicts poor prognosis in lung cancer. *Cell Death Dis* 11, 506

151. Juneja, V.R. *et al.* (2017) PD-L1 on tumor cells is sufficient for immune evasion in immunogenic tumors and inhibits CD8 T cell cytotoxicity. *Journal of Experimental Medicine* 214, 895–904

152. Zhao, B. *et al.* (2020) Efficacy of PD-1/PD-L1 blockade monotherapy in clinical trials. *Ther Adv Med Oncol* 12, 175883592093761

153. Mourad, D. *et al.* (2021) Immune Checkpoint Inhibitor-Induced Diabetes Mellitus: Potential Role of T Cells in the Underlying Mechanism. *Int J Mol Sci* 22, 2093

154. Scherm, M.G. *et al.* (2022) Beta cell and immune cell interactions in autoimmune type 1 diabetes: How they meet and talk to each other. *Mol Metab* 64, 101565

155. Bottazzo, G.F. (1986) Death of a Beta Cell: Homicide or Suicide? *Diabetic Medicine* 3, 119–130

156. Mallone, R. and Eizirik, D.L. (2020) Presumption of innocence for beta cells: why are they vulnerable autoimmune targets in type 1 diabetes? *Diabetologia* 63, 1999–2006

157. Kracht, M.J.L. *et al.* (2017) Autoimmunity against a defective ribosomal insulin gene product in type 1 diabetes. *Nat Med* 23, 501–507

158. McLaughlin, R.J. *et al.* (2016) Human islets and dendritic cells generate post-translationally modified islet autoantigens. *Clin Exp Immunol* 185, 133–140

159. Delong, T. *et al.* (2016) Pathogenic CD4 T cells in type 1 diabetes recognize epitopes formed by peptide fusion. *Science (1979)* 351, 711–714

160. Hutton, J.C. and Davidson, H.W. (2010) Cytokine-Induced Dicing and Splicing in the β-Cell and the Immune Response in Type 1 Diabetes. *Diabetes* 59, 335–336

161. Baker, R.L. *et al.* (2019) Hybrid Insulin Peptides Are Autoantigens in Type 1 Diabetes. *Diabetes* 68, 1830–1840

162. Moore, F. *et al.* (2011) STAT1 Is a Master Regulator of Pancreatic β-Cell Apoptosis and Islet Inflammation. *Journal of Biological Chemistry* 286, 929–941

163. Liang, R. *et al.* (2021) Cytohistologic analyses of β cell dedifferentiation induced by inflammation in human islets. *Eur J Inflamm* 19, 205873922110144

164. Ramos-Rodríguez, M. *et al.* (2019) The impact of proinflammatory cytokines on the β-cell regulatory landscape provides insights into the genetics of type 1 diabetes. *Nat Genet* 51, 1588–1595

165. Chen, J. *et al.* (2018) Mitochondrial Reactive Oxygen Species and Type 1 Diabetes. *Antioxid Redox Signal* 29, 1361–1372

166. Marhfour, I. *et al.* (2012) Expression of endoplasmic reticulum stress markers in the islets of patients with type 1 diabetes. *Diabetologia* 55, 2417–2420

167. Meyerovich, K. *et al.* (2016) Endoplasmic reticulum stress and the unfolded protein response in pancreatic islet inflammation. *J Mol Endocrinol* 57, R1–R17

168. Sahin, G.S. *et al.* (2021) An accomplice more than a mere victim: The impact of β-cell ER stress on type 1 diabetes pathogenesis. *Mol Metab* 54, 101365

169. Thompson, P.J. *et al.* (2019) Targeted Elimination of Senescent Beta Cells Prevents Type 1 Diabetes. *Cell Metab* 29, 1045-1060.e10

170. Richardson, S.J. *et al.* (2016) Islet cell hyperexpression of HLA class I antigens: a defining feature in type 1 diabetes. *Diabetologia* 59, 2448–2458

171. Quesada-Masachs, E. *et al.* (2022) Upregulation of HLA class II in pancreatic beta cells from organ donors with type 1 diabetes. *Diabetologia* 65, 387–401

172. Roep, B.O. *et al.* (2010) Islet inflammation and CXCL10 in recent-onset type 1 diabetes. *Clin Exp Immunol* 159, 338–343

173. Mohan, J.F. *et al.* (2017) Imaging the emergence and natural progression of spontaneous autoimmune diabetes. *Proceedings of the National Academy of Sciences* 114

174. Damond, N. *et al.* (2019) A Map of Human Type 1 Diabetes Progression by Imaging Mass Cytometry. *Cell Metab* 29, 755-768.e5

175. Babon, J.A.B. *et al.* (2016) Analysis of self-antigen specificity of islet-infiltrating T cells from human donors with type 1 diabetes. *Nat Med* 22, 1482–1487

176. Cerosaletti, K. *et al.* (2017) Single-Cell RNA Sequencing Reveals Expanded Clones of Islet Antigen-Reactive CD4+ T Cells in Peripheral Blood of Subjects with Type 1 Diabetes. *The Journal of Immunology* 199, 323–335

177. Anderson, A.M. *et al.* (2021) Human islet T cells are highly reactive to preproinsulin in type 1 diabetes. *Proceedings of the National Academy of Sciences* 118

178. Skowera, A. *et al.* (2008) CTLs are targeted to kill β cells in patients with type 1 diabetes through recognition of a glucose-regulated preproinsulin epitope. *Journal of Clinical Investigation* 118(10), 3390-402

179. Bender, C. *et al.* (2020) The healthy exocrine pancreas contains preproinsulin-specific CD8 T cells that attack islets in type 1 diabetes. *Sci Adv* 6

180. Cosentino, C. and Regazzi, R. (2021) Crosstalk between Macrophages and Pancreatic β-Cells in Islet Development, Homeostasis and Disease. *Int J Mol Sci* 22

181. Rodriguez-Calvo, T. *et al.* (2021) Neoepitopes in Type 1 Diabetes: Etiological Insights, Biomarkers and Therapeutic Targets. *Front Immunol* 12

182. Mukherjee, R. *et al.* (2015) Non-Classical monocytes display inflammatory features: Validation in Sepsis and Systemic Lupus Erythematous. *Sci Rep* 5, 13886

183. Thornley, T.B. *et al.* (2016) Contrasting Roles of Islet Resident Immunoregulatory Macrophages and Dendritic Cells in Experimental Autoimmune Type 1 Diabetes. *PLoS One* 11, e0150792

184. Wang, Y.J. *et al.* (2019) Multiplexed In Situ Imaging Mass Cytometry Analysis of the Human Endocrine Pancreas and Immune System in Type 1 Diabetes. *Cell Metab* 29, 769-783.e4

185. Uno, S. *et al.* (2007) Macrophages and dendritic cells infiltrating islets with or without beta cells produce tumour necrosis factor-α in patients with recent-onset type 1 diabetes. *Diabetologia* 50, 596–601

186. Ortis, F. *et al.* (2012) Differential usage of NF-κB activating signals by IL-1β and TNF-α in pancreatic beta cells. *FEBS Lett* 586, 984–989

187. Ortis, F. *et al.* (2008) Induction of nuclear factor-κB and its downstream genes by TNF-α and IL-1β has a pro-apoptotic role in pancreatic beta cells. *Diabetologia* 51, 1213–1225

188. Vomund, A.N. *et al.* (2015) Beta cells transfer vesicles containing insulin to phagocytes for presentation to T cells. *Proceedings of the National Academy of Sciences* 112

189. Walker, L.S.K. and von Herrath, M. (2015) CD4 T cell differentiation in type 1 diabetes. *Clin Exp Immunol* 183, 16–29

190. Sandor, A.M. *et al.* (2019) Immune cell trafficking to the islets during type 1 diabetes. *Clin Exp Immunol* 198, 314–325

191. Arif, S. *et al.* (2011) Peripheral and Islet Interleukin-17 Pathway Activation Characterizes Human Autoimmune Diabetes and Promotes Cytokine-Mediated β-Cell Death. *Diabetes* 60, 2112–2119

192. Ferraro, A. *et al.* (2011) Expansion of Th17 Cells and Functional Defects in T Regulatory Cells Are Key Features of the Pancreatic Lymph Nodes in Patients With Type 1 Diabetes. *Diabetes* 60, 2903–2913

193. Ferreira, R.C. *et al.* (2015) IL-21 production by CD4+ effector T cells and frequency of circulating follicular helper T cells are increased in type 1 diabetes patients. *Diabetologia* 58, 781–790

194. Martinov, T. *et al.* (2019) Programmed Death-1 Restrains the Germinal Center in Type 1 Diabetes. *The Journal of Immunology* 203, 844–852

195. Knight, R.R. *et al.* (2013) Human β-Cell Killing by Autoreactive Preproinsulin-Specific CD8 T Cells Is Predominantly Granule-Mediated With the Potency Dependent Upon T-Cell Receptor Avidity. *Diabetes* 62, 205–213

196. Chee, J. *et al.* (2014) Effector-Memory T Cells Develop in Islets and Report Islet Pathology in Type 1 Diabetes. *The Journal of Immunology* 192, 572–580

197. Radenkovic, M. *et al.* (2017) Characterization of resident lymphocytes in human pancreatic islets. *Clin Exp Immunol* 187, 418–427

198. Abdelsamed, H.A. *et al.* (2020) Beta cell-specific CD8+ T cells maintain stem cell memory-associated epigenetic programs during type 1 diabetes. *Nat Immunol* 21, 578–587

199. Gearty, S. V. *et al.* (2022) An autoimmune stem-like CD8 T cell population drives type 1 diabetes. *Nature* 602, 156–161

200. Smith, M.J. *et al.* (2018) Loss of B-Cell Anergy in Type 1 Diabetes Is Associated With High-Risk HLA and Non-HLA Disease Susceptibility Alleles. *Diabetes* 67, 697–703

201. Menard, L. *et al.* (2011) The PTPN22 allele encoding an R620W variant interferes with the removal of developing autoreactive B cells in humans. *J Clin Invest* 121, 3635–44

202. Christie, M.R. (2016) Delving Into the Type 1 Diabetic Islet: Evidence That B-Cell Infiltration of Islets Is Linked to Local Hyperimmunity and Accelerated Progression to Disease. *Diabetes* 65, 1146–1148

203. Mariño, E. *et al.* (2012) B-Cell Cross-Presentation of Autologous Antigen Precipitates Diabetes. *Diabetes* 61, 2893–2905

204. Hu, C. *et al.* (2007) Treatment with CD20-specific antibody prevents and reverses autoimmune diabetes in mice. *Journal of Clinical Investigation* 117, 3857–3867

205. Dufort, M.J. *et al.* (2019) Cell type-specific immune phenotypes predict loss of insulin secretion in new-onset type 1 diabetes. *JCI Insight* 4

206. Pescovitz, M.D. *et al.* (2014) B-Lymphocyte Depletion With Rituximab and β-Cell Function: Two-Year Results. *Diabetes Care* 37, 453–459

207. Linsley, P.S. *et al.* (2019) Elevated T cell levels in peripheral blood predict poor clinical response following rituximab treatment in new-onset type 1 diabetes. *Genes Immun* 20, 293–307

208. de Boer, P. *et al.* (2020) Large-scale electron microscopy database for human type 1 diabetes. *Nat Commun* 11, 2475

209. Vecchio, F. *et al.* (2018) Abnormal neutrophil signature in the blood and pancreas of presymptomatic and symptomatic type 1 diabetes. *JCI Insight* 3

210. Diana, J. *et al.* (2013) Crosstalk between neutrophils, B-1a cells and plasmacytoid dendritic cells initiates autoimmune diabetes. *Nat Med* 19, 65–73

211. Apaolaza, P.S. *et al.* (2021) Islet expression of type I interferon response sensors is associated with immune infiltration and viral infection in type 1 diabetes. *Sci Adv* 7

212. Marroqui, L. *et al.* (2017) Interferon-α mediates human beta cell HLA class I overexpression, endoplasmic reticulum stress and apoptosis, three hallmarks of early human type 1 diabetes. *Diabetologia* 60, 656–667

213. Gur, C. *et al.* (2010) The activating receptor NKp46 is essential for the development of type 1 diabetes. *Nat Immunol* 11, 121–128

214. Poirot, L. *et al.* (2004) Natural killer cells distinguish innocuous and destructive forms of pancreatic islet autoimmunity. *Proc Natl Acad Sci U S A* 101, 8102–7

215. Alba, A. *et al.* (2008) Natural killer cells are required for accelerated type 1 diabetes driven by interferon-β. *Clin Exp Immunol* 151, 467–475

216. Perricone, R. *et al.* (2008) NK cells in autoimmunity: A two-edg'd weapon of the immune system. *Autoimmun Rev* 7, 384–390

217. Sabetkam, S. *et al.* (2023) The dysfunction of natural killer cells is essential for the development of type 1 diabetes. *Pathol Res Pract* 247, 154556

218. Genuth, S. (2006) Insights from The Diabetes Control and Complications Trial/Epidemiology of Diabetes Interventions and Complications Study on The Use of Intensive Glycemic Treatment to Reduce The Risk of Complications of Type 1 Diabetes. *Endocrine Practice* 12, 34–41

219. Brown, S.A. *et al.* (2019) Six-Month Randomized, Multicenter Trial of Closed-Loop Control in Type 1 Diabetes. *New England Journal of Medicine* 381, 1707–1717

220. Stiller, C.R. *et al.* (1984) Effects of Cyclosporine Immunosuppression in Insulin-Dependent Diabetes Mellitus of Recent Onset. *Science (1979)* 223, 1362–1367

221. Mastrandrea, L. *et al.* (2009) Etanercept Treatment in Children With New-Onset Type 1 Diabetes. *Diabetes Care* 32, 1244–1249

222. Rosenzwajg, M. *et al.* (2015) Low-dose interleukin-2 fosters a dose-dependent regulatory T cell tuned milieu in T1D patients. *J Autoimmun* 58, 48–58

223. Pescovitz, M.D. *et al.* (2009) Rituximab, B-Lymphocyte Depletion, and Preservation of Beta-Cell Function. *New England Journal of Medicine* 361, 2143–2152

224. Rigby, M.R. *et al.* (2015) Alefacept provides sustained clinical and immunological effects in new-onset type 1 diabetes patients. *Journal of Clinical Investigation* 125, 3285–3296

225. Orban, T. *et al.* (2014) Reduction in CD4 Central Memory T-Cell Subset in Costimulation Modulator Abatacept-Treated Patients With Recent-Onset Type 1 Diabetes Is Associated With Slower C-Peptide Decline. *Diabetes* 63, 3449–3457

226. Herold, K.C. *et al.* (2013) Teplizumab (Anti-CD3 mAb) Treatment Preserves C-Peptide Responses in Patients With New-Onset Type 1 Diabetes in a Randomized Controlled Trial. *Diabetes* 62, 3766–3774

227. Keymeulen, B. *et al.* (2010) Four-year metabolic outcome of a randomised controlled CD3-antibody trial in recent-onset type 1 diabetic patients depends on their age and baseline residual beta cell mass. *Diabetologia* 53, 614–623

228. von Herrath, M. *et al.* (2021) Anti-interleukin-21 antibody and liraglutide for the preservation of β-cell function in adults with recent-onset type 1 diabetes: a randomised, double-blind, placebo-controlled, phase 2 trial. *Lancet Diabetes Endocrinol* 9, 212–224

229. Velloso, L.A. (2023) The first immunotherapy for type 1 diabetes. *American Journal of Physiology-Endocrinology and Metabolism* 324, E185–E186

230. Bluestone, J.A. *et al.* (2015) Type 1 diabetes immunotherapy using polyclonal regulatory T cells. *Sci Transl Med* 7

231. Giannoukakis, N. *et al.* (2011) Phase I (Safety) Study of Autologous Tolerogenic Dendritic Cells in Type 1 Diabetic Patients. *Diabetes Care* 34, 2026–2032

232. de Groot, P. *et al.* (2021) Faecal microbiota transplantation halts progression of human new-onset type 1 diabetes in a randomised controlled trial. *Gut* 70, 92–105

233. Zala, A. and Thomas, R. (2023) Antigen-specific immunotherapy to restore antigen-specific tolerance in Type 1 diabetes and Graves' disease. *Clin Exp Immunol* 211, 164–175

234. Clemente-Casares, X. *et al.* (2016) Expanding antigen-specific regulatory networks to treat autoimmunity. *Nature* 530, 434–440

235. Almenara-Fuentes, L. *et al.* (2023) A new platform for autoimmune diseases. Inducing tolerance with liposomes encapsulating autoantigens. *Nanomedicine* 48, 102635

236. Lablanche, S. *et al.* (2015) Five-Year Metabolic, Functional, and Safety Results of Patients With Type 1 Diabetes Transplanted With Allogenic Islets Within the Swiss-French GRAGIL Network. *Diabetes Care* 38, 1714–1722

237. Qi, M. *et al.* (2014) Five-year follow-up of patients with type 1 diabetes transplanted with allogeneic islets: the UIC experience. *Acta Diabetol* 51, 833–843

238. Mullard, A. (2023) FDA approves first cell therapy for type 1 diabetes. *Nat Rev Drug Discov* 22, 611–611

239. Pagliuca, F.W. *et al.* (2014) Generation of Functional Human Pancreatic β Cells In Vitro. *Cell* 159, 428–439

240. Millman, J.R. *et al.* (2016) Generation of stem cell-derived β-cells from patients with type 1 diabetes. *Nat Commun* 7, 11463

241. Keymeulen, B. *et al.* (2023) Encapsulated stem cell–derived β cells exert glucose control in patients with type 1 diabetes. *Nat Biotechnol* 10.1038/s41587-023-02055-5

242. Gerace, D. *et al.* (2023) Engineering human stem cell-derived islets to evade immune rejection and promote localized immune tolerance. *Cell Rep Med* 4, 100879

243. Abdul-Rasoul, M. *et al.* (2006) "The honeymoon phase" in children with type 1 diabetes mellitus: frequency, duration, and influential factors. *Pediatr Diabetes* 7, 101–7

244. JACKSON, R.L. (1940) STABILIZATION OF THE DIABETIC CHILD. *Arch Pediatr Adolesc Med* 59, 332

245. Mayer-Davis, E.J. *et al.* (2018) ISPAD Clinical Practice Consensus Guidelines 2018: Definition, epidemiology, and classification of diabetes in children and adolescents. *Pediatr Diabetes* 19 Suppl 27, 7–19

246. Mortensen, H.B. *et al.* (2009) New definition for the partial remission period in children and adolescents with type 1 diabetes. *Diabetes Care* 32, 1384–90

247. Nagl, K. *et al.* (2017) Factors contributing to partial remission in type 1 diabetes: analysis based on the insulin dose-adjusted HbA1c in 3657 children and adolescents from Germany and Austria. *Pediatr Diabetes* 18, 428–434

248. Max Andersen, M.L.C. *et al.* (2014) Partial remission definition: validation based on the insulin dose-adjusted HbA1c (IDAA1C) in 129 Danish children with new-onset type 1 diabetes. *Pediatr Diabetes* 15, 469–76

249. Nwosu, B.U. (2022) Partial Clinical Remission of Type 1 Diabetes: The Need for an Integrated Functional Definition Based on Insulin-Dose Adjusted A1c and Insulin Sensitivity Score. *Front Endocrinol (Lausanne)* 13

250. Buchanan, K. *et al.* (2019) An improved clinical model to predict stimulated C-peptide in children with recent-onset type 1 diabetes. *Pediatr Diabetes* 20, 166–171

251. Passanisi, S. *et al.* (2020) Influence of Age on Partial Clinical Remission among Children with Newly Diagnosed Type 1 Diabetes. *Int J Environ Res Public Health* 17

252. Marino, K.R. *et al.* (2017) A predictive model for lack of partial clinical remission in new-onset pediatric type 1 diabetes. *PLoS One* 12, e0176860

253. Wong, T.W.C. *et al.* (2021) Features of partial remission in children with type 1 diabetes using the insulin dose-adjusted A1c definition and risk factors associated with nonremission. *Ann Pediatr Endocrinol Metab* 26, 118–125

254. de Vries, S.A.G. *et al.* (2023) Do sex differences in paediatric type 1 diabetes care exist? A systematic review. *Diabetologia* 66, 618–630

255. Podolakova, K. *et al.* (2023) Complete remission in children and adolescents with type 1 diabetes mellitus—prevalence and factors. *Sci Rep* 13, 6790

256. Zhong, T. *et al.* (2020) The remission phase in type 1 diabetes: Changing epidemiology, definitions, and emerging immuno-metabolic mechanisms. *Diabetes Metab Res Rev* 36(2):e3207

257. Moole, H. *et al.* (2015) Spontaneous complete remission of type 1 diabetes mellitus in an adult – review and case report. *J Community Hosp Intern Med Perspect* 5, 28709

258. Karges, B. *et al.* (2004) Complete long-term recovery of beta-cell function in autoimmune type 1 diabetes after insulin treatment. *Diabetes Care* 27, 1207–8

259. Murillo, M. *et al.* (2017) Sustained spontaneous partial remission in a pediatric patient with type 1 diabetes. *J Clin Transl Endocrinol Case Rep* 6, 11–13

260. Brown, R.J. and Rother, K.I. (2008) Effects of beta-cell rest on beta-cell function: a review of clinical and preclinical data. *Pediatr Diabetes* 9, 14–22

261. Fonolleda, M. *et al.* (2017) Remission Phase in Paediatric Type 1 Diabetes: New Understanding and Emerging Biomarkers. *Horm Res Paediatr* 88, 307–315

262. Aly, H. and Gottlieb, P. (2009) The honeymoon phase: intersection of metabolism and immunology. *Curr Opin Endocrinol Diabetes Obes* 16, 286–92

263. Li, X. *et al.* (2020) PD-1 and PD-L1 Expression in Peripheral CD4/CD8+ T Cells Is Restored in the Partial Remission Phase in Type 1 Diabetes. *J Clin Endocrinol Metab* 105, 1947–1956

264. Karges, B. *et al.* (2006) Immunological mechanisms associated with long-term remission of human type 1 diabetes. *Diabetes Metab Res Rev* 22, 184–9

265. Akirav, E. *et al.* (2008) β-Cell Mass and Type 1 Diabetes. *Diabetes* 57, 2883–2888

266. Rui, J. *et al.* (2017) β Cells that Resist Immunological Attack Develop during Progression of Autoimmune Diabetes in NOD Mice. *Cell Metab* 25, 727–738

267. Fasolino, M. *et al.* (2022) Single-cell multi-omics analysis of human pancreatic islets reveals novel cellular states in type 1 diabetes. *Nat Metab* 4, 284–299

268. Chen, C. *et al.* (2017) Human beta cell mass and function in diabetes: Recent advances in knowledge and technologies to understand disease pathogenesis. *Mol Metab* 6, 943–957

269. Doke, M. *et al.* (2023) Dynamic scRNA-seq of live human pancreatic slices reveals functional endocrine cell neogenesis through an intermediate ducto-acinar stage. *Cell Metab* 35, 1944-1960.e7

270. Tang, R. *et al.* (2019) The Remission Phase in Type 1 Diabetes: Role of Hyperglycemia Rectification in Immune Modulation. *Front Endocrinol (Lausanne)* 10, 824

271. Nwosu, B.U. *et al.* (2020) Mechanisms and early patterns of dyslipidemia in pediatric type 1 and type 2 diabetes. *J Pediatr Endocrinol Metab* 33, 1399–1408

272. Ozen, G. *et al.* (2020) The Association of Autoimmune Diseases with Type 1 Diabetes Mellitus in Children Depends Also by the Length of Partial Clinical Remission Phase (Honeymoon). *Int J Endocrinol* 2020, 2630827

273. Nwosu, B.U. *et al.* (2021) Partial Clinical Remission Reduces Lipid-Based Cardiovascular Risk in Adult Patients With Type 1 Diabetes. *Front Endocrinol (Lausanne)* 12

274. Jaberi-Douraki, M. *et al.* (2014) Predictive models of type 1 diabetes progression: understanding T-cell cycles and their implications on autoantibody release. *PLoS One* 9, e93326

275. Fyvie, M.J. and Gillespie, K.M. (2023) The importance of biomarker development for monitoring type 1 diabetes progression rate and therapeutic responsiveness. *Front Immunol* 14

276. Ziegler, A.G. *et al.* (2013) Seroconversion to Multiple Islet Autoantibodies and Risk of Progression to Diabetes in Children. *JAMA* 309, 2473

277. Kwon, B.C. *et al.* (2022) Progression of type 1 diabetes from latency to symptomatic disease is predicted by distinct autoimmune trajectories. *Nat Commun* 13, 1514

278. Krischer, J.P. *et al.* (2015) The 6 year incidence of diabetes-associated autoantibodies in genetically at-risk children: the TEDDY study. *Diabetologia* 58, 980–987

279. Parikka, V. *et al.* (2012) Early seroconversion and rapidly increasing autoantibody concentrations predict prepubertal manifestation of type 1 diabetes in children at genetic risk. *Diabetologia* 55(7), 1926-1936

280. Kallionpää, H. *et al.* (2014) Innate Immune Activity Is Detected Prior to Seroconversion in Children With HLA-Conferred Type 1 Diabetes Susceptibility. *Diabetes* 63, 2402–2414

281. Vecchione, A. *et al.* (2020) Reduced PD-1 expression on circulating follicular and conventional FOXP3+ Treg cells in children with new onset type 1 diabetes and autoantibody-positive at-risk children. *Clinical Immunology* 211, 108319

282. Starosz, A. *et al.* (2022) Immunological balance between Treg and Th17 lymphocytes as a key element of type 1 diabetes progression in children. *Front Immunol* 13

283. Glisic, S. and Jailwala, P. (2012) Interaction between Treg Apoptosis Pathways, Treg Function and HLA Risk Evolves during Type 1 Diabetes Pathogenesis. *PLoS One* 7, e36040

284. Snowhite, I. V. *et al.* (2017) Association of serum microRNAs with islet autoimmunity, disease progression and metabolic impairment in relatives at risk of type 1 diabetes. *Diabetologia* 60, 1409–1422

285. Brenu, E.W. *et al.* (2023) Circulating biomarkers during progression to type 1 diabetes: A systematic review. *Front Endocrinol (Lausanne)* 14

286. Sims, E.K. *et al.* (2016) Elevations in the Fasting Serum Proinsulin–to–C-Peptide Ratio Precede the Onset of Type 1 Diabetes. *Diabetes Care* 39, 1519–1526

287. Zhang, K. *et al.* (2017) Circulating unmethylated insulin DNA as a potential non-invasive biomarker of beta cell death in type 1 Diabetes: a review and future prospect. *Clin Epigenetics* 9, 44

288. Ferrat, L.A. *et al.* (2020) A combined risk score enhances prediction of type 1 diabetes among susceptible children. *Nat Med* 26, 1247–1255

289. Suomi, T. *et al.* (2023) Gene expression signature predicts rate of type 1 diabetes progression. *EBioMedicine* 92, 104625

290. Snowhite, I. *et al.* (2021) Baseline Assessment of Circulating MicroRNAs Near Diagnosis of Type 1 Diabetes Predicts Future Stimulated Insulin Secretion. *Diabetes* 70, 638–651

291. Zhong, T. *et al.* (2020) Frequency, clinical characteristics, and determinants of partial remission in type 1 diabetes: Different patterns in children and adults. *J Diabetes* 12, 761–768

292. Chobot, A. *et al.* (2019) Remission phase in children diagnosed with type 1 diabetes in years 2012 to 2013 in Silesia, Poland: An observational study. *Pediatr Diabetes* 20, 286–292

293. Narendran, P. *et al.* (2017) Exercise to preserve β-cell function in recent-onset Type 1 diabetes mellitus (EXTOD) - a randomized controlled pilot trial. *Diabet Med* 34, 1521–1531

294. Coomans de Brachène, A. *et al.* (2023) Exercise as a non-pharmacological intervention to protect pancreatic beta cells in individuals with type 1 and type 2 diabetes. *Diabetologia* 66, 450–460

295. Chetan, M.R. *et al.* (2019) The Type 1 diabetes "honeymoon" period is five times longer in men who exercise: a case-control study. *Diabet Med* 36, 127–128

296. Pfleger, C. *et al.* (2008) Association of IL-1ra and adiponectin with C-peptide and remission in patients with type 1 diabetes. *Diabetes* 57, 929–37

297. Alizadeh, B.Z. *et al.* (2006) Association of interferon-gamma and interleukin 10 genotypes and serum levels with partial clinical remission in type 1 diabetes. *Clin Exp Immunol* 145, 480–4

298. Sanda, S. *et al.* (2008) Islet antigen specific IL-10+ immune responses but not CD4+CD25+FoxP3+ cells at diagnosis predict glycemic control in type 1 diabetes. *Clin Immunol* 127, 138–43

299. Narsale, A. *et al.* (2021) CD4+CD25+CD127hi cell frequency predicts disease progression in type 1 diabetes. *JCI Insight* 6

300. Fitas, A.L. *et al.* (2018) Immune cell and cytokine patterns in children with type 1 diabetes mellitus undergoing a remission phase: A longitudinal study. *Pediatr Diabetes* 19, 963–971

301. Moya, R. *et al.* (2016) A pilot study showing associations between frequency of CD4(+) memory cell subsets at diagnosis and duration of partial remission in type 1 diabetes. *Clin Immunol* 166–167, 72–80

302. Glisic-Milosavljevic, S. *et al.* (2007) Dynamic changes in CD4+ CD25+(high) T cell apoptosis after the diagnosis of type 1 diabetes. *Clin Exp Immunol* 150, 75–82

303. Cabrera, S.M. *et al.* (2018) Innate immune activity as a predictor of persistent insulin secretion and association with responsiveness to CTLA4-Ig treatment in recent-onset type 1 diabetes. *Diabetologia* 61, 2356–2370

304. Musthaffa, Y. *et al.* (2021) Proinsulin-specific T-cell responses correlate with estimated c-peptide and predict partial remission duration in type 1 diabetes. *Clin Transl Immunology* 10, e1315

305. Nakayamada, S. and Tanaka, Y. (2023) Immune Phenotype as a Biomarker for Systemic Lupus Erythematosus. *Biomolecules* 13, 960

306. Pascual-García, S. *et al.* (2023) Analysis of Novel Immunological Biomarkers Related to Rheumatoid Arthritis Disease Severity. *Int J Mol Sci* 24, 12351

307. Teniente-Serra, A. *et al.* (2019) Distinct pattern of peripheral lymphocyte subsets in Graves' disease with persistency of anti-TSHR autoantibodies. *Autoimmunity* 52, 220–227

308. Priyadarssini, M. *et al.* (2016) Immunophenotyping of T cells in the peripheral circulation in psoriasis. *Br J Biomed Sci* 73, 174–179

309. Quirant-Sánchez, B. *et al.* (2018) Predicting therapeutic response to fingolimod treatment in multiple sclerosis patients. *CNS Neurosci Ther* 24, 1175–1184

310. Hedman, Å.K. *et al.* (2023) Peripheral blood cellular dynamics of rheumatoid arthritis treatment informs about efficacy of response to disease modifying drugs. *Sci Rep* 13, 10058

311. Hull, C.M. *et al.* (2017) Regulatory T cell dysfunction in type 1 diabetes: what's broken and how can we fix it? *Diabetologia* 60, 1839–1850

312. Villalba, A. *et al.* (2019) Partial remission and early stages of pediatric type 1 diabetes display immunoregulatory changes. A pilot study. *Transl Res* 210, 8–25

313. Kurozumi, A. *et al.* (2016) Pancreas-protective effect of rituximab for acute-onset type 1 diabetes in the honeymoon period: a case report. *Endocrinol Diabetes Metab Case Rep* 2016, 160020

314. Zieliński, M. *et al.* (2022) Combined therapy with CD4+ CD25highCD127- T regulatory cells and anti-CD20 antibody in recent-onset type 1 diabetes is superior to monotherapy: Randomized phase I/II trial. *Diabetes Obes Metab* 24, 1534–1543

315. Wiedeman, A.E. *et al.* (2020) Autoreactive CD8+ T cell exhaustion distinguishes subjects with slow type 1 diabetes progression. *J Clin Invest* 130, 480–490

316. Tucker, C.G. *et al.* (2021) The Role of Programmed Death-1 in Type 1 Diabetes. *Curr Diab Rep* 21, 20

317. Ansari, M.J.I. *et al.* (2003) The programmed death-1 (PD-1) pathway regulates autoimmune diabetes in nonobese diabetic (NOD) mice. *J Exp Med* 198, 63–9

318. Pfleger, C. *et al.* (2008) Relation of circulating concentrations of chemokine receptor CCR5 ligands to C-peptide, proinsulin and HbA1c and disease progression in type 1 diabetes. *Clin Immunol* 128, 57–65

319. MacIver, N.J. *et al.* (2013) Metabolic regulation of T lymphocytes. *Annu Rev Immunol* 31, 259–83

320. Tang, R. *et al.* (2022) Enhanced T Cell Glucose Uptake Is Associated With Progression of Beta-Cell Function in Type 1 Diabetes. *Front Immunol* 13

321. Sen, P. *et al.* (2020) Metabolic alterations in immune cells associate with progression to type 1 diabetes. *Diabetologia* 63, 1017–1031

322. Tang, R. *et al.* (2023) Recovery of intracellular glucose uptake in T cells during partial remission of type 1 diabetes. *Diabetologia* 66, 1532–1543

323. Shyer, J.A. *et al.* (2020) Metabolic signaling in T cells. *Cell Res* 30, 649–659

324. Martins, C.P. *et al.* (2021) Glycolysis Inhibition Induces Functional and Metabolic Exhaustion of CD4+ T Cells in Type 1 Diabetes. *Front Immunol* 12

325. Pinheiro, M.M. *et al.* (2016) Four-year clinical remission of type 1 diabetes mellitus in two patients treated with sitagliptin and vitamin D3. *Endocrinol Diabetes Metab Case Rep* 2016

326. Pinheiro, M.M. *et al.* (2023) Association between sitagliptin plus vitamin D3 (VIDPP-4i) use and clinical remission in patients with new-onset type 1 diabetes: a retrospective case-control study. *Arch Endocrinol Metab* 67, e000652

327. Pinheiro, M.M. *et al.* (2017) Sitagliptin inhibit human lymphocytes proliferation and Th1/Th17 differentiation in vitro. *Eur J Pharm Sci* 100, 17–24

328. Kim, S.-J. *et al.* (2009) Dipeptidyl peptidase IV inhibition with MK0431 improves islet graft survival in diabetic NOD mice partially via T-cell modulation. *Diabetes* 58, 641–51

329. Shi, M. *et al.* (2021) Three-phasic pattern of C-peptide decline in type 1 diabetes patients with partial remission. *Diabetes Metab Res Rev* 37

330. Pollé, O.G. *et al.* (2022) Glycemic Variability Patterns Strongly Correlate With Partial Remission Status in Children With Newly Diagnosed Type 1 Diabetes. *Diabetes Care* 45, 2360–2368

331. Mørk, F.C.B. *et al.* (2022) Differences in insulin sensitivity in the partial remission phase of childhood type 1 diabetes; a longitudinal cohort study. *Diabet Med* 39, e14702

332. Nwosu, B.U. (2022) The Theory of Hyperlipidemic Memory of Type 1 Diabetes. *Front Endocrinol (Lausanne)* 13

333. Nwosu, B.U. *et al.* (2019) Pubertal Lipid Levels Are Significantly Lower in Youth With Type 1 Diabetes Who Experienced Partial Clinical Remission. *J Endocr Soc* 3, 737–747

334. Nwosu, B.U. *et al.* (2018) Children with type 1 diabetes who experienced a honeymoon phase had significantly lower LDL cholesterol 5 years after diagnosis. *PLoS One* 13, e0196912

335. Moosavi, M. *et al.* (2017) Effect of autoimmunity risk loci on the honeymoon phase in type 1 diabetes. *Pediatr Diabetes* 18, 459–462

336. Pujol-Autonell, I. *et al.* (2013) Efferocytosis promotes suppressive effects on dendritic cells through prostaglandin E2 production in the context of autoimmunity. *PLoS One* 8, e63296

337. Chen, Y. *et al.* (2022) The Unfavorable Impact of DR9/DR9 Genotype on the Frequency and Quality of Partial Remission in Type 1 Diabetes. *J Clin Endocrinol Metab* 107, e293–e302

338. Nakanishi, K. and Inoko, H. (2006) Combination of HLA-A24, -DQA1*03, and -DR9 contributes to acute-onset and early complete beta-cell destruction in type 1 diabetes: longitudinal study of residual beta-cell function. *Diabetes* 55, 1862–8

339. Jin, F. *et al.* (2018) Serum microRNA Profiles Serve as Novel Biomarkers for Autoimmune Diseases. *Front Immunol* 9, 2381

340. Carrascosa Lezcano, A. *et al.* (2008) Estudio transversal español de crecimiento 2008. Parte II: valores de talla, peso e índice de masa corporal desde el nacimiento a la talla adulta. *An Pediatr (Engl Ed)* 68, 552–569

341. Appay, V. *et al.* (2008) Phenotype and function of human T lymphocyte subsets: Consensus and issues. *Cytometry Part A* 73A, 975–983

342. Maecker, H.T. *et al.* (2012) Standardizing immunophenotyping for the Human Immunology Project. *Nat Rev Immunol* 12, 191–200

343. Vlachos, I.S. *et al.* (2015) DIANA-miRPath v3.0: deciphering microRNA function with experimental support. *Nucleic Acids Res* 43, W460–W466

344. Vlachos, I.S. *et al.* (2015) DIANA-TarBase v7.0: indexing more than half a million experimentally supported miRNA:mRNA interactions. *Nucleic Acids Res* 43, D153–D159

345. Supek, F. *et al.* (2011) REVIGO summarizes and visualizes long lists of gene ontology terms. *PLoS One* 6, e21800

346. Smith, M.D. *et al.* (2022) Haemolysis Detection in MicroRNA-Seq from Clinical Plasma Samples. *Genes (Basel)* 13

347. Livak, K.J. and Schmittgen, T.D. (2001) Analysis of Relative Gene Expression Data Using Real-Time Quantitative PCR and the 2−ΔΔCT Method. *Methods* 25, 402–408

348. Andersen, C.L. *et al.* (2004) Normalization of Real-Time Quantitative Reverse Transcription-PCR Data: A Model-Based Variance Estimation Approach to Identify Genes Suited for Normalization, Applied to Bladder and Colon Cancer Data Sets. *Cancer Res* 64, 5245–5250

349. Chicaybam, L. *et al.* (2013) An Efficient Low Cost Method for Gene Transfer to T Lymphocytes. *PLoS One* 8, e60298

350. Bongiovanni, C. *et al.* (2024) BMP7 promotes cardiomyocyte regeneration in zebrafish and adult mice. *Cell Rep* 43, 114162

351. Sugimoto, H. *et al.* (2007) BMP-7 functions as a novel hormone to facilitate liver regeneration. *The FASEB Journal* 21, 256–264

352. Qadir, M.M.F. *et al.* (2018) P2RY1/ALK3-Expressing Cells within the Adult Human Exocrine Pancreas Are BMP-7 Expandable and Exhibit Progenitor-like Characteristics. *Cell Rep* 22, 2408–2420

353. Marciniak, A. *et al.* (2014) Using pancreas tissue slices for in situ studies of islet of Langerhans and acinar cell biology. *Nat Protoc* 9, 2809–2822

354. Qadir, M.M.F. *et al.* (2020) Long-term culture of human pancreatic slices as a model to study real-time islet regeneration. *Nat Commun* 11, 3265

355. Bray, N.L. *et al.* (2016) Near-optimal probabilistic RNA-seq quantification. *Nat Biotechnol* 34, 525–7

356. Love, M.I. *et al.* (2014) Moderated estimation of fold change and dispersion for RNA-seq data with DESeq2. *Genome Biol* 15, 550

357. Garcia-Alonso, L. *et al.* (2019) Benchmark and integration of resources for the estimation of human transcription factor activities. *Genome Res* 29, 1363–1375

358. Bentsi-Barnes, K. *et al.* (2011) Detailed protocol for evaluation of dynamic perifusion of human islets to assess β-cell function. *Islets* 3, 284–290

359. Alba, A. *et al.* (2004) IFN beta accelerates autoimmune type 1 diabetes in nonobese diabetic mice and breaks the tolerance to beta cells in nondiabetes-prone mice. *J Immunol* 173, 6667–75

360. Villalba, A. *et al.* (2020) Antigen-specific immunotherapy combined with a regenerative drug in the treatment of experimental type 1 diabetes. *Sci Rep* 10, 18927

361. Gomez-Muñoz, L. *et al.* (2023) Immunoregulatory Biomarkers of the Remission Phase in Type 1 Diabetes: miR-30d-5p Modulates PD-1 Expression and Regulatory T Cell Expansion. *Noncoding RNA* 9, 17

362. Gomez-Muñoz, L. *et al.* (2022) Candidate Biomarkers for the Prediction and Monitoring of Partial Remission in Pediatric Type 1 Diabetes. *Front Immunol* 13, 825426

363. Gomez-Muñoz, L. *et al.* (2021) NK Cell Subsets Changes in Partial Remission and Early Stages of Pediatric Type 1 Diabetes. *Front Immunol* 11

364. Jaberi-Douraki, M. *et al.* (2015) Continuum model of T-cell avidity: Understanding autoreactive and regulatory T-cell responses in type 1 diabetes. *J Theor Biol* 383, 93–105

365. Wegrzyn, A.S. *et al.* (2023) Identification and classification of distinct surface markers of T regulatory cells. *Front Immunol* 13

366. Fraker, C. and Bayer, A.L. (2016) The Expanding Role of Natural Killer Cells in Type 1 Diabetes and Immunotherapy. *Curr Diab Rep* 16, 109

367. Lee, J.-H. *et al.* (2021) TGF-β Signaling in Pancreatic Islet β Cell Development and Function. *Endocrinology* 162

368. Henquin, J. *et al.* (2017) Pharmacological approach to understanding the control of insulin secretion in human islets. *Diabetes Obes Metab* 19, 1061–1070

369. Rabiee, A. *et al.* (2018) Distinct signalling properties of insulin receptor substrate (IRS)-1 and IRS-2 in mediating insulin/IGF-1 action. *Cell Signal* 47, 1–15

370. Zick, Y. (2005) Ser/Thr phosphorylation of IRS proteins: a molecular basis for insulin resistance. *Sci STKE* 268, pe4

371. Braun, M. *et al.* (2012) Autocrine regulation of insulin secretion. *Diabetes Obes Metab* 14, 143–151

372. Hao, Y. *et al.* (2022) ZBP1: A Powerful Innate Immune Sensor and Double-Edged Sword in Host Immunity. *Int J Mol Sci* 23

373. Van Belle, T.L. *et al.* (2012) Interleukin-21 Receptor-Mediated Signals Control Autoreactive T Cell Infiltration in Pancreatic Islets. *Immunity* 36, 1060–1072

374. Meng, Z.X. *et al.* (2012) Aberrant activation of liver X receptors impairs pancreatic beta cell function through upregulation of sterol regulatory element-binding protein 1c in mouse islets and rodent cell lines. *Diabetologia* 55, 1733–44

375. Bohuslavova, R. *et al.* (2023) ISL1 controls pancreatic alpha cell fate and beta cell maturation. *Cell Biosci* 13, 53

376. Ediger, B.N. *et al.* (2014) Islet-1 Is essential for pancreatic β-cell function. *Diabetes* 63, 4206–17

377. Refai, E. *et al.* (2005) Transthyretin constitutes a functional component in pancreatic β-cell stimulus-secretion coupling. *Proceedings of the National Academy of Sciences* 102, 17020–17025

378. Becker, A. *et al.* (2021) Cavβ3 Regulates Ca2+ Signaling and Insulin Expression in Pancreatic β-Cells in a Cell-Autonomous Manner. *Diabetes* 70, 2532–2544

379. Shah, S.R. *et al.* (2008) A role for BMPR1B in differentiation of pancreatic endocrine progenitors. *J Am Coll Surg* 207, S46

380. Sun, M. *et al.* (2003) Activation of Phosphatidylinositol 3-Kinase/Akt Pathway by Androgen through Interaction of p85α, Androgen Receptor, and Src. *Journal of Biological Chemistry* 278, 42992–43000

381. Rorsman, P. and Ashcroft, F.M. (2018) Pancreatic β-Cell Electrical Activity and Insulin Secretion: Of Mice and Men. *Physiol Rev* 98, 117–214

382. Aref, S. *et al.* (2017) Upregulation of CD200 is associated with regulatory T cell expansion and disease progression in multiple myeloma. *Hematol Oncol* 35, 51–57

383. Zhang, J. *et al.* (2009) Patterns of microRNA expression characterize stages of human B-cell differentiation. *Blood* 113, 4586–4594

384. Phillip, M. *et al.* (2024) Consensus guidance for monitoring individuals with islet autoantibody-positive pre-stage 3 type 1 diabetes. *Diabetologia* 47(8), 1276-1298

385. Herold, K.C. *et al.* (2019) An Anti-CD3 Antibody, Teplizumab, in Relatives at Risk for Type 1 Diabetes. *New England Journal of Medicine* 381, 603–613

386. Cherubini, V. *et al.* (2024) Follow-up and monitoring programme in children identified in early-stage type 1 diabetes during screening in the general population of Italy. *Diabetes Obes Metab* 26, 10, 4197-4202

387. Inshaw, J.R.J. *et al.* (2018) The chromosome 6q22.33 region is associated with age at diagnosis of type 1 diabetes and disease risk in those diagnosed under 5 years of age. *Diabetologia* 61, 147–157

388. Bosi, E. *et al.* (2017) Impact of Age and Antibody Type on Progression From Single to Multiple Autoantibodies in Type 1 Diabetes Relatives. *J Clin Endocrinol Metab* 102, 2881–2886

389. Endesfelder, D. *et al.* (2019) Time-Resolved Autoantibody Profiling Facilitates Stratification of Preclinical Type 1 Diabetes in Children. *Diabetes* 68, 119–130

390. Perri, V. *et al.* (2015) Expression of PD-1 Molecule on Regulatory T Lymphocytes in Patients with Insulin-Dependent Diabetes Mellitus. *Int J Mol Sci* 16, 22584–22605

391. Xiao, Y. *et al.* (2021) The Multiple Roles of B Lymphocytes in the Onset and Treatment of Type 1 Diabetes: Interactions between B Lymphocytes and T Cells. *J Diabetes Res* 2021, 1–8

392. Hu, Y. *et al.* (2023) γδ T cells: origin and fate, subsets, diseases and immunotherapy. *Signal Transduct Target Ther* 8, 434

393. Velikkakam, T. *et al.* (2022) Double-negative T cells: Setting the stage for disease control or progression. *Immunology* 165, 371–385

394. Zubkiewicz-Kucharska, A. *et al.* (2016) Abnormal Distribution of Gamma-Delta T Lymphocytes and Their Subsets in Type 1 Diabetes. *Advances in Clinical and Experimental Medicine* 25, 665–671

395. Nigi, L. *et al.* (2020) From immunohistological to anatomical alterations of human pancreas in type 1 diabetes: New concepts on the stage. *Diabetes Metab Res Rev* 36

396. Planas, R. *et al.* (2009) Gene expression profiles for the human pancreas and purified islets in Type 1 diabetes: new findings at clinical onset and in long-standing diabetes. *Clin Exp Immunol* 159, 23–44

397. Chowdhury, M.Z.I. and Turin, T.C. (2020) Variable selection strategies and its importance in clinical prediction modelling. *Fam Med Community Health* 8, e000262

398. Kaas, A. *et al.* (2010) Association of adiponectin, interleukin (IL)-1ra, inducible protein 10, IL-6 and number of islet autoantibodies with progression patterns of type 1 diabetes the first year after diagnosis. *Clin Exp Immunol* 161, 444–452

399. Schloot, N.C. *et al.* (2007) Association of immune mediators at diagnosis of Type 1 diabetes with later clinical remission. *Diabetic Medicine* 24, 512–520

400. Nigi, L. *et al.* (2020) Pancreatic Alpha-Cells Contribute Together With Beta-Cells to CXCL10 Expression in Type 1 Diabetes. *Front Endocrinol (Lausanne)* 11, 630

401. Oras, A. *et al.* (2019) A study of 51 subtypes of peripheral blood immune cells in newly diagnosed young type 1 diabetes patients. *Clin Exp Immunol* 198, 57–70

402. Coppieters, K.T. *et al.* (2012) Demonstration of islet-autoreactive CD8 T cells in insulitic lesions from recent onset and long-term type 1 diabetes patients. *Journal of Experimental Medicine* 209, 51–60

403. Gonzalez-Duque, S. *et al.* (2018) Conventional and Neo-antigenic Peptides Presented by β Cells Are Targeted by Circulating Naïve CD8+ T Cells in Type 1 Diabetic and Healthy Donors. *Cell Metab* 28, 946-960.e6

404. Serr, I. *et al.* (2016) Type 1 diabetes vaccine candidates promote human Foxp3+Treg induction in humanized mice. *Nat Commun* 7, 10991

405. Hamari, S. *et al.* (2016) Analyses of regulatory CD4+CD25+FOXP3+ T cells and observations from peripheral T cell subpopulation markers during the development of type 1 diabetes in children. *Scand J Immunol* 83, 279–287

406. Brusko, T. *et al.* (2007) No Alterations in the Frequency of FOXP3+ Regulatory T-Cells in Type 1 Diabetes. *Diabetes* 56, 604–612

407. Thompson, W.S. *et al.* (2014) Multi-parametric flow cytometric and genetic investigation of the peripheral B cell compartment in human type 1 diabetes. *Clin Exp Immunol* 177, 571–585

408. Catalán, D. *et al.* (2021) Immunosuppressive Mechanisms of Regulatory B Cells. *Front Immunol* 12

409. Simon, Q. *et al.* (2016) In-depth characterization of CD24 high CD38 high transitional human B cells reveals different regulatory profiles. *Journal of Allergy and Clinical Immunology* 137, 1577-1584.e10

410. Wang, Y. *et al.* (2020) Decrease in the proportion of CD24hiCD38hi B cells and impairment of their regulatory capacity in type 1 diabetes patients. *Clin Exp Immunol* 200, 22–32

411. El-Mokhtar, M.A. *et al.* (2020) Altered Regulatory B Cell Subsets in Children with Type 1 Diabetes Mellitus. *J Immunol Res* 2020, 1–8

412. Tripathy, S.K. *et al.* (2008) Continuous engagement of a self-specific activation receptor induces NK cell tolerance. *J Exp Med* 205, 1829–1841

413. Ogasawara, K. *et al.* (2004) NKG2D Blockade Prevents Autoimmune Diabetes in NOD Mice. *Immunity* 20, 757–767

414. Ogasawara, K. *et al.* (2003) Impairment of NK Cell Function by NKG2D Modulation in NOD Mice. *Immunity* 18, 41–51

415. Rodacki, M. *et al.* (2007) Altered Natural Killer Cells in Type 1 Diabetic Patients. *Diabetes* 56, 177–185

416. Deniz, G. *et al.* (2008) Regulatory NK Cells Suppress Antigen-Specific T Cell Responses. *The Journal of Immunology* 180, 850–857

417. Ferlazzo, G. *et al.* (2002) Human Dendritic Cells Activate Resting Natural Killer (NK) Cells and Are Recognized via the NKp30 Receptor by Activated NK Cells. *J Exp Med* 195, 343–351

418. Ong, S.-M. *et al.* (2018) The pro-inflammatory phenotype of the human non-classical monocyte subset is attributed to senescence. *Cell Death Dis* 9, 266

419. Rossol, M. *et al.* (2012) The CD14(bright) CD16+ monocyte subset is expanded in rheumatoid arthritis and promotes expansion of the Th17 cell population. *Arthritis Rheum* 64, 671–7

420. Ramírez, R. *et al.* (2011) CD14+CD16+ monocytes from chronic kidney disease patients exhibit increased adhesion ability to endothelial cells. *Contrib Nephrol* 171, 57–61

421. Kawanaka, N. *et al.* (2002) CD14+,CD16+ blood monocytes and joint inflammation in rheumatoid arthritis. *Arthritis Rheum* 46, 2578–86

422. Samassa, F. *et al.* (2024) Cross Talk between β Cells and Immune Cells: What We Know, What We Think We Know, and What We Should Learn. *Cold Spring Harb Perspect Med* a041604

423. Ferreira, R.C. *et al.* (2014) A Type I Interferon Transcriptional Signature Precedes Autoimmunity in Children Genetically at Risk for Type 1 Diabetes. *Diabetes* 63, 2538–2550

424. Lu, J. *et al.* (2020) Cytokines in type 1 diabetes: mechanisms of action and immunotherapeutic targets. *Clin Transl Immunology* 9

425. Sobel, D.O. *et al.* (2002) Gamma Interferon Paradoxically Inhibits the Development of Diabetes in the NOD Mouse. *J Autoimmun* 19, 129–137

426. Driver, J.P. *et al.* (2017) Interferon-γ Limits Diabetogenic CD8+ T-Cell Effector Responses in Type 1 Diabetes. *Diabetes* 66, 710–721

427. Campbell, I.L. *et al.* (1985) Interferon-γ Enhances the Expression of the Major Histocompatibility Class I Antigens on Mouse Pancreatic Beta Cells. *Diabetes* 34, 1205–1209

428. Sarvetnick, N. *et al.* (1988) Insulin-dependent diabetes mellitus induced in transgenic mice by ectopic expression of class II MHC and interferon-gamma. *Cell* 52, 773–782

429. Vukkadapu, S.S. *et al.* (2005) Dynamic interaction between T cell-mediated β-cell damage and β-cell repair in the run up to autoimmune diabetes of the NOD mouse. *Physiol Genomics* 21, 201–211

430. Rajendran, S. *et al.* (2021) IL-17 is expressed on beta and alpha cells of donors with type 1 and type 2 diabetes. *J Autoimmun* 123, 102708

431. Grieco, F.A. *et al.* (2014) IL-17A increases the expression of proinflammatory chemokines in human pancreatic islets. *Diabetologia* 57, 502–511

432. Jörns, A. *et al.* (2020) Remission of autoimmune diabetes by anti-TCR combination therapies with anti-IL-17A or/and anti-IL-6 in the IDDM rat model of type 1 diabetes. *BMC Med* 18, 33

433. Fraga, M.F. *et al.* (2005) Epigenetic differences arise during the lifetime of monozygotic twins. *Proceedings of the National Academy of Sciences* 102, 10604–10609

434. Beekman, M. *et al.* (2010) Genome-wide association study (GWAS)-identified disease risk alleles do not compromise human longevity. *Proceedings of the National Academy of Sciences* 107, 18046–18049

435. Zheng, Y. *et al.* (2017) miRNAs: novel regulators of autoimmunity-mediated pancreatic β-cell destruction in type 1 diabetes. *Cell Mol Immunol* 14, 488–496

436. Condrat, C.E. *et al.* (2020) miRNAs as Biomarkers in Disease: Latest Findings Regarding Their Role in Diagnosis and Prognosis. *Cells* 9, 276

437. Ventriglia, G. *et al.* (2020) miR-409-3p is reduced in plasma and islet immune infiltrates of NOD diabetic mice and is differentially expressed in people with type 1 diabetes. *Diabetologia* 63, 124–136

438. Marchand, L. *et al.* (2016) miRNA-375 a Sensor of Glucotoxicity Is Altered in the Serum of Children with Newly Diagnosed Type 1 Diabetes. *J Diabetes Res* 2016, 1–7

439. Santos, A.S. *et al.* (2019) Increased Expression of Circulating microRNA 101-3p in Type 1 Diabetes Patients: New Insights Into miRNA-Regulated Pathophysiological Pathways for Type 1 Diabetes. *Front Immunol* 10

440. Zurawek, M. *et al.* (2018) miR-487a-3p upregulated in type 1 diabetes targets CTLA4 and FOXO3. *Diabetes Res Clin Pract* 142, 146–153

441. Zhang, X. *et al.* (2020) MiR-885-3p is down-regulated in peripheral blood mononuclear cells from T1D patients and regulates the inflammatory response via targeting TLR4/NF-κB signaling. *J Gene Med* 22

442. Samandari, N. *et al.* (2017) Circulating microRNA levels predict residual beta cell function and glycaemic control in children with type 1 diabetes mellitus. *Diabetologia* 60, 354–363

443. Tsukita, S. *et al.* (2017) MicroRNAs 106b and 222 Improve Hyperglycemia in a Mouse Model of Insulin-Deficient Diabetes via Pancreatic β-Cell Proliferation. *EBioMedicine* 15, 163–172

444. Mandelbaum, A.D. *et al.* (2019) miR-17-92 and miR-106b-25 clusters regulate beta cell mitotic checkpoint and insulin secretion in mice. *Diabetologia* 62, 1653–1666

445. Xin, Y. *et al.* (2016) miR-20b Inhibits T Cell Proliferation and Activation via NFAT Signaling Pathway in Thymoma-Associated Myasthenia Gravis. *Biomed Res Int* 2016, 1–12

446. Ji, H. *et al.* (2022) Let7b-5p inhibits insulin secretion and decreases pancreatic β-cell mass in mice. *Mol Cell Endocrinol* 540, 111506

447. Sung, Y. *et al.* (2019) Lin28a expression protects against streptozotocin-induced β-cell destruction and prevents diabetes in mice. *Cell Biochem Funct* 37, 139–147

448. Zurawek, M. *et al.* (2020) Upregulation of FOXO3 in New-Onset Type 1 Diabetes Mellitus. *J Immunol Res* 2020, 1–4

449. Wang, H.-L. *et al.* (2022) Role of TGF-Beta Signaling in Beta Cell Proliferation and Function in Diabetes. *Biomolecules* 12, 373

450. Fauth, M. *et al.* (2019) Validation of extracellular miRNA quantification in blood samples using RT-qPCR. *FASEB Bioadv* 1, 481–492

451. Alpert, A. *et al.* (2019) A clinically meaningful metric of immune age derived from high-dimensional longitudinal monitoring. *Nat Med* 25, 487–495

452. Shearer, W.T. *et al.* (2003) Lymphocyte subsets in healthy children from birth through 18 years of age. *Journal of Allergy and Clinical Immunology* 112, 973–980

453. Tang, X. *et al.* (2009) Identification of glucose-regulated miRNAs from pancreatic β cells reveals a role for miR-30d in insulin transcription. *RNA* 15, 287–293

454. Zhao, X. *et al.* (2012) MicroRNA-30d Induces Insulin Transcription Factor MafA and Insulin Production by Targeting Mitogen-activated Protein 4 Kinase 4 (MAP4K4) in Pancreatic β-Cells. *Journal of Biological Chemistry* 287, 31155–31164

455. Gaziel-Sovran, A. *et al.* (2011) miR-30b/30d Regulation of GalNAc Transferases Enhances Invasion and Immunosuppression during Metastasis. *Cancer Cell* 20, 104–118

456. Liu, S. *et al.* (2019) Oral Administration of miR-30d from Feces of MS Patients Suppresses MS-like Symptoms in Mice by Expanding Akkermansia muciniphila. *Cell Host Microbe* 26, 779-794.e8

457. Seyhan, A.A. *et al.* (2016) Pancreas-enriched miRNAs are altered in the circulation of subjects with diabetes: a pilot cross-sectional study. *Sci Rep* 6, 31479

458. Frørup, C. *et al.* (2021) Plasma Exosome-Enriched Extracellular Vesicles From Lactating Mothers With Type 1 Diabetes Contain Aberrant Levels of miRNAs During the Postpartum Period. *Front Immunol* 12

459. Qian, X. *et al.* (2018) Regulation of fatty acid synthesis in immune cells. *Scand J Immunol* 88

460. Harris, E. *et al.* (2021) Nonviral gene delivery to T cells with Lipofectamine LTX. *Biotechnol Bioeng* 118, 1674–1687

461. Kalos, M. *et al.* (2011) T Cells with Chimeric Antigen Receptors Have Potent Antitumor Effects and Can Establish Memory in Patients with Advanced Leukemia. *Sci Transl Med* 3

462. Pule, M.A. *et al.* (2008) Virus-specific T cells engineered to coexpress tumor-specific receptors: persistence and antitumor activity in individuals with neuroblastoma. *Nat Med* 14, 1264–1270

463. Butt, M. *et al.* (2022) Appraisal for the Potential of Viral and Nonviral Vectors in Gene Therapy: A Review. *Genes (Basel)* 13, 1370

464. Pohl-Guimarães, F. *et al.* (2019) RNA-Modified T Cells Mediate Effective Delivery of Immunomodulatory Cytokines to Brain Tumors. *Molecular Therapy* 27, 837–849

465. Gehl, J. (2003) Electroporation: theory and methods, perspectives for drug delivery, gene therapy and research. *Acta Physiol Scand* 177, 437–447

466. Roth, T.L. *et al.* (2018) Reprogramming human T cell function and specificity with non-viral genome targeting. *Nature* 559, 405–409

467. Schutsky, K. *et al.* (2015) Rigorous optimization and validation of potent RNA CAR T cell therapy for the treatment of common epithelial cancers expressing folate receptor. *Oncotarget* 6, 28911–28928

468. Ang, W.X. *et al.* (2017) Intraperitoneal immunotherapy with T cells stably and transiently expressing anti-EpCAM CAR in xenograft models of peritoneal carcinomatosis. *Oncotarget* 8, 13545–13559

469. Mitchell, D.A. *et al.* (2008) Selective Modification of Antigen-Specific T Cells by RNA Electroporation. *Hum Gene Ther* 19, 511–521

470. Roberts, P. *et al.* (2006) miRCURY™ LNA research tools for microRNA. *Nat Methods* 3, I–II

471. Buchbinder, E.I. and Desai, A. (2016) CTLA-4 and PD-1 Pathways. *Am J Clin Oncol* 39, 98–106

472. Pauken, K.E. *et al.* (2013) PD-1, but Not PD-L1, Expressed by Islet-Reactive CD4+ T Cells Suppresses Infiltration of the Pancreas During Type 1 Diabetes. *Diabetes* 62, 2859–2869

473. Pauken, K.E. *et al.* (2015) Cutting Edge: Identification of Autoreactive CD4+ and CD8+ T Cell Subsets Resistant to PD-1 Pathway Blockade. *The Journal of Immunology* 194, 3551–3555

474. Paterson, A.M. *et al.* (2011) The Programmed Death-1 Ligand 1:B7-1 Pathway Restrains Diabetogenic Effector T Cells In Vivo. *The Journal of Immunology* 187, 1097–1105

475. Kanzaki, M. *et al.* (2012) Galectin-9 and T Cell Immunoglobulin Mucin-3 Pathway Is a Therapeutic Target for Type 1 Diabetes. *Endocrinology* 153, 612–620

476. Zhu, C. *et al.* (2005) The Tim-3 ligand galectin-9 negatively regulates T helper type 1 immunity. *Nat Immunol* 6, 1245–1252

477. Bettini, M. *et al.* (2011) Cutting Edge: Accelerated Autoimmune Diabetes in the Absence of LAG-3. *The Journal of Immunology* 187, 3493–3498

478. Kavvoura, F.K. and Ioannidis, J.P.A. (2005) CTLA-4 Gene Polymorphisms and Susceptibility to Type 1 Diabetes Mellitus: A HuGE Review and Meta-Analysis. *Am J Epidemiol* 162, 3–16

479. Bruzzaniti, S. *et al.* (2022) High levels of blood circulating immune checkpoint molecules in children with new-onset type 1 diabetes are associated with the risk of developing an additional autoimmune disease. *Diabetologia* 65, 1390–1397

480. Jones, B.E. *et al.* (2022) Fewer LAG-3+ T Cells in Relapsing-Remitting Multiple Sclerosis and Type 1 Diabetes. *The Journal of Immunology* 208, 594–602

481. Fujisawa, R. *et al.* (2015) Low programmed cell death-1 (PD-1) expression in peripheral CD4+ T cells in Japanese patients with autoimmune type 1 diabetes. *Clin Exp Immunol* 180, 452–457

482. Granados, H.M. *et al.* (2017) Programmed cell death-1, PD-1, is dysregulated in T cells from children with new onset type 1 diabetes. *PLoS One* 12, e0183887

483. Colli, M.L. *et al.* (2018) PDL1 is expressed in the islets of people with type 1 diabetes and is up-regulated by interferons-α and-γ via IRF1 induction. *EBioMedicine* 36, 367–375

484. Osum, K.C. *et al.* (2018) Interferon-gamma drives programmed death-ligand 1 expression on islet β cells to limit T cell function during autoimmune diabetes. *Sci Rep* 8, 8295

485. Keir, M.E. *et al.* (2006) Tissue expression of PD-L1 mediates peripheral T cell tolerance. *J Exp Med* 203, 883–895

486. Joller, N. *et al.* (2024) LAG-3, TIM-3, and TIGIT: Distinct functions in immune regulation. *Immunity* 57, 206–222

487. Fuertes Marraco, S.A. *et al.* (2015) Inhibitory Receptors Beyond T Cell Exhaustion. *Front Immunol* 6

488. Guo, L. *et al.* (2023) The role of TEMRA cell-mediated immune senescence in the development and treatment of HIV disease. *Front Immunol* 14

489. Mandai, M. *et al.* (2016) Dual Faces of IFNγ in Cancer Progression: A Role of PD-L1 Induction in the Determination of Pro- and Antitumor Immunity. *Clinical Cancer Research* 22, 2329–2334

490. Sivakumar, R. *et al.* (2019) Organotypic tumor slice cultures provide a versatile platform for immuno-oncology and drug discovery. *Oncoimmunology* 8, e1670019

491. Bailey, S.R. *et al.* (2022) Blockade or Deletion of IFNγ Reduces Macrophage Activation without Compromising CAR T-cell Function in Hematologic Malignancies. *Blood Cancer Discov* 3, 136–153

492. Bailey, S.R. *et al.* (2021) Blocking IFNγ in CAR-T Reduces Checkpoint Inhibitors and Cell-Mediated Toxicity without Compromising Therapeutic Efficacy in CD19 +malignancies. *Blood* 138, 1723–1723

493. Rodríguez-Galán, A. *et al.* (2018) Control of Immunoregulatory Molecules by miRNAs in T Cell Activation. *Front Immunol* 9

494. Coles, S.J. *et al.* (2012) Increased CD200 expression in acute myeloid leukemia is linked with an increased frequency of FoxP3+ regulatory T cells. *Leukemia* 26, 2146–2148

495. Gorczynski, R. *et al.* (2013) sCD200 Present in Mice Receiving Cardiac and Skin Allografts Causes Immunosuppression In Vitro and Induces Tregs. *Transplantation* 95, 442–447

496. Fife, B.T. *et al.* (2006) Insulin-induced remission in new-onset NOD mice is maintained by the PD-1–PD-L1 pathway. *J Exp Med* 203, 2737–2747

497. O'Kell, A.L. *et al.* (2017) Comparative Pathogenesis of Autoimmune Diabetes in Humans, NOD Mice, and Canines: Has a Valuable Animal Model of Type 1 Diabetes Been Overlooked? *Diabetes* 66, 1443–1452

498. Elmén, J. *et al.* (2008) LNA-mediated microRNA silencing in non-human primates. *Nature* 452, 896–899

499. Krützfeldt, J. *et al.* (2005) Silencing of microRNAs in vivo with 'antagomirs.' *Nature* 438, 685–689

500. Elmén, J. *et al.* (2008) Antagonism of microRNA-122 in mice by systemically administered LNA-antimiR leads to up-regulation of a large set of predicted target mRNAs in the liver. *Nucleic Acids Res* 36, 1153–1162

501. Lim, C.Y. *et al.* (2018) Organotypic slice cultures of pancreatic ductal adenocarcinoma preserve the tumor microenvironment and provide a platform for drug response. *Pancreatology* 18, 913–927

502. Lim, C.Y. *et al.* (2022) CD40 Agonists Alter the Pancreatic Cancer Microenvironment by Shifting the Macrophage Phenotype toward M1 and Suppress Human Pancreatic Cancer in Organotypic Slice Cultures. *Gut Liver* 16, 645–659

503. Russ, H.A. *et al.* (2009) Epithelial-Mesenchymal Transition in Cells Expanded In Vitro from Lineage-Traced Adult Human Pancreatic Beta Cells. *PLoS One* 4, e6417

504. Dor, Y. *et al.* (2004) Adult pancreatic β-cells are formed by self-duplication rather than stem-cell differentiation. *Nature* 429, 41–46

505. Thorel, F. *et al.* (2010) Conversion of adult pancreatic α-cells to β-cells after extreme β-cell loss. *Nature* 464, 1149–1154

506. Furuyama, K. *et al.* (2019) Diabetes relief in mice by glucose-sensing insulin-secreting human α-cells. *Nature* 567, 43–48

507. Domínguez-Bendala, J. *et al.* (2019) Pancreatic Progenitors: There and Back Again. *Trends in Endocrinology & Metabolism* 30, 4–11

508. Sui, L. *et al.* (2013) Role of BMP Signaling in Pancreatic Progenitor Differentiation from Human Embryonic Stem Cells. *Stem Cell Rev Rep* 9, 569–577

509. Klein, D. *et al.* (2015) BMP-7 Induces Adult Human Pancreatic Exocrine-to-Endocrine Conversion. *Diabetes* 64, 4123–4134

510. Mao, Y. *et al.* (2022) Transgenic overexpression of microRNA-30d in pancreatic beta-cells progressively regulates beta-cell function and identity. *Sci Rep* 12, 11969

511. Mziaut, H. *et al.* (2020) MiR-132 controls pancreatic beta cell proliferation and survival through Pten/Akt/Foxo3 signaling. *Mol Metab* 31, 150–162

512. Poy, M.N. *et al.* (2009) miR-375 maintains normal pancreatic α- and β-cell mass. *Proceedings of the National Academy of Sciences* 106, 5813–5818

513. Lang, H. *et al.* (2024) Repressing miR-23a promotes the transdifferentiation of pancreatic α cells to β cells via negatively regulating the expression of SDF-1α. *PLoS One* 19, e0299821

514. Wang, Y. *et al.* (2013) MicroRNA-7 Regulates the mTOR Pathway and Proliferation in Adult Pancreatic β-Cells. *Diabetes* 62, 887–895

515. Joglekar, M. V. *et al.* (2009) The miR-30 family microRNAs confer epithelial phenotype to human pancreatic cells. *Islets* 1, 137–147

516. Henquin, J.-C. (2019) The challenge of correctly reporting hormones content and secretion in isolated human islets. *Mol Metab* 30, 230–239

517. Reaven, E.P. *et al.* (1979) Effect of age on glucose-stimulated insulin release by the beta-cell of the rat. *Journal of Clinical Investigation* 64, 591–599

518. Du, A. *et al.* (2009) Islet-1 is required for the maturation, proliferation, and survival of the endocrine pancreas. *Diabetes* 58, 2059–69

519. Hyltén-Cavallius, L. *et al.* (2017) Patients With Long-QT Syndrome Caused by Impaired hERG-Encoded Kv11.1 Potassium Channel Have Exaggerated Endocrine Pancreatic and Incretin Function Associated With Reactive Hypoglycemia. *Circulation* 135, 1705–1719

520. Maczewsky, J. *et al.* (2017) The LXR Ligand T0901317 Acutely Inhibits Insulin Secretion by Affecting Mitochondrial Metabolism. *Endocrinology* 158, 2145–2154

521. Gerin, I. *et al.* (2005) LXRβ Is Required for Adipocyte Growth, Glucose Homeostasis, and β Cell Function. *Journal of Biological Chemistry* 280, 23024–23031

522. Ning, J. *et al.* (2019) Opposing roles and potential antagonistic mechanism between TGF-β and BMP pathways: Implications for cancer progression. *EBioMedicine* 41, 702–710

523. Petrocca, F. *et al.* (2008) Emerging Role of miR-106b-25/miR-17-92 Clusters in the Control of Transforming Growth Factor β Signaling. *Cancer Res* 68, 8191–8194

524. Li, X.-Y. *et al.* (2015) Notch Signaling in Pancreatic Development. *Int J Mol Sci* 17, 48

525. Siveke, J.T. *et al.* (2008) Notch Signaling Is Required for Exocrine Regeneration After Acute Pancreatitis. *Gastroenterology* 134, 544-555.e3

526. Xu, K. *et al.* (2022) DDX5 and DDX17—multifaceted proteins in the regulation of tumorigenesis and tumor progression. *Front Oncol* 12

527. Sajiir, H. *et al.* (2024) Pancreatic beta-cell IL-22 receptor deficiency induces age-dependent dysregulation of insulin biosynthesis and systemic glucose homeostasis. *Nat Commun* 15, 4527

528. Smith, M.R. *et al.* (2023) STAT5b: A master regulator of key biological pathways. *Front Immunol* 13

529. Zhong, W. *et al.* (2014) Activation of the MAPK11/12/13/14 (p38 MAPK) pathway regulates the transcription of autophagy genes in response to oxidative stress induced by a novel copper complex in HeLa cells. *Autophagy* 10, 1285–1300

530. Wang, N. *et al.* (2017) Amelioration of streptozotocin-induced pancreatic β cell damage by morin: Involvement of the AMPK-FOXO3-catalase signaling pathway. *Int J Mol Med* 41, 3, 1410–1418

531. Kops, G.J.P.L. *et al.* (2002) Forkhead transcription factor FOXO3a protects quiescent cells from oxidative stress. *Nature* 419, 316–321

532. Good, A.L. *et al.* (2019) JUND regulates pancreatic β cell survival during metabolic stress. *Mol Metab* 25, 95–106

533. Tinklepaugh, J. and Mamrak, N.E. (2023) Imaging in Type 1 Diabetes, Current Perspectives and Directions. *Mol Imaging Biol* 25, 1142–1149

SCIENTIFIC PRODUCTION

Publications

- **Gomez-Muñoz L**, Dominguez-Bendala J, Pastori RL, Vives-Pi M. Immunometabolic biomarkers for partial remission in type 1 diabetes mellitus. *Trends Endocrinol Metab*. 2024 Feb;35(2):151-163. doi: 10.1016/j.tem.2023.10.005. Epub 2023 Nov 8. PMID: 37949732.
- **Gomez-Muñoz L**, Perna-Barrull D, Murillo M, Armengol MP, Alcalde M, Catala M, Rodriguez-Fernandez S, Sunye S, Valls A, Perez J, Corripio R, Vives-Pi M. Immunoregulatory Biomarkers of the Remission Phase in Type 1 Diabetes: miR-30d-5p Modulates PD-1 Expression and Regulatory T Cell Expansion. *Noncoding RNA*. 2023 Feb 28;9(2):17. doi: 10.3390/ncrna9020017. PMID: 36960962; PMCID: PMC10037622.
- **Gomez-Muñoz L**, Perna-Barrull D, Caroz-Armayones JM, Murillo M, Rodriguez-Fernandez S, Valls A, Vazquez F, Perez J, Corripio R, Castaño L, Bel J, Vives-Pi M. Candidate Biomarkers for the Prediction and Monitoring of Partial Remission in Pediatric Type 1 Diabetes. *Front Immunol*. 2022 Feb 23;13:825426. doi: 10.3389/fimmu.2022.825426.
- **Gomez-Muñoz L**, Perna-Barrull D, Villalba A, Rodriguez-Fernandez S, Ampudia RM, Teniente-Serra A, Vazquez F, Murillo M, Perez J, Corripio R, Bel J, Vives-Pi M. NK Cell Subsets Changes in Partial Remission and Early Stages of Pediatric Type 1 Diabetes. *Front Immunol*. 2021 Jan 25;11:611522. doi: 10.3389/fimmu.2020.611522.

Publications from scientific collaborations

- Salvia R, Cañaveras M, Rico G. L, Drozdowskyj A, Ward D. M, Jurado R, **Gomez-Muñoz L**, Vives-Pi M, Martinez-Caceres E, Petriz J. Prospective Investigation of Nanoplastic Accumulation in Healthy Subjects, Autoimmune Diseases, Hematological Malignancies, Lung Cancer, and Murine Models. OSF. Preprint. 2024 June. doi: 10.31219/osf.io/ey2sp
- Garcia-Loza I, Perna-Barrull D, Aguilera E, Almenara-Fuentes L, **Gomez-Muñoz L**, Greco D, Vila M, Salvado M, Mancera-Arteu M, Olszowy MW, Petriz J, Dalmases M, Rodriguez-Vidal S, Barneda-Zahonero B, Vives-Pi M. Targeting macrophages with phosphatidylserine-rich liposomes as a potential antigen-specific immunotherapy for type 1 diabetes. *J Autoimmun*. 2024 May;145:103196. doi: 10.1016/j.jaut.2024.103196. Epub 2024 Mar 8. PMID: 38458075.
- Salvia R, Rico LG, Bradford JA, Ward MD, Olszowy MW, Martínez C, Madrid-Aris ÁD, Grífols JR, Ancochea Á, **Gomez-Muñoz L**, Vives-Pi M, Martínez-Cáceres E,

Fernández MA, Sorigue M, Petriz J. Fast-screening flow cytometry method for detecting nanoplastics in human peripheral blood. *MethodsX*. 2023 Feb 6;10:102057. doi: 10.1016/j.mex.2023.102057. PMID: 36851978; PMCID: PMC9958479.

- Perna-Barrull D, **Gomez-Muñoz L**, Rodriguez-Fernandez S, Gieras A, Ampudia-Carrasco RM, Almenara-Fuentes L, Risueño RM, Querol S, Tolosa E, Vives-Pi M. Impact of Betamethasone Pretreatment on Engrafment of Cord Blood-Derived Hematopoietic Stem Cells. *Arch Immunol Ther Exp* (Warsz). 2022 Dec 18;71(1):1. doi: 10.1007/s00005-022-00666-5. PMID: 36528821; PMCID: PMC9760591.
- Perna-Barrull D, Murillo M, Real N, **Gomez-Muñoz L**, Rodriguez-Fernandez S, Bel J, Puig-Domingo M, Vives-Pi M. Prenatal Betamethasone Exposure and its Impact on Pediatric Type 1 Diabetes Mellitus: A Preliminary Study in a Spanish Cohort. *J Diabetes Res*. 2022 Mar 10;2022:6598600. doi: 10.1155/2022/6598600. PMID: 35308094; PMCID: PMC8930272.
- Rodriguez-Rosales YA, Langereis JD, Gorris MAJ, van den Reek JMPA, Fasse E, Netea MG, de Vries IJM, **Gomez-Muñoz L**, van Cranenbroek B, Körber A, Sondermann W, Joosten I, de Jong EMGJ, Koenen HJPM. Immunomodulatory aged neutrophils are augmented in blood and skin of psoriasis patients. *J Allergy Clin Immunol*. 2021 Oct;148(4):1030-1040. doi: 10.1016/j.jaci.2021.02.041. Epub 2021 Mar 19. PMID: 33745888.
- Villalba A, Rodriguez-Fernandez S, Perna-Barrull D, Ampudia RM, **Gomez-Muñoz L**, Pujol-Autonell I, Aguilera E, Risueño RM, Cano-Sarabia M, Maspoch D, Vázquez F, Vives-Pi M. Antigen-specific immunotherapy combined with a regenerative drug in the treatment of experimental type 1 diabetes. *Sci Rep*. 2020 Nov 3;10(1):18927. doi: 10.1038/s41598-020-76041-1. PMID: 33144616; PMCID: PMC7609712.
- Villalba A, Rodriguez-Fernandez S, Perna-Barrull D, Ampudia RM, **Gomez-Muñoz L**, Pujol-Autonell I, Aguilera E, Coma M, Cano-Sarabia M, Vázquez F, Verdaguer J, Vives-Pi M. Repurposed Analog of GLP-1 Ameliorates Hyperglycemia in Type 1 Diabetic Mice Through Pancreatic Cell Reprogramming. *Front Endocrinol* (Lausanne). 2020 May 13;11:258. doi: 10.3389/fendo.2020.00258. PMID: 32477262; PMCID: PMC7237704.
- Rodriguez-Fernandez S, Murillo M, Villalba A, Perna-Barrull D, Cano-Sarabia M, **Gomez-Muñoz L**, Aguilera E, Maspoch D, Vazquez F, Bel J, Vives-Pi M. Impaired Phagocytosis in Dendritic Cells From Pediatric Patients With Type 1 Diabetes Does Not Hamper Their Tolerogenic Potential. *Front Immunol*. 2019 Nov 28;10:2811. doi: 10.3389/fimmu.2019.02811. PMID: 31849983; PMCID: PMC6892968.

Communications at national and international congresses

- **Gomez-Muñoz L**, Perna-Barrull D, Murillo M, Alcalde M, Catala M, Rodriguez-Fernandez S, Valls A, Perez J, Corripio R, Vives-Pi M. Partial Remission of Type 1 Diabetes: Circulating microRNAs and the immunoregulatory role of miR-30d-5p. Poster communication at: *19th Immunology of Diabetes Society Congress*. Paris, France, 23–27 May 2023.
- **Gomez-Muñoz L**, Perna-Barrull D, Caroz-Armayones JM, Valls A, Perez J, Corripio R, Murillo M, Vives Pi M. Predicting Partial Remission in Type 1 Diabetes using Immunological Parameters. Poster communication at: *44 Congreso de la Sociedad Española de Inmunología*. Bilbao, Spain, 10-13 May 2023.
- **Gomez-Muñoz L**, Perna-Barrull D, Murillo M, Valls A, Perez J, Corripio R, Vives-Pi M. MiRNAs circulantes en diabetes tipo 1 pediátrica: Biomarcadores de remisión y dianas terapéuticas. Oral communication at: *XXXIV Congreso de la Sociedad Española de Diabetes*. Valencia, Spain, 19-21 Apr 2023.
- **Gomez-Muñoz L**, Perna-Barrull D, Rodriguez-Fernandez S, Real N, Valls A, Perez J, Corripio R, Murillo M, Vives-Pi M. MicroRNA signature in children with type 1 diabetes and its role in autoimmunity. Oral communication at: *XVI Congrés de la Societat Catalana d'Immunologia*. Barcelona, Spain, 24-25 Nov 2022.
- **Gomez-Muñoz L**, Perna-Barrull D, Caroz-Armayones JM, Murillo M, Rodriguez-Fernandez S, Valls A, Vazquez F, Pérez J, Corripio R, Bel J, Vives-Pi M. A predictive model for partial remission in pediatric type 1 diabetes using immunological data. Poster communication at: *18th Immunology of Diabetes Society Congress*, 1-4 Nov 2021.
- **Gomez-Muñoz L**, Murillo M, Perna-Barrull D, Valls A, Pérez J, Vives-Pi M. Biomarcadores inmunológicos candidatos de remisión parcial en pacientes pediátricos con diabetes tipo 1. Oral communication (**winner**) at: *43 Congreso Sociedad Española de Endocrinología Pediátrica*. Santiago de Compostela, Spain, 9-11 Jun 2021.
- **Gomez-Muñoz L**, Perna-Barrull D, Murillo M, Villalba A, Rodriguez-Fernandez S, Vazquez F, Perez J, Corripio R, Teniente A, Bel J, Vives-Pi M. Peripheral immune cell patterns behind type 1 diabetes partial remission. Poster communication at: *42 Congreso de la Sociedad Española de Inmunología*. Madrid, Spain, 24-26 Mar 2021.
- Murillo M, **Gomez-Muñoz L**, Perna-Barrull D, Ventura PS, Castiello F, Valls A, Vives-Pi M. Endotypes in diabetes, different diabetes, different management? Poster communication at: *the 62nd Annual European Society for Pediatric Endocrinology Meeting 2024*. Liverpool, UK, 16-18 Nov 2024.

- Perna-Barrull D, Garcia-Loza I, Aguilera E, **Gomez-Muñoz L**, Domenech-Garcia R, Petriz J, Dalmases M, Rodriguez-Vidal S, Barneda-Zahonero B, Vives-Pi M. Harnessing macrophages for advanced type 1 diabetes immunotherapies. *20th Immunology of Diabetes Society Congress*. Bruges, Belgium, 4–8 Nov 2024.
- Murillo M, **Gomez-Muñoz L**, Perna-Barrull D, Castiello F, Ventura PS, Valls A, Vives-Pi M. Endotipos en diabetes, diabetes diferentes ¿seguimiento diferente? Poster communication at: *46 Congreso de la Sociedad Española de Endocrinología Pediátrica*. Las Palmas de Gran Canaria, Spain, 8-10 May 2024.
- Salvia R, Rico G. L, Ward D. M, **Gomez-Muñoz L**, Cañaveras M, Vives-Pi M, Martínez-Cáceres E, Jurado R, Petriz J. Nanoplastics accumulate in human tissues, overcome biological barriers and a significant fraction appear to enter through inhalation. Poster communication at: *37th Congress of the International Society for the Advancement of Cytometry* (CYTO). Edinburgh, Scotland, 4-8 May 2024.
- Salvia R, Rico LG, Ward MD, Bradford J, **Gómez-Muñoz L**, Vives-Pi M, Martínez-Cáceres E, Sorigué M, and Petriz J. Nanoplastics represent a significant fraction of inhaled air, can overcome biological barriers and accumulate in human tissues. Oral communication at: *XVIII Congress of the Iberian Society of Cytometry*. Madrid, Spain, 19-21 Apr 2023.
- Murillo M, **Gomez-Muñoz L**, Perna-Barrull D, Vives-Pi M, Valls A, Pérez J, Corripio R. Reserva pancreática en pacientes pediátricos con diabetes tipo 1 durante los primeros 12 meses tras el diagnostico. Poster communication at: *43 Congreso Sociedad Española de Endocrinología Pediátrica*. Santiago de Compostela, Spain, 9-11 Jun 2021.
- Adrian Villalba, Silvia Rodriguez-Fernandez, David Perna-Barrull, Rosa Maria Ampudia, Federico Vazquez, **Laia Gomez-Muñoz**, Irma Pujol-Autonell, Eva Aguilera, Mary Cano-Sarabia, Marta Vives-Pi. Novel combined therapy for autoimmune diabetes designed by drug repositioning. Oral and poster communications at: *DZD Diabetes Research School*. Barcelona, Spain, 14-16 Sep 2019.
- Adrian Villalba, Silvia Rodriguez-Fernandez, David Perna-Barrull, Rosa Maria Ampudia, Federico Vazquez, **Laia Gomez-Muñoz**, Eva Aguilera, Daniel Maspoch, Joan Verdaguer, Marta Vives-Pi. Novel compound identified by drug repositioning ameliorates experimental autoimmune diabetes. Oral communication at: *XIII Congrés de la Societat Catalana d'Immunologia*. Barcelona, Spain, 14-15 Nov 2019.

Scientific dissemination

- **Gómez-Muñoz L**, Vives-Pi M. Periodo de remisión parcial en la diabetes mellitus tipo 1. Implicaciones inmunológicas. Revista Diabetes (SED), nº 83. 30 Oct 2023.

Project as principal investigator

Awarded a competitive Grant for Diabetes Research Projects led by Young Researchers issued by the Spanish Society of Diabetes (SED). *Immune checkpoints as predictive and diagnostic biomarkers of remission in T1DM*. 2023-2024, 20.000€.

ACKNOWLEDGEMENTS

Quiero empezar recordando el momento en el que decidí ser científica, o al menos intentarlo. Estaba en clase de tutoría de cuarto de la ESO, tenía 16 años. Nos dijeron que cerráramos los ojos y nos viéramos en un futuro. "¿Qué os veis haciendo?" Por aquel entonces sabía que me encantaban las matemáticas y la biología, pero poco más. Hice caso, cerré los ojos y me imaginé con una bata blanca mirando por el microscopio. Creo que todas las decisiones que he ido tomando a lo largo de mi vida me han llevado hasta esa imagen que proyecté hace ya 12 años. Me siento orgullosa de haber conseguido hacer realidad el sueño de mi yo adolescente. ¿Y la inmunología? Pues bien, también tiene su historia. Me acuerdo que estaba en segundo de bachillerato, dos años después, y que el profesor de Biología (Carlos, aún te guardo en mi memoria) nos dijo que tocaba el tema del sistema inmunitario, pero que como era un poco complicado, solo nos íbamos a aprender la presentación antigénica. La explicó por encima y dijo "da igual, no os preocupéis porque esto no saldrá en selectividad". Yo me acuerdo que me fascinó el hecho de tener unas células que eran capaces de reconocer agentes externos y crear todo un ejército para luchar contra él. Fui y le comenté que quería saber más. Aunque no me supo responder, me dijo que buscara información e hiciera un resumen. Y así hice, busqué en internet y en libros cómo funcionaba este sistema que nos defiende y del que no tenía ni idea. Aunque se quedó ahí, yo ya sabía cuál iba a ser mi asignatura favorita en la universidad, y no me equivocaba.

Así que supongo que, en parte, era inevitable que acabara haciendo el doctorado en inmunología, decisión de la que no me arrepiento en absoluto. Es verdad todo lo que dicen de hacer un doctorado: requiere mucho esfuerzo y sacrificio, tiempo, dolores de cabeza, está mal pagado, tienes que lidiar con la frustración… Pero también que es enriquecedor, te desafía cada día y te demuestra que puedes hacerlo, hace que seas resolutivo, creativo, ambicioso. Y cuando un experimento sale como quieres, es la hostia. Me siento orgullosa haber llegado hasta aquí, con todos los cambios que ha comportado, porque me siento una persona más capaz y más segura. Pero de lo que más orgullosa me siento y lo que de verdad me ha hecho feliz, es haber compartido este camino con gente increíble. Esto va por vosotros.

Primer de tot, agrair a la **Marta** per acollir-me tan bé en el seu laboratori fa ja 5 anys, i per confiar en mi per a seguir amb la línia de recerca de la remissió parcial. Qui ens anava a dir que acabaríem sent expertes en miRNAs! Crec que l'empatia i el saber escoltar és el que diferència a un bon supervisor, i tu sens dubte ho has fet amb mi. Gràcies per tots aquests anys d'aprenentatge constant. També als integrants del laboratori (ara ja tots doctors) que em van guiar des del primer moment i sempre amb un somriure: la **Silvia**, qui em va explicar com fer els experiments des del dia 1 amb la seva excel·lència característica. L'**Adrian**, qui em va ensenyar que fer ciència i estar concentrat no és

incompatible amb passar-s'ho bé (gràcies per totes les nostres conversacions i tot el que vam riure mentre tallàvem pàncrees i intentàvem identificar cèl·lules doble positives per insulina i glucagó; capaz no vuelves de París!). I per suposat el **David**, qui m'ha acompanyat i ajudat com ningú en el desenvolupament d'aquesta tesi i a bregar amb el caos que suposa la vida. Gràcies i mil gràcies per sempre tenir una resposta llesta a tots els meus dubtes, per escoltar-me, pels moments de pensar i decidir què fer amb els ratolins (i sobreviure als seus salts mortals o anades d'olla), i per sempre (i quan dic sempre, és sempre) donar-me un cop de mà quan ho he necessitat. Al menys puc dir que et vaig salvar d'uns seguratas a la discoteca, estem en pau, oi? També la **Rosa**, per ajudar-me amb els experiments *in vivo* i per ser una persona tan carinyosa, bondadosa i professional. No puc seguir sense mencionar a les noies d'Ahead. La **Lidia**, per ser no només una companya de laboratori genial, sinó també una amiga que em porto amb mi per sempre. Gràcies per tot el que hem compartit i viscut que només nosaltres dos sabem. Per acompanyar-me en la meva locura d'anar a Bilbao havent d'escriure un abstracte en dos dies i en la de fer-nos un tattoo, per la nostra visita exprés a París, per les tardes de birres, rocòdrom, o les nits de festa, per ser la meva confident i donar-me els millors consells. I sobre tot, i perquè no ho oblidem mai, per rebre el broncote a la sala de cultius de l'Edifici Muntanya. Mai deixis de ser la pistacho lover més maca del món! **Daniela**, thank you for letting yourself be seduced by Taylor Swift, now we can fangirl over her together. Never stop passing me reels of celebrities and gossip. Ti adoro. **Maria**, dona gust arribar al laboratori i veure't sempre amb el teu somriure característic. Fas que tot sigui més fàcil i lleuger. Llàstima que no haguem pogut anar a un concert de Berri Txarrak juntes, però ens queda el de La Raíz (esperem que sense més lesions, sisplau!). I l'ultim en arribar, l'**Ivan**, que em va robar el cor des del primer dia. Ets increïble, però ja ho saps, i encara que et trobi a faltar com a compi de taula, sé que aconseguiràs tot el que et proposis.

También he tenido la suerte de coincidir y compartir espacio con grandes personas del Servicio de Inmunología. Quiero agradecer a **Eva** todos sus comentarios constructivos que hacen que no dejemos de mejorar. Me has enseñado que la inmunología avanza rápido, por lo que hay que trabajar duro y ponerse al día. A dos personas muy especiales con las que tuve el placer de coincidir durante el máster, **Coral** e **Íñigo**. Gracias por todas risas en el lab y fuera de él, y por nuestra aparición dramática como público virtual en la semifinal de OT. **Noelia**, urte hauetan nire aurkikuntzarik handiena izan zara. Ez utzi inori inoiz kendu nahi duzuna egiteko ilusioa, asko balio duzu eta adoragarria zara. **Diego**, gracias por la conexión desde el minuto 0, por compartir los dramas del laboratorio y de la vida. Por muchas más tardes de hacer pulseras, ir al Taylor fest o hacernos fotos. Lo que ha unido Taylor Swift no lo separará nada ni nadie. **Fede**, empezamos el doctorado

juntos y lo acabamos juntos, pero seguro que el camino no nos separa aquí. **Roser**, amb tu també vaig coincidir al màster però després la vida ens ha tornat a ajuntar a la segona planta de l'Edifici Mar. Gràcies per les xerrades i les quedades, i per decorar el laboratori per Nadal. No perdis mai el teu encant tant característic. Y, en definitiva, a todos los del grupo "Fiestaaa" que han hecho que formemos un equipo de inmunólogos como no lo ha habido ni habrá, y por apuntarse a un bombardeo, en especial a **Joan**, **Marc** (también conocido como papuchi o conductor borracho), **Jana** y **María**. No quiero dejar de mencionar a los que ya no están, a los que llevan más tiempo que yo y a los que acaban de llegar, por siempre echar una mano, dejar un reactivo, hacer un escape room o comentar cualquier tontería para distraernos unos segundos de la monotonía: **Yoli** (por estar dispuesta a ayudar siempre), **Bibi** y **Aina** (por vuestros consejos con los paneles de citometría), **Roger**, **Joana**, **Andrea**, **Miriam**, **Laura**, **Jordi**, **Cristina**, **Alex**, **Berta**, y **Maria José**. Y, por último, a todos los técnicos de asistencia, por darle vida al laboratorio, compartir poyata y ayudarnos en todo: **Ana Amaro** (gracias por lo que tú y yo sabemos), **Aroa** (echo de menos girarme y que no estés, pero me alegra que hayas encontrado tu sitio), **Ian** (nadie como tú para poner tecno, he validado que los linfocitos crecen mejor con tu música), **Armando**, **Álex, María**, **Ester** (compartimos la alegría que solo tienen los de Santako), **Arnau**, **Patri**, **Ana Belén**, **Laura, María** e **Imán**.

Quiero continuar mencionando a todas las personas del campus Can Ruti que me han ayudado en algún momento y han contribuido a que este trabajo se terminara de la mejor manera posible. A **Marta Murillo** por ser una médica excelente, involucrada como nadie en la investigación. Gracias por reclutar las muestras necesarias para este estudio, al lado de **Aina Valls** y **Nati Real** y de los compañeros del Parc Taulí, **Jacobo Pérez** y **Raquel Corripio**. Sin vuestro seguimiento de la remisión parcial, este trabajo no hubiera sido posible. Tampoco habría salido bien sin el mejor citometrista del mundo, **Marco Fernández**, y sin la ayuda de **Hammad Alzayat** con la citometría espectral y de **Gerard Requena** con el FACS. Gracias por hacer que aprenda de citometría más de lo que podría llegar a imaginar. También agradezco a **Pilar Armengol** y su equipo (**Irina**, **Anna** y **Xavi**) por ayudarme con el small RNA-seq y a **Clara Prats**, **Marta Alcalde**, **Martí Català** y **Lauro Sumoy** con el análisis. No me olvido de la ayuda con los ratones por parte del equipo del CMCiB, en especial de **Sergi** y **Yaiza**. Por último, agradecer al equipo de comunicación del IGTP por difundir nuestro trabajo de la mejor manera posible. Gracias en especial a **Tamara**, por apoyar todas mis ideas y confiar siempre en mí.

A la gente del Diabetes Research Institute por acogerme desde el primer día con los brazos abiertos y enseñarme todo lo que saben sobre las slices pancreáticas y las células β. A **Juan Domínguez** y **Ricardo Pastori** por toda su ayuda, conocimientos, y consejos. To **Dagmar**, for teaching me everything she knows about miRNAs and for her total

confidence. We started a bit blindly trying to see how it would be to transfect miRNAs into the slices and it has not gone badly at all (not counting the pancreas with suspicious black spheres...). A **Silvia**, por haber sido mi "mami" en USA y por su buena energía. Gracias por prepararnos cada mañana café (sí, el único café solo que he bebido en toda mi vida), por las veces que hemos cortado páncreas juntas con tu banda sonora favorita de fondo, por tus consejos y ayuda. También a **Isa** por estar siempre disponible cuando lo he necesitado y a **Mayur** for his help with the bioinfomatic analysis. And to all the people on floor 5 who have been with me during these four months: **Francesca**, **Kate**, **Lisbeth**, **Arthur**, **Oscar**, **Sung-Ting**, **Giacomo**... I especially want to thank **Estefania** for all her advice and her predisposition to always give me a hand. Thank you all for contributing to make my first experience in the USA a great one.

En el terreno personal, quiero empezar agradeciendo a mis amigas de siempre: **Desy**, **Paula**, **Andy**, **Eva** y **Nerea**. Pocos me conocen como vosotras, y es que no muchos pueden decir "nos conocemos desde P-3". Si estoy hoy aquí es, en gran parte, gracias a vosotras. Juntas hemos crecido, hemos aprendido a ser, a saber lo que nos gusta y lo que no, a aceptarnos y saber qué queremos. Hemos vivido momentos increíbles, de risas infinitas que no olvidaremos jamás. Pero también otros no tan buenos (*teenage years hit hard*), donde nos hemos sabido apoyar y hacernos ver lo que valemos. Por seguir creciendo juntas y ver los caminos por los que nos lleva la vida.

A mis biomédicos, porque si no fuera por vosotros nada sería igual. A **Sergi**, por ser mi mejor amigo desde que te dije en primero de carrera "a mí también me gusta MCR". Podría poner las mil y una anécdotas que he vivido contigo, pero no acabaría esta dedicatoria. Solo destacaré los meses de enero y junio estudiando hasta las 3–4 de la mañana sabiendo que íbamos igual de mal (porque nos gusta eso de procrastinar y somos unos *tryhard*). Gracias, porque sin ti la carrera y lo de después habría molado mucho menos. A **Dani**, por ser la persona en la que puedo confiar a ciegas. Gracias por estar y escucharme siempre, darme los mejores consejos, por hacer que crea en mí, por hacerme reír con tus bromas, por ser tan tú: tan inteligente, carismático y buena persona. Y además un apoyo en el mundo de la ciencia, futuro Dr Medina (hehe). A **Belén** y **Paula**, por quererme y aceptarme tal y como soy. Sois mi apoyo incondicional. Así que solo os pido muchas meriendas contándonos el día a día, muchos viajes más, bailando y disfrutando de las pequeñas cosas de la vida. Gracias por seguir a mi lado 10 años después. A **Laura**, por ser *my partner in crime* desde el primer día. Por todas las locuras que hemos hecho, todos los conciertos que hemos compartido, las prácticas de laboratorio infinitas donde siempre la liábamos (ups... jajaja). Por ser las inmunólogas que somos y siempre de la mano. A todos, espero devolveros –al menos– la mitad de lo que me habéis dado.

También quiero mencionar a otras personas que son muy importantes para mí y que me han acompañado en este camino. La **Natàlia**, la meva compi de pis a Nijmegen. Si alguna cosa m'ha donat l'Erasmus, és tu. Gràcies per convertir-te en "responder" i ser la mostra més important del meu TFG, per les pizzes dels divendres, per enganxar-te a OT per la meva culpa, per les conversacions fins a les tantes de la nit. I gràcies per continuar sent-hi. And talking about Erasmus, I would like to mention the Laboratory of Medical Immunology of Prof. **Hans JPM Koenen**, who treated me just like one of the family. I think that the first experience in a lab is very important and determines to a large extent whether or not you want to continue in the world of science. To them, thank you for motivating me to do it. Sobre todo, a mi supervisora, ahora ya Dr. **Yessica Alina Rodriguez**, por enseñarme a hacer un Ficoll y a cultivar linfocitos y neutrófilos. Nunca olvidaré tus palabras: "vales para esto". Gracias por confiar siempre en mí. And of course, my lab partners and friends, **Alexandra** and **Nurcan**. Even though we were from very different parts of the world (Spain, Hungary, Turkey), we created a bond that still exists today. And I am very proud of it, because it reflects all the support and love we gave each other in those six months. También a **Josep**, por acompañarme durante tantos años en este camino y por toda su ayuda tanto en lo profesional como en lo personal.

A las personas que más quiero. A mis iaios **Cecilia** y **Lorenzo**. Iaia, te echo de menos y sé que te habría encantado verme hoy aquí. Siempre me decías que era más buena que el pan, y muy, muy lista. Siempre presumiendo de tu nieta. Pero ahora presumo yo de iaia, sé que fuiste la mejor abuela, madre y mujer de todas. Una mujer fuerte, valiente, divertida, alegre como ninguna y que no paraba de dar amor. Aún recuerdo el olor de tus guisos (ojalá haber aprendido todas tus recetas), tus villancicos marranos (que los recordabas aún con el Alzheimer), los nísperos que cogíamos del árbol, las nueces y almendras que partíamos, los paseos por la montaña. Siempre seguirás aquí conmigo. Iaio, gracias por tu fortaleza y amor durante todos estos años. Me enorgullece decir que entre tu i la iaia me habéis criado. A mi padre **Ramón**, porque si de alguien he aprendido a ser curiosa y a preguntarme el porqué de las cosas, es de ti. Me has enseñado tanto… desde el simple hecho de montar en bici o bucear hasta los valores que me hacen ser quien soy. Gracias por haber luchado tanto para dármelo todo. A mi madre **Virginia**, mi ejemplo a seguir. Gracias por hacerme "cafés descafeinados" –sin efecto, claro– cuando me tenía que quedar estudiando hasta tarde, por haberte sacado la ESO y el bachillerato otra vez conmigo, escuchando cómo me había empollado todo "de pe a pa", aunque fuera muy aburrido, pero así sabías que yo me quedaba tranquila y segura. A los dos, porque sé que siempre vais a estar ahí para mí, incondicionalmente, y yo lo estaré de vuelta. A mi hermano **Iker**, porque me has hecho reír como nadie siempre que necesitaba desconectar. Gracias por ser la persona más divertida que conozco y tener un meme

siempre listo. A mi tita **Merche** y mi primo **Pau** por estar siempre ahí, apoyarme en todo lo que hago y por hacer que cualquier momento sea divertido. A mi primer –y sé que el mejor– perro que tendré jamás, **Aegon**. Gracias por tanta, TANTA compañía durante las horas de estudio o teletrabajo, y por darme tanto amor, cariño y felicidad. Por los paseos infinitos en la montaña o en la playa, por nuestros juegos de "estirar la rama", "no me pillas" o "buscar la chuche". Por bailar conmigo Taylor Swift, aunque no te guste. Por tantos besitos y abrazos, por escucharme y aprender todo lo que te enseño, por alegrarte como nadie cada vez que me ves. Espero darte la mejor vida posible, porque es lo mínimo que te mereces. Gracias por ser el mejor amigo del mundo.

I per últim, però no menys important, al **Gerard**, per fer-me la vida més bonica i fàcil des de que vas arribar, i sobre tot, per ser la meva inspiració. T'admiro i per mi ets un exemple. Gràcies infinites pel teu suport incondicional durant aquest últim any de tesi, pels teus súper scripts de R perquè aprengui una mica de bioinfo, per estar disposat a ajudar-me en tot, des de fer una figura per la review fins a revisar tots el texts que et passo. Sé que ens queda molt camí per recórrer i no puc esperar a viure mil aventures més amb tu. Em fa feliç pensar que podré veure com et converteixes en el millor científic del món (encara que per mi ja ho ets).